



The
University
Of
Sheffield.

**Membrane Microdomains as Therapeutic
Targets to Control Respiratory Syncytial
Virus**

Joanne McKenzie

Submitted for the Degree of Doctor of Philosophy

University of Sheffield

Department of Infection, Immunity, and Cardiovascular
Disease

June 2022

Abstract

Respiratory syncytial virus (RSV) infects most individuals by the age of two years old with reinfections occurring throughout life. RSV causes a wide spectrum of disease, contributing to high rates of morbidity and mortality in very young, elderly, and immunocompromised individuals. Severe RSV infections have been linked to an excessive and deleterious host immune response that can lead to pulmonary complications such as bronchiolitis. There are currently no established vaccines against RSV, and new treatments for infection are still in development and not established in routine practice.

Membrane microdomains (MM) are specialised regions of host cell membranes that play crucial roles in inflammatory cell signalling and are utilised as platforms for the adsorption and infection of enveloped viruses such as RSV. Previous studies have reported that a naturally occurring phosphatidylserine lipid species, SAPS, can perturb MM and the associated proinflammatory response induced by rhinovirus. I hypothesised that SAPS may be used to disrupt MM, modulating the immune response and the life cycle of RSV in airway epithelial cells (AEC)s. I further hypothesised that SAPS inhibitory effects may also prevent subsequent bacterial co-infection in RSV-infected cells.

AECs were infected with RSV and incubated with SAPS either during infection or at a range of times post-infection. RSV infected AECs co-incubated with SAPS exhibited significantly decreased release of CXCL8 and CCL5 up to 48 hours when compared to untreated cells alone or RSV infected cells co-incubated with the comparative liposome PAPC. Furthermore, AECs infected with RSV in the presence of SAPS had significantly reduced numbers of infected cells and subsequent viral replication in comparison to controls. Preliminary data has also demonstrated that SAPS can significantly reduce the adhesion of *Streptococcus pneumoniae* to AECs directly and inhibit subsequent adhesion in RSV-infected cells.

These data demonstrate that SAPS may have potential therapeutic value as a prophylactic treatment to modulate both RSV infection of AECs and the ensuing inflammatory response.

Acknowledgements

I would like to start by thanking Dr Lisa Parker for giving me the opportunity to work on such an exciting project for my PhD and the help and support provided over these last few years. I would also like to say a huge thank you to Professor Ian Sabroe who has helped me develop as a scientist and who made me realise that it is ok to ask for help in difficult times. Ian vowed to see me through to the end of this project despite retirement and I am very grateful! I would also like to thank Professor Colin Bingle who stepped up to help supervise me during the COVID-19 pandemic and who has always been there for a chat during both my MSc and PhD. In addition, thank you to my MSc supervisor Dr Clare Stokes who taught me so much in the lab alongside Dr Grace Manley.

Thank you to the University of Sheffield, the British Lung Foundation, and The Children's Hospital Charity for generously funding me and this work.

I would also like to acknowledge 'Team Lung', a terrible nickname for an amazing group of people who started their PhD journeys with me and who made some of the hardest days more bearable. A special thank you goes to Dr Kirsty Leigh Bradley whom without her support I would not have made it through these last 4 years. You have been there through the toughest times, not only for the PhD, but also outside of work and I am forever grateful. I am so proud of your amazing achievements so far and you truly deserve it.

Lastly, a huge thank you goes to my mum who is always there no matter what and whose strength and determination never fails to amaze me, you are incredible. This thesis is dedicated to you and in loving memory of dad, who managed to keep smiling even in the hardest of times.

Abbreviation List

A549	Adenocarcinomic human alveolar basal epithelial cell
AEC	Airway epithelial cell
ALI	Air-liquid interface
ATCC	American Type Culture Collection
ATP	Adenosine triphosphate
BEAS-2B	Bronchial airway epithelial cells
BHI	Brain heart infusion (broth)
BPE	Bovine pituitary extract
c-BD1	Chinchilla β -defensin 1
CCL5	Chemokine (C-C motif) ligand 5 (also known as RANTES)
CD14	Cluster of differentiation 14
CDK	Cyclin-dependent kinase
cDNA	Complimentary DNA
CFU	Colony-forming units
CbpA	Choline-binding protein A
COPD	Chronic obstructive pulmonary disease
CPE	Cytopathic effect
CTxB	Cholera toxin
CXCL8	Chemokine (C-X-C) motif ligand 8 (also known as IL-8)
CXR	Carboxy-X-rhodamine
CX3CL1	Chemokine (C-X ₃ -C) motif ligand 1
CX3CR1	Chemokine (C-X ₃ -C) motif receptor 1
DAB	3,3'-Diamino-benzidine
DAPI	4',6-diamidino-2-phenylindole
DRM	Detergent resistant membranes
dsRNA	double stranded RNA
<i>E. coli</i>	<i>Escherichia coli</i>
ELISA	Enzyme-linked immunosorbent assay
F	RSV fusion glycoprotein
FBS	Foetal bovine serum
FFU	Focus forming units
FRET	Fluorescence resonance energy transfer

G	RSV attachment glycoprotein
GA-1000	Gentamicin sulfate-amphotericin 1000
GP	General practitioner
GPI	Glycosylphosphatidylinisitol
GPMV	Giant plasma membrane vesicles
h	Hour
HBEC3-KT	Human bronchial epithelial cell
HEp-2	Human epithelial type 2
HIV	Human immunodeficiency deficiency virus
HMPV	Human metapneumovirus
HRP	Horseradish peroxidase
hTERT	Human telomerase reverse transcriptase
IAV	Influenza A virus
ICAM-1	Intercellular Adhesion Molecule 1
IFN	Interferon
IFN- λ	Interferon lambda
IL-1 β	Interleukin 1 beta
IRF	Interferon regulatory factor
ISG	Interferon-stimulated gene
L	Large polymerase protein
LB	Luria-Bertani
L _d	Liquid disordered
L _o	Liquid ordered
LPS	Lipopolysaccharide
LRT	Lower respiratory tract
LRTI	Lower respiratory tract infection
M	Matrix protein
M Φ	Macrophage
M β CD	Methyl-beta-cyclodextrin
MD-2	Myeloid differentiation factor 2
MDA-5	Melanoma differentiation-associated protein 5
MDBK	Madin-Darby bovine kidney
MFI	Mean fluorescent intensity
MM	Membrane microdomain

MOI	Multiplicity of infection
MTT	3-(4,5-Dimethylthiazol-2-yl)-2,5-diphenyltetrazolium bromide
MyD88	Myeloid differentiation primary response 88
N	Nucleoprotein
NK	Natural killer (cell)
NADPH	Nicotinamide adenine dinucleotide phosphate
NF- κ B	Nuclear factor kappa-light-chain-enhancer of activated B cells
NHBE	Normal human bronchial epithelial
<i>NTHi</i>	Non-typeable <i>Haemophilus influenzae</i>
NOD2	Nucleotide binding oligomerisation domain containing 2
NS	Non-structural
<i>NTHi</i>	<i>Non-typeable Haemophilus influenzae</i>
OM	Otitis media
P	Phosphoprotein
PA	Phosphatidic acid
PAF-R	Platelet-activating factor receptor
PAMP	Pathogen associated molecular pattern
PAPC	1-palmitoyl-2-arachidonoyl-sn-glycero-3-phosphocholine
PBMC	Peripheral blood mononuclear cell
PBP1a	penicillin binding protein 1a
PC	Phosphocholine
PCR	Polymerase chain reaction
PE	Phosphatidylethanolamine
PFA	Paraformaldehyde
PFU	Plaque forming unit
PG	Phosphatidylglycerol
PI	Phosphatidylinositol
PICU	Paediatric intensive care unit
PRR	Pattern recognition receptor
PS	Phosphatidylserine
RIG-I	Retinoic acid-inducible gene-I
RLR	RIG-I-like receptor
RNA	Ribonucleic acid
RNP	Ribonucleoprotein

RSV	Respiratory syncytial virus
RT qPCR	Real time quantitative polymerase chain reaction
RV	Rhinovirus
S	Staurosporine
SAPS	1-stearoyl-2-arachidonoyl-sn-glycero-3-phospho-L-serine
SARS-CoV	Severe acute respiratory syndrome-coronavirus
SEM	Standard error of the mean
SH	Small hydrophobic
SP-A	Surfactant protein A
<i>Spn</i>	<i>Streptococcus pneumoniae</i>
ssRNA	Single-stranded RNA
Th1/ Th2	T helper cell type 1/ 2
TLR	Toll-like receptor
TNF α	Tumor necrosis factor-alpha
TNS	Trypsin neutralisation solution
TRIF	TIR-domain-containing adapter-inducing interferon- β
URT	Upper respiratory tract
URTI	Upper respiratory tract infection
WD-PAEC	Well-differentiated primary paediatric airway epithelial cells

Table of Contents

Abstract.....	i
Acknowledgements.....	iv
Abbreviation List	vi
Table of Contents.....	xi
List of Figures	xvi
List of Tables	xix
Chapter 1: Introduction.....	1
1.1 Respiratory syncytial virus	1
1.1.1 RSV life cycle	3
1.2 Immune responses to RSV	6
1.2.1 Airway epithelium	6
1.2.2 Innate and adaptive immunity to RSV	7
1.3 Health burden of respiratory syncytial virus	12
1.3.1 RSV disease in infants and the elderly.....	13
1.3.4 Bacterial co-infections.....	16
1.3.4.1 Destruction of the epithelial cell barrier.....	19
1.3.4.2 Modulation of immune signalling	19
1.3.4.3 The use of antibiotics for viral-bacterial co-infections	21
1.3.4.4 The need for new anti-virals for RSV	22
1.4 Membrane microdomains	22
1.4.1 Membrane microdomain controversy	25
1.4.2 The role of membrane microdomains in viral infection	26
1.4.3 Modulating membrane microdomains using SAPS – project hypothesis	29
Chapter 2: Materials and Methods	31
2.1 Materials.....	31
2.1.1 Cell culture media reagents.....	31
Table 2.1 Cell culture media and reagents (alphabetical)	31
2.1.2 Buffers and substrates	32
Table 2.2 Buffers and substrates for ELISA, plaque assay, confocal and MTT cell viability	32
2.1.3 Detection reagents	33
Table 2.3 Detection reagents for ELISA, plaque assay, cell viability	33
2.1.4 Detection antibodies.....	34
Table 2.4 Antibodies and dyes for imaging (prepared according to manufacturer’s instruction).....	34
2.1.5 Commercial kits.....	35
Table 2.5 Commercial kits used for RNA extraction, cDNA synthesis and RT-qPCR	35

2.1.6 Primer-probes	36
Table 2.6 Quantitative RT-qPCR primer probes	36
2.1.7 Experimental liposomes	37
Table 2.7 SAPS/ PAPC Liposomes	37
2.2 Methods	38
2.2.1 BEAS-2B cell culture	38
2.2.2 HEp-2 cell culture	38
2.2.3 HBEC3-KT cell culture	39
2.2.4 NHBE cell culture	39
2.2.4.1 Arrival of new donor cells in lab	39
2.2.4.2 Subculture of NHBE cells from liquid nitrogen	41
2.2.4.3 Passaging of NHBE cells	41
2.2.5 Mycoplasma testing	42
2.2.6 Respiratory syncytial virus	42
2.2.6.1 Growing viral stocks	42
2.2.6.2 RSV titration	43
2.2.7 RSV experimental infection of airway epithelial cells	44
2.3 Sample collection and preparation	45
2.3.1 Supernatants	45
2.3.2 RNA	45
2.4 Cell viability assay	46
2.4.1 MTT cell viability assay	46
2.4.2 Cell Titer-Glo® assay	46
2.5 Quantitative real-time PCR (RT q-PCR)	47
2.5.1.1 RNA extraction of BEAS-2B cells	47
2.5.1.2 RNA purification of BEAS-2B cells	47
2.5.2 RNA extraction of HBEC3-KT and NHBE cells	48
2.5.3 cDNA synthesis	49
2.5.4 Absolute quantification RT-qPCR	49
2.5.4.1 Plasmid preparation	49
2.5.4.1a Transformation of <i>Escherichia coli</i> (<i>E. coli</i>)	49
2.5.4.1b Growing up transformed <i>E. coli</i> stocks	50
2.5.4.1c Isolation and purification of plasmid	50
2.5.4.2 RT-qPCR	50
2.6 Enzyme-Linked Immunosorbent Assay (ELISA)	51
2.7 Plaque assay for viral infection	52
2.8 Liposome preparation SAPS/ PAPC	53
2.8.1 Lipid hydration	53
2.8.2 Characterisation of SAPS and PAPC	54

2.8.3 Peripheral blood mononuclear cells (PBMC)	54
2.9 Confocal microscopy	54
2.9.1 Coverslip preparation	54
2.9.2 Infection of cells	55
2.9.2.1 RSV infection for optimisation of anti-RSV fusion (F) antibody	55
2.9.2.2 RSV infection of HBEC3-KT cells at different temperatures for distinguishing binding and fusion events of RSV	55
2.9.3 Fixing cells	56
2.9.4 Primary antibody staining	56
2.9.5 Secondary antibody staining and mounting of coverslips	56
2.9.6 Actin staining.....	57
2.9.7 Confocal microscopy	57
2.10 Bacterial culture.....	57
2.10.1 <i>Streptococcus pneumoniae</i> (<i>Spn</i>) stock preparation	57
2.10.2 Preparation of pHrodo-stained <i>Spn</i>	61
2.10.2.1 Imaging pHrodo-stained <i>Spn</i> in RSV-infected HBEC3-KT cells.....	61
2.10.3 Miles Misra viable bacterial count.....	62
2.11 RSV-bacterial co-Infections of HBEC3-KT cells.....	63
2.11.1 Optimisation of <i>Spn</i> infections of HBEC3-KT cells.....	63
2.11.2 Bacterial challenge with SAPS	63
2.11.3 Co-infected cells: Bacterial adherence assay	64
2.11.4 Co-infected cells: Bacterial invasion	65
2.11.4.1 Bacterial invasion via flow cytometry	65
2.11.4.2 Bacterial invasion via confocal	66
2.12 Data Analysis.....	67
Chapter 3: Results – Investigating the Ability of SAPS Treatment to Modulate the Response of Airway Epithelial Cells to RSV Infection	68
3.1 Hypothesis and aims	68
3.2 Confirming the activity of SAPS and PAPC to modulate inflammatory signalling in PBMCs.....	69
3.3 Modulation of inflammatory signalling in RSV-infected BEAS-2B cells using SAPS/PAPC	73
3.3.1 SAPS significantly reduces the production of CXCL8 and CCL5 from RSV-infected BEAS-2B cells	74
3.3.2 SAPS does not reduce BEAS-2B cell viability or impact RSV-induced cell death	79
3.4 Optimisation of RSV infection of normal human bronchial epithelial (NHBE) and HBEC3-KT cells	82
3.4.1 Optimisation of NHBE and HBEC3-KT cell cultures	82
3.4.1.1 Identification of contaminant in RSV stocks.....	85
3.4.2 RSV induces CXCL8 and CCL5 release in an MOI-dependent manner with limited effects on cell viability	87

3.4.3 RSV moderately reduces cell viability of HBEC3-KT and NHBE cells.....	87
3.4.4 SAPS significantly reduces CXCL8 and CCL5 release from RSV-infected NHBE cells	91
3.4.5 SAPS significantly reduces CXCL8 and CCL5 release from RSV-infected HBEC3-KT cells.....	97
3.5 The efficacy of SAPS as a post-treatment	99
3.5.1 Exploring the immunomodulatory effects of SAPS when applied after an established RSV infection	99
3.5.2 Investigating the effect of multiple SAPS post-treatments in HBEC3-KT cells and cytokine release	103
3.5.3 Investigating the effect of multiple SAPS post-treatments on HBEC3-KT cell viability.....	108
3.5.4 Exploring the effect of 100 µg/ml of SAPS/PAPC on cytokine release from HBEC3-KT cells.....	113
3.5.5 Exploring the effect of 100 µg/ml of SAPS/PAPC on HBEC3-KT cell viability	118
3.6 Chapter summary	123
Chapter 4: Results – SAPS Modulates the Life Cycle of RSV in Airway Epithelial Cell Cultures	124
4.1 Hypothesis and Aims.....	124
4.2 SAPS significantly reduces RSV infection of NHBE cells.....	125
4.2.1 Viral plaque assay optimisation in NHBE cells	125
4.2.2 SAPS significantly reduces the number of NHBE cells infected with RSV	129
4.3 SAPS may modulate RSV infection of, and subsequent viral replication within, airway epithelial cells.....	131
4.3.1 Viral replication in BEAS-2B cells.....	131
4.3.2 SAPS significantly reduces viral RNA from RSV-infected NHBE cells	133
4.3.3 SAPS significantly reduces viral RNA in RSV-infected HBEC3-KT cells.....	135
4.3.4 SAPS does not impact viral replication in HBEC3-KT cells when applied as a post-treatment.....	137
4.4 Confocal microscopy for visualising RSV infection.....	139
4.4.1 Optimisation of RSV anti-fusion (F) antibody in BEAS-2B	139
4.4.2 Optimisation of RSV F antibody staining in NHBE Cells	143
4.4.3 Phalloidin staining in HBEC3-KT cells to visualise the interaction of RSV at filament rich microdomains	146
4.4.4 SAPS visibly reduces levels of viral infection in HBEC3-KT cells	149
4.5 Section summary.....	160
4.6 Exploring the efficacy of SAPS to perturb bacterial co-infections in RSV-infected cells	161
4.6.1 HBEC3-KT infections with <i>Streptococcus pneumoniae</i>	161
4.6.2 Optimising <i>Streptococcus pneumoniae</i> infection of HBEC3-KT cells.....	162
4.6.3 SAPS significantly reduces the number of viable <i>Spn</i> after 1 h incubation	165
4.6.4 Adherence of <i>Streptococcus pneumoniae</i> is upregulated in RSV-infected HBEC3-KT cells but significantly inhibited with SAPS	167

4.6.5 Exploring if RSV infection predisposes to increased rates of bacterial invasion with <i>Streptococcus pneumoniae</i> in HBEC3-KT cells.....	169
4.6.5.1 Optimisation of techniques to investigate pHrodo-labelled <i>Spn</i> invasion in HBEC3-KT cells	169
4.6.5.2 Investigating flow cytometry techniques to quantify <i>Spn</i> uptake in HBEC3-KT cells	174
4.6.5.3 Increased incubation periods of <i>Spn</i> on HBEC3-KT cells does not increase invasion	175
4.6.5.4 Investigating the occurrence of bacterial invasion in RSV-infected HBEC3-KT cells using confocal microscopy	177
4.6.5.5 Investigating the effect of SAPS treatment on bacterial invasion in HBEC3-KT cells using confocal microscopy	181
4.7 Chapter summary	185
Chapter 5: Discussion	186
5.1 Airway epithelial cell models	186
5.2 Mechanism of SAPS when co-incubated during RSV infection	194
5.2.1 SAPS possible mechanism on chemokine production	197
5.2.2 Viral infection and replication.....	201
5.3 Mechanism of SAPS when applied post RSV infection	204
5.4 SAPS interactions with cell receptors and virus	209
5.5 RSV-bacterial co-infections.....	214
5.6 Limitations and future work	219
5.7 Conclusion.....	222
References	225
Appendix.....	248
Appendix 1: Troubleshooting bacterial contaminated RSV stocks	248

List of Figures

Figure 1.1 (A) Structure of Respiratory Syncytial Virus & (B) Life Cycle of RSV.....	5
Figure 1.2 Innate Immune Cell Signalling in Response to RSV Infection.....	11
Figure 1.3 Schematic Diagram Illustrating how RSV can cause Tissue Damage and Severe Pathology in the Airway Epithelium.....	18
Figure 1.4 (A) Membrane Microdomain & (B) The Role of MM During RSV Infection	24
Figure 2.1 NHBE Donor Cell Characteristics.....	40
Figure 2.2 Growth Curve of <i>Streptococcus pneumoniae</i> FP22.....	60
Figure 3.1 SAPS Inhibits CXCL8 Release from PBMCs Stimulated with LPS but not IL-1 β	72
Figure 3.2 Summary Timeline Indicating the Times at which Cells are Infected with RSV and Incubated with SAPS or PAPC.....	77
Figure 3.3 SAPS Significantly Reduces CXCL8 and CCL5 Production from RSV-Infected BEAS-2B Cells.....	78
Figure 3.4 The Effect of SAPS/PAPC Treatment on BEAS-2B Cell Viability.....	81
Figure 3.5 The Effect of Increased RSV MOI on the Release of CXCL8 and CCL5 and Cell Viability in Two Independent NHBE Donors.....	89
Figure 3.6 The Effect of Increased RSV MOI on the Release of CXCL8 and CCL5 and Cell Viability in HBEC3-KT Cells.....	90
Figure 3.7 SAPS Significantly Reduces CXCL8 Release from RSV-Infected NHBE Cells.....	92
Figure 3.8 SAPS Significantly Reduces CCL5 Release from RSV-Infected NHBE Cells.....	94
Figure 3.9 Comparative Investigations in Two Independent NHBE Donors.....	96
Figure 3.10 SAPS Significantly Reduces CXCL8 and CCL5 Release from RSV-Infected HBEC3-KT Cells.....	98
Figure 3.11 Summary Timeline Indicating the Times at which Cells are Infected with RSV and Incubated with SAPS or PAPC.....	101
Figure 3.12 SAPS has Limited Inhibitory Effects on CXCL8 Release from RSV-Infected Cells when Applied as a Post-Treatment.....	102
Figure 3.13 SAPS as a Post-Treatment has some Effects on CCL5 Release.....	103

Figure 3.14 Summary Timeline Indicating the Times at which Cells are Infected with RSV and Incubated with SAPS or PAPC.....	106
Figure 3.15 Multiple SAPS Treatments on HBEC3-KT cells.....	107
Figure 3.16 Multiple SAPS or PAPC Treatments may be Detrimental to HBEC3-KT Viability.....	110
Figure 3.17 Multiple SAPS or PAPC Treatments Causes Visible Cytotoxic Effects on HBEC3-KT Monolayers.....	111-112
Figure 3.18 Summary Timeline Indicating the Times at which Cells are Infected with RSV and Incubated with SAPS or PAPC.....	115
Figure 3.19 Higher Concentrations of SAPS or PAPC are Cytotoxic to HBEC3-KT Cells and Perturb the Production of CXCL8.....	116
Figure 3.20 Higher Concentrations of SAPS or PAPC are Cytotoxic to HBEC3-KT Cells and Perturb the Production of CCL5.....	117
Figure 3.21 Higher Concentrations of SAPS or PAPC are Cytotoxic to HBEC3-KT Cells.....	120
Figure 3.22 100 µg/ml SAPS/PAPC Treatments Causes Visible Cytotoxic Effects on HBEC3-KT monolayers.....	121-122
Figure 4.1 Images from Viral Plaque Assay Optimisation.....	127
Figure 4.2 Optimising Viral Plaque Assay in NHBE Cells.....	128
Figure 4.3 Both Concentrations of SAPS Significantly Inhibit Viral Infection of NHBE Cells.....	130
Figure 4.4 SAPS Treatment may Reduce RSV Viral Copies at 24 and 48 h.....	132
Figure 4.5 NHBE Cells Treated with SAPS have Significantly Lower Levels of Detectable Viral RNA at 24 and 48 h.....	134
Figure 4.6 HBEC3-KT Cells Treated with SAPS have Significantly Lower Levels of Detectable Viral RNA at 24 and 48 h.....	136
Figure 4.7 SAPS Post-Treatment does not Impact on Viral Replication in HBEC3-KT.....	138
Figure 4.8 Confocal Microscopy to Visualise and Quantify RSV Infection.....	141-142
Figure 4.9 Confocal Microscopy can be used to Quantify Viral Infected Cells.....	144-145
Figure 4.10 Optimisation of Phalloidin Staining in RSV-Infected Cells.....	147-148
Figure 4.11 Summary Timeline Indicating the Times at which Cells are Infected with RSV and Incubated with SAPS.....	152

Figure 4.12 Investigating the Effect of SAPS on Viral Infection within HBEC3-KT Cells and the Role of Actin Rearrangement.....	153-157
Figure 4.13 Images Demonstrating the Interactions of RSV at Actin-Rich Membranes of HBEC3-KT Cells.....	158
Figure 4.14 Images Demonstrating the Morphology of HBEC3-KT Cells Infected with RSV in the Presence of SAPS.....	159
Figure 4.15 Optimisation of <i>Streptococcus pneumoniae</i> Infection Conditions.....	164
Figure 4.16 Investigating the Direct Impact of SAPS (25 µg/ml) on <i>Streptococcus pneumoniae</i> (<i>Spn</i>) Growth.....	166
Figure 4.17 The Adherence of <i>Streptococcus pneumoniae</i> is Upregulated in RSV-Infected Cells but Significantly Inhibited with the Addition of SAPS.....	168
Figure 4.18 Investigating the Application of pHrodo-Stained <i>Spn</i> to Visualise Internalisation in HBEC3-KT Cells.....	171-173
Figure 4.19 Investigating the Application of Flow Cytometry to Quantify Intracellular <i>Spn</i> within HBEC3-KT Cells.....	175
Figure 4.20 Optimisation of Fluorescent <i>Streptococcus pneumoniae</i> (<i>Spn</i>) to Visualise and Quantify Bacterial Invasion in HBEC3-KT Cells.....	178-180
Figure 4.21 Investigating the Effect of SAPS on RSV Infection and Subsequent <i>Streptococcus pneumoniae</i> (<i>Spn</i>) Invasion in HBEC3-KT Cells.....	182-184

List of Tables

Table 1.1 Mechanisms in which Viral Infection can Result in Concurrent or Secondary Bacterial Infection within the Respiratory Tract.....	17
Table 1.2 Summary of Viral Pathogens and their Interactions with MM.....	28
Table 2.1 Cell Culture Media and Reagents (Alphabetical).....	31-32
Table 2.2 Buffer and Substrates for ELISA, Plaque Assay, Confocal and MTT Cell Viability.....	32-33
Table 2.3 Detection Reagents for ELISA, Plaque Assay, Cell Viability.....	33
Table 2.4 Antibodies and Dyes for Imaging (Prepared According to Manufacturer's Instruction)	34-35
Table 2.5 Commercial Kits used for RNA Extraction, cDNA Synthesis and RT-qPCR.....	35
Table 2.6 Quantitative RT-qPCR Primer Probes.....	36
Table 2.7 SAPS/PAPC Liposomes.....	37
Table 3.1 Steps Taken to Optimise NHBE Culture.....	84
Table 4.1 Summary of the Steps Taken to Optimise Viral Plaque Assay to Quantify RSV-Infected Cells.....	127

Chapter 1: Introduction

Respiratory syncytial virus (RSV) is a highly ubiquitous virus that infects around 90% of infants before the age of two years old (Lambert et al., 2014; Openshaw et al., 2017; Vandini et al., 2017). In the majority of individuals, infection with RSV is localised to the upper respiratory tract (URT) and disease is characterised by mild, common cold-like symptoms such as a cough, excess mucus production, and a sore throat. However in immunocompromised individuals, infants and the elderly, RSV may progress into a symptomatic lower respiratory tract infection (LRTI) associated with a more severe disease phenotype with hyperinflammation, tissue damage and opportunistic bacterial infections (Openshaw et al., 2017; Vareille et al., 2011). RSV-induced LRTIs can result in life-threatening bronchiolitis or pneumonia and has also been attributed to the development of pulmonary complications in later life such as recurrent wheeze or asthma (Cromer et al., 2017; Griffiths et al., 2017). Despite the initial characterisation of RSV back in 1956 (Morris et al., 1956), there is still no vaccine against RSV and treatments remain limited and expensive and therefore new therapeutics and antivirals are urgently required to tackle RSV disease.

1.1 Respiratory syncytial virus

RSV is a negative sense, single-stranded RNA (ssRNA) virus that belongs to the *Orthopneumovirus* genus within the (recently defined) *Pneumoviridae* family (Thornhill and Verhoeven, 2020). RSV is a seasonal virus where peaks of infection in the UK are demonstrated between September and December (Coultas et al., 2019). However, these regular seasonal epidemics were recently impacted by the global coronavirus disease (COVID-19) pandemic and it is not known whether the epidemiology of RSV (along with other viruses such as influenza and metapneumovirus) will be permanently modified in future outbreaks (Binns et al., 2022). There are two subtypes of RSV: A (most common circulating

strain) and B, where subtypes are characterised by the antigenicity of virion attachment glycoprotein (G) (Vandini et al., 2017).

RSV virions can be spherical or filamentous where the spherical structure of RSV and its associated structural proteins are depicted in **Figure 1.1 A**. The ssRNA genome of RSV contains 10 genes that can encode a total of 11 structural and non-structural proteins (Lambert et al., 2014; Vandini et al., 2017). Embedded in the viral lipid envelope are three transmembrane glycoproteins; small hydrophobic (SH) which has proposed roles in immune modulation, and the major surface glycoproteins; attachment (G) and fusion (F) that help mediate the attachment and fusion of RSV to host cells during infection (Griffiths et al., 2017). Both G and F are immunogenic proteins that therefore elicit protective neutralising antibodies from an infected host (Tang et al., 2019). Of interest, a secreted isoform of attachment glycoprotein (G) has also been described that may act as a decoy target antigen for host cell neutralising antibodies (Bukreyev et al., 2008). Additional research has also demonstrated that secreted G protein may diminish the antibody-mediated restraint of RSV replication, allowing for increased viral spread in the host (Bukreyev et al., 2012) indicating some of the key immunomodulatory roles that G protein plays. In addition, the F protein can mediate the fusion of RSV-infected cells with adjacent host cells to create multinucleated cells (syncytia), a characteristic that helped give rise to the name of this virus. The formation of syncytia allow RSV to readily spread between cells in the airway epithelium, and is associated with cytopathic effects (Lambert et al., 2014; Tian et al., 2013). The large polymerase (L), phosphoprotein (P) and nucleoprotein (N) associate with the viral RNA to make up the functional polymerase complex. Non-structural (NS) proteins 1 (NS1) and 2 (NS2) are involved in innate immune modulation during infection by inhibiting interferon (IFN) responses and apoptosis, but are not packaged into new virions after replication and are therefore omitted from **Figure 1.1 A** (Spann et al., 2005). The matrix (M) protein lies beneath the lipid envelope and helps give the virion its structural shape. Lastly, the *M2* gene has two open reading frames which can differentially encode either M2-1 (essential factor for viral RNA complex) and M2-2 (mediates transcription to replication) (Kiss et al., 2014).

1.1.1 RSV life cycle

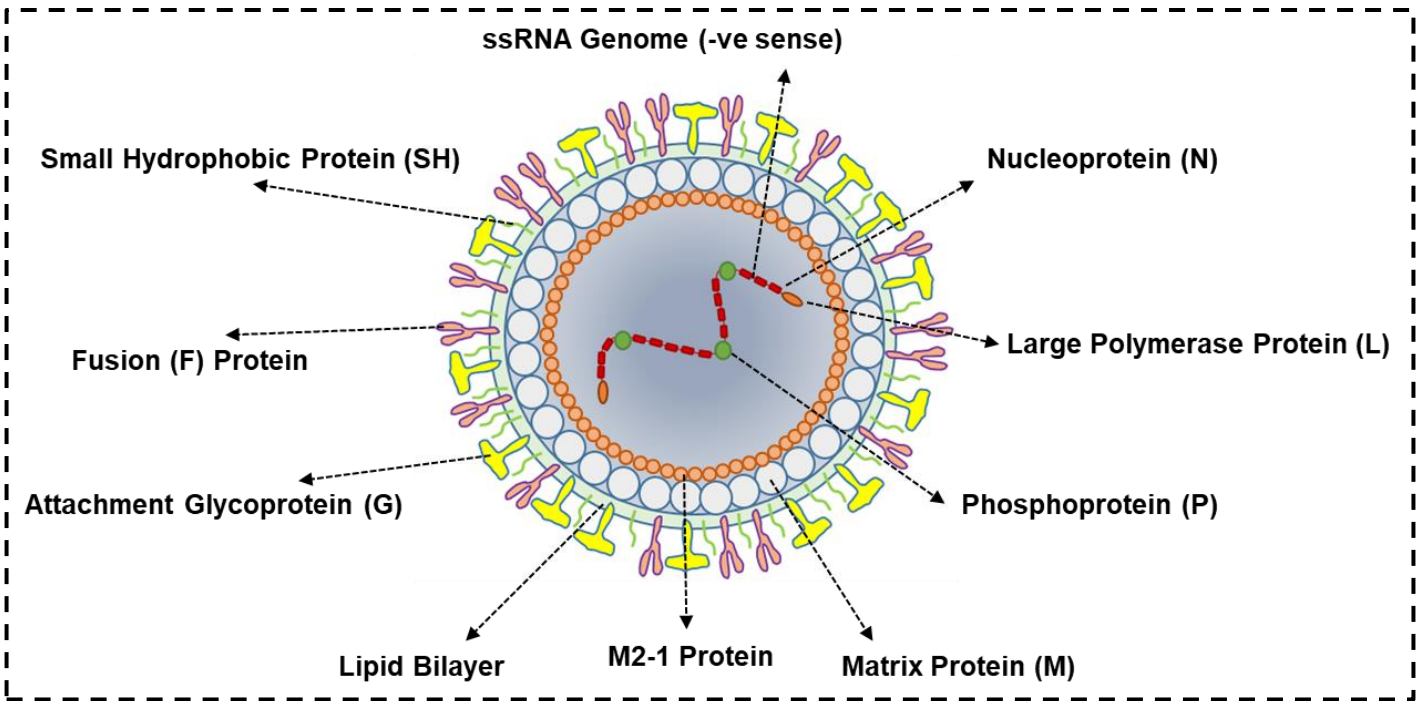
RSV can be readily spread between an infected person to a new permissible host via nasal/oral secretions that contain RSV-infected droplets of saliva or mucus (Shahriari et al., 2016). The virus displays tropism for airway epithelial cells in the URT where it can bind receptors via attachment glycoprotein G (Haynes et al., 2001). Several host cell receptors have been identified as possible targets of viral G protein binding, including CX3C chemokine receptor 1 (also known as fractalkine receptor, CX3CR1), heparan sulfate proteoglycans and nucleolin (Anderson et al., 2020; Harcourt et al., 2006; Haynes et al., 2001; Kurt-Jones et al., 2000; Marr and Turvey, 2012). The full scope of receptors that RSV may utilise during infection however, remains ambiguous particularly as some studies have presented data indicating that recombinant strains of RSV lacking G protein are not essential for viral infection and replication *in vitro* but required *in vivo* (Teng et al., 2001; Teng and Collins, 2002). These studies suggest that interactions and receptors for RSV G protein may be cell type dependent, and proposed receptors listed above may not demonstrate fully the interactions of RSV with cognate receptors present in the respiratory tract (Feng et al., 2022; King et al., 2021). The binding and fusion of RSV to cells has been demonstrated to occur at specialised regions of the host cell membrane (termed membrane microdomains; MM), that congregate the required host cell receptors into specific areas of the membrane to allow for efficient viral-host interactions (Chang et al., 2012; Griffiths et al., 2017; Ke et al., 2018).

Successful attachment to a host cell triggers conformational changes in the F protein (from the pre-fusion to post-fusion form) which allows the lipid envelope of the virus and that of the host cell membrane to come into close proximity, at which point lipid mixing enables the viral RNA to be delivered inside the cell (Battles et al., 2016). RSV then hijacks the host cell machinery in order to transcribe its viral RNA from the negative sense template into positive sense RNA, using its viral RNA-dependent RNA polymerase complex. This positive sense RNA intermediate is then ready for efficient translation to produce new copies of the negative

sense genomes which can be packaged together with viral proteins to form new virions that accumulate and bud from the host cell membrane (**Figure 1.1 B**) (Collins et al., 2013).

Most individuals are infected with RSV before the age of two but primary infection does not lead to robust, life-long immunity and therefore reinfection (sometimes with the same serotype of virus) can occur throughout life (Openshaw et al., 2017; Varese et al., 2022).

1.1 A



1.1 B

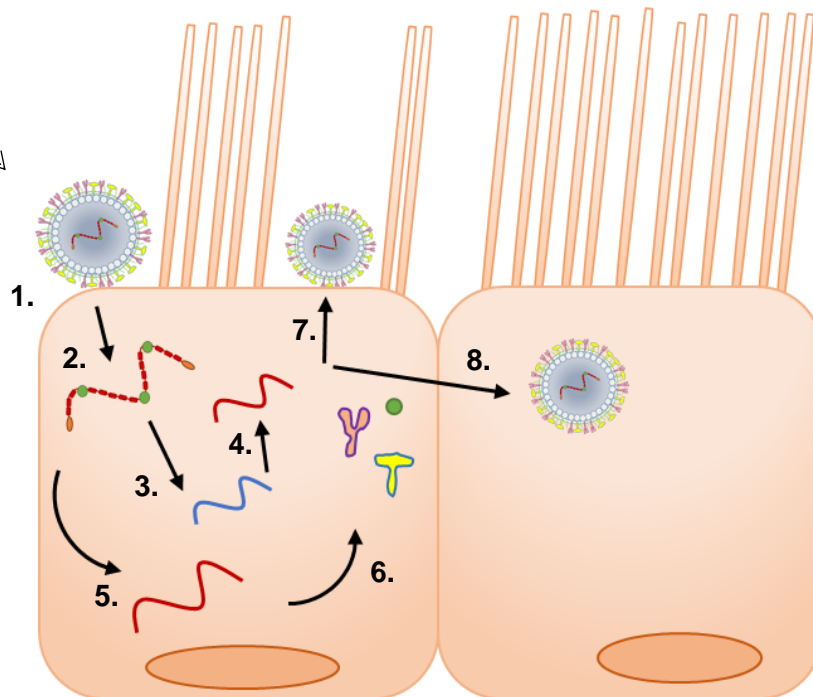


Figure 1.1 (A) Structure of respiratory syncytial virus. The single-stranded RNA genome is surrounded by nucleoproteins (N). Attached to the nucleocapsid are two large polymerase proteins (L) and three phosphoproteins (P). Matrix proteins (M) encase the nucleocapsid and are enveloped by a lipid bilayer. Three transmembrane glycoproteins can be found in the lipid bilayer: small hydrophobic (SH) proteins, attachment protein (G) and fusion protein (F).

(B) Life cycle of RSV. RSV preferentially attaches to a ciliated cell within a host via surface glycoprotein G (1). Fusion protein F allows the virus to merge with the host cell membrane and release the viral genome (2). The viral RNA is transcribed into a positive sense RNA intermediate (3) then translated back into negative-sense viral RNA (4). Viral RNA is translated using host cell machinery (5) to generate more viral protein (6). Newly generated viral RNA and proteins aggregate at the host cell membrane where they form a ribonucleoprotein complex that is enveloped by host cell membrane as it buds (7). Alternatively, new virion may infect neighbouring cells forming syncytia (8).

1.2 Immune responses to RSV

1.2.1 Airway epithelium

The airway epithelium of the respiratory tract is a first line defence against potential pathogens and other environmental stimuli (Vareille et al., 2011). The nasopharynx comprises the nasal cavity, mouth and throat, and is the primary site for RSV infections (Jumat et al., 2015). However, in some individuals, RSV can progress into the lower respiratory tract (comprising the bronchioles and alveoli) and this can lead to a more severe disease (Coultas et al., 2019).

RSV is not the only potential threat however and, in order to deal with infectious agents and environmental infiltrates, the respiratory tract has developed an array of defences (Vareille et al., 2011). The airway epithelium itself acts as the physiological first line of defence and is composed of mucus-secreting goblet cells which trap pathogens or debris, and ciliated cells, that feature hairlike projections (cilia) that can beat in a rhythmic motion. Together, these cells work collaboratively to help clear the airways in a process termed mucociliary clearance (Johnston et al., 2021; Kuek and Lee, 2020; Wright, 2005). In addition, the secreted mucus contain antimicrobial peptides including cathelicidin LL-37, which, in combination with human β -defensins, have been shown to inhibit RSV infection of airway epithelial cells and have roles in promoting inflammatory signalling in response to pathogens such as RSV (Teclé et al., 2010). Pulmonary surfactant is composed of lipids and proteins which have also been shown to have roles in pathogen clearance from the airways as well as immunoregulatory roles (Kuronuma et al., 2009; Numata et al., 2010). Pulmonary surfactant also mediates the required low surface tension within the lung in which perturbation of surfactant can result in respiratory distress syndrome (Wright, 2005). Of note, surfactant protein A (SP-A) has demonstrated direct anti-viral effects during RSV infection by binding the F protein of RSV and preventing its uptake into epithelial cells (Lüfgren et al., 2002). However, in cases where the pathogen has penetrated these first lines of defence, the airway is also able to coordinate the induction of innate and adaptive immunity by directly secreting pro- and anti-inflammatory cytokines to

recruit leukocytes such as alveolar macrophages, neutrophils and eosinophils (Hiemstra, 2001).

1.2.2 Innate and adaptive immunity to RSV

In many instances, RSV may penetrate the physiochemical barrier of the respiratory tract and successfully bind airway epithelial cells within the host, triggering innate and adaptive immune responses. The host utilises a range of specialised pattern recognition receptors (PRR)s that can detect specific pathogen associated molecular patterns (PAMP)s throughout different stages of viral infection (**Figure 1.2**) (Goritzka et al., 2015; Satkunanathan et al., 2014). Damage-associated molecular patterns (DAMPs) have also been shown to interact with PRRs where damaged cells may release endogenous molecules (such as high mobility group box 1 and S100A9) after RSV infection and drive chronic inflammation in the lungs (Bolourani et al., 2021; Foronjy et al., 2016; Gong et al., 2020; Hosakote et al., 2016).

During viral attachment, PRRs such as TLR4 and TLR2/6 can detect RSV PAMPs such as the surface glycoproteins. Within the host cell, endosomal TLR7/8 can identify ssRNA upon its release into the host cell where TLR3 can detect double stranded (ds)RNA during viral replication (Goritzka et al., 2015). Of interest, and contrary to prevalent research, the intracellular expression of TLR2 and TLR4 has also been documented in epithelial cells (Hornef et al., 2003; Ueta et al., 2004). In addition, the surface expression of TLR3 and TLR7 at the apical membrane of human tracheal epithelial cells has also been demonstrated (Ioannidis et al., 2013). For this reason, TLR4, TLR3 and TLR7 have been marked with an asterisk (**Figure 1.2**) to indicate their potential expression at alternative sites within airway epithelial cells and highlights that there is still much to learn about the interactions and roles of TLRs with RSV. RIG-I like receptors; RIG-I, Nucleotide Binding Oligomerisation Domain Containing 2 (NOD2) and melanoma differentiation-associated protein 5 (MDA-5) are cytoplasmic and are also able to detect dsRNA during RSV replication (Kawai and Akira, 2010; Kurt-Jones et al., 2000; Li and Wu, 2021).

The detection of RSV by PRRs lead to the recruitment of specialist adaptor proteins such as TIR-domain-containing adapter-inducing interferon- β (TRIF) and myeloid differentiation primary response 88 (MyD88), whose downstream signalling includes the activation of transcription factors including interferon regulatory factor (IRF) and nuclear factor kappa-light-chain-enhancer of activated B cells (NF- κ B) (**Figure 1.2**) (Haynes et al., 2001; Kawai and Akira, 2010). These signalling pathways collectively lead to the increased recruitment of immune cells such as alveolar macrophages and dendritic cells alongside the coordinated production of proinflammatory cytokines such as interleukin (IL) 1-beta (IL-1 β), IL-18 and interferons (IFN) (Ascough et al., 2018; Sun and López, 2017). Type-I (IFN- α/β) and type-III (IFN- λ) IFNs, have both been shown to play crucial anti-viral roles during RSV infection (Ascough et al., 2018; Cormier et al., 2014; Okabayashi et al., 2011). Cormier et al. (2014) demonstrated that neonatal mice that had diminished IFN- α led to increased disease severity with Th₂-skewed responses however Okabayashi et al. (2011) revealed that IFN- λ was the predominant IFN released from both primary and immortalised nasal epithelial cells infected with RSV. RSV-infected airway epithelial cells also produce chemokines including (C-C motif) ligand 2 (CCL2)/MCP1, CCL4/MIP-1 β , CCL5/RANTES, (C-X-C motif) ligand 8 (CXCL8)/IL-8 and CXCL10/IP-10 which recruit leukocytes such as neutrophils, alveolar macrophages, eosinophils and T cells to sites of infection (Broadbent et al., 2018; Culley et al., 2002; Haynes et al., 2001; McNamara et al., 2005). Although these chemokines play key roles in protective immunity, when in excess (as seen in severe RSV disease) they can also drive disease pathogenesis (Cromer et al., 2017; Murawski et al., 2009; Shi et al., 2017). The combination of recruited innate immune cells and soluble cytokine mediators helps establish a sequential regulated inflammatory response within the lung which helps mediate the ensuing adaptive immune response later in infection (Coultas et al., 2019; Varese et al., 2022).

Innate and adaptive immune responses work collaboratively to generate a robust and protective response to viral pathogens such as RSV. The key lymphocytes activated during

the adaptive immune response are T and B leukocytes which are crucial for resolution of RSV infections (Ascough et al., 2018). There are two major T cell types that are sub-categorised based on their surface markers; the CD4⁺ (helper T cell) which help prime other immune cells during viral infection and stimulate the production of antibodies from B cells, and the CD8⁺ (cytotoxic T cells) which can directly kill viral infected cells (Ascough et al., 2018; Openshaw et al., 2017).

CD4⁺ T helper cells can be further subdivided into distinct groups based on their cytokine production and activities; Th₁ (secrete IFN- γ and TNF- β that help generate cell mediated immunity), Th₂ (secrete IL-4, IL-10 and help to prime B cells to secrete antibodies), Th₁₇ (secrete IL-17 which contributes to a more proinflammatory phenotype) and T regulatory (Treg) cells (help regulate and suppress T cell activation and proliferation) (Legg et al., 2003; Mangoldt et al., 2015, p. 17). In the majority of individuals infected with RSV, a Th₁ dominant adaptive immune response ensues where B cells are activated to secrete neutralising antibodies such as immunoglobulin (Ig) A from the nasal epithelium and IgG in the serum that help control the spread of RSV throughout the lung (Ascough et al., 2018; Walsh and Falsey, 2004). However, the immune response in severe RSV disease has been linked to the progression of a Th₂ type response characterised by increased leukocytes such as eosinophils and decreased production of antiviral IFN- γ (Delgado et al., 2009; Lambert et al., 2014; Openshaw et al., 2017; Walsh and Falsey, 2004).

CD8⁺ T cells can also be subdivided into effector (activated during proliferation and release cytokines such as IFN- γ and TNF- β) or memory cells which reside in the host and can rapidly proliferate upon recognition of cognate antigen (Schmidt and Varga, 2020). Although research has indicated that complete immunity is not achieved during “natural” infection with RSV, human challenge studies have indicated that CD8⁺ resident memory T cells have been linked to protective immunity against reinfection with RSV and are correlated with reduced viral load and symptom severity (Jozwik et al., 2015; Varese et al., 2022). CD8⁺ T cells are crucial for viral clearance by targeting and killing viral infected cells through the production of effector

molecules such as granzyme B and inflammatory cytokines, however, these actions can lead to immunopathology within the lung if not controlled properly (Schmidt et al., 2018; Schmidt and Varga, 2020).

A fine balance exists between a robust immune response to clear the virus, and an excessive inflammatory response that can in turn, lead to further pathology. In the majority of individuals, RSV infection is retained in the URT and associated with milder common cold-like symptoms that normally resolve in around 7 – 14 days without complication (Bont, 2013). However, in immunocompromised individuals, and often in the very young or elderly, RSV infection may progress into the lower respiratory tract with hyperinflammation and pulmonary complications such as bronchiolitis and pneumonia. (Openshaw et al., 2017; Vareille et al., 2011). In addition, there is also evidence to suggest that DAMPs associated with RSV infection may contribute to chronic airway inflammation and requires further investigation (Bolourani et al., 2021; Foronjy et al., 2016; Gong et al., 2020; Hosakote et al., 2016). The reasons why immune responses differ so much, particularly between specific age groups, is still an area of active research (See Section 1.3.1) (Coultas et al., 2019; Culley et al., 2002; Lambert et al., 2014; Openshaw et al., 2017).

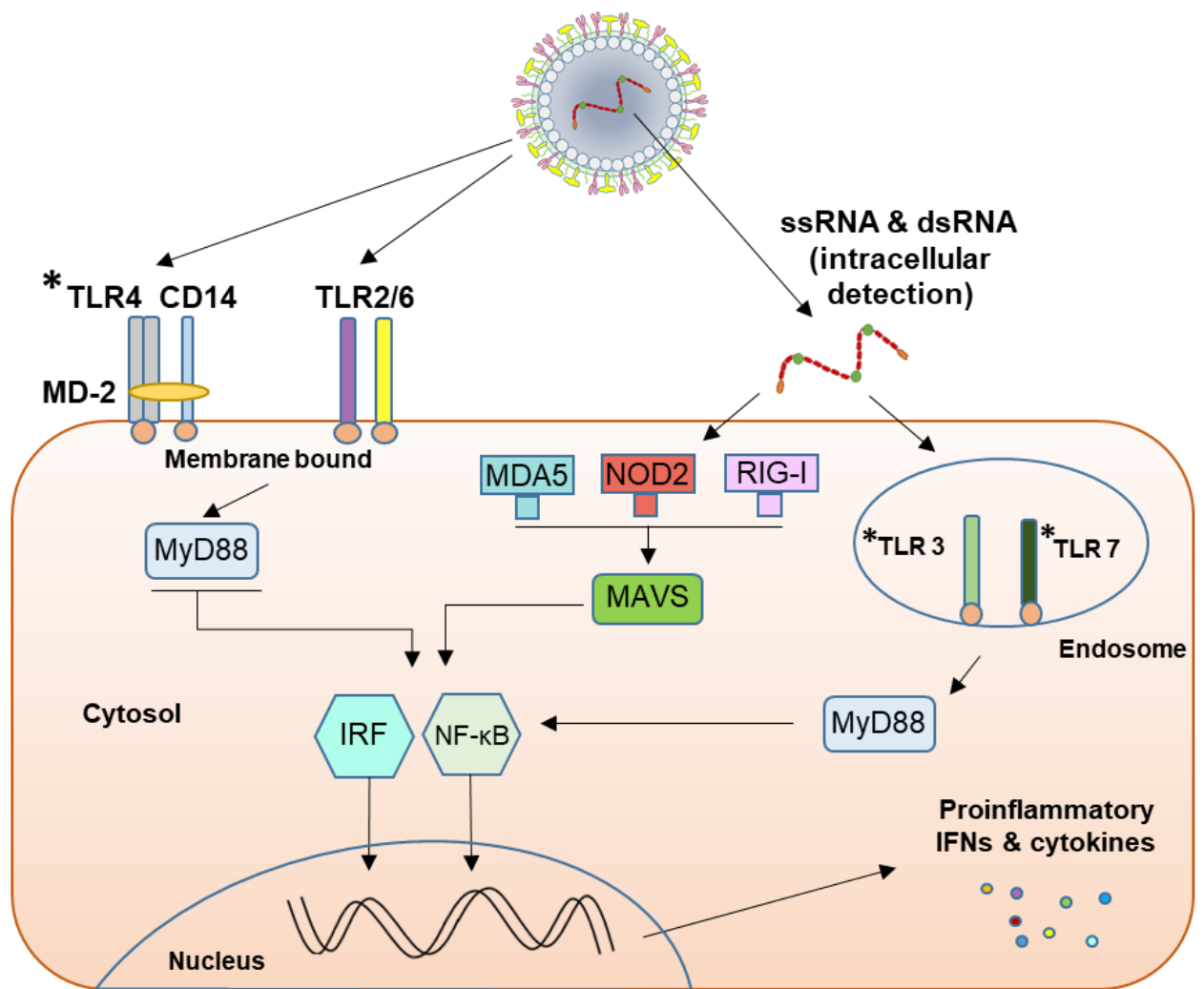


Figure 1.2 Innate immune cell signalling in response to RSV infection. Detection of RSV infection occurs at many specialised PRRs. These lead to the recruitment of specialised adaptor proteins that trigger the translocation of IRF and NF-κB into the nucleus to initiate the production of proinflammatory cytokines & chemokines that help recruit immune cells such as neutrophils and natural killer cells. TLRs that are marked with an asterisk indicate that these receptors may also be expressed in alternative sites contrary to their well-established locations depicted in the diagram.

1.3 Health burden of respiratory syncytial virus

The ability of RSV to cause a wide spectrum of disease and where primary infection does not induce complete, protective immunity, has impacted the successful development of a vaccine and there remains an increasing disease burden associated with RSV (Coultas et al., 2019). One of the first vaccine attempts against RSV was conducted in the 1960s using formalin-inactivated RSV which unfortunately heightened pathology in response to viral challenge in vaccinated infants and subsequently led to the deaths of two participants (Fulginiti et al., 1969). Since then, there was hesitation over subsequent attempts to develop vaccines against RSV. However, a pivotal discovery made at the National Institutes of Health (NIH) by Dr Jason McLellan was that neutralising RSV antibodies were better induced against the pre-fusion form of RSV F protein rather than the previously targeted post-fusion form (McLellan et al., 2013b, 2013a). This knowledge has helped boost the rapid development of potential vaccines and therapies against RSV and to date, there are four RSV vaccine candidates in phase 3 testing from GlaxoSmithKline, Janssen, Moderna and Pfizer which have been designed to induce neutralising antibodies against pre-F RSV protein (GlaxoSmithKline, 2021; Janssen Vaccines & Prevention B.V., 2022; ModernaTX, Inc., 2022; Pfizer, 2022).

In addition, the structural information of RSV F protein has been applied to increase the efficacy of prophylactic therapeutics against RSV. Currently, there are only two approved prophylactic therapies for RSV; palivizumab - a humanised monoclonal antibody which targets the F protein of RSV, and ribavirin – a nucleoside analogue which inhibits viral replication (Eiland, 2009). Due to its high cost and limited efficacy during active infection, palivizumab is reserved for prophylactic use in infants that are at high risk of severe RSV disease such as premature birth during RSV seasons (Lambert et al., 2014; Nuijten et al., 2007). However, a promising new monoclonal antibody called nirsevimab is currently in phase 3 trials which has demonstrated increased levels of neutralising antibody against the highly conserved 0 region of the pre-fusion form of F and, has also demonstrated an increased half-life to that of

palivizumab (Griffin et al., 2020). The only other current therapeutic used against RSV is ribavirin which is often prescribed to infected, immunocompromised individuals, however it is reported to have limited efficacy (Subcommittee on Diagnosis and Management of Bronchiolitis, 2006). Treatment therefore remains mostly supportive through supplemental oxygen and fluids, contributing to an increased health burden for certain groups of the population.

RSV is one of most common causative agents for lower respiratory tract infection (LRTI) in infants, the elderly, and immunocompromised and is therefore associated with high rates of morbidity and mortality across the world (Falsey et al., 2009; Shi et al., 2017). Despite this, the health burden of RSV is often overshadowed by other well-known respiratory viruses such as influenza (Cromer et al., 2017). However, a public health study has shown that in comparison to influenza, RSV infections result in twice as many general practitioners (GP) consultations and five times as many hospitalisations (Ackerson et al., 2019; Cromer et al., 2017). RSV infections impose a huge health burden on healthcare systems where, in England alone, the associated annual healthcare cost of RSV infections in children under 5 years old is around £54 million (Cromer et al., 2017).

1.3.1 RSV disease in infants and the elderly

Infants, particularly those aged under 2 years, have been shown to be at an increased risk of severe RSV disease. In 2005 around 66,000-199,000 deaths worldwide were recorded in children younger than 5 years old with 99% occurring in developing countries (Nair et al., 2010). One of the physiological factors for severe RSV disease in this age group is that the airways are much smaller and therefore RSV-induced mucus production and immune cell infiltration within the airways appears more likely to cause blockages and reduced gas exchange (Lambert et al., 2014). Genetic factors (in association with environmental stimuli) have also been described that may predispose children to severe RSV disease. Caballero et al. (2015) described mutations in *Tlr4* genotype whereby two single nucleotide

polymorphisms, Asp299Gly and Thr399Ile, were shown to skew the immune response to LPS which binds TLR4. As TLR4 is also a major receptor in which RSV interacts with, genetic mutations that alter the functions of this receptor during RSV infection have also been linked to a causative hyperinflammatory response (Caballero et al., 2015, p. 4). Of interest, separate studies have demonstrated that these two specific mutations have also been shown to result in decreased expression of TLR4 and thus impaired innate immune responses to RSV which resulted in more severe disease (Halfhide et al., 2009; Tal et al., 2004). However, one of the major factors that has been attributed to severe RSV disease is the production of proinflammatory cytokines associated with a Th₂ biased immune response with poor neutralising Th₁ activity (Kollmann et al., 2009). This leads to increased production of proinflammatory cytokines/chemokines that recruit eosinophils and neutrophils which can have increased cytopathic effects on airway epithelial cells (Habibi et al., 2020).

Severe RSV disease during primary infection of infants has been (sometimes controversially) linked to the development of asthma in later life (Homaira et al., 2017; Knudson and Varga, 2015; Lambert et al., 2014; Sigurs et al., 2000; Wu and Hartert, 2011). There is debate as to whether RSV infection predisposes individuals to asthma because of a period of RSV-induced airway inflammation and associated tissue damage, or if certain individuals are predisposed (either genetically or environmentally) to asthma and severe RSV infection merely accelerates this development (Lambert et al., 2014; Sigurs et al., 2000; Wu and Hartert, 2011). Evidence to support the former argument are that severe RSV infection can result in a skewed immune response (predominantly Th₂) whereby eosinophils and neutrophils are recruited into the lungs (Culley et al., 2002; Habibi et al., 2020; Lambert et al., 2014). This can contribute to delayed viral clearance and increase hypersensitivity to aeroallergens within the lung environment (Jackson et al., 2016). Of particular importance was a study by Culley et al. (2002) using BALB/c mice that demonstrated that age of primary RSV infection can affect immune responses during reinfection and drive disease severity. Data indicated that neonatal mice were more likely to have Th₂ dominant responses which is subsequently triggered upon

reinfection. This indicates how RSV infection in young infants may impede subsequent immune responses of the airway which may contribute to respiratory disease (Culley et al., 2002). Tourdot et al. (2008) have also demonstrated, in their murine model of chronic allergen exposure, that RSV infection may contribute to airway remodelling and sensitisation of the lungs to subsequent allergen exposure. RSV-infected mice that were then challenged with allergen demonstrated phenotypic changes, such as increased production of collagen and thickening of bronchial basal membrane cells, characteristics that resemble asthmatic airways (Tourdot et al., 2008). Together, these studies demonstrate the long-term immunological and structural effects that RSV can have that may predispose individuals to subsequent incidence of asthma. In addition, some studies have indicated that the risk of developing asthma appears to coincide with episodes of childhood wheezing that occurred as a response to RSV or rhinovirus (RV) (Jackson et al., 2016; Stein et al., 1999). The likelihood of bronchiolitis and wheeze occurring during childhood RSV infection is higher due to an immature immune response and smaller airway, therefore, it is plausible that infection with RSV may contribute to the development of asthma (Jackson et al., 2016; Knudson and Varga, 2015; Lloyd and Saglani, 2017; Lloyd and Snelgrove, 2018).

There is a large spectrum of disease severity in infants and there are still many unanswered questions about why there is such a large variability in response to RSV infection. It is hypothesised that severe disease may be due to the immature immune system in infants or that some individuals are more susceptible to the virus, leading to an increased viral burden (Delgado et al., 2009; Griffiths et al., 2017).

Adults aged over 65 years have been identified as another high risk group for severe RSV disease, where it has been claimed that the disease burden attributable to RSV infection may match that of non-pandemic influenza (Falsey et al., 2009; Falsey and Walsh, 2005). RSV is particularly troublesome for those with chronic obstructive pulmonary disease (COPD) (Falsey et al., 2009). In comparison to infants, elderly populations have been linked to severe RSV disease through a process now described as inflammaging. This has been linked to the

inability to produce an effective inflammatory response, however characterising the exact changes in adaptive immunity are complex and may involve genetic or environmental changes or even moderations in the microbiome as people age (Falsey et al., 2009; Openshaw et al., 2017). There have also been reports that have found a reduction in both IFN- γ and CD8⁺ T cells, which coincided with increased levels of viral replication and ineffective clearance (de Bree et al., 2005).

1.3.4 Bacterial co-infections

Increasing evidence has revealed that the respiratory tract is not a sterile environment and contrary to initial theories, both the upper and lower airways host a diverse array of microbial species including bacteria, fungi, virus, and protozoa (Ursell et al., 2012). The genes of these different microbes that reside in the same ecological niche are collectively described as the microbiome (Ursell et al., 2012). Much like the gastrointestinal tract, the lung microbiome is enriched with different microbial species that normally co-exist in a state of equilibrium. The microbiome has been shown to help prevent infection with opportunistic pathogens as well as help stimulate and develop the immune system in the developing lung during early years (Shukla et al., 2017) However, the equilibrium of this microbiome can be perturbed by pathogenic virus such as RSV, leading to the disruption of this microbial community and the occurrence of viral-bacterial co-infections (Beck et al., 2012; Gao et al., 2014; Yagi et al., 2021).

Bacterial co-infection can occur in RSV infection, and often results in prolonged hospital stays, reliance on supportive therapy and in extreme cases, the development of bronchiolitis, sepsis or bacterial pneumonia (Suárez-Arrabal et al., 2015; Thorburn et al., 2006). Studies have shown that the higher rates of bacterial pneumonia often coincide with seasonal peaks of RSV and influenza outbreaks (Deng, 2013) and that there are multiple predisposing factors that can contribute to viral-bacterial co-infection in the airways (**Figure 1.3**) (**Table 1.1**) (Bakaletz, 2017; Morens et al., 2008; Vareille et al., 2011).

Effect of Viral Infection	Attributing Factor for Bacterial Co-Infection
Altering microbiome (de Steenhuijsen Piters et al., 2015; Ichinohe et al., 2011; Wang et al., 2013)	Disruption of protective, commensal bacterial species – allows opportunistic colonisation with harmful bacteria/virus
Direct damage to airway epithelium (Iverson et al., 2011; Nicolas de Lamballerie et al., 2019; Rezaee et al., 2013)	Disruption of tight epithelial junctions – exposing basal cell membrane to pathogens
	Hyperplasia – increased mucous production and decreased mucociliary clearance
Altered immune response (Nakamura et al., 2011; Sun and Metzger, 2014)	Increased expression of host cell receptors – aids bacterial adherence
	Disruption of immune cells – inhibited activation of immune cells and thus clearance of pathogens
Disruption of bacterial biofilms (Hendricks et al., 2016; Laufer et al., 2011; Marks et al., 2013; Pettigrew et al., 2014; Reddinger et al., 2016)	Release of planktonic bacteria – outgrowth within airway or promotion of biofilm formation

Table 1.1 Mechanisms in which viral infection can result in concurrent or secondary bacterial infection within the respiratory tract.

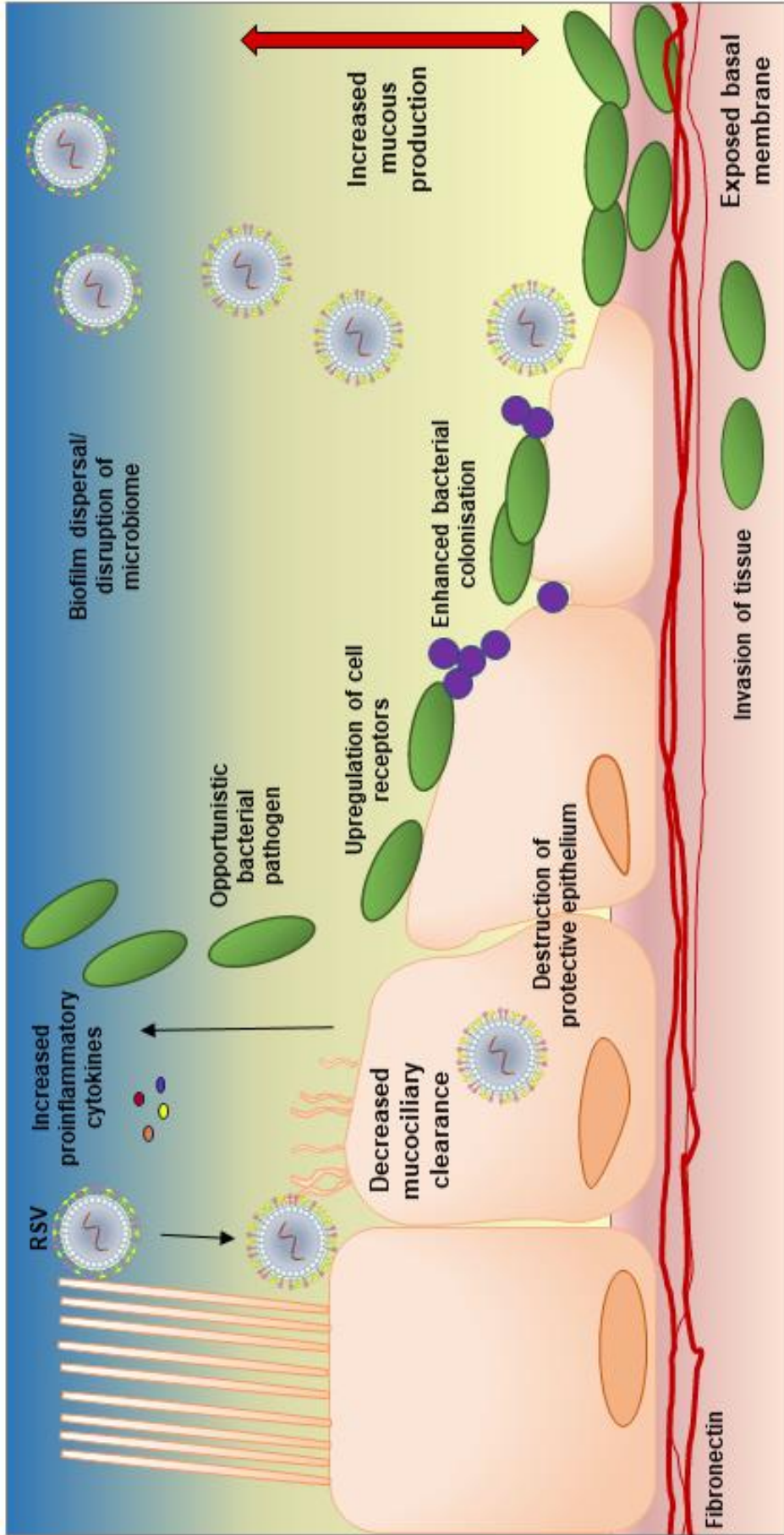


Figure 1.3 Schematic diagram illustrating how RSV can increase susceptibility to bacterial co-infection. RSV infection can progress into the lower airways and cause more severe disease. Excessive inflammation as well as direct tissue damage are linked to decreased mucociliary clearance, hyperplasia of ciliated cells to goblet cells resulting in excessive mucous production leading to the narrowing of airways, occurrence of respiratory wheeze and mucus plugs. Destruction of the protective airway epithelium can also lead to exposed cell receptors that aids the attachment of opportunistic bacteria to airway epithelium of ev adapted from into the tissue. Figure adapted from Bosch et al., (2013).

1.3.4.1 Destruction of the epithelial cell barrier

RSV replication can directly impact cell viability and in addition, viral infected cells can be targeted and lysed by host immune cells attempting to reduce viral spread (Gao et al., 2014). Viral infection can therefore lead to a diminished protective barrier, exposing a niche that may be permissible for opportunistic bacterial pathogens to attach or even disseminate into the submucosa (de Steenhuijsen Piters et al., 2015; Vareille et al., 2011). Phenotypic changes that occur within the infected airway epithelium can lead to decreased ciliated cells and the upregulation of goblet cells (termed hyperplasia) that contributes to excess mucus production, aiding the transition of commensal bacteria from the URT to the LRT (Griffiths et al., 2017; Smith et al., 2014a; Stark et al., 2006; Vareille et al., 2011). With this first line of defence compromised, the respiratory microbiome, that normally maintains homeostasis by preventing colonisation with harmful pathogens, is disrupted, which can allow opportunistic bacterial infections to occur (de Steenhuijsen Piters et al., 2015). The main commensal bacteria that can act as opportunistic pathogens within the URT are: *Staphylococcus aureus*, *Streptococcus pneumoniae* (*Spn*), *Haemophilus influenzae* and *Moraxella catarrhalis*, which in health can exist in equilibrium without causing harm to the host, though are all capable of causing respiratory infection and pneumonia (Bosch et al., 2013). Children in particular are colonised by large numbers of these bacterial species, which may make them more susceptible to bacterial co-infection when their microbiomes are disrupted after infection with RSV (de Steenhuijsen Piters et al., 2015). In addition, direct infection of airway epithelial cells with RSV has been shown to upregulate the expression of viral G protein at the membranes of infected cells, in which *Spn* has been demonstrated to use as a receptor to adhere (Avadhanula et al., 2006; Hament et al., 2004).

1.3.4.2 Modulation of immune signalling

Investigating the interactions between RSV and the host immune response in terms of immune modulation and disease severity may offer insight into why some people respond more

potently to RSV infection than others. Furthermore, this may provide evidence regarding increased susceptibility of certain individuals to subsequent bacterial co-infection.

RSV infection initiates host cell immune signalling with increased production of chemokines such as CXCL8 (also known as IL-8) and IL-6, which have many functions, including facilitating the recruitment of neutrophils to sites of infection (Culley et al., 2002; Lambert et al., 2014; Openshaw et al., 2017). IL-6 also results in upregulation of intercellular adhesion molecule 1 (ICAM-1), which acts to assist the influx and attachment of immune cells, like eosinophils and neutrophils, into sites of infection (Avadhanula et al., 2006). Further to this, Avadhanula et al. (2006) also demonstrated that immortalised (BEAS-2B) and normal human bronchial epithelial (NHBE) cells infected with RSV or influenza had increased intercellular adhesion molecule 1 (ICAM-1) expression at both 48 and 72 h post infection, and this correlated with increased bacterial adhesion with non-typeable *Haemophilus influenzae* (*NTHi*) and *Spn*.

Defensins are antimicrobial peptides produced by epithelial cells, phagocytes and lymphocytes, which often serve as signals to induce an adaptive immune response upon bacterial infection, and have anti-viral roles by binding the lipid envelope and surface glycoproteins to neutralise viral binding (Oppenheim et al., 2003; Wilson et al., 2013). However, there is compelling evidence that RSV actively downregulates host defensins. McGillivray et al. (2009) demonstrated this using an *in vivo* chinchilla model, where 7 days post RSV infection the levels of chinchilla β -defensin 1 (c-BD1) were reduced by 50%, which correlated with increased levels of *NTHi* in the lung.

Extreme pathogenesis in infants with RSV have also been linked to a Th₂ dominant response, leading to severe pathology and prolonged infection due to inefficient clearance of the virus (Culley et al., 2002; Openshaw et al., 2017). A Th₂ dominant response has also been linked to the suppression of IL-12 and which leads to subsequent impaired immunity to bacterial pathogens and possible outgrowth of *Spn* (Bakaletz, 2017; Barthelemy et al., 2017). This indicates how a skewed immune response not only heightens viral infection, but also

predisposes to further bacterial complications where bacterial pathogens are not efficiently cleared from the airways. The decreased efficiency of the immune response, coupled with factors that promote bacterial growth, indicate how bacterial infections may develop from acute to chronic pathogenesis. In some cases, viral infection has also been shown to contribute to the development of bacterial biofilms within the lungs, therefore decreasing the efficacy of some antibiotics (Beadling and Slifka, 2004; Hendricks et al., 2016).

1.3.4.3 The use of antibiotics for viral-bacterial co-infections

Primary care consultants or GPs are responsible for up to 90% of all antibiotics that are prescribed to patients, the majority of which are to treat respiratory infections/illness (Llor and Bjerrum, 2014). In fact, URIs account for up to 57% of antibiotic use and LRTIs account for up to 30% (Llor and Bjerrum, 2014). The main antibiotics that are used are beta-lactams (i.e. penicillin, with or without beta lactamase inhibitors), some tetracyclines (e.g. doxycycline), some quinolones (e.g. levofloxacin) and macrolides (Suárez-Arrabal et al., 2015). These are often provided without excluding a possible viral infection first (Hay and Tilling, 2014; Quintos-Alagheband et al., 2017). Otitis media (OM) is one of the most common reasons for antibiotics being administered to children (Marom et al., 2012). The ability of respiratory viral infections to predispose the airways to subsequent bacterial infection highlights the role that viruses indirectly play in leading to antibiotic use in healthcare settings.

Evidence indicates that the administration of antibiotics to infants immediately upon their arrival at hospital may decrease bacterial loads by up to 50% in comparison to those who do not receive immediate treatment (Llor and Bjerrum, 2014). However, the same study also revealed that individuals who received antibiotics required longer treatment in paediatric intensive care unit (PICU), where gastrointestinal or neurological complications can occur (Llor and Bjerrum, 2014). It has also been shown that antibiotics used for respiratory infections may also lead to prolonged harbouring of resistant bacteria for up to 12 months or even colonisation of other sites such as the gut with more harmful bacteria such as *Clostridium difficile* (Budnitz

et al., 2006; Llor and Bjerrum, 2014). This may also result in more second line antibiotics being required to treat late infections during this period (Budnitz et al., 2006).

There are huge discrepancies that exist in terms of antibiotic treatment for viral-bacterial co-infections, as often healthcare workers would rather issue antibiotics as a precautionary measure, especially where rapid and accurate diagnostics are unavailable (Llor and Bjerrum, 2014).

1.3.4.4 The need for new anti-virals for RSV

Viral infection alone can cause severe cytopathic effects and inflammation in the lung but can also concurrently increase susceptibility to bacterial infections, driving severe pathogenesis. The diverse interactions that drive these responses suggest that a multidisciplinary approach is required to tackle the occurrence of bacterial superinfections and the reliance on antimicrobials as a first line treatment. The development of novel anti-virals may have multiple benefits to health by reducing hyperinflammation, severe disease and the potential of bacterial co-infection. The use of anti-viral agents may also reduce the reliance on antibiotics to treat the subsequent bacterial infections associated with primary viral infection.

1.4 Membrane microdomains

The original concept of biological membranes in living cells was the 'fluid mosaic model' where it was proposed that phospholipids existed in a homogenous distribution across both the cytoplasmic (inner) and exoplasmic (external) membrane leaflets with proteins randomly integrated throughout the membrane (Singer and Nicolson, 1972). By 1974 however, research was already beginning to interrogate this simplified model and it was further proposed that distinct areas may exist in the lipid bilayer consisting of heterogenous lipid species (Lee et al., 1974). Some years later it was demonstrated that these heterogenous areas of the membrane may consist of distinct lipid-protein species that enabled specific signalling or transport events within the cell (Simons and Ikonen, 1997). Simons proposed the

term “lipid raft” to capture the character of these transient, highly ordered domains in the fluid membrane. Of note, lipid rafts are also commonly referred to as membrane microdomains (MM)s which is the nomenclature adopted throughout this thesis.

MMs are currently characterised as distinct regions of cell membranes that are composed of sphingolipids, phospholipids, and are rich in cholesterol (responsible for the fluidity of the membrane), with key roles in lipid/protein trafficking and cell signalling (**Figure 1.4 A**) (Simons and Ikonen, 1997; Simons and Toomre, 2000). MMs are transient platforms that help congregate different classes of phospholipids into small (25 nm) or larger (up to 700 nm) domains whereby the specific geometric and chemical properties of the lipids can dictate functional properties of the membrane microdomain (Chazal and Gerlier, 2003). Furthermore, the heterogenous nature of membranes allows for the simultaneous existence of distinct phases within the same membrane. For example, saturated lipids have a natural affinity for sphingolipids and sterols which allows these components to pack tightly together in an orderly fashion within the membrane, giving rise to what is termed a liquid ordered (L_o) phase and that allows lipids to laterally diffuse through the membrane and is thought to be the model for MMs (Kaiser et al., 2009). In contrast, unsaturated lipids repel cholesterol present in the membrane and do not pack as tightly with sphingolipids and sterols, which may alter the properties of the membrane and allow for what is termed liquid disordered (L_d) regions to form that are separate from the L_o phase (Brown and London, 1998; Kaiser et al., 2009).

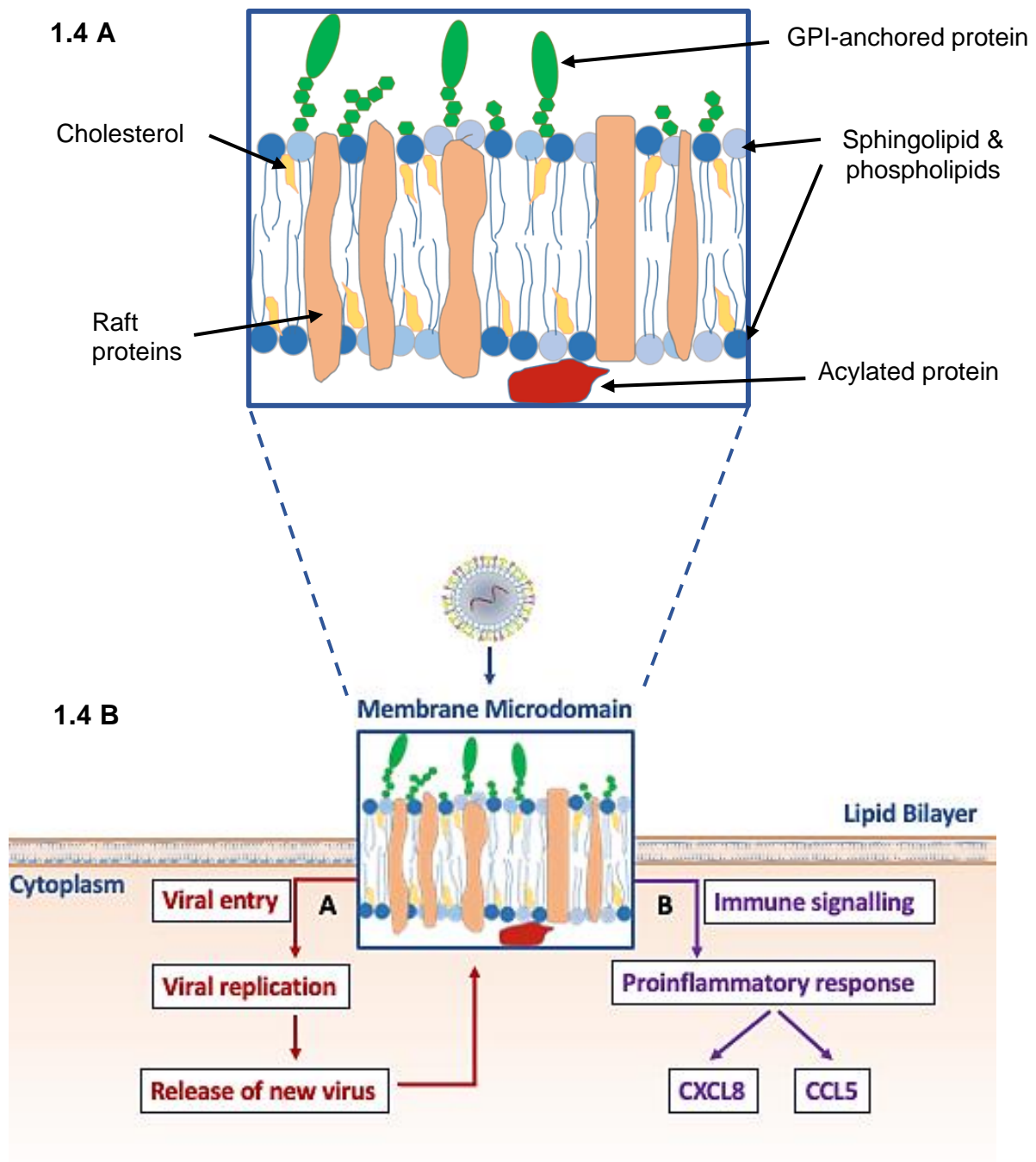


Figure 1.4 A Membrane microdomain. The bilayer is composed of phospholipids and sphingolipids. Embedded within the membrane are transmembrane raft proteins that congregate within the bilayer to produce large, stable rafts or smaller rafts that disassemble quickly. MM are rich in cholesterol and therefore create highly stable, liquid-ordered structures. Glycosylphosphatidylinositol (GPI)-anchored proteins are key molecules for carrying out biological functions where Acylated proteins are crucial for signal transduction and are located on the inner plasmic layer. (Image adapted from (Simons and Gerl, 2010).

Figure 1.4 B The Role of MM During RSV Infection. MM are rich in phospholipids, sphingolipids and cholesterol, a composition that gives rise to a highly stable but liquid ordered structure within the lipid bilayer. MM are utilised for various stages of the viral life cycle such as the attachment and egress of new RSV particles (A). RSV infection simultaneously triggers TLR-dependent signalling within MM which can result in an overexuberant immune response often characterised by increased levels of CXCL8 and CCL5 (B).

1.4.1 Membrane microdomain controversy

Despite much research over the years, there is still some controversy surrounding the nature of MMs. Due to their small size and transient properties, visualisation of MMs has proven difficult and previous efforts to try and identify MMs have applied crude techniques to artificially modulate or generate MMs.

Previous research that has attempted to separate MMs from the cell membrane have utilised the knowledge that areas of the membrane will exist in either L_o or L_d with different characteristics. As the L_o phase that makes up MM is rich in cholesterol and sphingolipids, it is therefore insoluble to non-ionic detergents when incubated at low temperatures, which allows for the separation of MM from the rest of the membrane in the L_d phase (Brown and Rose, 1992). This technique gave rise to what was termed detergent resistant membranes (DRM)s and was a popular technique to try and identify lipids and proteins enriched in these segregated areas of the membrane. DRMs isolated from biologically relevant cells however, lack the characteristic asymmetry of relevant membranes and are therefore seen as artificial models of MM (Lichtenberg et al., 2005; London and Brown, 2000).

To overcome this, a pioneering study from Baumgart et al. (2007) developed an alternative technique to interrogate the functions and properties of MMs by isolating giant plasma membrane vesicles (GPMVs) from living cells, whereby both the lipid and protein content of the living cell it was derived from were retained. By applying confocal microscopy techniques, it was demonstrated that L_o and L_d regions could coexist within the same membrane and illustrated the natural formation of L_o regions (Baumgart et al., 2007). The formation of L_o phase in the membrane helped support the model that MM can form transient platforms within cell membranes without superficial stimulus.

In addition, the development of optical technologies such as fluorescence resonance energy transfer (FRET), electron microscopy and single molecule tracking have helped elucidate

membrane biology (Eggeling et al., 2009; Parker et al., 2008; Sengupta et al., 2007). In addition, the co-localisation of specific proteins into MM has been visualised in fixed cell imaging, where correlation of activity have been linked to the composition of proteins and lipids in the MM (Chang et al., 2012; McCurdy and Graham, 2003; Zhou et al., 2015). With these advances in microscopy have come increased discoveries about the role of MMs during microbial infection and human disease.

1.4.2 The role of membrane microdomains in viral infection

Due to the crucial roles that MM have in coordinating host cell signalling and protein-lipid interactions, it is not surprising that over the years, MMs have been shown to play numerous roles in human disease such as cancer, cardiovascular disease and neurological disorders (Gajate and Mollinedo, 2006; Hicks et al., 2012; Hussain et al., 2019; Maguy et al., 2006; Vona et al., 2021). What's more, many human infectious pathogens including, fungi, bacteria, and viral species have been demonstrated to interact with MM during different stages of infections, opening up the option for potential modulation for therapeutic benefit (Knodler et al., 2003; Lafont and Van Der Goot, 2005; Rosenberger et al., 2000; Turris et al., 2015; Vieira et al., 2010; Zaas et al., 2005). **Table 1.2** highlights some important research that has been conducted for various viruses and the suggested roles of MM during host-pathogen interaction.

MM have been reported to have crucial roles in cell signalling events by enabling the association or disassociation of cell receptors into specified areas of the membrane to mediate signalling transduction events (Hueber, 2003; Katagiri et al., 2001; Kowalski and Pier, 2004; Simons and Toomre, 2000). In terms of immune signalling in response to virus, much research has reported that TLR signalling occurs in MM (Fessler and Parks, 2011; Ruyschaert and Loney, 2015; San-Juan-Vergara et al., 2012; Simons and Gerl, 2010). Surface TLRs (including TLR2 and TLR4) have been identified as some of the main receptors that can detect RSV during infection and therefore play crucial roles in host cell inflammatory signalling (Broadbent et al., 2018; Kurt-Jones et al., 2000). The accumulation and association of host cell PRRs with

their associated co-receptors within MM enables cell signalling in response to PAMPs (Carter et al., 2009; Parker et al., 2008; Stokes et al., 2016). In addition, MM have been reported to play crucial roles in viral infection where enveloped viruses such as RSV preferentially attach and bud from MM of the host cell (**Figure 1.4 B**) (Carter et al., 2009; Chang et al., 2012; San-Juan-Vergara et al., 2012). It is hypothesised that this may be due to the abundance of cholesterol found in MM in which enveloped virus can incorporate into their own membranes to allow for rapid attachment and fusion of virus to the host cell during infection and also egress out of the cell during viral budding (Carter et al., 2009; Chang et al., 2012; Charlton et al., 2019; Simons and Gerl, 2010).

Due to the important roles that MM perform during viral-induced cell signalling and infection, they have been identified as potential targets for therapeutic modification. Previous studies have commonly used pharmaceutical agents such as cholesterol chelator methyl- β -cyclodextrin (M β CD) to modulate MM and their associated functions during infection with RSV or other clinically relevant enveloped viruses (Bajimaya et al., 2017; Chang et al., 2012; Charlton et al., 2019; San-Juan-Vergara et al., 2012; Sun and Whittaker, 2003; Yeo et al., 2009). The results indicated that depletion of cholesterol reduced the efficiency of virus such as RSV, influenza, human immunodeficiency virus (HIV), and bunyavirus to either fuse with the host cell membrane or egress from a range of cell types including; human airway epithelial A549, NHBE, human epithelial type 2 (HEp-2) and Madin-Darby bovine kidney (MDBK) cells (Bajimaya et al., 2017; Chang et al., 2012; Charlton et al., 2019; San-Juan-Vergara et al., 2012; Sun and Whittaker, 2003; Yeo et al., 2009). When cholesterol was experimentally recovered in cell culture, the infectivity of virions was recovered (Bajimaya et al., 2017). Although these methods reduced viral infection and spread in cell culture, the use of these pharmaceutical substances were limited due to their toxic effect on whole cell viability (Zidovetzki and Levitan, 2007).

Virus	Interaction with MM	Reference
Coxsackievirus A9, A21 and B4	Entry	(Shafren, 1998; Triantafilou and Triantafilou, 2004, 2003)
Dengue virus	Replication	(Lee et al., 2008)
Ebola	Fusion	(Empig and Goldsmith, 2002)
Hepatitis C virus	Replication	(Aizaki et al., 2004)
Herpes simplex virus	Fusion	(Bender et al., 2003)
HIV-1	Fusion, assembly/egress	(Brügger et al., 2007, 2006; Ding et al., 2003; Kozak et al., 2002; Popik et al., 2002; Waheed and Freed, 2009)
Influenza A	Binding and endocytosis	(Verma et al., 2018)
Marburg	Fusion	(Empig and Goldsmith, 2002)
Measles	Assembly/egress	(Manié et al., 2000; Vincent et al., 2000)
Rhinovirus	Entry	(Grassmé et al., 2005)
Rotavirus	Entry, assembly/egress	(Iša et al., 2004)
RSV	Attachment/entry/assembly/egress	(Brown et al., 2004; Chang et al., 2012; Jumat et al., 2015; Ludwig et al., 2017; McCurdy and Graham, 2003; Triantafilou et al., 2013; Yeo et al., 2009)
SARS-CoV-1	Entry	(Wang et al., 2008)
SARS-CoV-2	Entry	(Li et al., 2021)
SARS-CoV-2 (Reviews)	(Proposed roles in entry, replication)	(Palacios-Rápalo et al., 2021; Theken et al., 2021)
West Nile virus	Entry	(Medigeshi et al., 2008)

Table 1.2 Summary of viral pathogens and their interactions with MM.

1.4.3 Modulating membrane microdomains using SAPS – project hypothesis

Published work from my lab group investigated whether a specific liposome species called SAPS (1-stearoyl-2-arachidonoyl-sn-glycero-3-phospho-L-serine) could be used to modulate TLR signalling events that take place within MMs. SAPS is composed of a naturally occurring lipid species, phosphatidylserine (PS) which has been studied when reconstituted and applied as a unilamellar liposome. PS is ordinarily retained within the cytoplasmic leaflet of mammalian cells with key roles in orchestrating cell signalling during apoptotic events, where PS is flipped to the outer membrane and is involved in the controlled clearance of apoptotic cells (Henson and Bratton, 2013). It has been reported that the exposure of PS on the cell membrane can instigate an anti-inflammatory response (Henson and Bratton, 2013; Ma et al., 2011). Because of these anti-inflammatory properties, Parker et al. (2008) hypothesised that PS may orchestrate anti-inflammatory effects on epithelial and endothelial cells challenged with a range of TLR ligands. In these studies, it was demonstrated that the PS-containing liposome, SAPS, was able to diminish TLR-dependent inflammatory responses in cells stimulated with a range of stimuli such as lipopolysaccharide (LPS). Through the use of FRET technology, it was reported that SAPS could disrupt TLRs within MM by inhibiting the association of TLR4 with its coreceptor CD14 (a MM-associated glycosylphosphatidylinositol-anchored protein), a normal requirement for potent inflammatory signalling (Parker et al., 2008). Based on these initial findings and in conjunction with evidence for MM involvement in viral life cycles, research was then conducted to investigate the potential of SAPS to disrupt inflammatory signalling events in airway epithelial cells infected with human rhinovirus (RV) (Stokes et al., 2016). The results showed that both immortalised and primary airway epithelial cells infected with RV, in the presence of SAPS, had significantly reduced TLR signalling and inflammatory cytokine production compared to untreated cells (Stokes et al., 2016). However, SAPS only had modest effects on viral replication, suggesting that MM disruption did not perturb the life cycle of RV (Stokes et al., 2016). It was therefore postulated that SAPS may have broader effects against

an enveloped virus, such as RSV, which may utilise MMs to a greater extent for viral binding and egress.

The hypothesis for this project was that SAPS may be used to disrupt MM and therefore modulate the immune response to RSV and the attachment, replication, and egress of RSV in airway epithelial cells. It was also hypothesised that by using SAPS to reduce RSV infection, consecutive bacterial infections that are commonly associated with RSV would be reduced.

The main aims of this research were to:

- Investigate the ability of SAPS to disrupt multiple stages of the RSV life cycle and subsequent proinflammatory cytokine production in a range of airway epithelial cell types,
- Explore the mechanism of SAPS using fluorescent microscopy,
- Investigate how RSV-infected airway epithelial cells can promote subsequent co-infection with *Streptococcus pneumoniae*,
- Explore whether SAPS can modify bacterial co-infection of RSV-infected airway epithelial cells.

Chapter 2: Materials and Methods

2.1 Materials

2.1.1 Cell culture media reagents

Table 2.1 Cell culture media and reagents (alphabetical)

Name	Composition (Supplier)	Application
BEAS-2B complete media	RPMI-1640 medium containing 2 mM L-glutamine (Gibco, UK), supplemented with 10% heat treated foetal bovine serum (FBS) (Gibco), 1% penicillin, 1% streptomycin (10,000 U/ml) (Sigma-Aldrich, UK)	BEAS-2B maintenance
BEAS-2B infection/ basal media	RPMI-1640 medium supplemented with 2% heat treated FBS, 1% penicillin, 1% streptomycin	Equilibrating BEAS-2B cell growth pre-infection
BEAS-2B/ HEp-2 subculture reagents	10X Trypsin/EDTA (Sigma-Aldrich) diluted to 1X in sterile PBS	BEAS-2B/ HEp-2 maintenance
Cryo-SFM	Full composition not disclosed: consists of methylcellulose, DMSO and other cryoprotectants (Promocell, Germany)	Freezing down NHBE cells
HBEC3-KT complete media	Keratinocyte-SFM (1X) (Gibco, UK) containing 2 mM L-glutamine supplemented with 0.05 mg/mL BPE, 0.005 µg/mL epidermal growth factor (EGF) (Gibco), 1% penicillin, 1% streptomycin	HBEC3-KT cell maintenance
HBEC3-KT infection and recovery media	Keratinocyte-SFM (1X) containing 2 mM L-glutamine supplemented with 1% penicillin, 1% streptomycin	Equilibrating HBEC3-KT cell growth for viral infection
HBEC3-KT infection and recovery media	Keratinocyte-SFM (1X) (Gibco, UK) containing 2 mM L-glutamine	Equilibrating HBEC3-KT cell growth for bacterial infection
HBEC3-KT subculture reagents	Trypsin/EDTA, trypsin neutralising solution (Promocell, Germany) and Hanks' balanced salt solution (HBSS) (Gibco, UK)	HBEC3-KT cell maintenance
HEp-2 complete media	DMEM (Gibco, UK) supplemented with 10% heat treated FBS, 1% non-essential amino acids (Gibco), 2% L-	HEp-2 cell maintenance

	glutamine and 1% penicillin, 1% streptomycin	
HEp-2 infection media	DMEM without supplement or antibiotic	HEp-2 infection with virus
HEp-2 viral propagation /recovery media	DMEM supplemented with 10% FBS	Used to growing viral stocks of RSV and to recover cells after infection with virus
NHBE complete media	Bronchial epithelial cell growth basal medium (Lonza, Switzerland) supplemented with 0.4% Bovine Pituitary Extract, 0.1% Insulin, 0.50 ml hydrocortisone, 0.1% Gentamicin sulfate-Amphotericin – 1000, 0.1% Retinoic Acid, 0.1% Transferrin, 0.1% Triiodothyronine, 0.1% Epinephrine and 0.1% human epidermal growth factor (Lonza)	NHBE cell maintenance
NHBE infection media	Bronchial epithelial cell growth basal medium supplemented with 0.1% Gentamicin sulfate-Amphotericin– 1000	Equilibrating NHBE cell growth pre-infection
NHBE recovery media	Same as complete media except no BPE	To recover cell growth after infection with virus
NHBE subculture reagents	Trypsin/EDTA, trypsin neutralising solution and HEPES- buffered saline solution (Lonza, Switzerland)	NHBE cell maintenance
<i>Spn</i> culture broth	Brain Heart Infusion Broth (Sigma-Aldrich, UK)	Growth of <i>Spn</i>

2.1.2 Buffers and substrates

Table 2.2 Buffers and substrates for ELISA, plaque assay, confocal and MTT cell viability

Reagent	Composition	Application
Coating buffer	0.14 M NaCl, 2.7 mM KCl, 1.5 mM KH ₂ PO ₄ , 8.1 mM Na ₂ HPO ₄	ELISA
Wash buffer	0.5 M NaCl, 2.5 mM NaH ₂ PO ₄ , 7.5 mM Na ₂ HPO ₄ , 0.1% TWEEN-20 pH to 7.2 with NaOH	ELISA
Methanol /2% H ₂ O ₂	4 ml of CH ₃ OH and 80 µl H ₂ O ₂	Plaque assay
PBS/1% BSA/ 0.1 % sodium azide	12 ml of phosphate-buffered saline solution, 0.12 g of bovine serum albumin and 0.012 g NaN ₃	Plaque assay

PBS/1% BSA	20 ml of phosphate-buffered saline solution and 0.2 g of bovine serum albumin	Plaque assay
MTT 5 mg	0.125 g MTT into 25 ml sterile phosphate-buffered saline solution	MTT assay
10 % SDS (0.01 M HCL)	1 g Sodium dodecyl sulfate and 8 µl HCL	MTT assay
Collagen	0.05 mg/ml collagen 1 mixed with 0.02 M acetic acid	Coating coverslips
Blocking buffer (25ml)	2.5ml 10X PBS, 1.25 ml normal goat serum, 21.25 ml dH ₂ O and 0.5 ml 5% Saponin	Immunofluorescence
Antibody dilution buffer (40ml)	4 ml 10X PBS, 36 ml dH ₂ O, 0.4 g BSA and 0.8 ml 5% saponin	Immunofluorescence
Diamond antifade mountant with DAPI (Invitrogen # P36962)	Antifade and mounting solution	Immunofluorescence

2.1.3 Detection reagents

Table 2.3 Detection reagents for ELISA, plaque assay, cell viability

Reagent (supplier & product code)	Concentration	Application
Streptavidin – HRP (R&D Systems # DY998)	1:200	Antibody detection in ELISA
Streptavidin – HRP (R&D Systems # DY998)	1:100	Antibody detection in plaque assay
Substrate solution(R&D Systems # DY999)	Equal parts of solution A and solution B	Initiates colour reaction for ELISA
3,3' – Diaminobenzidine (DAB) substrate (Sigma Aldrich # D4293)	1 of each tablet into 5 ml of dH ₂ O	Detects and stains viral infected cells
Cell Titer-Glo (Promega # G7570)	Equal parts of substrate and buffer	Cell viability

2.1.4 Detection antibodies

Table 2.4 Antibodies and dyes for imaging (prepared according to manufacturer's instruction)

Antibody (supplier & product code)	Isotype (immunogen)	Working concentration	Application
Anti-RSV antibody (BIO-RAD # 7950-0104)	Polyclonal goat IgG (Human RSV isolate)	40 µg/ml	Plaque assay
Anti-RSV fusion antibody (Abcam # 24011)	Monoclonal mouse IgG2b (Bovine RSV strains, 127, SNK and 9007. Human RSV strains; Long, Randall, 8/60, and A/2)	3.3 µg/ml	Immunofluorescence
Isotype control (Abcam # 18469)	Monoclonal mouse IgG2b kappa (Trinitrophenol and KLH)	3.3 µg/ml	Immunofluorescence
Alexa fluor® 488 anti-mouse (Invitrogen # A11001)	Polyclonal IgG goat (Gamma Immunoglobins Heavy and Light chains)	2 µg/ml	Immunofluorescence
Texas Red™- X Phalloidin (Invitrogen # T7471)	N/A	1:50	Immunofluorescence
pHrodo™ Red Succinimidyl ester	N/A	2.55 mM	Immunofluorescence
CXCL8, anti-human antibody (R&D # MAB208)	Capture: Mouse IgG (E. coli-derived recombinant human IL-8/CXCL8)	0.3 µg/ml	ELISA
CXCL8, anti-human antibody (R&D # BAF208)	Detection: Biotinylated goat IgG (E. coli-derived recombinant human IL-8/CXCL8)	0.32 µg/ml	ELISA
CCL5, anti-human antibody (R&D # MAB678)	Capture: Mouse IgG (E. coli-derived recombinant human CCL5/RANTES)	2 µg/ml	ELISA

CCL5, anti-human antibody (R&D # BAF273)	Detection: Biotinylated goat IgG (E. coli-derived recombinant human CCL5/RANTES)	0.08 µg/ml	ELISA
--	--	------------	-------

2.1.5 Commercial kits

Table 2.5 Commercial kits used for RNA extraction, cDNA synthesis and RT-qPCR

Name (supplier & product code)	Components	Application
DNA – free (Ambion # AM1906M)	10x DNase I buffer rDNase I DNase inactivation reagent	RNA extraction (BEAS-2B protocol) – removal of genomic DNA
Monarch® Total RNA Miniprep Kit (New England Biolabs #T2010S)	RNA purification columns RNA wash buffer DNase 1/DNase Buffer RNA priming buffer	RNA extraction of NHBE and HBEC3-KT cells
High – capacity cDNA reverse transcription (Applied Biosystems # 4368814)	10x RT buffer 10x random primers 25x dNTP mix Multiscribe Reverse Transcriptase RNase inhibitor	Synthesis of RNA to cDNA
GoTaq Probe q-PCR master mix (Promega #A6101)	GoTaq Probe q-PCR mastermix CXR Reference Dye	RT – qPCR (real time quantitative PCR)
Monarch® Plasmid Miniprep Kit (New England Biolabs #T1010)	DNA Elution buffer Plasmid Wash Buffer (1&2) Plasmid Neutralisation Buffer Plasmid Lysis Buffer Plasmid Resuspension Buffer	Isolation and purification of plasmid DNA

2.1.6 Primer-probes

Table 2.6 Quantitative RT-qPCR primer probes

Target	Sequence (5' -3')	Annealing Temp (°C)	Working Concentration (nM)	Supplier
RSV L-gene (Forward Primer)	GAACTCAGTGTAGGTAGAATGTTTGCA	65.2	900	Sigma Aldrich
RSV L-gene (Reverse Primer)	TTCAGCTATCATTTTCTCTGCCAAT	65.6	300	Sigma Aldrich
RSV L-gene Probe	[6FAM]TTTGAACCTGTCTGAACATTCCCGGTT[TAM]	73.1	100	Sigma Aldrich

2.1.7 Experimental liposomes

Table 2.7 SAPS/ PAPC Liposomes

Name	Stock Concentration	Supplier and Product Code
1-stearoyl-2-arachidonoyl-sn-glycero-3-phospho-L-serine (SAPS)	1.0 mg/ml	Avanti Polar Lipids (Alabaster, AL) # 840064
1-palmitoyl-2-arachidonoyl-sn-glycero-3-phosphocholine (PAPC)	1.0 mg/ml	Avanti Polar Lipids (Alabaster, AL) # 850459

2.2 Methods

2.2.1 BEAS-2B cell culture

The immortalised, normal human bronchial airway epithelial cell line (BEAS-2B) was obtained from American Type Culture Collection (ATCC). Cells were cultured from frozen and maintained in 75 cm² tissue culture flasks (Thermo Fisher) with RPMI-1640 complete media (Table 2.1). Cells were grown in a humidified incubator at a temperature of 37°C and 5% CO₂ until a confluent monolayer (80-90%) was achieved and subsequent passaging completed. Spent media was discarded and cells washed twice using 5 ml of sterile PBS before adding 2 ml of trypsin (Sigma-Aldrich). Flasks were placed back into the incubator (37°C/5% CO₂) for approximately 5 mins until cells had rounded up and began to detach from the bottom of the flask (flasks were gently tapped to aid any remaining cells off). The trypsin was inactivated with 2 ml RPMI-1640 complete media (Table 2.1) before transferring the cell suspension media into a 15 ml centrifuge tube. The flask was washed with an additional 2 ml RPMI-1640 media to obtain any remaining cells and then subsequently added to the centrifuge tube. Cells were then centrifuged at 220 g for 5 mins, 20°C to form a pellet. The pellet was resuspended in 10 ml complete media (Table 2.1) before a cell count was obtained and new flasks seeded at a density of 0.8–2.0 x10⁶ cells/flask (depending on rate of growth). Cells were sub-cultured four times before being used in experiments and discarded after undergoing a total of 10 further passages.

2.2.2 HEp-2 cell culture

The immortalised human epithelial cell line (HEp-2) was obtained from ATCC and stored in liquid nitrogen until required. Cells were cultured from frozen and maintained as described in **Section 2.2.1** but with DMEM complete media (Table 2.1).

2.2.3 HBEC3-KT cell culture

The normal human bronchial epithelial cell line (HBEC3-KT) (ATCC) have been immortalised using cyclin dependent kinase 4 (CDK4) and telomerase reverse transcriptase (hTERT) to extend their lifespan in cell culture. Cells were brought up from storage in liquid nitrogen and rapidly defrosted in a 37°C water bath for up to 90 seconds. Cells were placed into a 75 cm² tissue culture flask (Thermo Fisher) containing 10 ml pre-warmed HBEC3-KT complete media (Table 2.1). Cells were passaged at 70-80% confluence where spent media was removed and the cell monolayer rinsed 3X with 10 ml of Hanks' balanced salt solution (HBSS, Table 2.1). A 3 ml aliquot of Trypsin/EDTA (Promocell, Germany, Table 2.1) was added into the flask to cover the monolayer and placed into an incubator at 37°C, 5% CO₂. Cells were checked after 5-6 mins to determine cell rounding and cell detachment. Flasks were then gently tapped to aid the remaining cells off the bottom of the flask and 3 ml trypsin neutralisation solution (TNS) (Table 2.1) was added into the flask to deactivate the trypsin. The cell suspension was moved into a 50 ml centrifuge tube and 4 ml of HBSS added into the flask to rinse and collect any remaining cells. Cells were centrifuged at 220 g for 5 mins, 20°C to form a pellet. The cell pellet was resuspended in 10 ml HBEC3-KT complete media and a haemocytometer used to determine cell count. Cells were seeded between 0.3 x10⁶ and 1.2 x10⁶ based on proliferation rate. Cells were used up until passage 29 and each passage was categorised as a separate N.

2.2.4 NHBE cell culture

2.2.4.1 Arrival of new donor cells in lab

Normal human bronchial epithelial (NHBE) cells were obtained from healthy donors and purchased from Lonza (**Figure 2.1**). New donor cells that arrived into the lab were labelled passage (P) number 2, defrosted rapidly (within 90 seconds) in 37°C water then split into 75 cm² tissue culture flasks (Thermo Fisher) containing 15 ml pre-warmed NHBE complete media (Table 2.1). Cells were seeded at a density of 3500 cells/cm² as recommended by the

manufacturer. Cells were grown until 80-90% confluent and then subcultured into new 75 cm² tissue culture flasks (Thermo Fisher) at a seeding density of 0.75 x10⁶ cells/ml. Cells were frozen down at passage 4 in Cryo-SFM (Promocell) (Table 2.1) and at a density of 0.5 x10⁶ cells/ml. Vials were stored in liquid nitrogen until required.

Donor Number	Lot Number	Sex	Age (Years)	Race	Smoker	Alcohol	Cell Viability (%)	Cell Count (cells/ml)	Doubling Time (h)	Seeding Efficiency (%)
29521	0000527924	M	47	C	N	Y	90	1,310,000	28	23
36585	18TL269120	M	36	C	N	N	92	773,300	22	100
30996*	0000596064	F	52	H	N	N	72	754,500	26	38

Figure 2.1 NHBE donor cells characteristics. Characteristics of the different NHBE donor cells purchased from Lonza. Donors that were identified as non-smokers were preferentially selected. Donors marked with an * indicate that this donor was not used in subsequent experiments as cells failed to grow. C=Caucasian, H=Hispanic.

2.2.4.2 Subculture of NHBE cells from liquid nitrogen

Per 1 vial of cells, two 25 cm² flasks were prepared with 5 ml complete media (Table 2.1), preheated to 37°C. Each vial of cells was rapidly defrosted in a 37°C water bath then 500 µl of cells added to each flask. 1 ml of media from one flask was dispensed back into the vial to capture any remaining cells. Sealed flasks were moved gently backwards and forwards on a benchtop then left to sit at room temperature for 5 mins to allow an equal distribution of cells across the base of the flask to adhere. Cells were placed in an incubator at 37°C, 5% CO₂ and media replaced every other day until cells were 80–90% confluent. Cells were then cultured into larger 75 cm² tissue culture flasks as per Lonza protocol (Section 2.2.4.3).

2.2.4.3 Passaging of NHBE cells

In brief, spent media was removed and replaced with 10 ml of HEPES-BSS (Table 2.1). The flask was tilted to wash the monolayer of cells, then the HEPES-BSS was removed. A volume of 5 ml Trypsin (Lonza, Switzerland) was gently dispensed over the cells and the flask placed into an incubator at 37°C, 5% CO₂. Cells were checked after 5 mins (maximum 7 mins) for indications of cell rounding and cell detachment. Flasks were then gently tapped to aid the remaining cells off the bottom of the flask before 10 ml of TNS (Table 2.1) was added into the flask to deactivate the trypsin. The cell suspension was moved into a 50 ml centrifuge tube and 5 ml of HEPES-BSS added back into the flask to rinse and collect any remaining cells. Cells were centrifuged at 220 g for 5 mins, 20°C to form a pellet. Supernatant was discarded and the cell pellet gently mixed in 5 ml complete media. A cell count was completed using a 10 µl sample volume from the centrifuge tube and new flasks seeded at 0.75 x10⁶. Plates were seeded between 0.6 x10⁶– 0.9 x10⁶ depending on when cells were required. Each vial of cells was used from passage 4 up until (and including) passage 7 where after cells were discarded.

2.2.5 Mycoplasma testing

Routine checks for mycoplasma were carried out by a departmental technician once every quarter, using EZ-PCR mycoplasma kit (Geneflow), in accordance with the manufacturer's instructions.

2.2.6 Respiratory syncytial virus

2.2.6.1 Growing viral stocks

New stocks of RSV strain A2 were grown using a previous batch (passage 5) of RSV strain A2, originally purchased from ATCC. Three 175 cm² flasks were seeded with HEp-2 cells (Section 2.2.2) at a density of 3 x10⁶ cells/ml in DMEM (Gibco, UK) viral propagation media (Table 2.1). Flasks were incubated overnight at 37°C/5% CO₂ or until cells had reached 50% confluence. Spent media was removed and flasks washed once with 15 ml DMEM (Gibco, UK) infection media (Table 2.1). Two 175 cm² flasks were infected with RSV at 0.1 plaque forming units (PFU)/cell (diluted in 7.5 ml DMEM infection media [Table 2.1] per flask). The third 175 cm² flask received 7.5 ml DMEM infection media only to act as the control antigen flask. All three flasks were then incubated for 2 h at 37°C/5% CO₂, with periodic rotations every 15 mins to allow viral binding to the cells. An additional 22.5 ml of viral propagation (Table 2.1) media was added to each flask before being incubated for 24 h at 37°C/ 5% CO₂. The following day, cells were checked under the microscope to assess any cytopathic effects and 25 ml of spent media removed from each individual flask and placed into separate 50 ml centrifuge tubes. Each centrifuge tube was then centrifuged at 1000 g, 4°C for 5 mins to produce a small pellet of cells. Each pellet was resuspended in 25 ml DMEM infection media (Table 2.1) before being added back into its respective flask. Flasks were then placed back into the incubator overnight at 37°C/5% CO₂. The next day, a sonicator (Fisherbrand FB11002) was filled with ice and cooled to 4°C. Cells were visualised under an inverted light microscope to determine levels of cytopathic effect (50% is optimal). A cell scraper (Sarstedt) was used to perturb the flask monolayer and detach the HEp-2 cells until suspended within spent media. The

media/cell suspension from each flask was transferred into a separate 50 ml centrifuge tube. Each centrifuge tube was then placed into the precooled sonicator for 20 seconds at 100% power (ensuring the bottom of the tube was touching the base of the sonicator) to lyse the HEp-2 cells and release virions. Each centrifuge tube was then centrifuged for 5 mins at 1000 g 4°C to separate the supernatant (containing virus or media in control flask) from the pellet (cell debris). The supernatant was transferred to a new 50 ml centrifuge tube and then aliquoted into 1 ml cryovials. Each cryovial was dipped into liquid nitrogen until frozen (snap-frozen) and then stored temporarily at –80°C before being moved to liquid nitrogen for long-term storage.

2.2.6.2 RSV titration

To determine the number of infectious particles present in the newly propagated RSV A2 P6 virus (Section 2.2.6.1), a viral plaque assay was completed. HEp-2 cells were brought up from liquid nitrogen and subcultured (Section 2.2.3) into 75 cm² flasks four times before being used for the experiment. Cells were resuspended in DMEM propagation media (Table 2.1) and then seeded into 96 well plates (Costar) at a density of 2 x10⁴ cells/well in 100 µl. Cells were then incubated at 37°C/5% CO₂ overnight. Cells were checked the following day to confirm that they had reached a confluence of around 90% with minimal patches/detachment. Twelve 1.5 ml Eppendorf tubes were prepared as follows; tube 1 received 990 µl of HEp-2 infection media (Table 2.1) and the remaining tubes received 200 µl HEp-2 infection media. This was completed in duplicate to test the control antigen (CA-cells propagated without RSV) and the propagated RSV (Section 2.2.6.1). An initial 1:100 dilution was completed whereby 10 µl of either CA or virus was added to tube 1 containing 990 µl of infection media and then mixed with pipetting. Subsequent doubling dilutions were completed by removing 200 µl from tube 1 into tube 2 and mixed with pipetting. Serial dilutions were carried on until the final tube was mixed. Spent media was removed from the 96-well plate and 50 µl of the appropriate RSV dilution or media control were added, in triplicate, to each well. Plates were then incubated for

2 h at 37°C, 5% CO₂ after which, 150 µl of HEp-2 recovery media (Table 2.1) was added directly to each well. Plates were incubated for a further 24 h.

The plates were checked for any cytopathic effect and then a plaque assay completed to determine the number of infected cells (known as plaque forming units or focus forming units). Spent media was removed and each well washed with 100 µl PBS, moving from the most dilute to the highest concentration of virus. To fix the cells, 100 µl of methanol/2% H₂O₂ (Table 2.2) was added to each well of the plate and the plate left for 20 mins at room temperature. The plate was washed in 200 µl of PBS/1% BSA/0.1% sodium azide (Table 2.2). A 1:200 dilution of the RSV biotinylated ab (Table 2.4) was prepared in PBS/1% BSA and 100 µl added to each well and the plate incubated for 1 h. Each plate was washed 2X with 200 µl PBS/1% BSA and then 100 µl streptavidin HRP (Table 2.3) added to each well. The plates were wrapped in foil and incubated at room temperature for 30 mins. Two separate washes of 200 µl of PBS/1% BSA were completed and then 50 µl of 3,3' – Diaminobenzidine (Table 2.3) added to each well. The plates were wrapped in foil and then incubated at room temperature until brown spots appeared (usually between 2 – 24 h). Wells were washed with 100 µl PBS and left to air dry. Plaques (visible as brown spots) were counted using an inverted light microscope and the PFU/ml calculated using the following equation:

$$PFU \text{ per ml} = \text{no. of plaques} \times \text{dilution factor} \times 20$$

2.2.7 RSV experimental infection of airway epithelial cells

BEAS-2B, HBEC3-KT and NHBE cells were cultured as described (Section 2.2.1, 2.2.3 and 2.2.4 respectively) and seeded into 12–well plates (Costar) at a density of 50,000–70,000 cells/well (BEAS-2B), 80-100,000 cells/well (HBEC3-KT) or 60,000–80,000 cells/well (NHBE) depending on when required and in the appropriate complete media (Table 2.1). Cells were incubated at 37°C, 5% CO₂ and maintained until 80% confluent where upon complete media would be removed and replaced with the appropriate basal medium (Table 2.1) to ensure cells are all at the same growth phase. Cells were then incubated over night at 37°C, 5% CO₂.

The desired multiplicity of infection (MOI: which determines the ratio of virus to cell) was prepared (250 µl/well) of RSV A2 strain (ATCC) and control samples were prepared using appropriate basal media (Table 2.1). Controls included a UV inactivated virus where neat virus had been exposed to UV light at a wavelength of 999 for 10 mins. Filtrate virus was prepared by pipetting neat virus into a 0.5 ml Eppendorf tube with 30 kDa filter (Amicon) and then centrifuged at 1000 g for 5 mins at room temperature. Infection HEp-2 media (Table 2.1) that was used to propagate the virus was also included as well as normal basal media (Table 2.1) used during cell culture (cell type dependent).

Basal media was removed and each well washed with 1 ml basal medium. After the addition of the appropriate RSV dilution or control, plates were incubated at 37°C, 5% CO₂ for 2 h and tilted periodically every 15 mins. Media and/or virus was then removed and each well rinsed with 1 ml basal medium (Table 2.1 - cell type dependent) before the addition of 1 ml basal media/well (BEAS-2B) or 1 ml recovery media (NHBE) (Table 2.1). Plates were subsequently incubated at 37°C, 5% CO₂ for 24/48 h where upon supernatants (SN) and RNA were collected (Section 2.3 – 2.4) or cell viability assay performed (Section 2.4).

2.3 Sample collection and preparation

2.3.1 Supernatants

Cell free supernatants were collected from individual wells and placed into separate Eppendorf tubes then centrifuged for 2 mins at 1500 g to pellet cell debris. The overlying supernatant was then transferred (without disturbing the pellet) into a fresh tube and stored at –80°C until required for analysis via ELISA (Section 2.5). If RNA samples were desired, the remaining pelleted cells were kept and used as described (Section 2.3.2).

2.3.2 RNA

Supernatants/spent media were removed (Section 2.3.1), and 1 ml of TRI reagent® (Sigma-Aldrich) added to each well to lyse the cells. Lysed cells were collected and placed into the

Eppendorf tube containing the pelleted cells collected in (Section 2.3.1). The cell pellet was resuspended in the TRI reagent ® and tubes frozen at –80°C until required.

2.4 Cell viability assay

2.4.1 MTT cell viability assay

Quantification of viable BEAS-2B cells was measured using a 3-(4,5-Dimethylthiazol-2-yl)-2,5-diphenyltetrazolium bromide for (MTT) assay which measures levels metabolic of activity in the form of nicotinamide adenine dinucleotide phosphate (NADPH) production. Excess media from culture plates was removed and 400 µl of basal media (Table 2.1) added to each well. MTT (Table 2.2) was prepared in accordance with the manufacturer's instructions and added to each well (40 µl/well). The plate was wrapped in tin foil and incubated at 37°C, 5% CO₂ for 2 h where the tetrazolium dye of MTT may be reduced by living cells into an insoluble formazan. To solubilise the formazan, 200 µl 10% SDS, 0.01 M HCL (Table 2.2) is added to every well before an overnight incubation at 37°C, 5% CO₂. The solution was added in triplicate to an opaque 96-well plate (Costar) and absorbance determined using a Varioskan plate reader at 620 nm. Cell viability was determined as follows:

$$\% \text{ of viable cells} = \frac{(abs_{sample} - abs_{blank})}{abs_{control} - abs_{blank}} \times 100$$

2.4.2 Cell Titer-Glo® assay

A different cell viability assay was trialled for NHBE and HBEC3-KT cell optimisation experiments as it was a faster assay than the MTT assay (Section 2.4.1). Cellular metabolic activity was measured by scrutinising levels of cellular adenosine triphosphate (ATP). Spent media was removed from the plate and 200 µl of the appropriate recovery media (Table 2.1) was added to each sample well and an additional empty well (containing no cells) as a control. The CellTiter-Glo® reagent (Table 2.3) was prepared in accordance to manufacturer's instructions and added to each well to make a 1:2 dilution (200 µl/well). The plate was covered in foil and placed at room temperature for 2 mins with shaking to allow cell lysis. The plate

was then taken off the orbital shaker and left for an additional 10 mins incubation at room temperature. Duplicates of each sample were then added to a white opaque 96-well plate (Costar) and luminescence determined using a Varioskan at 480 nm. Viability was calculated:

$$\% \text{ of viable cells} = \frac{(abs_{sample} - abs_{blank})}{abs_{control} - abs_{blank}} \times 100$$

2.5 Quantitative real-time PCR (RT q-PCR)

2.5.1.1 RNA extraction of BEAS-2B cells

Samples were collected as described (Section 2.3.2). Chloroform was added directly into the sample and thoroughly mixed before standing the samples at room temperature for 10 mins. A cooled centrifuge at 4°C was used at 1200 *g* for 15 mins to separate the RNA into an aqueous layer, distinct from contaminating proteins, lipids and DNA. The aqueous layer containing RNA was then carefully removed and transferred into a new tube. To further purify the RNA from the solution, isopropanol was added to each tube, mixed vigorously and then samples left to stand for 10 mins at room temperature. An RNA pellet was formed using centrifugation at 4°C for 10 mins, 1200 *g*. The aqueous solution was removed, and the pellet (containing RNA) was washed with 70% ethanol before centrifugation at 1500 *g*, 4°C for 10 mins. Ethanol was removed and the pellet was allowed to air dry at room temperature before resuspension in 30 µl nuclease free, distilled H₂O.

2.5.1.2 RNA purification of BEAS-2B cells

Extracted RNA (Section 2.4.1), was further purified using a commercially available DNase kit (Table 2.5) to eliminate any contaminating genomic DNA. A master mix containing 3 µl of 10X buffer, and 1 µl DNase/sample, was prepared and added to each sample. After incubating the samples at 37°C for up to 30 mins, the reaction was halted with the addition of DNase inactivation solution (3 µl/sample). Samples were continually mixed (with pipetting) during a 2 min incubation period at room temperature. Contaminating DNA and excess DNase treatment

were removed through centrifugation: 1000 *g* for 2 mins at 4°C and the resulting supernatant (containing RNA) was transferred into a fresh tube before storing at –80°C.

2.5.2 RNA extraction of HBEC3-KT and NHBE cells

Samples were collected as described (Section 2.3.2) and prepared using the Monarch® Total RNA Miniprep Kit (Table 2.5) and according to the manufacturer's instructions. In brief, 200 µl of chloroform was added to each sample and thoroughly mixed before incubation of the samples at room temperature for 10 mins. Samples were centrifuged at 4°C, 12,000 *g* for 15 minutes. The uppermost, aqueous layer containing RNA was then carefully removed and transferred into a new tube and an equal volume of ethanol (≥ 95%) was added into the tube and mixed by inverting. Up to 800 µl was placed into an RNA purification column sat within a collection tube (this step was repeated where volumes were greater than 800 µl) and centrifuged for 30 seconds at 16,000 *g*, 4°C. The flow through was discarded and 500 µl of RNA wash buffer added into the purification column then centrifuged again at 16,000 *g* for 30 seconds at 4°C. DNase treatment was prepared in a separate Eppendorf - for each sample; 5 µl of DNase 1 and 75 µl DNase reaction buffer was added into the Eppendorf and inverted to mix. 80 µl of this DNase reaction mixture was added directly to the top of the matrix in the RNA purification column and incubated at room temperature for 15 mins. 500 µl of RNA priming buffer was then added to each column and tubes were centrifuged as previously described. The flow through was discarded and columns were washed with 500 µl RNA wash buffer and centrifuged as before. The wash step was repeated a second time however samples were centrifuged for 2 mins. The column was then placed in a fresh Eppendorf and 30 µl of nuclease free, distilled H₂O added to each column. Samples were centrifuged once more for 30 seconds at 16,000 *g*, 4°C then columns were removed and samples stored at -80°C until required.

2.5.3 cDNA synthesis

To quantify the levels of viral RNA using RT-qPCR, complimentary DNA had to be generated from the purified RNA (Section 2.5.1.1-2.5.2). The purity of each RNA sample was determined by a Nanodrop-1000 spectrophotometer (Thermo Fisher). Then, 1 µg of RNA could be prepared for each sample using a high-capacity cDNA reverse transcription kit (Applied Biosystems) (Table 2.5). A mastermix was prepared containing (per sample); 4 µl of 10X RT buffer, 1.6 µl 25X 100 nM dNTPs, 4 µl 10X random primers, 2 µl multiscribe reverse transcriptase, 2 µl RNase inhibitor and 6.4 µl of dH₂O. A thermal cycler (PTC-200) was used to transcribe the RNA samples into cDNA using the following cycles; 94°C for 2 mins, 40–60°C for 1 min and 70–74°C for 2 mins (20 cycles). The cDNA samples were frozen at –80°C until required for RT-qPCR.

2.5.4 Absolute quantification RT-qPCR

2.5.4.1 Plasmid preparation

In order to quantify the levels of viral RNA in each sample, a standard curve was generated using a plasmid encoding a specific fragment of the RSV large polymerase (L) – gene (Culley et al., 2002). The PCDNA3 plasmid containing an ampicillin resistance gene was gifted from Dr Fiona Culley at Imperial College London with the plasmid weight previously determined as 4.3×10^{-12} µg/molecule.

2.5.4.1a Transformation of *Escherichia coli* (*E. coli*)

To generate more stock of the plasmid, 1 µl of plasmid was added into 15 µl of *E. coli* (strain TOP10, kindly provided by Colin Bingle lab) in an Eppendorf and kept on ice for 30 mins. The tube was then placed into a water bath at 42°C for 30 seconds to heat shock the bacteria and enable the plasmid to enter into the cells. The tube was placed back on ice and 250 µl of S.O.C medium (Invitrogen) added to enable maximum transformation efficiency. The tube was placed in a shaker for 1 h at 37°C, 200 rpm. Around 100 µl of the bacteria suspension was

then spread onto an agar plate containing Luria-Bertani (LB) and ampicillin. The plate was allowed to dry for 30 mins then placed in an incubator overnight at 37°C.

2.5.4.1b Growing up transformed *E. coli* stocks

The following day, 1 bacterial colony was selected from the agar plate and inoculated in 2 ml of LB broth + ampicillin. The tube incubated overnight at 37°C, 200 rpm shaking.

2.5.4.1c Isolation and purification of plasmid

The plasmid DNA was isolated and purified using the Monarch® Plasmid Miniprep Kit (Table 2.5) according to the manufacturer's instructions. In brief, the bacterial culture was gently tapped to mix then 1.5 ml was placed into a fresh Eppendorf and briefly centrifuged for 30 seconds at 16,000 *g*. The supernatant was discarded, and the cell pellet (containing transformed bacteria) resuspended in 200 µl of Plasmid Resuspension Buffer and vortexed until clumps dispersed. To this, 200 µl of Plasmid Lysis Buffer was added and the tube inverted 5 – 6 times to mix. The suspension was then left at room temperature for 1 min. 400 µl of Plasmid Neutralization Buffer was added into the Eppendorf and the suspension inverted to mix before a further incubation at room temperature for 2 mins. The tube was then centrifuged at 16,000 *g* for 5 mins to remove contaminant RNA. The supernatant was then carefully removed, placed into a spin column and centrifuged at 16,000 *g* for 2 mins. The flow through was discarded and 200 µl of Plasmid Wash Buffer 1 added into the spin column before centrifugation at 16,000 *g* for 1 min. The flow through was once again discarded and 400 µl of Plasmid Wash Buffer 2 added into the spin column before centrifugation for 1 min, 16,000 *g*. The spin column was then placed into a fresh Eppendorf and 30 µl of DNA Elution Buffer added into the centre matrix of the column and incubated for 2 mins then centrifuged at 16,000 *g* for 1 min to elute the DNA. The plasmid was frozen at -20°C until required.

2.5.4.2 RT-qPCR

A standard curve was prepared using the generated plasmid (section 2.5.4.1) where an initial 1:100 dilution was completed to generate 10^8 copies/ μl and then subsequent dilutions completed at 1:10 until 10 copies/ μl .

Primers and probe (Table 2.6) were prepared at a final stock concentration of 100 μM as per the manufacturer's instructions.

Samples were prepared using a TaqMan kit from Promega (Table 2.5). Each sample was prepared as follows: 10 μl q-PCR Master Mix (Promega), 0.2 μl carboxy-X-rhodamine (CXR) (Promega), 5.8 μl water, 1 μl of the forward and reverse RSV primers, and RSV probe were added into each sample. For unknown samples, 0.025 μg of cDNA sample were added or 1 μl of the relevant dilution of the RSV plasmid for the standard curve. Duplicates of either sample or standard control was added to a 384 well plate then sealed (Starlab X-clear advanced polyolefin seal) to prevent evaporation of samples during temperate cycles. Plates were briefly centrifuged at 689 g for 2 mins to ensure sample collection in the bottom of the well. Samples were run on a Real-time PCR machine (ABI 7900HT) set at: 50°C for 2 mins, 95°C for 10 mins then 40 cycles at: 95°C for 15 seconds and 60°C for 60 seconds. The resulting data was analysed using SDS 2.2.1 software (ABI systems).

2.6 Enzyme–Linked Immunosorbent Assay (ELISA)

An ELISA was used to determine the quantity of CXCL8 and CCL5 from supernatant collected (Section 2.3.1). CCL5 or CXCL8 coating antibody (Table 2.4) were diluted (according to the manufacturer's guidelines) in coating buffer (Table 2.2). A volume of 100 μl was then added the wells of a high-binding 96 well plate (Costar). The plate was wrapped in cling film and incubated overnight at room temperature to use the following day or refrigerated for a maximum of 3 days. The plate was then rinsed 3 times in wash buffer (Table 2.2) using an automated plate washer (Labtech International). A blocking buffer comprising of 1% BSA (Sigma-Aldrich) and coating buffer, was added before placing the plate on an orbital shaker (300 rotations/min). The plate was left at room temperature for 1 hour to prevent unspecific

binding of the antibody. After incubation, the plate was washed as previously described, and designated sample preparations and standard (CXCL8: 19.6 to 5000 pg/ml or CCL5: 39 to 10000 pg/ml) were added in duplicate at 100 µl/well. To allow sufficient binding, the plate was placed back on to the orbital shaker for 1.5 – 2 h. The plate was washed as previously described and 100 µl of desired biotinylated detection antibody (Table 2.4) added to each well. The plate was placed back on the orbital shaker for 1.5-2 h. The plate was washed, as previously described, to remove any excess biotinylated antibody before the addition of 100 µl of Streptavidin-HRP (R&D Systems) (Table 2.4) to each well at a concentration of 1:200. The plate was wrapped in foil then incubated once more at room temperature for 20 mins with shaking. A wash was completed, and then equal parts of substrate A and B (R&D Systems) mixed to generate 100 µl/well. The plate was wrapped once more in foil and left to develop up to 20 mins with shaking. The reaction was stopped with the addition of 50 µl sulphuric acid (1 M) to each well. To determine the optical density (OD), the plate was read using a Thermo Multiskan at an optical density of 450 nm. A standard curve was generated from the OD values to indicate the levels of each standard (CXCL8: 19.6 to 5000 pg/ml and CCL5: 39 to 10000 pg/ml) which could be used to quantify levels in the samples.

2.7 Plaque assay for viral infection

NHBE cells were seeded into a 96-well plate and then incubated at 37°C, 5% CO₂ overnight. Cells were then checked the following day to confirm that they had reached a confluence of around 90% with minimal patches/detachment. Spent media was removed and each well washed with 500 µl of basal media (cell type dependent). A range of RSV MOI dilutions were prepared using basal media and 150 µl added to each well. Plates were incubated at 37°C, 5% CO₂ for 2 h and tilted periodically every 15 mins. Spent media was removed and each well washed with 500 µl basal media (Table 2.1). A volume of 500 µl recovery media (Table 2.1) were added to each well and the plate placed back into the incubator 37°C, 5% CO₂ overnight.

The next day, plates were checked for any cytopathic effect and then a plaque assay completed to determine the number of infected cells (known as plaque forming units or focus forming units). Spent media was removed and each well washed with 400 µl PBS, moving from the most dilute to the highest concentration of virus. To fix the cells, 300 µl of methanol/2% H₂O₂ (Table 2.2) was added to each well of the plate and the plate left for 20 mins at room temperature. The plate was washed in 400 µl of PBS/1% BSA/0.1% sodium azide (Table 2.2). A 1:100 dilution of the RSV biotinylated ab (Table 2.4) was prepared in PBS/1% BSA and 300 µl added to each well and the plate incubated for 1 h. Each plate was washed 2 times with 400 µl PBS/1% BSA and then 300 µl streptavidin HRP (Table 2.3) added to each well. The plates were wrapped in foil and incubated at room temperature for 30 mins. Two separate washes of 400 µl of PBS/1% BSA were completed and then 250 µl of 3,3' – Diaminobenzidine (Table 2.3) added to each well. The plates were wrapped in foil and then incubated at room temperature until brown spots appear (usually between 2 – 24 h). Wells were washed with 400 µl PBS and left to air dry. Plaques (visible as brown spots) were counted using an inverted light microscope and the PFU/ml calculated using the following equation:

$$PFU \text{ per ml} = \text{no. of plaques} \times \text{dilution factor} \times 20$$

2.8 Liposome preparation SAPS/ PAPC

2.8.1 Lipid hydration

The experimental liposome 1-stearoyl-2-arachidonoyl-*sn*-glycero-3-phospho-L-serine (SAPS) and control liposome 1-palmitoyl-2-arachidonoyl-*sn*-glycero-3-phosphocholine (PAPC) (Table 2.7) were purchased from Avanti Polar lipids (Alabaster, AL). Both liposomes were prepared in the lab using the lipid hydration method to obtain unilamellar liposomes at a concentration of 1.0 mg/ml. A rotary evaporator (Stuart RE300DB) was used to remove the majority of chloroform from each sample before being flushed with nitrogen (Techne Sample Concentrator) to remove any excess chloroform and produce a dry lipid film. Degassed PBS was then used to rehydrate the lipids, which results in swelling and formation of multilamellar

liposomes. To create uniform sized, unilamellar liposomes, sonication (Fisherbrand FB11002) was applied and then samples purified with a 0.22 µm filter. Liposomes were kept at 4°C in glass vials and their efficacy tested on peripheral blood mononuclear cells (PBMC)s (Section 2.8.2).

2.8.2 Characterisation of SAPS and PAPC

To determine that SAPS and PAPC prepared (Section 2.8.1) were perturbing specific signalling pathway, PBMCs were prepared (Section 2.8.3) and treated with two different concentrations of each liposome then incubated for 1 h at 37°C, 5% CO₂. Each well was then stimulated with either lipopolysaccharide (LPS) or Interleukin 1 beta (IL-1β) before incubation at 37°C 5% CO₂ for 24 h where supernatant samples were collected for analysis by ELISA (Section 2.6).

2.8.3 Peripheral blood mononuclear cells (PBMC)

In accordance with a protocol approved by the South Sheffield Local Ethics Committee (STH13927), venous blood was obtained from healthy volunteers (with fully informed consent). The peripheral blood mononuclear cells (PBMCs) were isolated from the whole blood sample by a departmental colleague using a Percoll™ density gradient as previously described (Wardle et al., 2011).

2.9 Confocal microscopy

2.9.1 Coverslip preparation

Coverslips measuring 13 mm, were sterilised in separate wells of a 12–well plate and exposed to UV radiation (999 wavelength) for 10 mins. Coverslips were coated with 500 µl collagen (collagen 1 diluted to 0.05 mg/ml in 0.02 M acetic acid) (Table 2.2) then incubated at room temperature for 1 h. Coverslips were rinsed twice with sterile PBS then allowed to air dry in a

sterile flow cabinet. Plates were sealed with parafilm and placed into a fridge at 4°C until required.

2.9.2 Infection of cells

2.9.2.1 RSV infection for optimisation of anti-RSV fusion (F) antibody

BEAS-2B, HBEC3-KT or NHBE cells were seeded at around 0.6×10^6 /12-well plate and maintained (Section 2.2) until 80% confluent. Plates were washed with basal media –cell type dependent (Table 2.1). Viral dilutions were prepared using appropriate cell type basal medium and 250 µl of RSV/ media added to the plate. The plate was placed into the incubator for 2 h at 37°C, 5% CO₂. Plates were tilted every 15 mins to allow sufficient exposure of cells to virus. Plates were removed and spent media discarded before an additional media wash to remove any unbound virus from the well (1 ml basal medium/well). Plates not requiring fixation until a later time point, received 1 ml fresh basal medium (BEAS-2B) or recovery media (HBEC3-KT or NHBE) and incubated 37°C, 5% CO₂. Plates designated 0 h were fixed immediately (Section 2.9.3).

2.9.2.2 RSV infection of HBEC3-KT cells at different temperatures for distinguishing binding and fusion events of RSV

Duplicate plates of HBEC3-KT cells were seeded at 0.8×10^6 /plate and maintained (Section 2.2) until 80% confluent. Both plates were infected with RSV A2 (MOI 0.4) or stimulated with basal media for 1 h at 4°C in the presence/absence of SAPS (25 µg/ml) with periodic rocking every 15 mins. One plate was immediately washed using ice cold PBS to remove any unbound virus and subsequently fixed with 4% PFA (Section 2.9.3). Plate 2 was transferred to a humidified incubator for an additional 1 h at 37°C, 5% CO₂ to allow viral fusion and infection of the HBEC3-KT cells. Plate 2 was washed to remove any unbound virus, required wells treated again with SAPS (25 µg/ml) then the plate put back into the incubator for 20 h at which point, cells were washed and fixed. Cells for this experiment were imaged using a Zeiss Airyscan confocal microscope.

2.9.3 Fixing cells

In order to visualise RSV attachment to cells immediately after infection, cells were fixed with 500 μ l 4% PFA after the final media wash during infection process (Section 2.9.2). The plate was placed at room temperature for 15 mins then PFA removed and plates washed twice with 500 μ l PBS. Fresh PBS was added to each well (500 μ l/well) then refrigerated at 4°C until required (no longer than 1 week) or stained immediately (Section 2.9.4).

2.9.4 Primary antibody staining

Cells were washed with sterile 1X PBS and incubated at room temperature for 5 mins with shaking. Spent PBS was removed and 1ml/well blocking buffer (Table 2.2) added to each well then left to incubate for 1 h at room temperature. Buffer was removed and 1ml/well of RSV anti-F ab (Table 2.4) added to all appropriate wells. An isotype control (Table 2.4) was added to one well and the plate wrapped in clingfilm before incubating overnight at 4°C with shaking.

2.9.5 Secondary antibody staining and mounting of coverslips

Cells were washed three times with 1ml/well sterile 1X PBS with 5 mins incubation periods and shaking. Secondary antibody (Table 2.4) was prepared in dilution buffer (Table 2.2) and 1 ml/ well added to the plate. The plate was wrapped in foil and incubated at room temperature for 1 h with shaking. Excess antibody was then washed off with 1X PBS (3 separate washes). Microscope slides measuring 1.0–1.2 mm thick (Academy) were prepared by adding 10 μ l of mountant (Invitrogen) (Table 2.2) directly to the slide. Coverslips were removed from tissue culture plates using tweezers, rinsed in d_2 H₂O, dabbed dry and then placed (cell side down) onto the mountant. Slides were covered to prevent light penetration and allowed to set for 1 h at room temperature before being stored at 4°C overnight.

2.9.6 Actin staining

Where staining of actin filaments was required, cells were fixed as previously described (Section 2.9.3). Cells were washed with sterile 1X PBS and incubated at room temperature for 5 mins with shaking. Spent PBS was removed and 1 ml/well blocking buffer (Table 2.2) added to each well then left to incubate for 1 h at room temperature. Buffer was removed and 250 μ l/well of Phalloidin (Table 2.4) added to all appropriate wells. The plate was incubated for 45 mins at room temperature under humid conditions by wrapping in a damp paper towel. Excess antibody was then washed off with 1X PBS (3 separate washes) and coverslips mounted as described (Section 2.9.5).

2.9.7 Confocal microscopy

Cells were imaged using a Nikon A1 or Airyscan confocal microscope using the 60X oil lens. Areas of visualisation were picked using the DAPI channel only to remove any bias and 3 separate areas were imaged to generate an average fluorescent intensity value. Images were processed using ImageJ software. Images that were captured and processed using the Airyscan confocal were kindly imaged by Dr Nick Van Hateren (Wolfson Light Microscopy Facility). Again, areas of the cells were selected at random through the DAPI channel only and imaged using the 40X lens with oil.

2.10 Bacterial culture

2.10.1 *Streptococcus pneumoniae* (*Spn*) stock preparation

Experiments were completed using FP22, the isogenic unencapsulated derivative of serotype 2 strain D39 (Pearce et al., 2002) that was originally gifted from Professor Tim Mitchell (University of Birmingham). For confocal microscopy studies, the unencapsulated, fluorescent *Spn* strain called FT4 was used, originally provided by Dr Andrew Fenton, University of

Sheffield. Fresh stocks were initially generated using a beaded stock generated by a fellow PhD student (Faith H Tolliday). The beaded stock was thawed at room temperature then flicked to mix. A sterile loop was used to select a bead and then streaked onto a Columbia blood agar plate (Thermo Fisher, UK). The plate was placed into an incubator overnight at 37°C, 5% CO₂. The following day, an overnight culture was prepared. Eight 15 ml centrifuge tubes were prepared with 10 ml of (previously autoclaved) BHI (Table 2.1). Serial dilutions were then prepared by inoculating the first tube with 10-30 bacterial colonies from the agar plate. The centrifuge tube was briefly vortexed to mix and then 5 µl of this suspension was carried over to tube 2. Tube 2 was inverted once to mix and then 5 µl removed and placed into tube 3. This process was repeated until tube 8 was inoculated. The centrifuge tubes were placed into an incubator (no shaking) overnight at 37°C, 5% CO₂ ensuring the lids were left loose.

The overnight cultures were observed and the centrifuge tube containing turbid supernatant (indicating bacterial growth) that also had minimal pellet formation (dead cells) was selected. Around 1- 2 ml of the selected overnight culture was then used to inoculate a fresh centrifuge tube containing 30 ml BHI. An extra 50 ml centrifuge tube was also prepared containing 10 ml of BHI only to be used for blank OD measurements to equilibrate the spectrophotometer. The bacterial suspension was briefly vortexed then an OD (600 nm) taken to confirm a starting OD of between 0.01 and 0.05. The lids on the bacterial suspension and blank control were loosened slightly before placing the suspensions into an incubator at 37°C, 5% CO₂ (without shaking). Hourly measurements were taken until an OD of 0.5 (mid log phase) was reached (**Figure 2.2**). Around 15 ml of the bacterial suspension was removed from the uppermost part of the centrifuge tube (to prevent collecting dead cells) and placed into a fresh tube. The bacterial suspension was then mixed with 50% glycerol at a ratio of 5:3 (9 ml of 50% glycerol added to 15 ml bacteria suspension). The suspension was vortexed to mix and then aliquoted into 1 ml Eppendorf's and frozen at -80°C.

The colony forming units (CFU) of the frozen stock aliquots were quantified using the Miles Misra technique (Section 2.10.3).

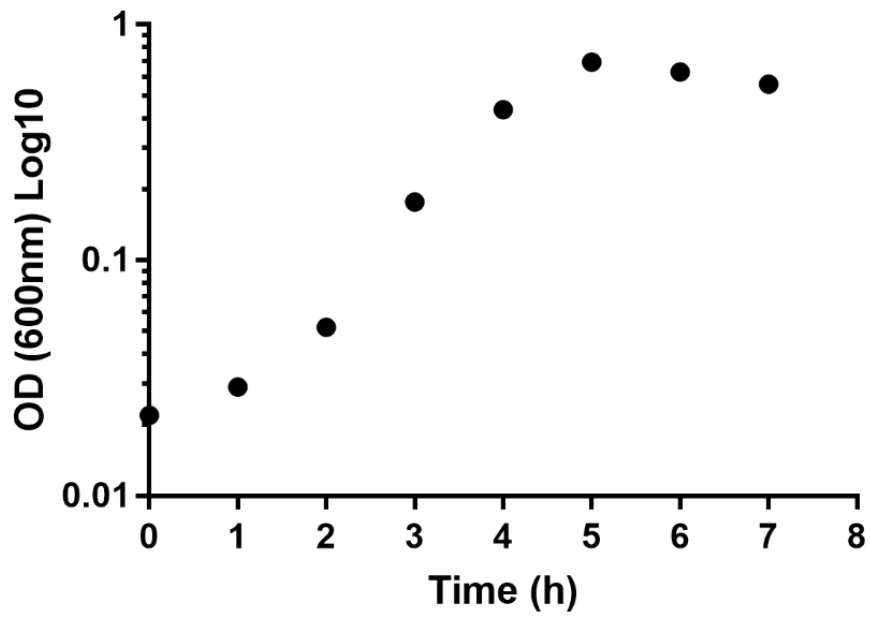


Figure 2.2 Growth curve of *Streptococcus pneumoniae* FP22. Overnight cultures of *Spn* were prepared and used to grow up *Spn* stocks in BHI until mid-log phase of growth was reached (as indicated by OD 0.5). OD measurements were taken using a spectrophotometer at 600 nm.

2.10.2 Preparation of pHrodo-stained *Spn*

A frozen aliquot of FP22 was defrosted at room temperature and centrifuged at 9000 *g* for 3 mins. Supernatant was removed and the pellet resuspended in 1 ml PBS before centrifugation again at 9000 *g* for 3 mins. Supernatant was removed and bacteria resuspended in 1 ml PBS then centrifuged once more at 9000 *g* for 3 mins. Supernatant was removed and bacteria were resuspended in 200 μ l of PBS. 0.5 μ l of pHrodo (Table 2.4) was added into the aliquot of *Spn* and the mixture pipetted up and down then vortexed to prevent clumping of the pHrodo dye. The bacterial suspension was wrapped in foil to prevent light penetrations and incubated at 37°C for 30 mins on a shaker. The bacteria were centrifuged as previously described and the pellet resuspended in 1 ml of Tris (25 mM, pH 8.4) and incubated at room temperature for 1 min in the dark. The aliquot was centrifuged as previously described and resuspended in 1 ml PBS to wash the pellet with another centrifugation step. The bacterial pellet was resuspended in 1 ml HBEC3-KT basal medium and wrapped in foil until required. Prepared samples were used within 24 hours to avoid degradation.

2.10.2.1 Imaging pHrodo-stained *Spn* in RSV-infected HBEC3-KT cells

Three independent experiments from three individual populations of cells were conducted simultaneously in a 24-well culture plate. Cells were seeded at 0.8×10^6 cells/plate using complete medium containing GA-1000 and grown overnight to reach 60% confluence the following day. Media was removed from the plate washed with 1 ml/well fresh basal media (no GA-1000) and cells were placed into 1 ml/well basal media (without GA-1000).

Cells were stimulated with basal media or infected with RSV A2 (MOI 0.4) for 2 h in the presence/absence of SAPS (25 μ g/ml) at 37 °C, 5% CO₂ with periodic rocking every 15 mins. Media and unbound virus removed, and SAPS re-added to required wells. The plate was incubated for 24 h.

The next day, one well was fixed with 250 μ l 4% PFA for 15 mins at room temperature to act as a control to ensure that no *Spn* should fluoresce unless intracellular. The plate was stimulated with media or infected with unlabelled *Spn* or pHrodo-stained (Section 2.10.2) *Spn* (FP22) (MOI 1). The plate was centrifuged for 5 mins at 150 *g* to ensure bacteria were in contact with the cell monolayer. The plate was incubated for 1 h at 37°C, 5% CO₂. Unbound bacteria were removed and the plate washed 3X with 500 μ l PBS washes. Cells were then incubated with 500 μ l antibiotic (20 μ g/ml gentamicin/ 40 μ g/ml streptomycin and 40 U/ml penicillin) for 30 minutes at 37°C, 5% CO₂ to kill any remaining extracellular bacteria. Samples were collected from each well and plated neat onto blood agar plates to ensure efficient killing of extracellular *Spn*. 1 ml fresh basal media was added to each well and the plate wrapped in foil to protect from light. The plate was imaged immediately using a ZOE Fluorescent Cell Imager (BIO-RAD) to detect red fluorescence indicative of intracellular, pHrodo-stained *Spn*. To ensure no bias in sample image collection, each well was aligned centrally on the imager using the brightfield setting before switching to the red channel to detect red fluorescence and capture images. Zoom is 100 μ m. The CFU/ml of each *Spn* stock prepared was quantified by Miles Misra (Section 2.10.3).

2.10.3 Miles Misra viable bacterial count

Viable bacteria from stock preparation (Section 2.10.1) and from experimental procedures were quantified using the Miles Misra technique (Miles et al., 1938). Six 10-fold serial dilutions were completed in sterile PBS and plated on blood agar plates with 3 x 10 μ l drops of each dilution to obtain average counts. Agar plates were allowed to air dry then incubated at 37°C, 5% CO₂ overnight. *Spn* colonies were confirmed through identification of α -haemolysis of the blood agar and quantified; number of colonies divided by 30 to acquire CFU/ μ l, then multiplied by the dilution factor of that sample and then multiplied by 1000 to give CFU/ ml.

2.11 RSV-bacterial co-Infections of HBEC3-KT cells

2.11.1 Optimisation of *Spn* infections of HBEC3-KT cells

HBEC3-KT cells were cultured (Section 2.2.3) and seeded into 24-well plates (Costar) at a density of 1.2×10^6 cells/plate. Cells were incubated at 37°C, 5% CO₂ and maintained until 70% confluent where upon complete media was removed and replaced with basal medium (without antibiotics) (Table 2.1) to ensure cells are all at the same growth phase. Cells were then incubated over night at 37°C, 5% CO₂. The following day, a fresh aliquot of *Spn* (FP22) was thawed at room temperature and centrifuged at 9000 *g* for 3 mins. The supernatant was removed and the bacterial pellet resuspended in 1 ml PBS before centrifugation at 9000 *g* for 3 mins. Supernatant was removed and the bacterial pellet gently resuspended in 1 ml PBS. Bacterial suspensions were prepared to generate MOI 0.5, 1, 1.5, 5 and 10 (diluted in HBEC3-KT basal media) to generate 200 µl/ well. A PBS control was also included to ensure PBS alone was not affecting viability and CXCL8 generation from the HBEC3-KT cells. The plate was centrifuged for 5 mins at 150 *g* to ensure bacteria were in contact with the cell monolayer and then incubated with the selected MOI of *Spn* for 1 h at 37°C, 5% CO₂. The bacteria and media were removed, and wells washed 3 x with 500 µl PBS to remove any unbound bacteria. Cells were then incubated with antibiotics (100 µg/ml gentamicin/ 100 µg/ml streptomycin and 100 U/ml penicillin) for 1 h. Media and antibiotics were removed, and wells washed as previously described. Fresh basal media was added to the plate and staurosporine (1 µM) added to a well to act as a positive control for cell death. The plate was incubated for 24 h at 37°C, 5% CO₂ and supernatants collected and analysed for CXCL8 via ELISA (Section 2.6) and cell viability assessed using CellTiter-Glo® (Section 2.4.2).

2.11.2 Bacterial challenge with SAPS

A fresh aliquot of *Spn* was thawed at room temperature and centrifuged at 9000 *g* for 3 mins. The supernatant was removed, and the bacterial pellet resuspended in 1 ml PBS before centrifugation at 9000 *g* for 3 mins. Supernatant was removed and the bacterial pellet gently

resuspended in 1 ml PBS. Bacteria were prepared in basal media to give approximately 2.3×10^5 CFU/ 200 μ l. Triplicate wells received 200 μ l of *Spn* only and separately, triplicate wells received 195 μ l *Spn* and 5 μ l SAPS (25 μ g/ml). The plate was incubated for 1 h at 37°C, 5% CO₂. The bacterial suspension in each well was drizzled ~ 10x to help dislodge any adherent bacteria to the base of the well. A sample of 100 μ l from each well was then removed and serially diluted (6x 10-fold dilutions) to complete Miles Misra counts (Section 2.10.3).

2.11.3 Co-infected cells: Bacterial adherence assay

HBEC3-KT cells were cultured (Section 2.2.3) and seeded into 24-well plates (Costar) at a density of 1.2×10^6 cells/ plate. Cells were incubated at 37°C, 5% CO₂ and maintained until 80% confluent where upon complete media was removed and replaced with basal medium (without antibiotics) (Table 2.1) to ensure cells are all at the same growth phase. Cells were then incubated over night at 37°C, 5% CO₂.

Cells were infected with RSV A2 (MOI 0.4) or stimulated with media for 2 h in the presence/absence of SAPS (25 μ g/ml). Unbound virus was removed from the cells and fresh basal medium added to the cells and SAPS re-added to the appropriate wells. Cells were incubated for 24 h before subsequent infection with *Spn*.

The following day, a fresh aliquot of *Spn* (FP22) was thawed at room temperature and centrifuged at 9000 *g* for 3 mins. The supernatant was removed, and the bacterial pellet resuspended in 1 ml PBS before centrifugation at 9000 *g* for 3 mins. Supernatant was removed and the bacterial pellet gently resuspended in 1 ml PBS. Bacterial suspensions were prepared using HBEC3-KT basal media to generate *Spn* MOI 1. Cells were stimulated with 200 μ l/ well basal media or *Spn* and the plate centrifuged for 5 mins at 150 *g* before incubation at 37°C, 5% CO₂ for 1 h. The bacteria and media were removed, and wells washed 3 x with 500 μ l PBS to remove any unbound bacteria. Cells were detached from the wells using 200 μ l/ well of 0.04% trypsin/EDTA and incubation at 37°C, 5% CO₂ for 5-7 mins or until cells detached from

the well. The bacterial-cell suspension was collected from each well and the Eppendorf placed on ice. PBS (200 µl) was added into each well and drizzled over 3x to collect any remaining bacteria from the well and resuspended into the appropriate Eppendorf containing the bacterial-cell suspension. Samples were prepared as in Section 2.10.3.

2.11.4 Co-infected cells: Bacterial invasion

HBEC3-KT cells were seeded into 12-well plates at 1×10^6 cells/plate in complete media and incubated overnight to reach 60-70% confluency after which complete media was removed and fresh basal medium added to each well overnight.

For co-infection studies, HBEC3-KT cells were infected with RSV A2 (MOI 0.4) or stimulated with media for 2 h in the presence/absence of SAPS (25 µg/ml). Unbound virus was removed from the cells and fresh basal medium and SAPS re-added. Cells were incubated for 24 h before subsequent infection with *Spn* as described below.

2.11.4.1 Bacterial invasion via flow cytometry

For co-infection studies and those looking at *Spn* alone (where the RSV infection day was omitted), cells were stimulated with 250 µl HBEC3-KT basal media or infected with pHrodo-labelled *Spn* (Section 2.10.2) at an MOI of 1. The plate was centrifuged at 150 g for 5 mins and then incubated for 1 h at 37°C, 5% CO₂. Bacteria and media were removed, and the plate washed 3 x with 500 µl PBS to remove any unbound bacteria. The plate was incubated for a further 30 mins with antibiotics (20 µg/ml gentamicin/40 µg/ml streptomycin and 40 U/ml penicillin). Supernatant was collected from bacterial-infected cells and plated neat onto blood agar to confirm the killing of any extracellular bacteria. The plate was washed 3 x with 500 µl PBS and cells detached with 250 µl/ well of 0.04% trypsin/EDTA and incubation at 37°C, 5% CO₂ for ~5-7 mins. The bacterial-cell suspension was collected from each well and the Eppendorf tube placed on ice. PBS (250 µl) was drizzled 3x over each well to collect any

remaining bacteria and resuspended into the appropriate Eppendorf containing the bacterial-cell suspension.

Cells were pelleted with centrifugation at 400 *g* for 5 mins and the supernatant carefully aspirated and cells resuspended in 500 μ l PBS. Centrifugation was repeated to pellet the cells where the supernatant was discarded, and cells resuspended in 250 μ l 4% PFA with a 1 h incubation at 4°C. Cells were centrifuged as previously described and supernatant removed. Cells were washed via centrifugation with 500 μ l PBS for 5 mins at 400 *g*. Cell pellets were resuspended in basal HBEC3-KT media and maintained in dark conditions at 4°C until analysis.

Samples were processed using LSRII (BD Biosciences) where two detection filters were selected (575 and 610 nm) to span the possible wavelength of pHrodo (pHrodo has excitation peak at 560 nm and emission at 587 nm) which can fluoresce differentially depending on pH. Analysis was undertaken using FlowJo V10.8.0 (Becton, Dickinson & Company, NJ, USA).

2.11.4.2 Bacterial invasion via confocal

HBEC3-KT cells were grown on collagen coated coverslips (Section 2.9.1) in 12-well plates to 80% confluence. For co-infection studies, cells were infected with RSV (Section 2.11.4) 24 h prior to bacterial infection with red fluorescent *Spn* (FT4). A fresh aliquot of *Spn* was thawed at room temperature and centrifuged at 9000 *g* for 3 mins. The supernatant was removed, and the bacterial pellet resuspended in 1 ml PBS before centrifugation at 9000 *g* for 3 mins. Supernatant was removed and the bacterial pellet gently resuspended in 1 ml PBS. Bacterial suspensions were prepared to generate the appropriate MOI (diluted in HBEC3-KT basal media) to generate 250 μ l/well. The plate was centrifuged for 5 mins at 150 *g* to ensure bacteria were in contact with the cell monolayer and then incubated with the selected MOI of *Spn* for 1 h at 37°C, 5% CO₂. The bacteria and media were removed, and wells washed 3 x with 500 μ l PBS to remove any unbound bacteria. Cells were then incubated with antibiotics (20 μ g/ml gentamicin/40 μ g/ml streptomycin and 40 U/ml penicillin) for 30 mins. Media and

antibiotics were removed, and wells washed as previously described. Cells were fixed in 4% PFA for 15 mins at room temperature, washed 3 x with 500 μ l PBS and incubated at 4°C until required for staining. In co-infection studies, RSV F protein was stained as described in Section 2.9.4 and 2.9.5 before DAPI staining and mounting of the samples (Section 2.9.5) and analysis via confocal microscopy (Section 2.9.7).

2.12 Data Analysis

Data are represented as mean \pm SEM (where N=3 or more) of separate experiments (BEAS-2B) or (HBEC3-KT) or separate donors (NHBE) as specified in the legend. GraphPad Prism (GraphPad Inc., La Jolla, CA) software version 7.0 was used to complete statistical analysis. Data were analysed using a two-way ANOVA and Tukey's multiple comparisons test or a one-way ANOVA with Dunnett's post-test to the control as specified in the figure legend. Data were analysed using repeated measures unless otherwise stated. Significant differences are indicated by *p <0.05, **p<0.01, ***p<0.001 and ****p<0.0001.

Chapter 3: Results – Investigating the Ability of SAPS Treatment to Modulate the Response of Airway Epithelial Cells to RSV Infection

3.1 Hypothesis and aims

Previous studies within my lab have explored the potential of the phosphatidylserine containing liposome, SAPS, to disrupt inflammatory signalling in response to a range of TLR agonists, and identified that SAPS mediated these actions by a mechanism that was likely to involve disruption of membrane microdomains (MM)s (Parker et al., 2008). More recently, SAPS was demonstrated to reduce the inflammatory response in immortalised and primary airway epithelial cells when infected with the non-enveloped, ssRNA respiratory virus; rhinovirus (RV) (Stokes et al., 2016). These data demonstrated that treatment of the immortalised human bronchial epithelial cell (BEAS-2B) line and normal human primary bronchial epithelial (NHBE) cells with SAPS significantly reduced the production of cytokines and chemokines such as CXCL8, CXCL10 and CCL5 seen in response to RV (Stokes et al., 2016). It was noted however that although inflammatory signalling was reduced, SAPS did not reduce levels of viral replication and thus had limited effects on RV's life cycle.

Based on my lab groups published data and increasing evidence that supports the role of MMs at multiple stages of many enveloped virus life cycles during infection of epithelial cells (Section 1.5), it was hypothesised that SAPS may also be able to modulate the response to the enveloped respiratory syncytial virus (RSV). My project hypothesis is that treatment of airway epithelial cells with SAPS can disrupt MM, modulating the immune response to RSV and potentially also the attachment, replication, and release of RSV during infection. To determine the importance of having the PS component for activity, a second liposome was included in the following investigations called 1-palmitoyl-2-arachidonoylsn-glycero-3-phosphocholine (PAPC), which is a larger, phosphocholine (PC) containing liposome (Parker et al., 2008; Treede et al., 2007). PAPC has been reported to have anti-inflammatory effects

when in an oxidised state (ox-PAPC) with no reported toxic effects in cell culture (Kawasaki and Ohnishi, 1992; Ke et al., 2017; Lichtenberger et al., 2001; Treede et al., 2007; Voelker and Numata, 2019). SAPS does not require oxidation to mediate its effects and therefore it was hypothesised that SAPS may offer broader potential as a therapeutic. The non-oxidised form of PAPC was used for comparative investigations.

The initial aims of this chapter were to therefore:

1. Confirm the activity of newly generated stocks of SAPS and comparative liposome PAPC in peripheral blood mononuclear cells (PBMC)s to validate their actions in established models.
2. Develop *in vitro* cell models for RSV infection studies.
3. Investigate how co-incubation of SAPS/PAPC liposomes in RSV-infected airway epithelial cells affects the inflammatory response by quantifying CXCL8 and CCL5 production.
4. Explore the potential of SAPS/PAPC as a post-treatment to control inflammatory responses in RSV-infected cells.

3.2 Confirming the activity of SAPS and PAPC to modulate inflammatory signalling in PBMCs

In line with previous studies within my lab, a comparative liposome called PAPC (1-palmitoyl-2-arachidonoyl-*sn*-glycero-3-phosphocholine) was used alongside SAPS to determine the effects of different lipid components on experimental outputs (Stokes et al., 2016). In previously published data (Stokes et al., 2016), the stability and characteristics of SAPS and PAPC liposomes generated through the lipid hydration method (as described in section 2.8.1) were determined. The mean size of SAPS was 203.6 ± 48.0 nm and PAPC 629.6 ± 90.7 nm, where the size distribution retained their uniformity up to the latest tested point (28 days) when stored at 4°C. My lab group also reported the targeted activity of SAPS to disrupt the crucial

signalling platforms required for TLR-dependent activation of the inflammatory response by perturbing MM (Parker et al., 2008; Stokes et al., 2016). The specificity of SAPS to inhibit MM, without affecting whole cell integrity, is a key characteristic of this liposome and it was therefore required that the activity of each new batch of SAPS and PAPC prepared within our lab (Section 2.8.1) was tested (Section 2.8.2) before its use in cell culture experiments.

Peripheral blood mononuclear cells (PBMC)s express a wide range of TLRs and have therefore been extensively used to investigate inflammatory signalling (Kwok et al., 2012; Morris et al., 2005; Parker et al., 2008; Ramírez-Pérez et al., 2020). PBMCs were therefore used in this study to investigate the inflammatory response of PBMCs to lipopolysaccharide (LPS) and interleukin-1 beta (IL-1 β). LPS and IL-1 β both signal through the adaptor complex MyD88, however, whilst LPS signalling via TLR4 occurs within MM, IL-1 β signalling via IL-1R1 does not depend on MM platforms (O'Neill and Bowie, 2007; Triantafilou et al., 2004b, 2004a). Therefore, SAPS has historically been found to perturb inflammatory signalling associated with LPS stimulation and not IL-1 β stimulated cells. These methods were used to assess that each prepared batch of SAPS or PAPC had the comparable characteristics detailed in our labs previously published data before they were applied in proceeding experiments.

For these experiments, PBMCs were treated with two different concentrations of SAPS or PAPC (10 or 50 μ g/ml) and then stimulated with either LPS or IL-1 β . Published work within this lab have previously investigated the use of LPS and IL-1 β to stimulate cocultures of epithelial cells and PBMCs with subsequent quantification of cytokines (Parker et al., 2008). Based on these published data, the concentrations used for LPS and IL-1 β stimulation were selected at 1 ng/ml and 10 ng/ml respectively. CXCL8 production was then quantified 24 h after stimulation, to determine the extent of pro-inflammatory cell signalling in response to LPS or IL-1 β , in the presence or absence of SAPS/PAPC.

Stimulation of PBMCs with LPS alone resulted in a substantial increase in CXCL8 production (37.6 \pm 9.7 ng/ml) in comparison to the unstimulated media control (1.2 \pm 0.6 ng/ml) (**Figure**

3.1). In line with previous findings (Parker et al., 2008) SAPS treatment resulted in a concentration dependent decrease in CXCL8 production from LPS stimulated PBMCs. These changes did not reach statistical significance but were in keeping with extensive previous published data and taken to indicate stable performance of the liposomes. These data also demonstrate that in comparison to SAPS, both concentrations of PAPC had only modest inhibitory effects on CXCL8 release (**Figure 3.1**). PBMCs stimulated with IL-1 β had increased CXCL8 production compared to the media control and as expected, neither concentration of SAPS nor PAPC had substantial inhibitory effects (**Figure 3.1**). Notably, the highest concentration (50 μ g/ml) of SAPS and PAPC appeared to potentiate CXCL8 production from IL-1 β stimulated PBMCs, though again changes did not reach statistical significance in comparison to PBMCs stimulated with IL-1 β only (**Figure 3.1**).

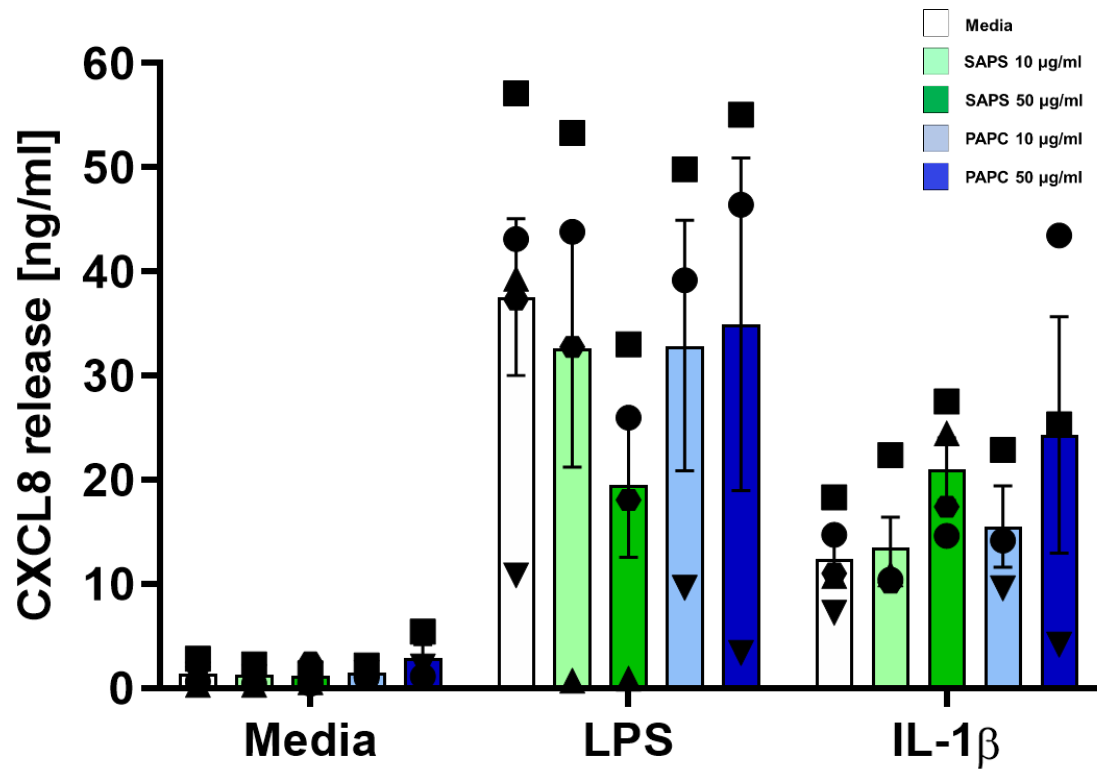


Figure 3.1 SAPS inhibits CXCL8 release from PBMCs stimulated with LPS but not IL-1β. Peripheral blood mononuclear cells (PBMCs) were seeded at 30,000 cells/well in a 24-well plate. Designated wells were treated with SAPS or PAPC (10/50 μg/ml) and incubated for 1 h. Cells were then stimulated with LPS (1 ng/ml), IL-1β (10 ng/ml) or media and incubated for a further 24 h. Cell-free supernatants were generated and levels of CXCL8 determined by ELISA. Data are mean (represented by filled bar) ± SEM of N=3-5 with each replicate performed on freshly prepared PBMCs from independent donors. Individual experiments can be identified by the different shaped symbols. Data were analysed using mixed effects analysis with Tukey's post-test where no significance was reported.

3.3 Modulation of inflammatory signalling in RSV-infected BEAS-2B cells using SAPS/PAPC

Severe RSV infection has often been characterised as an over-exuberant or dysregulated host immune response where excessive proinflammatory cytokines and chemokines such as CXCL8 and CCL5 are frequently detected in hospitalised infants (Culley et al., 2002; Openshaw et al., 2017; Ugonna et al., 2016). These, in part, drive a high influx of immune cells such as neutrophils (N Φ), natural killer (NK) cells and eosinophils that, when in excess, can lead to tissue damage and further pathology within the lungs (Lukens et al., 2010; Vareille et al., 2011). In addition, CXCL8 and CCL5 can serve as respective markers to indicate whether nuclear factor-kappa B (NF- κ B) and interferon regulatory factors (IRF)s have been activated during viral infection, since CCL5 has a greater dependence on IRFs for its production than CXCL8, and were therefore used to monitor the levels and broad patterns of inflammatory responses (Czerkies et al., 2018; Fitzgerald et al., 2003; Stokes et al., 2011).

Initial studies were completed using the immortalised human bronchial epithelial cell line (BEAS-2B). These cells have been extensively used within pulmonary research to study the interactions and responses of respiratory viral infection. Unlike primary cells, cell lines (such as BEAS-2B cells) do not undergo senescence as rapidly and retain many characteristics that resemble the human airways, such as the formation of tight junctions and ability to show relevant immune signalling (Edwards et al., 2016; Hillyer et al., 2018; Satkunanathan et al., 2014; Stokes et al., 2011; Touzelet et al., 2020; Yoon et al., 2007). Previously published research undertaken within my group investigated RV-induced inflammatory responses in BEAS-2B and NHBE cells with comparative results (Mills et al., 2019; Stokes et al., 2016, 2011). In addition, RSV has been historically investigated in BEAS-2B cells (Kalinowski et al., 2018; Numata et al., 2015, 2013; Yoon et al., 2007). These data therefore support the use of BEAS-2B cell culture as an initial model to investigate viral infections.

3.3.1 SAPS significantly reduces the production of CXCL8 and CCL5 from RSV-infected BEAS-2B cells

Preliminary investigations undertaken during my MSc and prior to commencing my PhD, investigated the use of two RSV multiplicities of infection (MOI) of 0.4 and 1 to infect BEAS-2B cells and assess the effect of SAPS/PAPC treatment on CXCL8 and CCL5 release when applied at a range of time points either pre, post or during RSV infection of the cells. These data indicated that SAPS was most efficacious when simultaneously incubated with RSV during the 2 h infection period and reapplied at 0 h (immediately after unbound RSV were removed) (data not shown). It was therefore decided that this treatment time point would be predominantly used (unless otherwise stated) for investigative experiments throughout this project. A summary timeline is provided which outlines the experimental procedure (**Figure 3.2**).

BEAS-2B cells were either mock infected with basal medium or infected with two different MOI of RSV where the ratio of virus to cell was either 0.4 or 1. Mock and RSV-infected cells were co-incubated with SAPS or PAPC (50 µg/ml) for the 2 h infection period (Section 2.2.7). After 24 and 48 h, supernatants were analysed to determine CXCL8 and CCL5 production via ELISA (Section 2.6). Standard viral controls were also included in these initial studies to confirm that any differences in cytokine release were attributable to RSV infection alone. Controls included ultraviolet (UV)-inactivated virus (intact virions with damaged viral RNA), filtrate RSV (containing no infective virions) and HEp-2 media alone (in which the RSV is propagated).

The results demonstrated that cells infected with RSV (MOI 0.4) showed a marked increase in CXCL8 production at both 24 h: 4.2 (\pm 1.4) ng/ml and 48 h: 6.1 (\pm 1.6) ng/ml post infection. However, RSV-infected cells that had been co-incubated with SAPS released significantly less CXCL8, with 1.7 (\pm 1.9) ng/ml at 24 h (**Figure 3.3 A**) and 2 (\pm 1.9) ng/ml at 48 h (**Figure 3.3 B**) compared to RSV alone. SAPS had a similar effect on cells infected with the higher concentration of RSV (MOI 1) where CXCL8 production was significantly reduced from 5.9 (\pm

1.4) ng/ml to 1.7 (\pm 0.3) ng/ml at 24 h post infection and 6.5 (\pm 0.9) ng/ml to 2 (\pm 0.4) ng/ml at 48 h (**Figure 3.3 A, B**). In contrast, the comparative liposome PAPC did not inhibit CXCL8 release at either time point or with either MOI of virus (**Figure 3.3 A, B**). Conversely, cells that were infected with RSV (MOI 1) and co-incubated with PAPC resulted in a significant increase in CXCL8 at 24 h and 48 h (**Figure 3.3 A, B**). There were therefore significant differences in CXCL8 production between RSV-infected cells that had been co-incubated with SAPS to those treated with PAPC (**Figure 3.3 A, B**).

The inhibitory effects of SAPS were more profound on CCL5 production from RSV-infected cells (**Figure 3.3 C, D**). At 24 h, cells infected with RSV (MOI 0.4) alone produced around 61.3 (\pm 9.3) ng/ml CCL5, whereas this was significantly decreased to 0.9 (\pm 0.2) ng/ml when cells had been co-incubated with SAPS (**Figure 3.3 C**). These inhibitory effects were maintained at 48 h (**Figure 3.3 D**) where SAPS significantly reduced CCL5 production from cells infected with both MOIs of RSV (**Figure 3.3 D**).

Unexpectedly, PAPC also demonstrated some inhibitory effects on CCL5 production from RSV-infected (MOI 0.4) cells at both time points at both 24 and 48 h in comparison to untreated cells (**Figure 3.3 C, D**). PAPC also had significant inhibitory effects on RSV-infected cells (MOI 1) at the 48-h time point where the levels of CCL5 were significantly reduced in comparison to untreated cells (**Figure 3.3 D**). However, significant differences between SAPS and PAPC treated cells were again observed, whereby SAPS had an overall stronger inhibitory effect on CCL5 production than PAPC.

UV-inactivated, filtrate RSV and HEp-2 media alone were included as initial controls to confirm that any differences in cytokine release were attributable to RSV infection alone (**Figure 3.3 A-D**). These results indicate that BEAS-2B cells stimulated with HEp-2 media and RSV filtrate alone did not induce a marked increase in CXCL8 (**Figure 3.3 A, B**) or CCL5 (**Figure 3.3 C, D**) at either time point. As expected, and based on published literature (Culley et al., 2006; Glaser et al., 2019; Kalinowski et al., 2018), UV-inactivated virus induced a slight increase in

CXCL8 (**Figure 3.3 A, B**) but not CCL5 (**Figure 3.3 C, D**). Of note, liposome treatment of uninfected cells with either SAPS or PAPC did not result in significantly induced levels of CXCL8 or CCL5 (**Figure 3.3 A-D**).

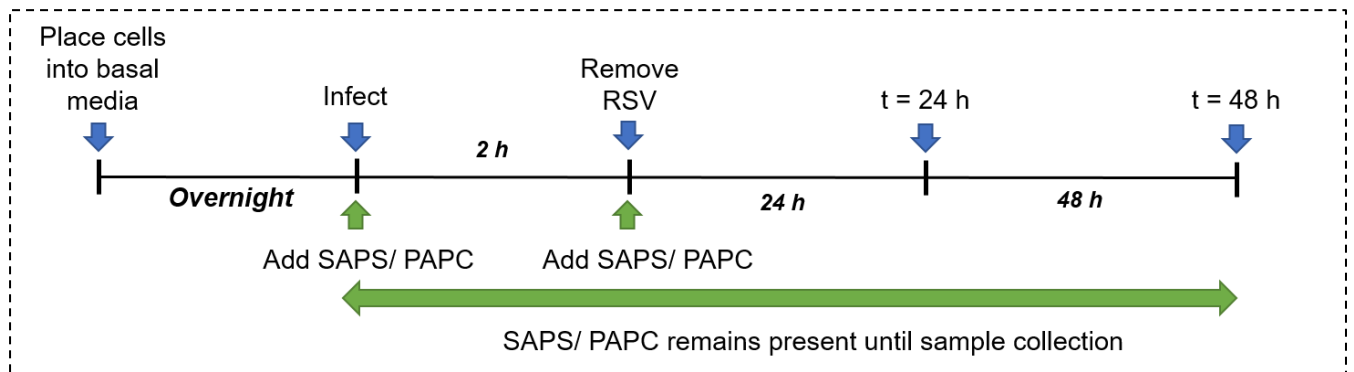


Figure 3.2 Summary timeline indicating the times at which cells are infected with RSV and incubated with SAPS or PAPC. BEAS-2B cells were either stimulated with basal medium or infected with two different multiplicities of infection (MOI) of RSV where the ratio of virus to cell was either 0.4 or 1. Cells stimulated with media or infected with RSV, were co-incubated with SAPS or PAPC (50 µg/ml) for the 2 h infection period. Unbound virus was removed and placed in fresh basal medium. Selected wells were treated once more with either SAPS/PAPC which remained present on the cells until sample collection at 24 and 48 h, where supernatants were collected and analysed to determine CXCL8 and CCL5 production via ELISA.

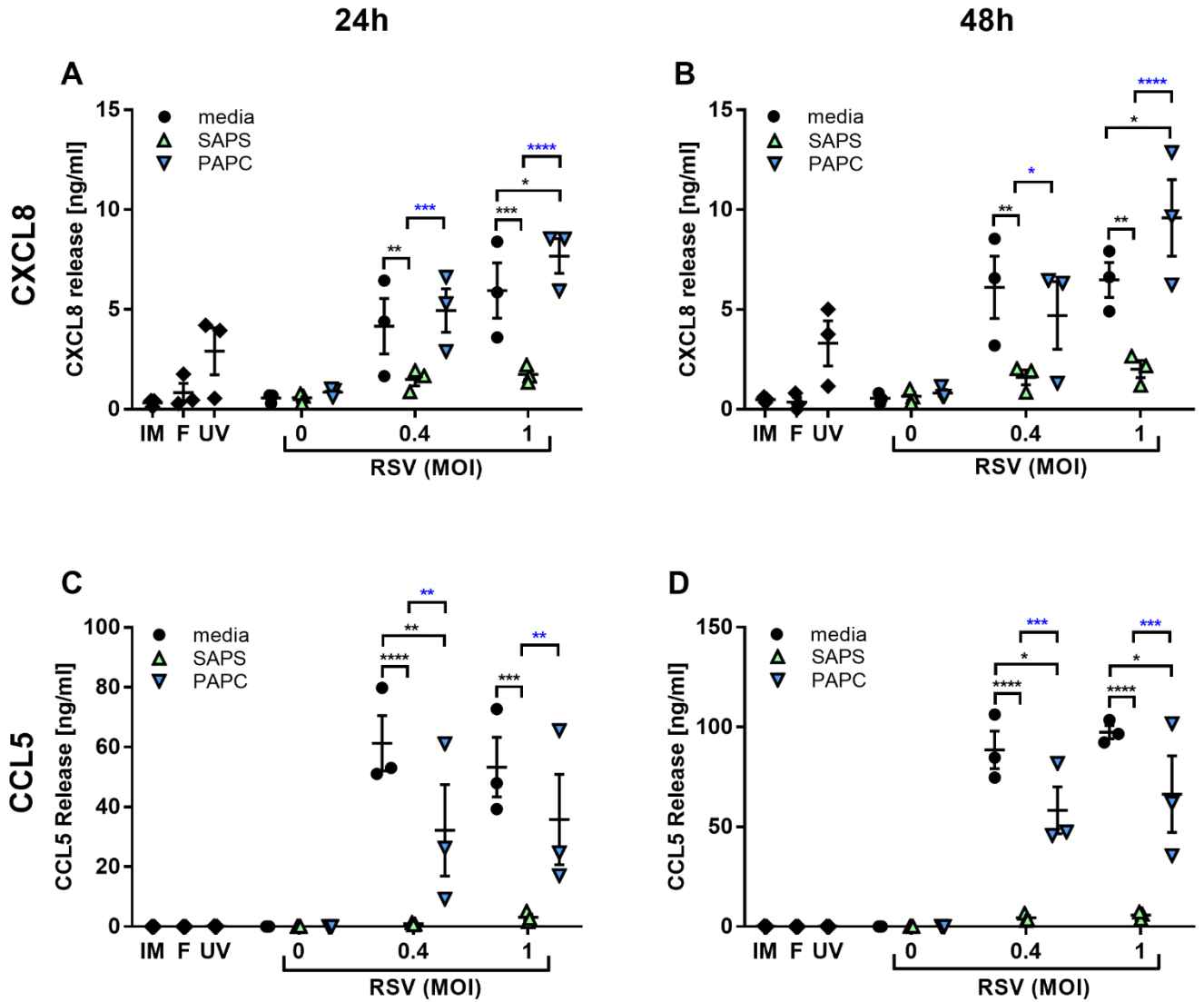


Figure 3.3 SAPS significantly reduces CXCL8 and CCL5 production from RSV-infected BEAS-2B cells. BEAS-2B cells were grown to 80% confluence in 12-well plates and infected with RSV A2 (MOI 0.4 or 1.0), UV-inactivated RSV (UV), RSV filtrate (F) or stimulated with infection media (IM) or normal (RPMI) growth media (0). Designated cells were simultaneously incubated with SAPS or PAPC (50 μ g/ml) which remained on the cells throughout. The cells were incubated for 2 h then washed to remove any unbound virus and designated wells treated once more with SAPS or PAPC (50 μ g/ml). After 24 (A, C) and 48 h (B, D), cell-free supernatants were generated and CXCL8 (A, B) and CCL5 (C, D) were quantified by ELISA. Data are mean \pm SEM of N=3 independent experiments, with each replicate performed on a separate passage of BEAS-2B cells. Data were analysed using a two-way ANOVA and Tukey's multiple comparisons test. Significant differences are indicated by * $p < 0.05$, ** $p < 0.01$, *** $p < 0.001$ and **** $p < 0.0001$. Blue stars indicate significant differences between SAPS and PAPC treated cells.

3.3.2 SAPS does not reduce BEAS-2B cell viability or impact RSV-induced cell death

Phosphatidylserine (lipid component of SAPS) and phosphatidylcholine (lipid component of PAPC) are naturally occurring lipid species that make up pulmonary surfactant (Agassandian and Mallampalli, 2013; Ji et al., 2021; Kuronuma et al., 2009; Milad and Morissette, 2021). Liposomes consisting of these naturally occurring lipids have been used not only within my research group, but have also been utilised in other published work, where it has been demonstrated that liposomes composed of naturally occurring lipids including phosphatidylinositol, phosphatidylethanolamine and phosphatidylglycerol) can be used both *in vitro* and *in vivo* to modulate viral infectivity and resulting immune responses without associated cytotoxic effects (Numata et al., 2015, 2012, 2010; Voelker and Numata, 2019). Our previously published data (Stokes et al., 2016) demonstrated that neither SAPS nor PAPC (up to 50 µg/ml) were cytotoxic in the immortalised BEAS-2B and primary bronchial epithelial cell cultures, however it was important to confirm these data and ensure that SAPS and/or PAPC were not potentiating cell death in RSV-infected BEAS-2B cells in this study. RSV can also impact on cell viability and therefore it was important to monitor BEAS-2B cell viability in response to RSV infection to ensure that any outputs (such as cytokine/chemokine production) were not downregulated because of overall decreased cell viability rather than a direct response to liposome treatment.

An MTT (3-(4,5-dimethylthiazol-2-yl)-2,5-diphenyltetrazolium bromide) assay (Section 2.4.1) was used to assess the viability of BEAS-2B cells. The levels of NADPH production from metabolically active cell cultures were quantified, serving as an indicator of cell viability. BEAS-2B cells were either stimulated with media or infected with RSV (MOI 0.4 or MOI 1). Selected cells were additionally co-incubated with SAPS/PAPC (50 µg/ml), and levels of viable cells were quantified 24 and 48 h after viral infection.

As expected, BEAS-2B cells that were infected with RSV had decreased cell viability over the 24 (**Figure 3.4 A**) and 48 h (**Figure 3.4 B**) period in comparison to uninfected media controls.

RSV (MOI 0.4) infected cells had significantly reduced cell viability at 48 h (22% reduction in comparison to uninfected cells) and the higher MOI of virus (MOI 1) resulted in a 42% decrease in viable cells (**Figure 3.4 A, B**). Conversely, RSV-infected cells (MOI 0.4 and 1) that had been co-incubated with SAPS did not have reduced cell viability at either time point (**Figure 3.4 A, B**). Cell viability as assessed by the MTT assay was modestly lower in RSV-infected cells treated with PAPC when compared with cells infected with RSV without a lipid treatment (**Figure 3.4 A, B**).

Cells treated with filtrate RSV, where RSV virions have been removed, had a non-significant increase in viable cells at 48 h (**Figure 3.4 C**) in comparison to the media control. Cells that were stimulated with UV-inactivated virus (where viral RNA has been degraded) (MOI 1) had some reduction of cell viability at 48 h only (**Figure 3.4 C**). Staurosporine, which is used as a positive control for cell death, resulted in a significant decrease of viable cells (as expected) at both 24 and 48 h (**Figure 3.4 C**). Uninfected BEAS-2B cells that were treated with SAPS or PAPC only, did not have significantly decreased cell viability at 24 or 48 h, however a slight reduction in viability (~20%) was observed 48 h after treatment for both liposomes relative to untreated cells (**Figure 3.4 C**).

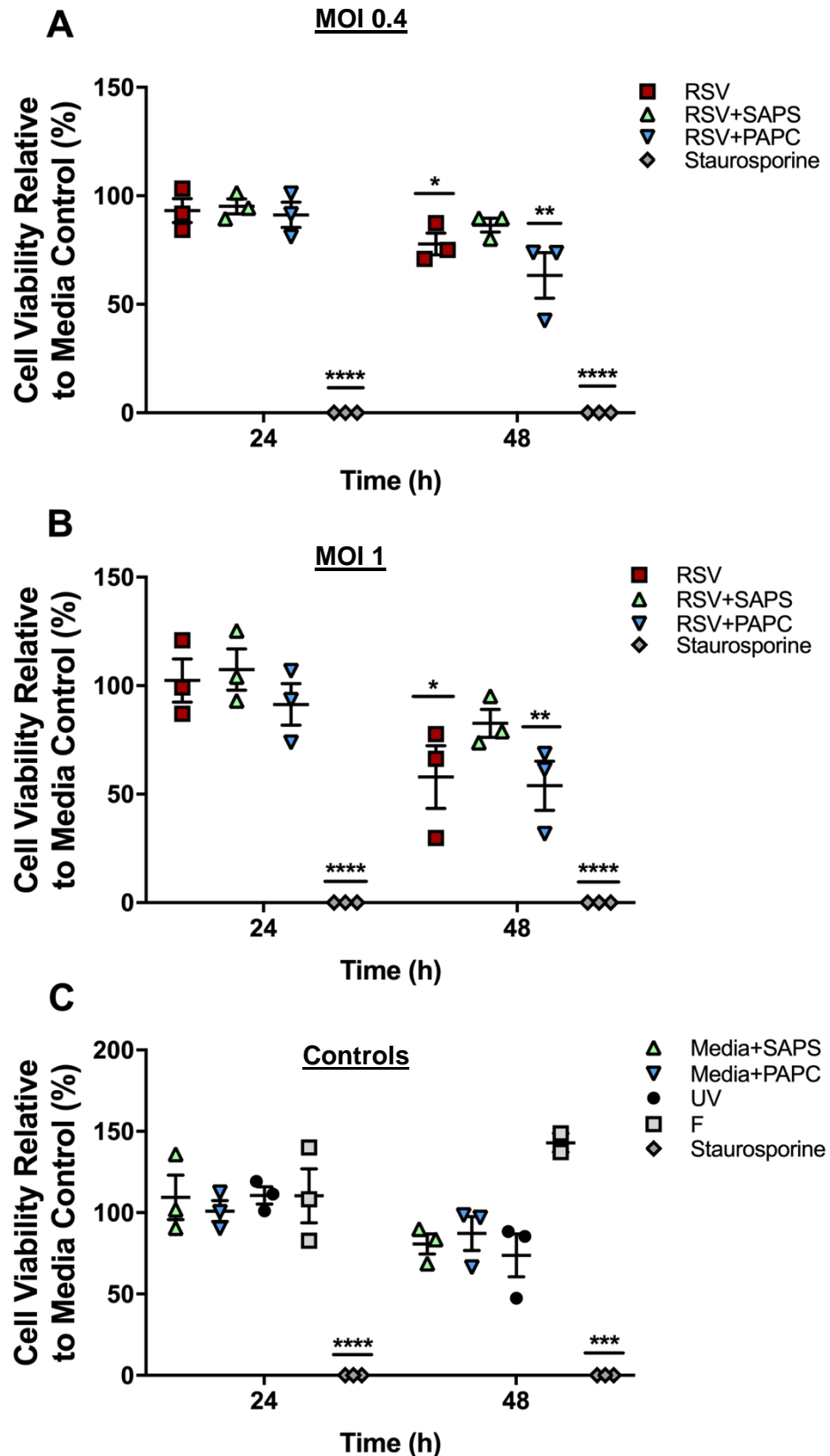


Figure 3.4 The effect of SAPS/PAPC treatment on BEAS-2B cell viability. BEAS-2B cells were infected with RSV A2 MOI 0.4 (A) or MOI 1.0 (B). Viral controls (C) were stimulated with UV-inactivated RSV (UV), RSV filtrate (F) or normal (RPMI) growth media. Designated cells were simultaneously incubated with SAPS or PAPC (50 μ g/ml) which remained on the cells throughout. The cells were incubated for 2 h then washed to remove any unbound virus and designated wells treated once more with SAPS or PAPC (50 μ g/ml). Staurosporine (S) was used as a positive control for cell death. Cell viability was determined at 24 or 48 h using an MTT assay. Data are mean \pm SEM of N=3 independent experiments, with each replicate performed on separate passages of BEAS-2B. Raw data were analysed using a two-way ANOVA with Dunnett's post-test comparing data to the media control only. Data presented indicates the cell viability relative to the relevant media control which has been normalised to 100%. Significant differences are indicated by * $p < 0.05$, ** $p < 0.01$, *** $p < 0.001$ and **** $p < 0.0001$.

3.4 Optimisation of RSV infection of normal human bronchial epithelial (NHBE) and HBEC3-KT cells

Whilst BEAS-2B cells are a valuable model system, using primary airway epithelial cells as the next step for our investigations was important, as these cells are a potentially more representative model of *in vivo* behaviours (Broadbent et al., 2020; Sims et al., 2008). However, primary cells are harder to culture in a lab setting in comparison to cell lines. In addition, normal human primary bronchial epithelial cells have limited life spans and reduced proliferation efficiency, making experimental work challenging (Broadbent et al., 2020; Bukowy-Bieryłło, 2021).

3.4.1 Optimisation of NHBE and HBEC3-KT cell cultures

NHBE cells were obtained from the commercial supplier Lonza. This supplier had been selected as they had cells available from healthy donors and those with airways disease. Lonza cells had not previously been used in our lab group and therefore required extensive optimisation to culture (Table 3.1). Our lab had extensive experience of using primary airway epithelial cells, airway smooth muscle cells and vascular endothelial and smooth muscle cells from other suppliers. Despite following the strict instructions outlined in the protocol from Lonza, many of the donor cells did not grow well in our lab. The cells were seeded into the recommended number of tissue culture flasks (based on the detailed seeding and viability numbers given to us by Lonza) however based on these recommendations, the cells did not grow to confluency and seemed to reach senescence very quickly, meaning there were no cells available for experimentation. Unfortunately, due to these ongoing issues with the NHBE cells and considerable time taken (14 months) to troubleshoot their growth, the decision was made to use an alternative cell model (HBEC3-KT cells) for any future studies with some of the main findings recapitulated in NHBE cells where possible. The normal human bronchial epithelial cells (HBEC3-KT) were originally obtained from commercial suppliers ATCC and were a kind gift from Professor Colin D Bingle from within our department. These cells were

life-span extended through transfection of human primary bronchial epithelial cells with a retroviral construct containing mouse cyclin-dependent kinase (CDK) 4 and human telomerase reverse transcriptase (hTERT), lending them to continued application in viral infection studies compared to the NHBE cells with senescent characteristic (Nakauchi et al., 2019; Ramirez et al., 2004). In addition, they have been successfully cultured at air-liquid-interface (ALI) and as such, have the potential to be a more representative model of normal airway cells than the immortalised BEAS-2B cell line, and act as a good intermediate step to extend investigations within this project where NHBE cells were unattainable. As such, the data within this thesis was conducted predominantly in HBEC3-KT cells with key experiments recapitulated in NHBE cells where possible.

To determine optimal experimental conditions for studies in both the HBEC3-KT and NHBE cells, a suitable MOI (multiplicity of infection) of RSV was first determined that would induce a measurable response in cytokine release but not have excessive detrimental effects on whole cell viability, particularly when collecting samples at 48 h post RSV-infection. Although an MOI of 1 was used in the BEAS-2B cells, the literature indicated that NHBE cells may be more susceptible to RSV infection, and thus a lower range of MOIs (from 0.1 to 0.8) was studied (Makris et al., 2016; Satkunanathan et al., 2014).

NHBE and HBEC3-KT cells were grown to 80% confluency in 12-well plates and then infected with increasing MOI of RSV A2 for 2 h. After unbound virus was removed, cells were placed in the appropriate basal medium (Section 2.2.7). Cell-free supernatant samples were generated, and cell viability analysed at 24 and/or 48 h post infection.

Table 3.1 Steps taken to optimise NHBE culture

Issue	Steps Taken	Result
Cells not detaching during split process	Increase volume of trypsin	Cells still remaining on bottom of flask
	Increased number of washes with HEPES-BSS	Slight improvement but not 100% reliable
	Visit from LONZA technical support – replaced trypsin	Detachment greatly improved
	Aliquot trypsin into smaller volumes to avoid constant freeze thawing.	Detachment more reliable
	Passage cells at 80% confluence	Cells detaching easier than when at 90% confluence
Seeding efficiency on arrival into the lab	Split cells into more 25 cm ² flasks to neutralise DMSO	Higher proportion of cells recoverable from initial split
Cells congregating into the middle of tissue culture plates	Keep plates on flat surface and move in horizontal motion then leave to settle for 5 mins before moving to incubator	Cells grow in even monolayer with minimal detachment in centre of well
Seeding time and viability	Confirm seeding efficiency, doubling time and viability of selected donors	Account for these variables when seeding cells for experiments
Gaining accurate cell count	Increased volume of trypsin in wells	Cells clumping, accurate count still difficult
	Increased washing of the wells and longer incubation in trypsin	More accurate cell count that coincides with data sheet

3.4.1.1 Identification of contaminant in RSV stocks

During the transition to HBEC3-KT cells, it was noted that the supernatant of the RSV-infected cells had a turbid appearance 24 h after RSV infection, indicative of possible bacterial/fungal contamination. Initial investigations were carried out to confirm whether the contamination may have been from the stock of HBEC3-KT cells we were using by seeding HBEC3-KT cells into a tissue culture plate alongside HBEC3-KT cells from Professor Colin Bingle's lab group. Cells were either stimulated with our stocks of culture medium or infected with the same stock of RSV (MOI 0.4 or 1.2) for 2 hours. Unbound virus was removed and the HBEC3-KT cells incubated for 24 h. Visual checks of the cell monolayers were carried out the following day (**Appendix 1, photo 1**). The uninfected HBEC3-KT cells from both our lab and Professor Colin Bingle's lab looked as normal whereas the supernatant from both populations of HBEC3-KT cells that had been infected with RSV had the distinctive cloudy appearance. From these observations, it was decided that the contamination may have stemmed from the RSV stocks. Supernatants were therefore collected from the plate and 50 µl aliquoted onto a Luria-Bertani (LB) agar plate to determine if bacterial colonies were present. A neat sample (100 µl) was also taken from one of the frozen RSV stock vials (RSV A2 P6) and streaked onto a LB agar plate. The agar plates were allowed to dry then placed in an incubator at 37°C, 5% CO₂ for 48 h. Visual observation indicated that there was bacterial growth in each of the RSV-infected supernatant samples and in the RSV stock vial (**Appendix 1, Photo 2 and Photo 3**). A Gram stain was completed by a fellow PhD student (Rebecca Hull) but the results were inconclusive regarding bacterial identification. Previous stock vials of RSV, including the original vial (P4) gifted from Dr Fiona Culley at Imperial College London also tested positive for bacterial growth indicating contamination in the original stock vials. The stocks at P5 and P6 including the control antigen are shown (**Appendix 1, Photo 4**). The control antigen stocks did not contain bacterial contamination indicating that the bacterial contaminant had originated from the older RSV stocks rather than the media or equipment.

Of note, the turbidity observed in the RSV-infected HBEC3-KT cells was not seen during the NHBE experimental investigations. It was reasoned that the antibiotics present in the NHBE cell culture medium (gentamicin sulfate-amphotericin-GA-1000) (Table 2.1), was more bactericidal than the antibiotics included in the HBEC3-KT media (penicillin-streptomycin-PS). To determine the differential effects of either GA-1000 or PS present in the HBEC3-KT culture medium to control the bacterial infected RSV stocks, HBEC3-KT cells were infected with RSV (MOI 0.4 or 1.2) in media containing either PS or GA-1000. Cells were incubated for 24 h then checked for visual signs of bacterial growth in the medium. Turbidity was noted in the RSV-infected cells that had been incubated with media containing PS, particularly with the higher MOI of 1.2. This was not seen in HBEC3-KT cells that were infected with RSV in the presence of GA-1000 (**Appendix 1, Photo 5**). Bacterial contamination was once again confirmed on LB agar plates.

Due to these findings, the decision was made to generate new RSV stocks (Section 2.2.6.1) however GA-1000 was included in the HEP-2 infection media to kill any bacteria present in the frozen stocks during the initial stages of propagation. After the first day of RSV propagation, spent media was removed from the flask and replaced with fresh HEP-2 infection media without antibiotics to ensure that no antibiotics would be present in the final frozen viral stocks. Titration was carried out as described (Section 2.2.6.2). In addition, four separate aliquots of the newly generated RSV stocks (P7) were tested once more on LB agar plates and incubated for up to 48 hours 37°C, 5% CO₂. No bacterial growth was observed from any of the vials.

Given the limited time (due to COVID-19) and issues acquiring new stocks of RSV from ATCC, the procedures (detailed above) were conducted to reduce the effects of the bacterial contamination in the RSV stocks. However, it cannot be confirmed with certainty that no bacteria or bacterial products remained that may have confounded signalling pathways and their outputs. Therefore, the following data should be interpreted with this in mind.

3.4.2 RSV induces CXCL8 and CCL5 release in an MOI-dependent manner with limited effects on cell viability

Pilot experiments were performed with HBEC3-KT and NHBE cells to gain insights into levels and patterns of chemokine production and cell viability prior to more extensive experiments with SAPS. RSV infection caused the release of CXCL8 and CCL5 in an MOI-dependent manner from both NHBE (**Figure 3.5 A, B**) and HBEC3-KT (**Figure 3.6 A-D**) cells. In NHBE cells, although the release of both CXCL8 (**Figure 3.5 A**) and CCL5 (**Figure 3.5 B**) increased in an MOI-dependent manner, some donor variability was observed in the overall levels of CXCL8 and CCL5 generated. Only two donors could be tested because of cell growth and maintenance issues discussed above.

In HBEC3-KT cells, the levels of CXCL8 and CCL5 increased further between the 24 and 48 h time period (**Figure 3.6 A-D**). This was particularly evident for CCL5, where the levels of CCL5 almost doubled from the initial 24 h time point to the 48-h period in HBEC3-KT cells, independent of RSV MOI (**Figure 3.6 C, D**).

The levels of CXCL8 produced from the HBEC3-KT cells (ranging from MOI 0.1 = 2.23 ng/ml up to MOI 0.8 = 11.28 ng/ml) by 48 h (**Figure 3.6 B**) were comparable to the overall levels of CXCL8 produced from the NHBE cells at the same time point, where MOI 0.1 = 2.13 ng/ml and up to 12.93 ng/ml in cells infected with MOI 0.8 (**Figure 3.6 A**). A similar range of CCL5 production was demonstrated between cell types at 48 h where CCL5 in the HBEC3-KT cells increased from MOI 0.1 = 17.05 ng/ml up to 57.43 ng/ml in MOI = 0.8 (**Figure 3.6 D**) and in NHBE cells MOI 0.1 = 9.62 up to 57.11 ng/ml in MOI 0.8 (**Figure 3.5 B**).

3.4.3 RSV moderately reduces cell viability of HBEC3-KT and NHBE cells

In these pilot experiments, the viability of RSV-infected cells, in comparison to uninfected cells, appeared lower at 24 and 48 h in HBEC3-KT (**Figure 3.6 E, F**) cells and at 48 h post infection in NHBE cells (**Figure 3.5 C**). As anticipated, cells infected with the highest RSV MOI (0.8) had the greatest reduction in cell viability at 48 h in both cell types with 27.81% decrease in

HBEC3-KT (**Figure 3.6 F**) and 14.86% average decrease in NHBE cells (**Figure 3.5 C**). Again, there was some variation between the two independent NHBE donors in their response to varying MOI infections and associated cell viability (**Figure 3.5 C**).

Based on these data, an MOI of 0.4 was selected for forthcoming experimental investigations. The MOI of 0.4 (also used previously in the BEAS-2B cells), did not reduce overall cell viability by more than 10% in both cell types which suggested it may be a good MOI to use in future experiments where sample collection would be required over a period of 48 h. In addition, the MOI of 0.4 induced measurable levels of CXCL8 and CCL5 which would enable elucidation of the effect of SAPS treatment on production in future challenge experiments.

The data also indicates that any decrease in cell viability induced by RSV at MOI 0.4 did not reduce the capacity of cells to produce CXCL8 and CCL5 at 24 or 48 h. In addition, although a small data set is shown, the optimisation data indicate that the response of NHBE and HBEC3-KT cells to RSV may be comparable and supports the use of HBEC3-KT cells as a suitable airway epithelial model when NHBE cells are unattainable.

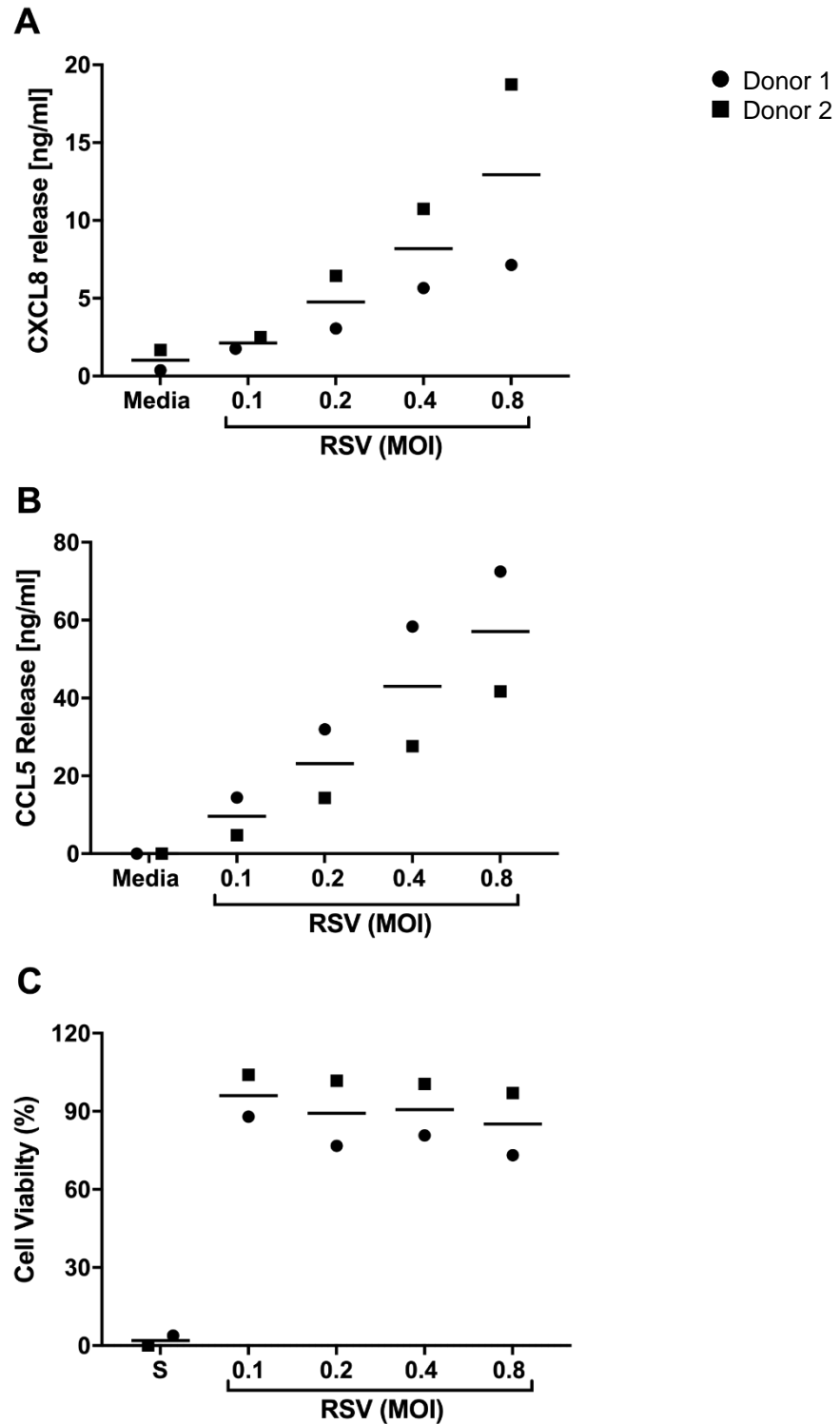


Figure 3.5 The effect of increased RSV MOI on the release of CXCL8 and CCL5 and cell viability in two independent NHBE donors. NHBE cells were infected with RSV A2 (MOI 0.1 – 0.8) or stimulated normal growth media. Cells were incubated for 2 h then cells were washed to remove any unbound virus and fresh medium added. After 48 h, supernatant samples were generated and levels of CXCL8 (A) and CCL5 (B) determined via ELISA. A CellTiter-Glo® assay was completed to determine cell viability (C). Cell viability is displayed relative to the media control which has been normalised to 100%. Data are the mean of two separate NHBE donors as indicated by the different symbols. S=staurosporine.

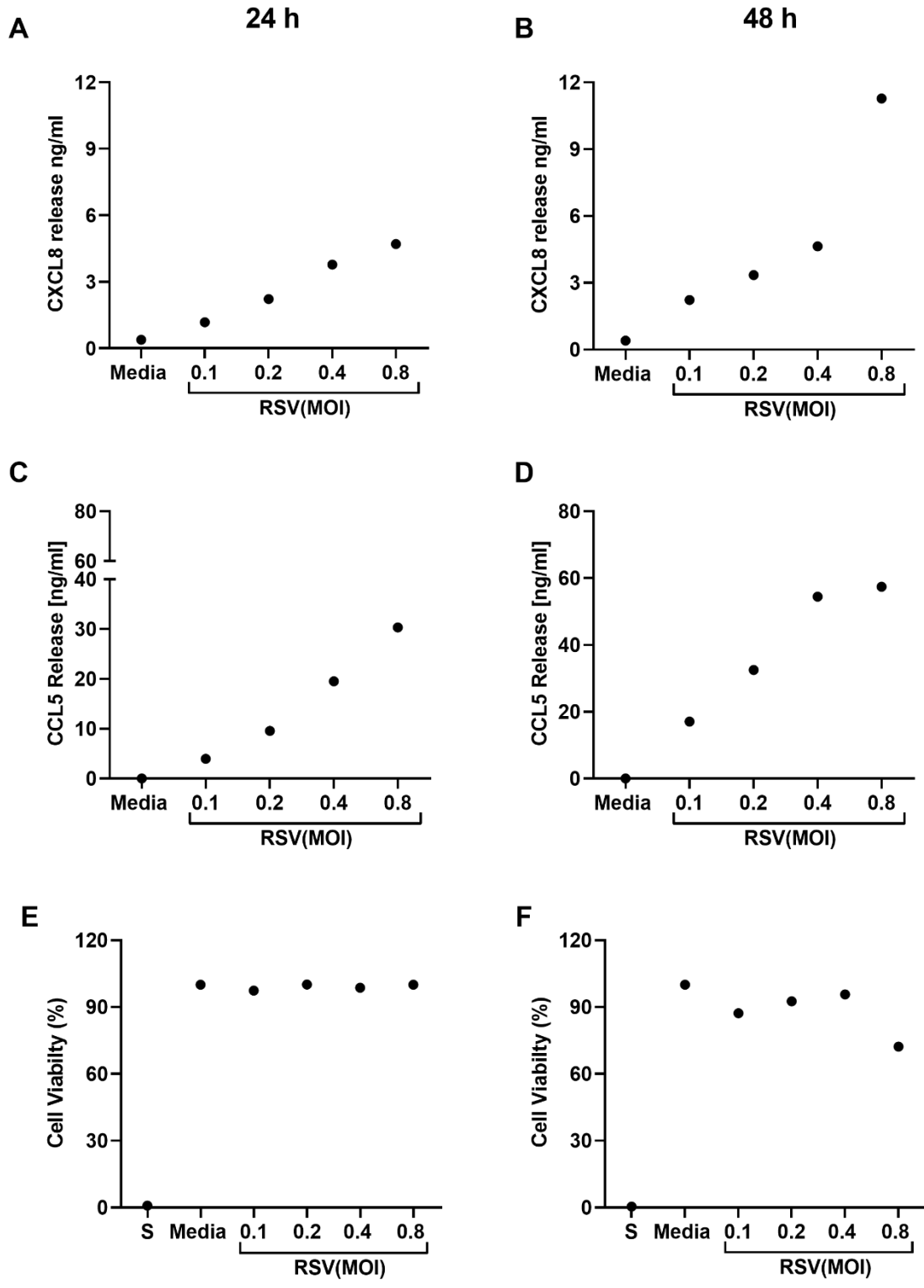


Figure 3.6 The effect of increased RSV MOI on the release of CXCL8 and CCL5 and cell viability in HBEC3-KT cells. HBEC3-KT cells were infected with RSV A2 (MOI 0.1 – 0.8) or stimulated normal growth media for 2 h. Cells were washed to remove any unbound virus and fresh media added. After 24 and 48 h, supernatant samples were generated and levels of CXCL8 (A, B) and CCL5 (C, D) determined via ELISA. A CellTiter-Glo® assay was completed to determine cell viability (E, F). Cell viability is displayed relative to the media control which has been normalised to 100%. Data are from one experiment. S=staurosporine.

3.4.4 SAPS significantly reduces CXCL8 and CCL5 release from RSV-infected NHBE cells

Based on the preceding results (Section 3.4), an MOI of 0.4 was selected for RSV infections in the NHBE and HBEC3-KT experiments. Concentrations of 10 and 25 µg/ml SAPS/PAPC were selected to investigate the modulation of CXCL8 and CCL5 production from RSV-infected cells. The decision to lower the concentration of SAPS/PAPC to be used in the NHBE and HBEC3-KT cells was due to previously published data from my lab group, showing that NHBE cells stimulated with SAPS at a concentration of 50 µg/ml showed minor production of CXCL8 from uninfected cells (Stokes et al., 2016). The lowest concentration used in the Stokes study was 10 µg/ml, which significantly reduced CXCL8 and CCL5 48 h post-RV infection. I therefore selected 10 and 25 µg/ml as the initial concentrations to investigate inflammatory responses from uninfected and RSV-infected NHBE or HBEC3-KT cells.

Because of difficulties culturing NHBE cells, data shown here are from multiple replicates of a single donor tested over sequential passages.

CXCL8 release from RSV-infected NHBE cells increased from 11.8 (\pm 3.9) ng/ml at 24 h (**Figure 3.7 A**) to 17.2 (\pm 6.4) ng/ml by 48 h (**Figure 3.7 B**) and this was significantly reduced by both concentrations of SAPS (10 and 25 µg/ml) by approximately 80% and 90% respectively, at both time points (**Figure 3.7 A, B**). Both concentrations of PAPC reduced CXCL8 from RSV-infected cells but only the highest concentration (25 µg/ml) significantly decreased levels of CXCL8 at both time points, and not to the same extent as SAPS (25 µg/ml) (**Figure 3.7 A, B**). As previously noted, both SAPS and PAPC had modest impacts on uninfected cells (media control) resulting in slightly elevated CXCL8 at both time points, but this was not statistically significant (**Figure 3.7 A, B**).

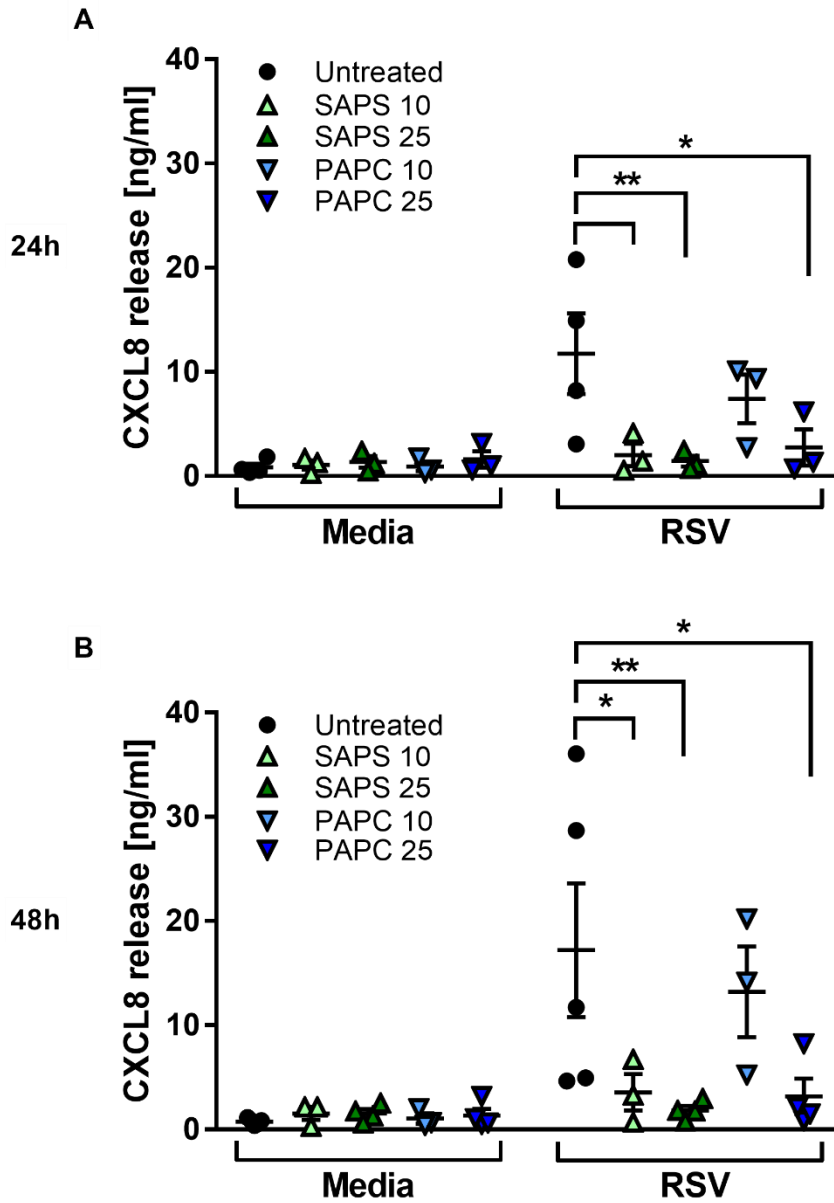


Figure 3.7 SAPS significantly reduces CXCL8 release from RSV-infected NHBE cells. NHBE cells were infected with RSV A2 (MOI 0.4) or stimulated normal growth media. Designated cells were incubated with SAPS or PAPC (10 or 25µg/ml) which remained on the cells throughout the 2 h incubation. After incubation, cells were washed to remove any unbound virus and designated cells treated once more with SAPS or PAPC (10 or 25 µg/ml). After 24 (**A**) and 48 h (**B**), supernatant samples were generated and CXCL8 quantified by ELISA. Data are mean ± SEM of N=3/4 individual experiments in D365. Data were analysed using a two-way ANOVA and Tukey's multiple comparisons test. Significant differences are indicated by *p <0.05, **p <0.01.

RSV infection also resulted in a marked increase of CCL5 24 h post infection with 23.5 (\pm 7.7) ng/ml (**Figure 3.8 A**) which further doubled by 48 h = 45.9 (\pm 15.1) ng/ml (**Figure 3.8 B**). In keeping with the effect on CXCL8 release, RSV-infected cells that had been co-incubated with SAPS had significant and markedly reduced levels of CCL5 production at both time points by approximately 90% (SAPS 10 μ g/ml) or 99% (SAPS 25 μ g/ml) (**Figure 3.8 A, B**). Cells that had been treated with the highest concentration of PAPC also had significantly reduced CCL5 release at both time points however the lowest concentration of PAPC did not greatly reduce CCL5 production at 24 h and contradictorily, induced CCL5 production at 48 h by 18% (**Figure 3.8 A, B**). As expected, and in line with previous data (**Figure 3.3, Figure 3.5, and Figure 3.6**), uninfected cells had no detectable CCL5 and was therefore assigned the lowest value of the standard curve (0.039 ng/ml) where neither SAPS nor PAPC treatment impacted on this (**Figure 3.8 A, B**).

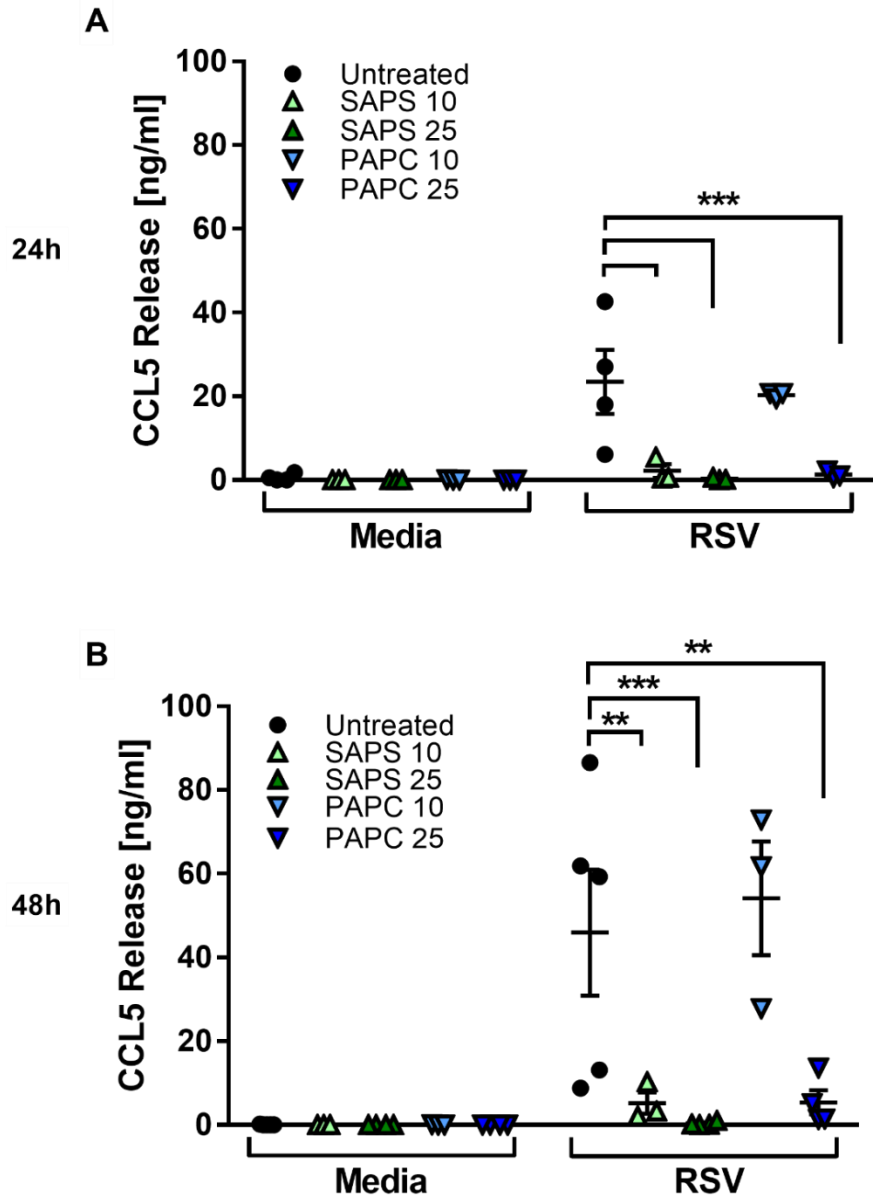


Figure 3.8 SAPS significantly reduces CCL5 release from RSV-infected NHBE cells. NHBE cells were infected with RSV A2 (MOI 0.4) or stimulated normal growth media. Designated cells were incubated with SAPS or PAPC (10 or 25 μ g/ml) which remained on the cells throughout the 2 h incubation. After incubation, cells were washed to remove any unbound virus and designated cells treated once more with SAPS or PAPC (10 or 25 μ g/ml). After 24 (A) and 48 h (B) supernatant samples were generated and CCL5 quantified by ELISA. All data are mean \pm SEM of N=3/5 individual experiments in D365. Data were analysed using a two-way ANOVA and Tukey's multiple comparisons test. Significant differences are indicated by **p <0.01, ***p <0.001.

A concentration of 25 µg/ml SAPS/PAPC was selected for future experimental work, as this concentration had the most significant effect on CXCL8 and CCL5 production without inducing high levels of CXCL8 in uninfected controls (**Figure 3.7 and 3.8**). As these data were generated using one NHBE donor (N=3/5 experimental replicates), the experiment was subsequently repeated in a second NHBE donor to identify any potential donor variation. These experiments were limited to N=1 for each cell donor because of difficulties with primary cell culture. Definitive conclusions cannot therefore be drawn from these experiments, but the cells from both donors appeared to behave similarly.

As shown in **Figure 3.9 A**; the average level of CXCL8 produced from two independent NHBE donors, infected with RSV, was approximately 5 ng/ml 48 h post infection. The NHBE cells that had been co-incubated with SAPS or PAPC (25 µg/ml) resulted in a notable reduction in CXCL8 production compared to untreated RSV-infected cells (**Figure 3.9 A**).

A similar trend was noted in both donors with CCL5 production where RSV-infected cells co-incubated with SAPS or PAPC during RSV infection had markedly reduced CCL5 production compared to untreated cells (**Figure 3.9 B**).

To determine that CXCL8 and CCL5 were not reduced solely due to a reduction in viable cells, a cell viability assay was conducted alongside supernatant analysis (Section 2.4.2). These data were also used to confirm (in line with previous published findings) that SAPS and PAPC (25 µg/ml) were not having a direct, detrimental effect on the NHBE cell viability 48 h post treatment. The results indicate that neither SAPS nor PAPC potentiated cell death in the uninfected or RSV-infected cells at 48 h (**Figure 3.9 C**). There were modest variations in the overall concentrations of CXCL8 and CCL5 produced from the two different donors but both donor cells demonstrated similar patterns in regard to SAPS/PAPC treatment (**Figure 3.9 A, B and C**).

3.4.5 SAPS significantly reduces CXCL8 and CCL5 release from RSV-infected HBEC3-KT cells

Because of substantial problems studying NHBE cells, I moved to examine the actions of SAPS and PAPC in models of RSV infection in HBEC3-KT cells. These cells were infected and stimulated with SAPS/PAPC (25 µg/ml) as previously described (**Figure 3.2**) and the levels of CXCL8 and CCL5 were quantified at 24 and 48 h post infection (**Figure 3.10**). HBEC3-KT cells that were infected with RSV in the presence of SAPS had significantly reduced (~ 85%) CXCL8 production at both 24 (**Figure 3.10 A**) and 48 h (**Figure 3.10 B**). There was a similar trend seen for CCL5 where RSV-infected cells treated with SAPS had significantly reduced (by ~ 99%) CCL5 production at both 24 (**Figure 3.10 C**) and 48 h (**Figure 3.10 C**).

In contrast, PAPC treatment did not inhibit the generation of CXCL8 or CCL5 in response to RSV infection (**Figure 3.10 A, B**).

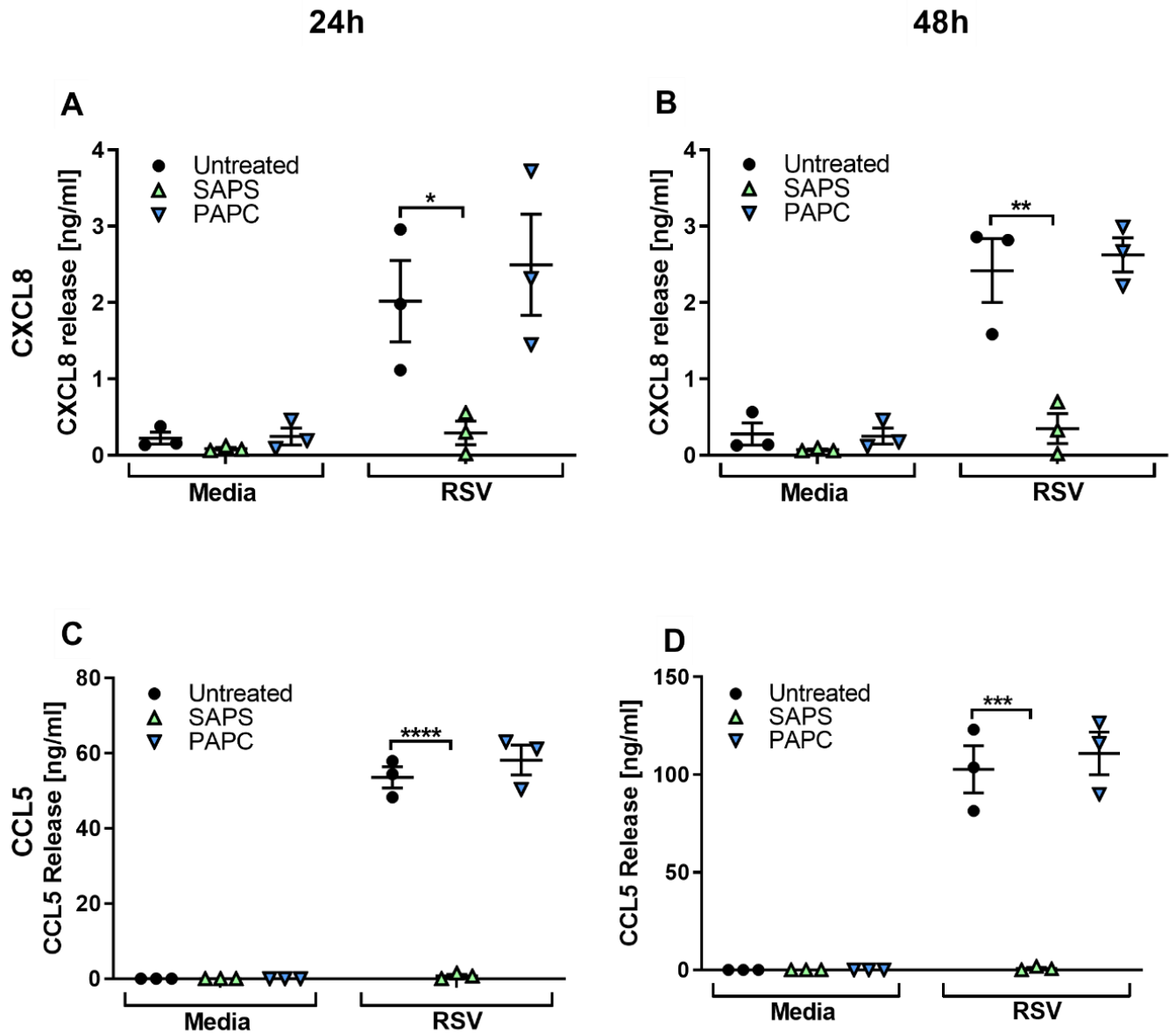


Figure 3.10 SAPS significantly reduces CXCL8 and CCL5 release from RSV-infected HBEC3-KT cells. HBEC3-KT cells were infected with RSV A2 (MOI 0.4) or stimulated with normal growth media. Designated cells were incubated with SAPS or PAPC (25 μ g/ml) which remained on the cells throughout the 2 h incubation. After incubation, cells were washed to remove any unbound virus and designated cells treated once more with SAPS or PAPC (25 μ g/ml). After 24 and 48 h, supernatant samples were generated and CXCL8 (A, B) and CCL5 (C, D) quantified by ELISA. All data are mean \pm SEM of N=3 individual experiments. Data were analysed using a two-way ANOVA and Tukey's multiple comparisons test. Significant differences are indicated by *p < 0.05, **p < 0.01, ***p < 0.001, and ****p < 0.0001.

3.5 The efficacy of SAPS as a post-treatment

The experiments in this chapter thus far have investigated the modulatory effect of SAPS treatment on CXCL8 and CCL5 release when it is applied at the same time as mock/RSV infection of the airway epithelial cells. In a clinical setting, individuals will already have an established RSV infection when presenting at the doctor or hospital and it was therefore important to investigate whether SAPS had similar modulatory effects on the release of CXCL8 and CCL5 when applied as a post-treatment. Previously published work (Stokes et al., 2016) demonstrated that SAPS was able to significantly reduce CXCL8 and CCL5 from RV-infected BEAS-2B and NHBE cells when applied either 1, 4 or 8 h after an established viral infection. Therefore, to determine if SAPS would have comparable inhibitory effects when applied as a post treatment in HBEC3-KT cells infected with RSV, a range of post treatment time points were investigated.

HBEC3-KT cells were either stimulated with media or infected with RSV (MOI 0.4) for 2 h after which, unbound virus was removed and fresh basal media added and designated time = 0 h. SAPS or PAPC (25 µg/ml) were added directly into the media of the appropriate well at either 2, 4, 8 or 24 h post RSV-infection/media stimulation. These time points were selected to determine what efficacy (if any) SAPS would have on CXCL8 and CCL5 production as RSV infection progressed within the cells. A summary timeline of the infection and treatment protocol is displayed (**Figure 3.11**).

3.5.1 Exploring the immunomodulatory effects of SAPS when applied after an established RSV infection

SAPS and PAPC both significantly reduced the production of CXCL8 at 24 h from RSV-infected cells when treatment was applied at 2, 4 and 8 h post infection in comparison to untreated cells (**Figure 3.12 C**). It is notable that, although still significant, the later the post treatment is applied to infected cells, the less inhibitory SAPS is on CXCL8 release; (2 h = 53%, 4 h = 43% and 8 h = 23% reduction) (**Figure 3.12 C**). In addition, the inhibitory effects

of SAPS and PAPC post treatments were not maintained at 48 h post RSV-infection (**Figure 3.12 D**). No significant effects were noted from the uninfected control cells (stimulated with media) that were also co-incubated with SAPS or PAPC 2, 4, 8 and 24 h post media stimulation (**Figure 3.12 A, B**).

SAPS and PAPC were less effective at reducing CCL5 production when administered post RSV-infection (**Figure 3.13 C, D**). The addition of SAPS at 2 or 4 h post RSV-infection significantly reduced the levels of CCL5 released from the cells at 24 h; (2 h = 20% and 4 h = 13% reduction in CCL5) in comparison to untreated cells or those treated with PAPC (**Figure 3.13 C**). As was noted when examining production of CXCL8, (**Figure 3.13**), neither SAPS nor PAPC had any inhibitory effects on CCL5 production by the 48 h sample time point, where the values between untreated and SAPS/PAPC-treated cells were similar to those of the untreated RSV-infected cells (**Figure 3.13 D**).

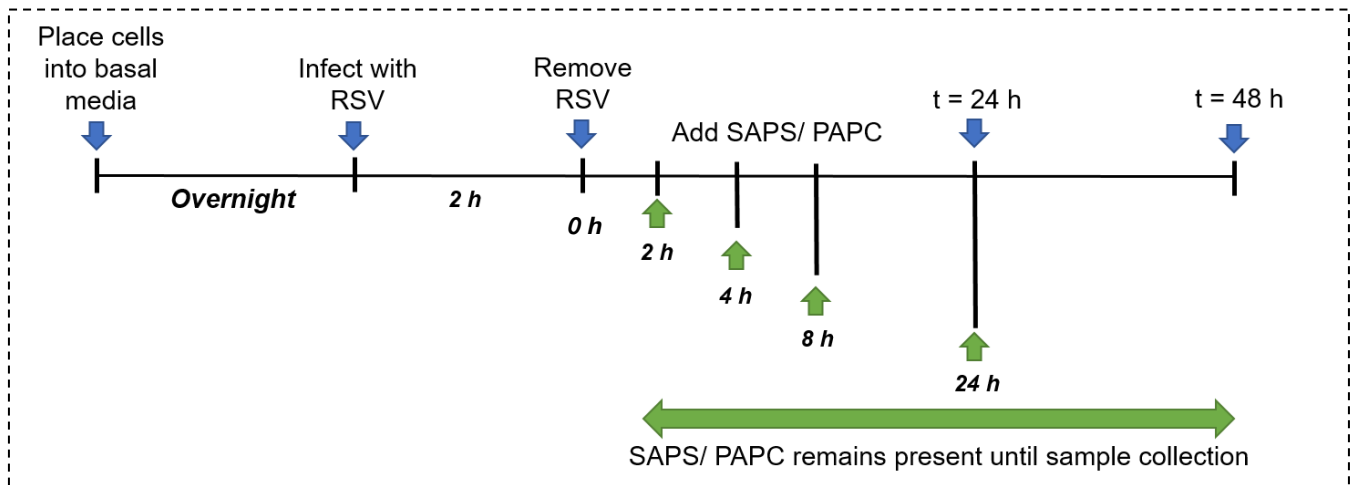


Figure 3.11 Summary timeline indicating the times when cells were infected with RSV and incubated with SAPS or PAPC. HBEC3-KT cells were either stimulated with media or infected with RSV A2 (MOI 0.4) for 2 h. Unbound virus was removed and fresh basal medium was added to the cells where time = 0 h. Selected wells were treated with either SAPS/PAPC (25 µg/ml) at either 2, 4, 8 or 24 h after RSV infection which remained present on the cells until sample collection at 24 and 48 h, where supernatants were collected and analysed to determine CXCL8 and CCL5 production via ELISA.

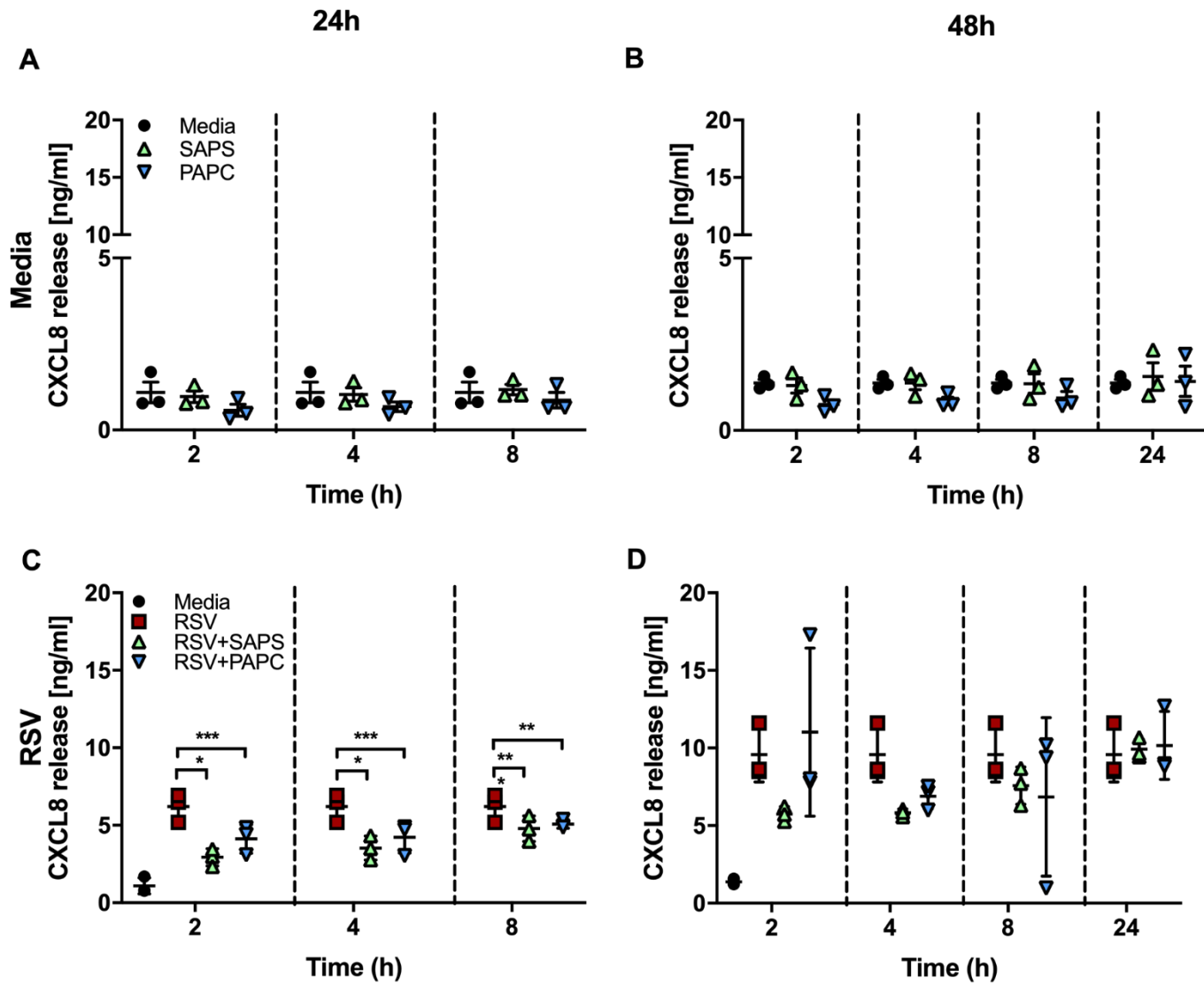


Figure 3.12 SAPS has limited inhibitory effects on CXCL8 release from RSV-infected cells when applied as a post-treatment. HBEC3-KT cells were infected with RSV A2 or stimulated with media control for 2 h. After the 2 h incubation, cells were washed to get rid of any unbound virus. Designated cells were then treated once with SAPS/PAPC (25 μ g/ml) at either 2, 4, 8 or 24 h after RSV infection. At 24 (A, C) and 48 h (B, D), supernatants were generated and the levels of CXCL8 were quantified via ELISA. All data are mean \pm SEM of N=3 individual experiments. Data were analysed using a two-way ANOVA and Tukey's multiple comparisons test. Significant differences are indicated by **p < 0.01, ***p < 0.001, and ****p < 0.0001.

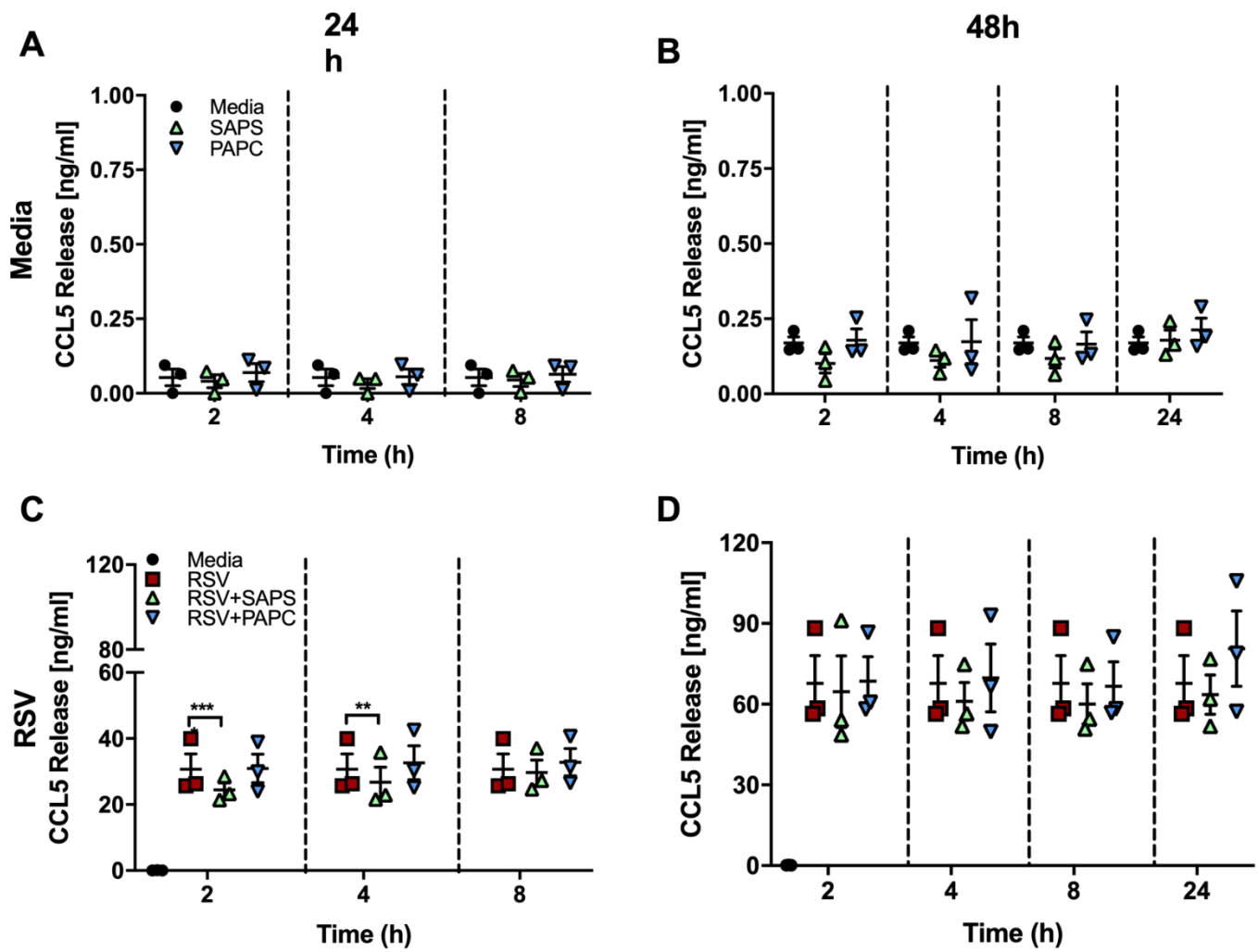


Figure 3.13 SAPS as a post-treatment has limited inhibition on CCL5 release. HBEC3-KT cells were infected with RSV A2 or stimulated with media control for 2 h. After the 2 h incubation, cells were washed to get rid of any unbound virus. Designated cells were then treated once with SAPS/PAPC (25 μ g/ml) at either 2, 4, 8 or 24 h after RSV infection. At 24 (A, C) and 48 h (B, D), supernatants were generated and the levels of CCL5 were quantified via ELISA. All data are mean \pm SEM of N=3 individual experiments. Data were analysed using a two-way ANOVA and Tukey's multiple comparisons test. Significant differences are indicated by **p < 0.01 and ****p < 0.0001.

3.5.2 Investigating the effect of multiple SAPS post-treatments in HBEC3-KT cells and cytokine release

Based on the results obtained in Section 3.5.1; when applied as a one-off post-treatment SAPS/PAPC had some inhibitory actions on CXCL8 release and CCL5 (SAPS only) at 24 h only but no significant effect at 48 h. To explore if the activity of SAPS (as a post-treatment) could be improved, the following experiments were conducted:

1. Reapplying SAPS (25 µg/ml) to the cells at multiple time points post RSV-infection over 24 and 48 h or,
2. Increasing the concentration of the one-off post-treatment with SAPS from 25 µg/ml to 100 µg/ml (explored in Section 3.5.4 & 3.5.5).

The first set of data demonstrates the results of repeated application of SAPS (25 µg/ml) on RSV-infected HBEC3-KT cells whereas the increased concentration of 100 µg/ml SAPS is detailed in the subsequent section (3.5.4 & 3.5.5).

In comparison to the experiments completed in Section 3.5.1 where HBEC3-KT cells were treated with SAPS/PAPC at one time point post-infection, these experiments investigated the application of SAPS/PAPC when applied multiple times throughout the infection process including 4 and 8 h only and 4, 8 and 24 h post-RSV infection, with the timelines illustrated (**Figure 3.14**). The 2 h post-treatment time point was removed as this was having the most significant impact on reducing CXCL8 and CCL5 but was very close to the initial infection time point and I wanted to focus on how well SAPS/PAPC would impact cytokine production at the later time points.

Previous experiments confirmed that SAPS/PAPC (up to 25 µg/ml) did not have a detrimental effect on the BEAS-2B or NHBE cell viability (**Figure 3.4** and **Figure 3.9**) however the repeated application of SAPS/PAPC had not been investigated before and it was therefore important to confirm that exposing the HBEC3-KT cells to multiple treatments with either liposome would not affect cell viability. Therefore, in addition to quantification of CXCL8 and CCL5 via ELISA, a CellTiter-glo® assay was completed to confirm cell viability at both 24 and

48 h and the airway epithelial cells were visually monitored for signs of cell death using the ZOE Fluorescent Cell Imager (BIO-RAD) microscope.

Repeated treatments of the airway epithelial cells with SAPS and PAPC did not significantly reduce CXCL8 release at 24 h (**Figure 3.15 A**) or 48 h (**Figure 3.15 B**) in comparison to the RSV-infected control cells. The response of the cells at 48 h was more variable, as indicated by the large error bars (**Figure 3.15 B**). The data also showed that multiple SAPS treatments on the uninfected media control cells resulted in a significant induction of CXCL8 in comparison to the untreated media control and PAPC-treated (**Figure 3.15 A**). In contrast, multiple treatments (4 and 8 h) of RSV-infected cells with SAPS significantly reduced CCL5 release at 24 h, whilst PAPC also reduced CCL5, but this did not reach significance (**Figure 3.15 C**). At 48 h, both SAPS and PAPC repeated treatments (4, 8 & 24 h) significantly reduced the production of CCL5 in comparison to the untreated cells, with PAPC having more of a significant effect than SAPS (**Figure 3.15 D**).

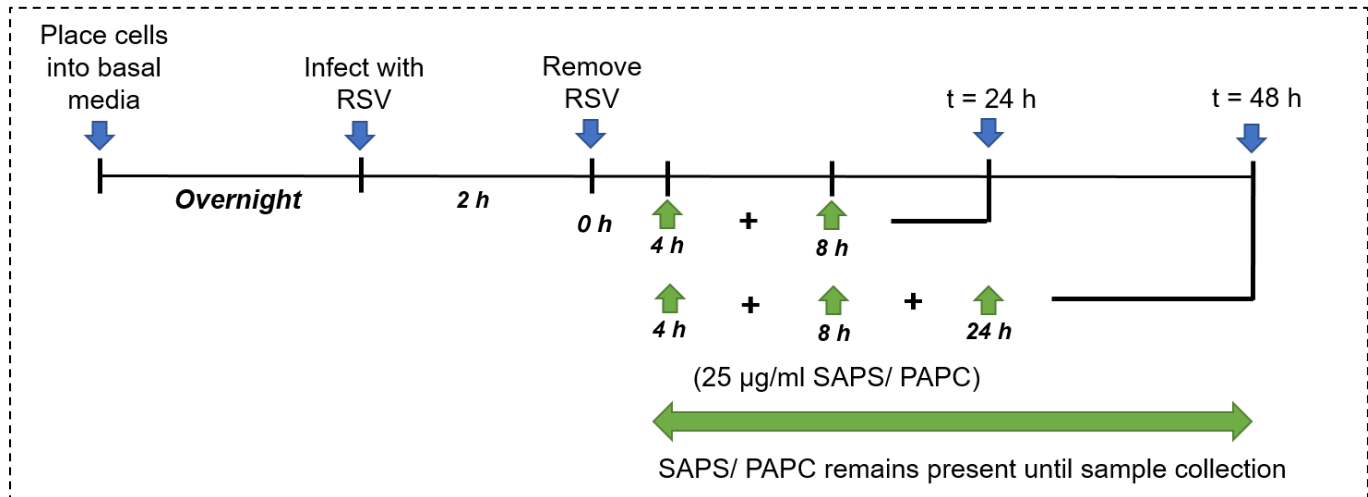


Figure 3.14 Summary timeline indicating the times at which cells are infected with RSV and incubated with SAPS or PAPC. HBEC3-KT cells were either stimulated with media or infected with RSV A2 (MOI 0.4) for 2 h. Unbound virus was removed and fresh basal medium was added to the cells where time = 0 h. Selected wells were treated multiple times with either SAPS/PAPC (25 µg/ml) post RSV-infection including 4 and 8 h (24 h sample collection) or 4, 8 and 24 h (48 h sample collection) after RSV infection. SAPS/PAPC remained present on the cells until sample collection at 24 and 48 h, where supernatants were collected and analysed to determine CXCL8 and CCL5 production via ELISA. Cell viability was also completed at 24 and 48 h.

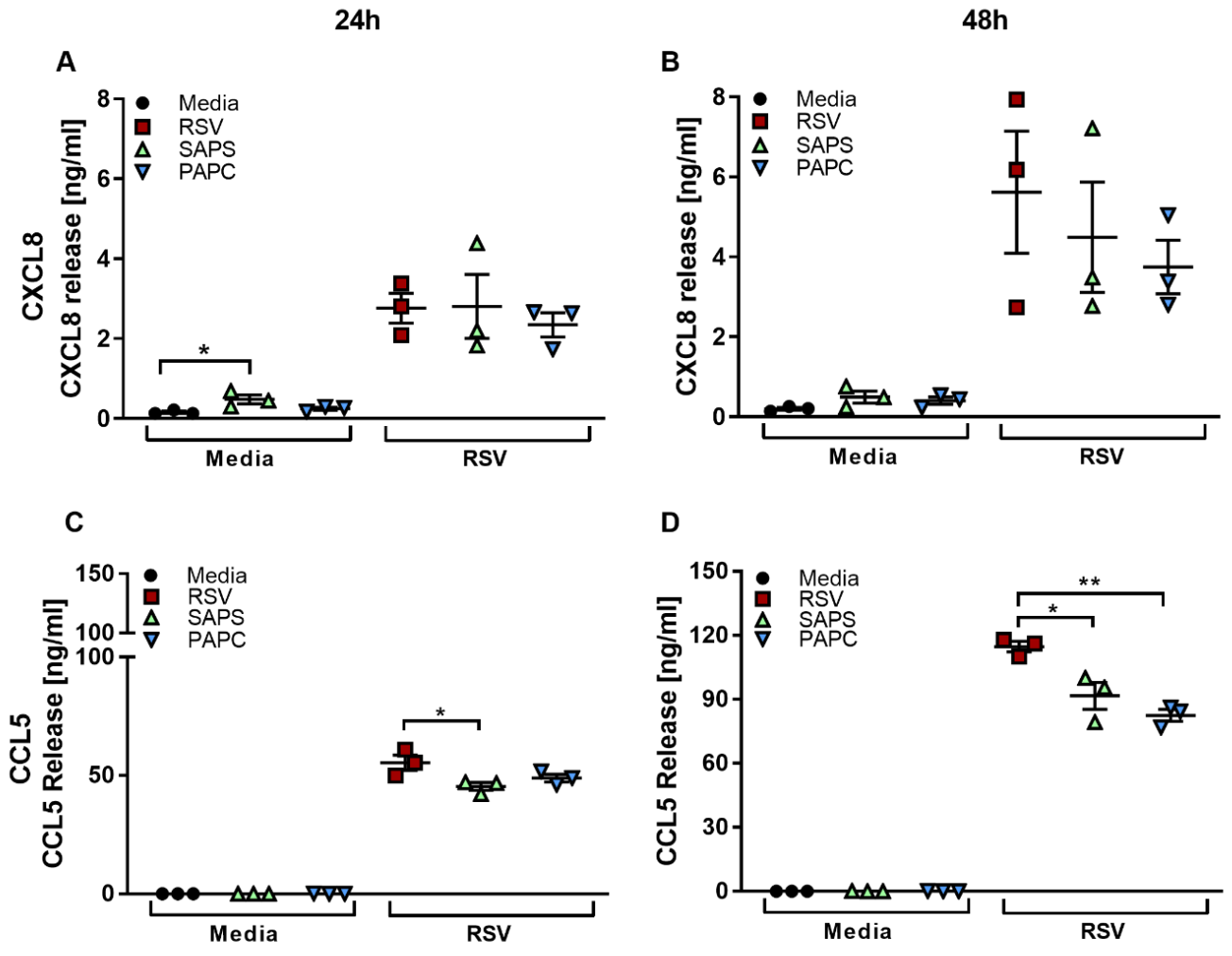


Figure 3.15 Multiple SAPS treatments on HBEC3-KT cells. SAPS as a post-treatment has some effects on CCL5 release. HBEC3-KT cells were infected with RSV A2 or stimulated with media control for 2 h. After the 2 h incubation, cells were washed to remove any unbound virus. Designated cells were then treated with SAPS/PAPC (25 µg/ml) at 4 and 8 h (A, C) or 4, 8 and 24 h (B, D) after RSV infection. At 24 (A, C) and 48 h (B, D), supernatants were generated and the levels of CCL5 were quantified via ELISA. Data are mean ± SEM of N=3 individual experiments. Data were analysed using a one-way ANOVA and Tukey's multiple comparisons test. Significant differences are indicated by *p <0.05, **p <0.01.

3.5.3 Investigating the effect of multiple SAPS post-treatments on HBEC3-KT cell viability

To confirm that repeated treatment of the cells with SAPS or PAPC was not having detrimental effects on whole cell viability, the viability of HBEC3-KT cells was monitored at both 24 and 48 h (**Figure 3.16 A, B**). Of interest, and in contrast with previous data (**Figure 3.4 and Figure 3.9**), SAPS treatment of uninfected cells decreased cell viability at the 24 h time point by approximately 5% relative to the media control (**Figure 3.16 A**). Repeated PAPC treatment of uninfected cells also reduced cell viability at 24 h and this was a significant effect with a decrease of around 29% (**Figure 3.16 A**). A similar observation was noted in RSV-infected cells at 24 h where, SAPS and PAPC treatment reduced cell viability (SAPS-treated = approximately 9% reduction, PAPC = 29% reduction) relative to RSV-infected cells alone, and again PAPC treatment had a significant impact (**Figure 3.16 A**).

Due to the low replicates at 48 h, statistical analysis was not performed on the data but there appeared to be a similar trend whereby SAPS and PAPC treatment decreased levels of viable cells at 48 h in comparison to the untreated media control, with PAPC having a more notable impact (**Figure 3.16 B**). SAPS and PAPC-treated cells that had been infected with RSV, also had reduced cell viability in relation to RSV-infected cells that had not received any liposome treatment (**Figure 3.16 B**).

The impact of repeated SAPS/PAPC treatment on the morphological appearance of the HBEC3-KT cells (uninfected and RSV-infected) are shown at 24 h (**Figure 3.17 A**) and 48 h (**Figure 3.17 B**). The media control cells that have not been infected with RSV or treated with either SAPS or PAPC and illustrate the common morphology and appearance of HBEC3-KT cells when viable and growing as expected. HBEC3-KT cells that have been repeatedly treated with SAPS appear more elongated and free moving debris above the monolayer appeared as darker particles. In comparison, cells treated with PAPC appear more rounded than the untreated control, though no notable free-moving debris was observed (**Figure 3.17**

A). The observations made at 24 h become more apparent in the 48 h images (**Figure 3.17 B**) where SAPS-treated cell cultures appear to have accumulated more debris as illustrated by the darker spots. The rounded appearance of the uninfected PAPC-treated cells at 24 h was also further augmented at 48 h but the cells appeared more granular relative to the uninfected and untreated control cells that, as expected, did not differ significantly in appearance to the relative 24 h images (**Figure 3.17 B**).

RSV-infected HBEC3-KT cells that had been repeatedly treated with either SAPS or PAPC had more evidential monolayer disruption associated with cell shrinkage, rounding and detachment of cells in comparison to RSV-infected cells that had not been treated with either liposome (**Figure 3.17 A, B**). It was again noted that the RSV-infected cells treated with SAPS resulted in visible debris that was moving across the monolayer when being observed in real time with the ZOE Fluorescent Cell Imager, demonstrated by the darker particles in the fixed image (**Figure 3.17 A, B**).

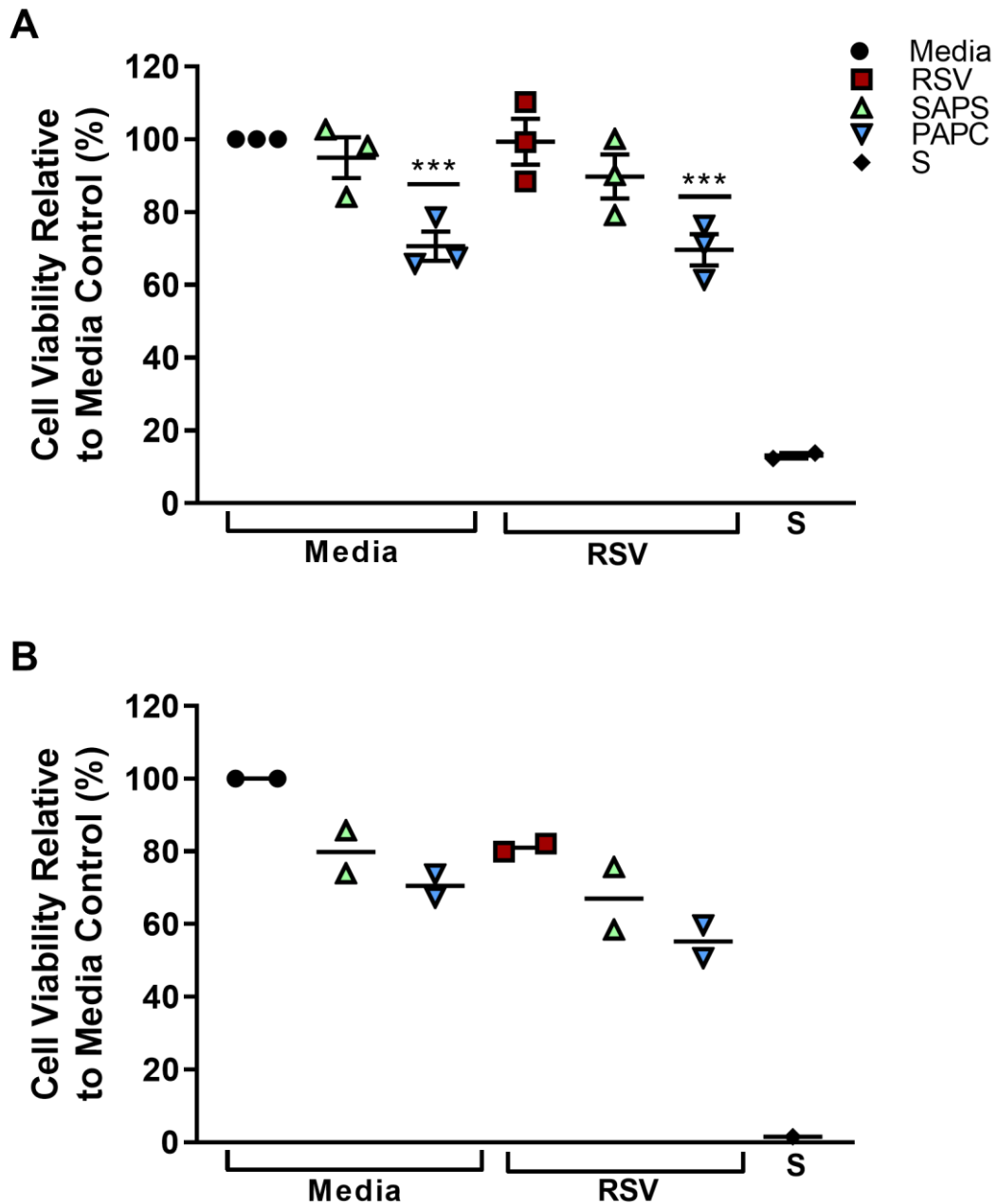
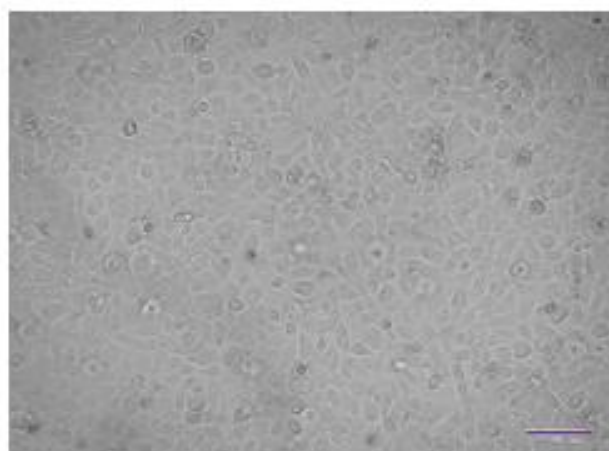
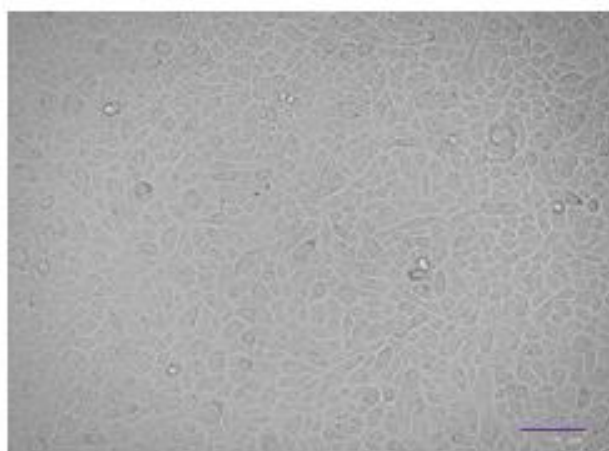
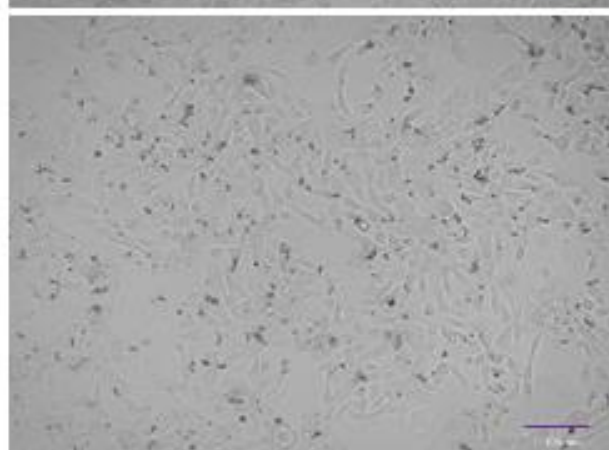
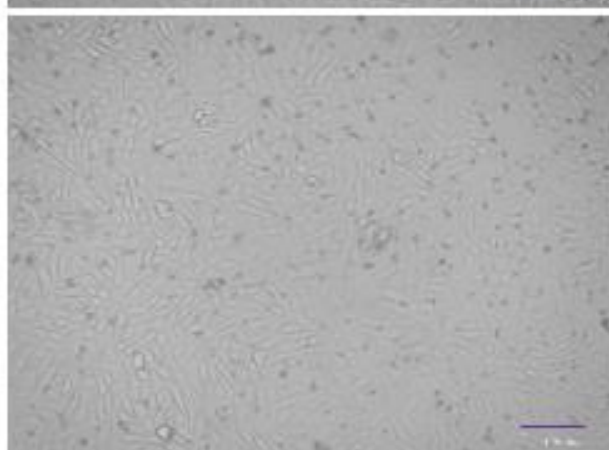
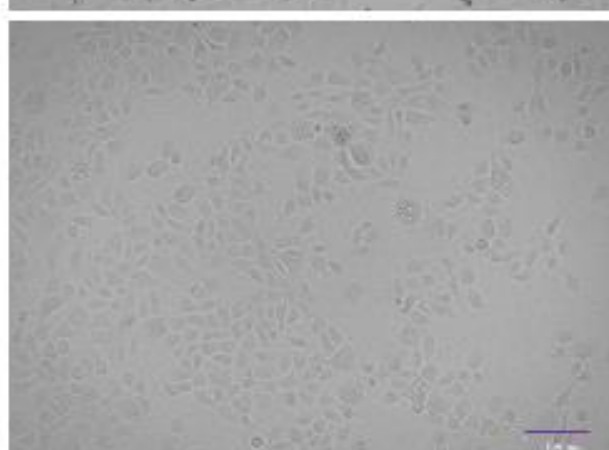
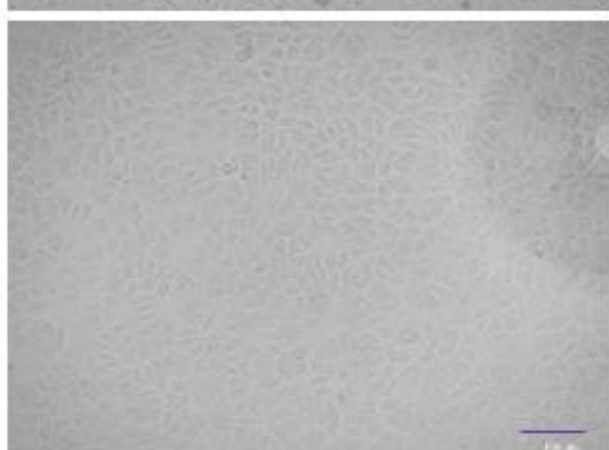


Figure 3.16 Multiple SAPS or PAPC treatments may be detrimental to HBEC3-KT viability. HBEC3-KT cells were infected with RSV A2 or stimulated with media control for 2 h. After the 2 h incubation, cells were washed to remove any unbound virus. Designated cells were then treated with SAPS/PAPC (25 µg/ml) at 4, 8 (A) or 4, 8 and 24 h (B) after RSV infection. At 24 (A) and 48 h (B) a CellTiter-glo® assay was used to determine cell viability. 24 h data are mean ± SEM of N=3 individual experiments and 48 h data are the mean of N=2 individual experiments. The 24 h raw data were analysed using a one-way ANOVA with Dunnett's post-test. The data displayed represents cell viability relative to the media control which has been normalised to 100%. Significant differences are indicated by ***p < 0.001. S=staurosporine.

A**Media****RSV****Untreated****+SAPS****+PAPC**

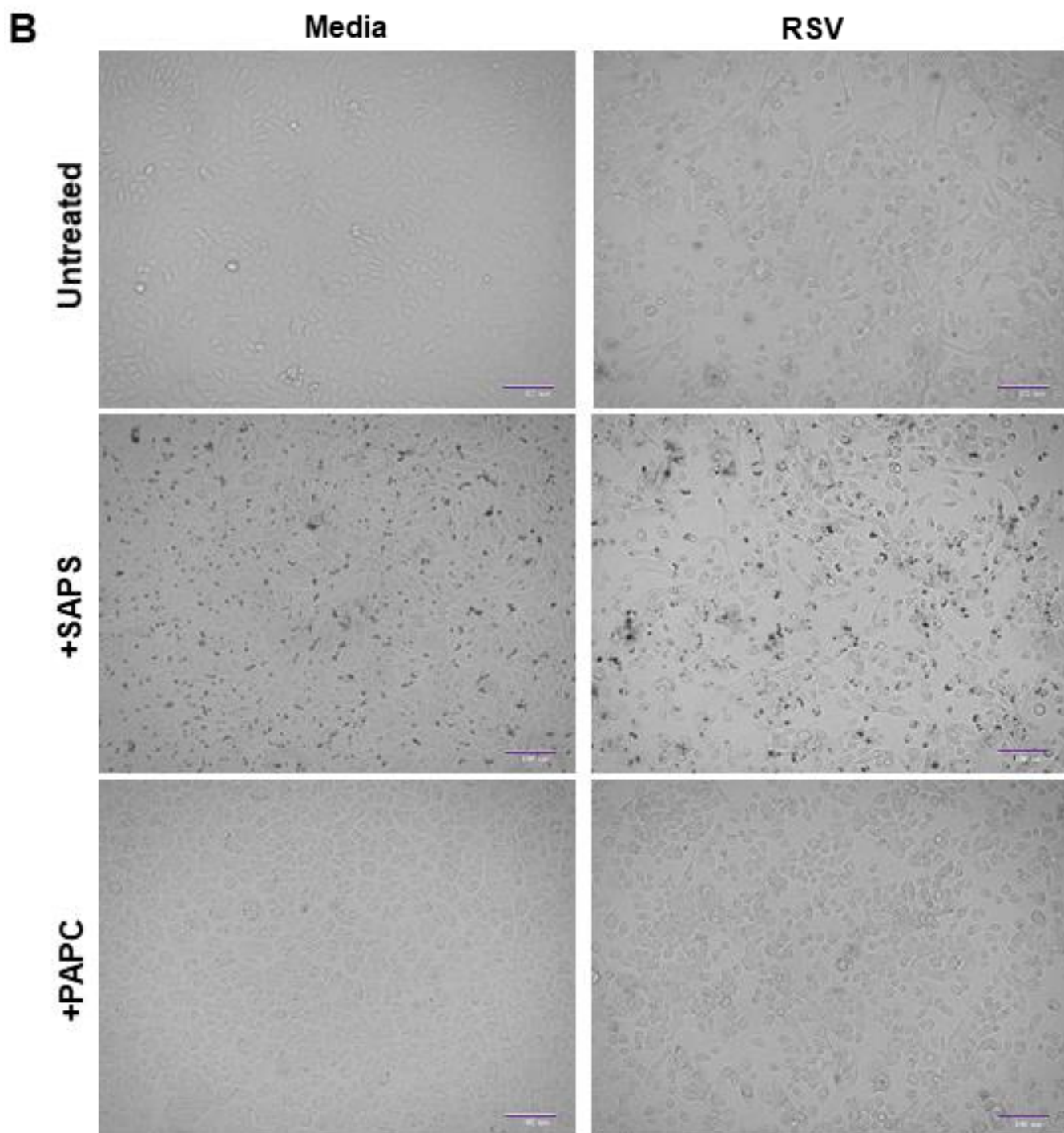


Figure 3.17 Multiple SAPS or PAPC treatments causes visible cytotoxic effects on HBEC3-KT monolayers. HBEC3-KT cells were infected with RSV A2 or stimulated with media control for 2 h. After the 2 h incubation, cells were washed to remove any unbound virus. Designated cells were then treated with SAPS/PAPC (25 $\mu\text{g}/\text{ml}$) at 4 and 8 (24 h samples only) or 4, 8 and 24 h (48 h samples only) post RSV infection. After 24 h (**A**) and 48 h (**B**), cell monolayers were imaged using BIO-RAD ZOE fluorescent cell imager. Scale bar is 100 μm . Images are from N=1 individual experiment but indicative of samples from N=3.

3.5.4 Exploring the effect of 100 µg/ml of SAPS/PAPC on cytokine release from HBEC3-KT cells

To determine if SAPS/PAPC would have longer lasting effects perturbing the production of CXCL8 and CCL5 if a higher initial concentration of liposomes were added to the cells, a comparative investigation was completed alongside the experiments conducted in Section 3.5.3. HBEC3-KT cells were treated with 100 µg/ml SAPS/PAPC at one time point only; 4, 8 or 24 h post-RSV or mock infection where CXCL8 and CCL5 production was quantified at 24 h and 48 h. Cell viability was monitored as described in section 3.5.3. A summary timeline for this experimental work is shown below (**Figure 3.18**).

Samples collected 24 h after viral infection or stimulated with media, indicated that there were no significant differences in CXCL8 production, except for uninfected cells that were treated with PAPC 4 h after media stimulation where levels of CXCL8 were significantly increased relative to the untreated media control (**Figure 3.19 A**).

At 48 h, both SAPS and PAPC significantly induced CXCL8 production from the uninfected cells relative to the untreated media control and these effects were more pronounced with the earlier liposome treatments (**Figure 3.19 B**). In contrast, in the presence of RSV infection, SAPS but not PAPC significantly reduced the production of CXCL8 at 48 h (**Figure 3.19 D**) compared to untreated cells infected with RSV. Once more, this effect was more pronounced the earlier the liposomes are administered to the cells but lost by 24 h post infection (**Figure 3.19 D**).

There were no significant differences in CCL5 production at 24 (**Figure 3.20 A**) or 48 h (**Figure 3.20 B**) between the uninfected media control cells and those treated with SAPS or PAPC. In contrast, in the presence of RSV and at both 24 (**Figure 3.20 C**) and 48 h (**Figure 3.20 D**), all the SAPS post-treatments significantly reduced the production of CCL5 compared to the untreated control cells and this was again more pronounced the earlier the post-treatment. RSV-infected cells treated with PAPC (4 and/or 8 h post-infection) also significantly reduced

CCL5 production at 24 and 48 h where once more, the earlier the liposomes were administered after infection, the greater the reduction in CCL5 (**Figure 3.20 C, D**).

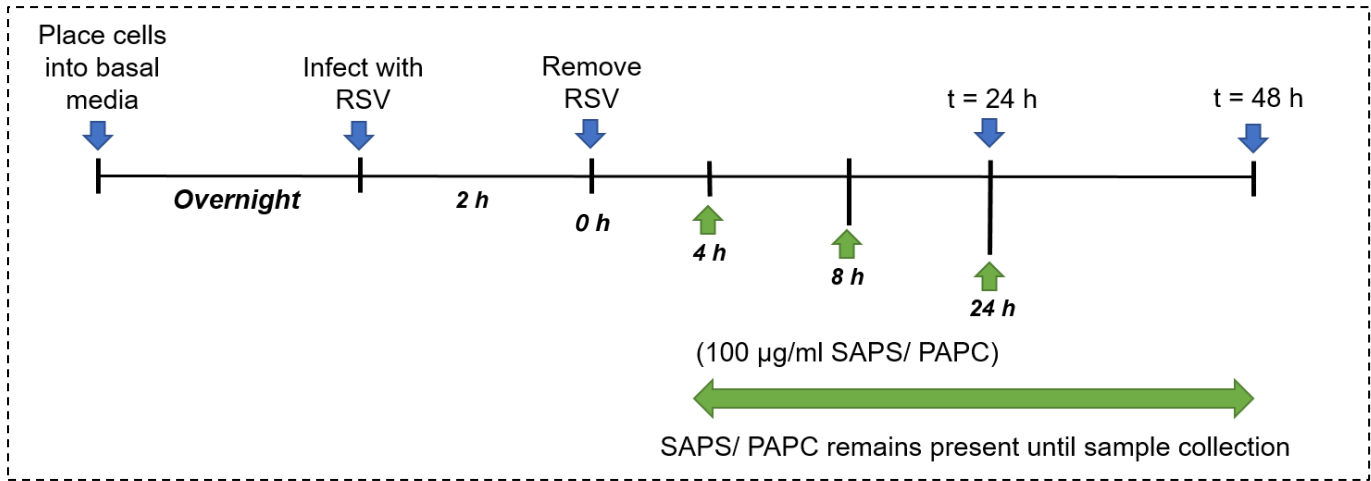


Figure 3.18 Summary timeline indicating the times at which cells are infected with RSV and incubated with SAPS or PAPC. HBEC3-KT cells were either stimulated with media or infected with RSV A2 (MOI 0.4) for 2 h. Unbound virus was removed, and fresh basal medium was added to the cells where time = 0 h. Selected wells were treated once with either SAPS/PAPC (100 µg/ml) at a range of times post RSV-infection including 4 or 8 h (24 h sample collection) or 4, 8 or 24 h (48 h sample collection) after RSV infection. SAPS/PAPC remained present on the cells until sample collection at 24 and 48 h, where supernatants were collected and analysed to determine CXCL8 and CCL5 production via ELISA. Cell viability was also completed at 24 and 48 h.

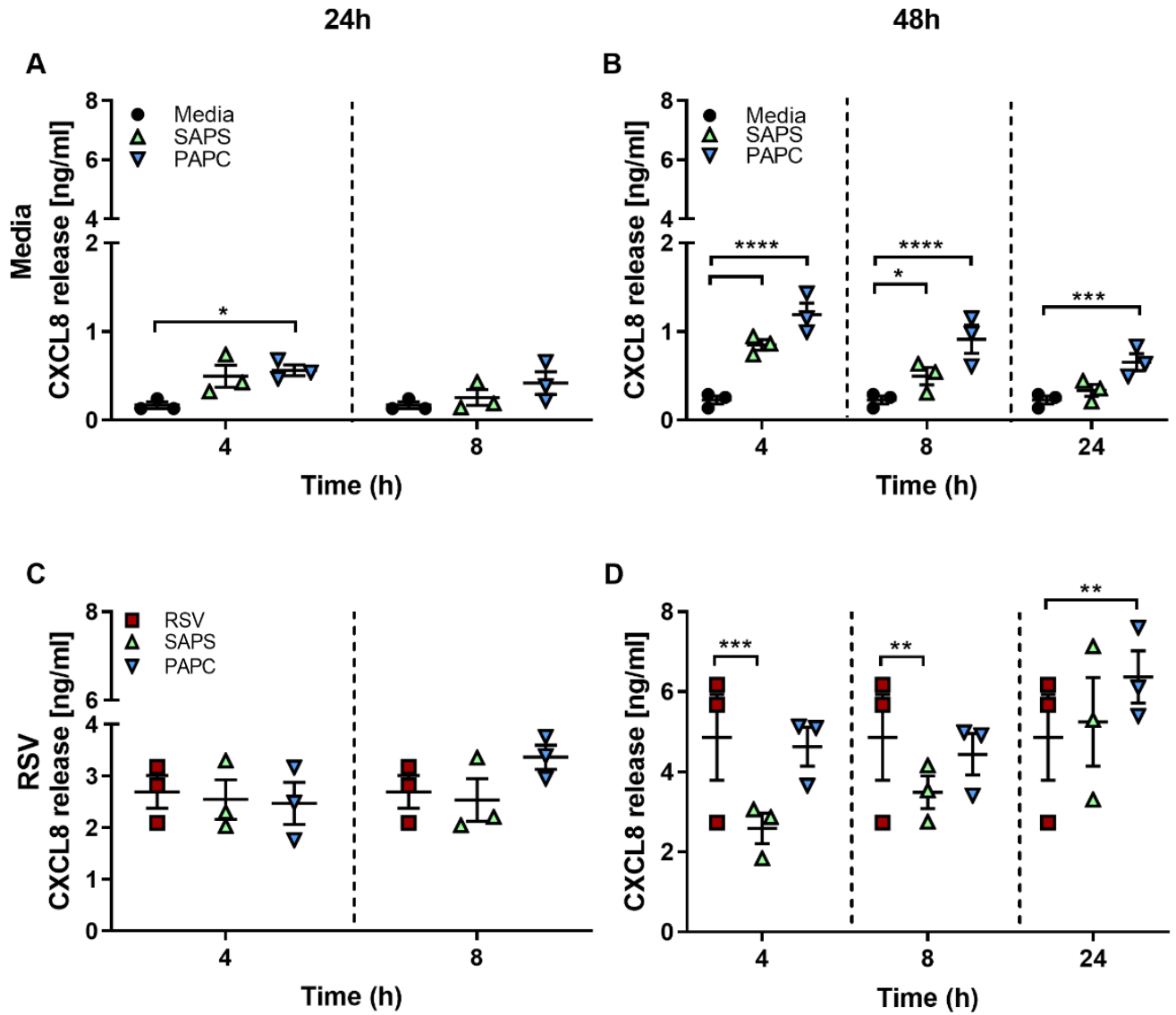


Figure 3.19 Higher concentrations of SAPS or PAPC are cytotoxic to HBEC3-KT cells and perturb the production of CXCL8. HBEC3-KT cells were infected with RSV A2 or stimulated with media control for 2 h. After the 2 h incubation, cells were washed to remove any unbound virus. Designated cells were then treated once with SAPS/PAPC (100 µg/ml) at either 4 or 8 h (A, C) or 4, 8 or 24 h (B, D). At 24 (A, C) and 48 h (B, D), supernatants were generated and the levels of CXCL8 were quantified via ELISA. Data are mean ± SEM of N=3 individual experiments. Data were analysed using a two-way ANOVA and Tukey's multiple comparisons test. Significant differences are indicated by *p <0.05, **p <0.01, ***p <0.001, and ****p <0.0001.

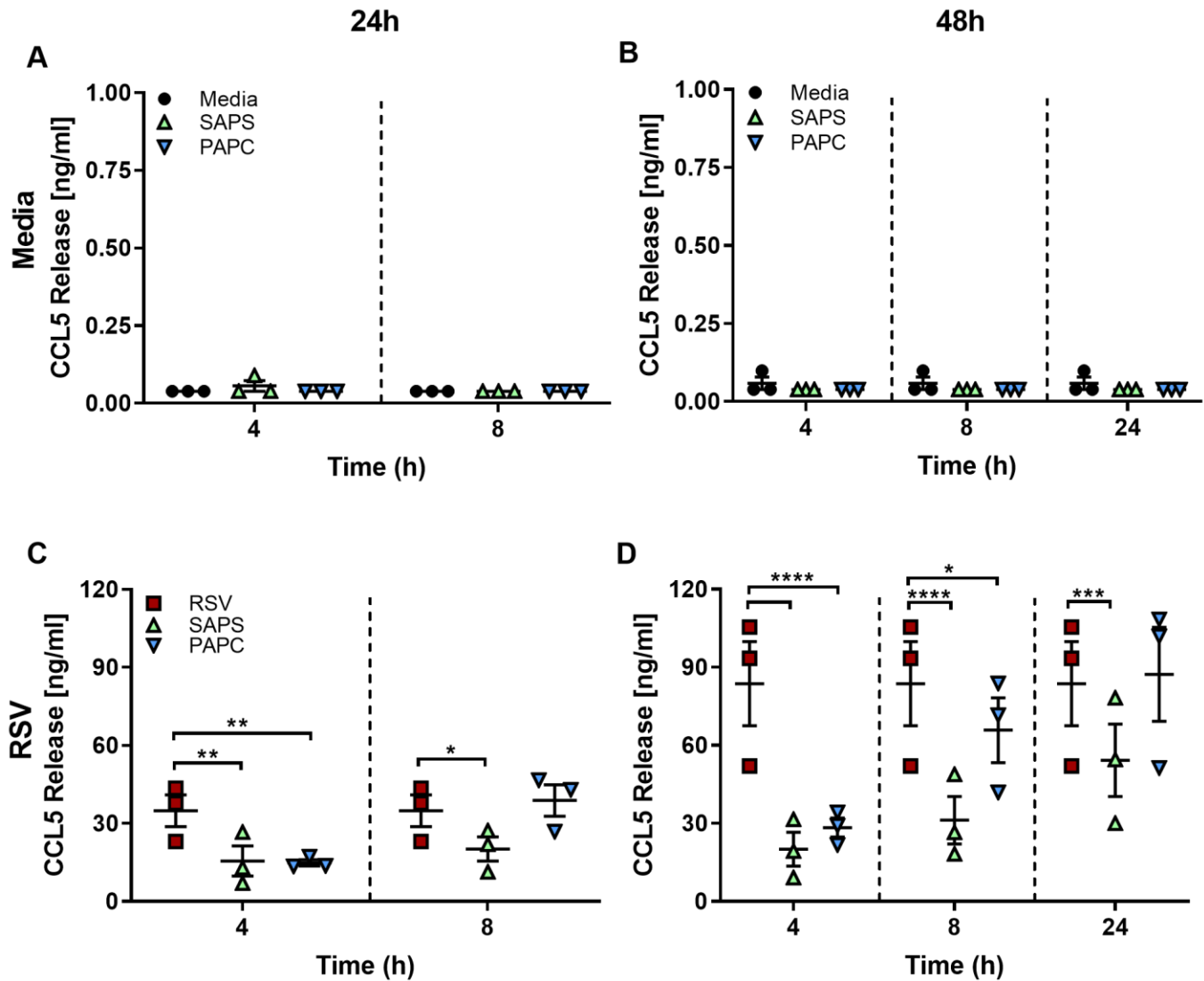


Figure 3.20 Higher concentrations of SAPS or PAPC are cytotoxic to HBEC3-KT cells and affect the production of CCL5. HBEC3-KT cells were infected with RSV A2 or stimulated with media control for 2 h. After the 2 h incubation, cells were washed to remove any unbound virus. Designated cells were then treated once with SAPS/PAPC (100 μ g/ml) at either 4 or 8 h (A, C) or 4, 8 or 24 h (B, D) after RSV infection. At 24 (A, C) and 48 h (B, D), supernatants were generated and the levels of CCL5 were quantified via ELISA. Data are mean \pm SEM of N=3 individual experiments. Data were analysed using a two-way ANOVA and Tukey's multiple comparisons test. Significant differences are indicated by *p < 0.05, **p < 0.01, ***p < 0.001, and ****p < 0.0001.

3.5.5 Exploring the effect of 100 µg/ml of SAPS/PAPC on HBEC3-KT cell viability

Cell viability after treatment with higher doses of lipids was evaluated. The results (**Figure 3.21 A-D**) indicate that 100 µg/ml SAPS/PAPC post-treatments had a significant impact on both the uninfected and RSV-infected HBEC3-KT cells at the 24 h time point. Due to the low number of repeats for the 48 h time point, statistical analysis was not performed, however there were still notable trends that mirrored those seen at 24 h where the cells that had been treated with SAPS/PAPC had greatly reduced cell viability compared to the appropriate untreated cell comparison (**Figure 3.21 B, D**).

To determine the impact of the higher liposome concentration on HBEC3-KT cells, representative images were taken at 24 and 48 h to help document the morphology of the cells in response to SAPS/PAPC treatments relative to their untreated control (mock-infected with media or RSV-infected) (**Figure 3.22 A, B**). The images share some common features that were previously noted in Section 3.5.2. Most notable was the accumulation of extracellular particles in the SAPS-treated cells (RSV-infected and uninfected). This was also associated with the disruption of the cell monolayer with notable areas of cell detachment and shrinkage at the 24 h time point, particularly 4 h post (mock)-infection where the monolayer differs greatest from the uninfected and RSV-infected cells that has not been treated with either liposome (**Figure 3.22 A**). By 48 h, large differences between the RSV-infected control cells and the RSV-infected cells that had received SAPS treatment, particularly the 24 h post-treatment cells where no visible monolayer is seen (**Figure 3.22 B**). In comparison to the SAPS-treated cells, PAPC-treated cells did not appear to result in the accumulation of particulate at either time point (**Figure 3.22 A, B**). There were visible morphological differences however in both the mock-infected and RSV-infected cells that had either received PAPC post-treatment or not. At 24 h, there were visibly more rounded cells (in the 4 and 8 h post-treated cells) in contrast to the untreated cells (**Figure 3.22 A**). These differences in morphology were also noted at 48 h but were additionally associated with shrinkage of the cell

monolayer particularly those that had been treated 4 or 8 h post mock/RSV-infection (**Figure 3.22 B**).

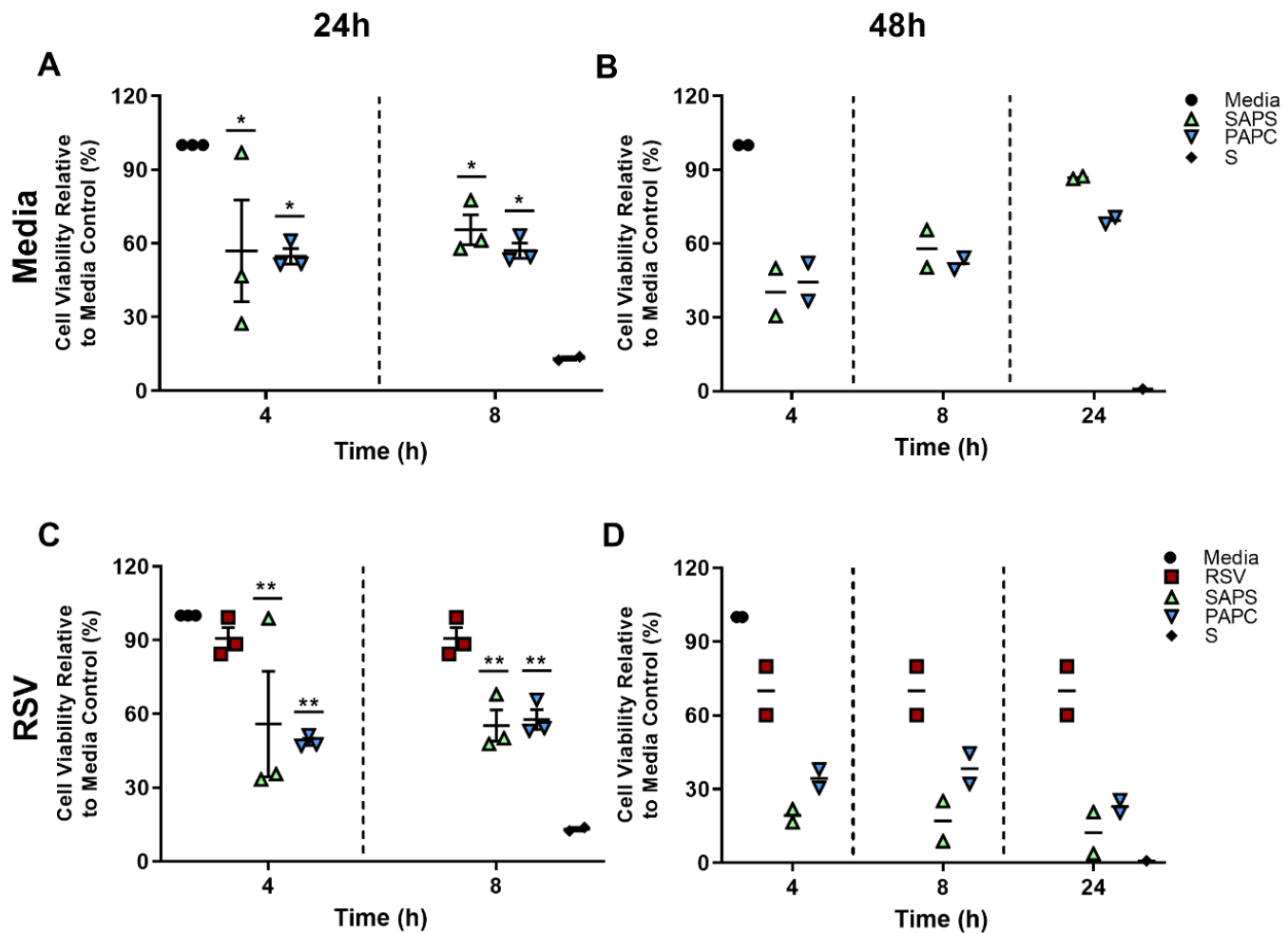
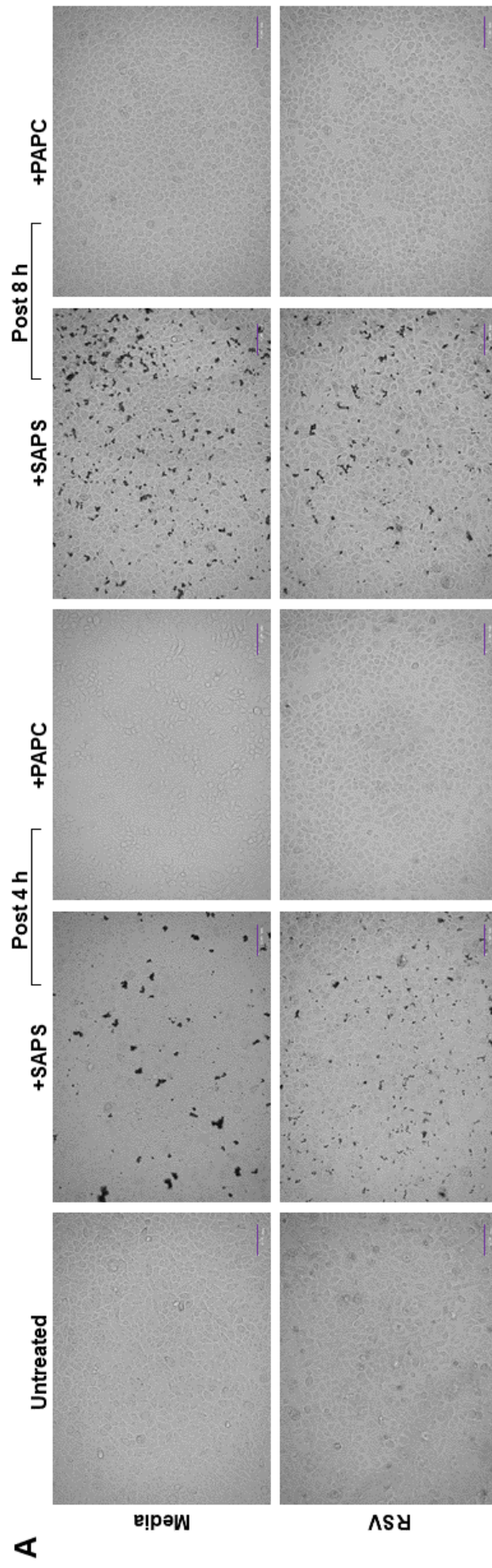


Fig 3.21 Higher concentrations of SAPS and PAPC are cytotoxic to HBEC3-KT cells. HBEC3-KT cells were infected with RSV A2 or stimulated with media control for 2 h. After the 2 h incubation, cells were washed to remove any unbound virus. Designated cells were then treated once with SAPS/PAPC (100 µg/ml) at either 4 or 8 h (A, C) or 4, 8 or 24 h (B, D) after RSV infection. At 24 (A, C) and 48 h (B, D) a CellTiter-Glo® assay was performed to determine cell viability. 24 h data are mean ± SEM of N=3 individual experiments and the 48 h data are mean of N=2 independent experiments. The 24 h raw data were analysed using a two-way ANOVA with Dunnett's post-test. Data are presented against the media control which has been normalised to 100%. Significant differences are indicated by *p < 0.05, **p < 0.01. S=staurosporine.



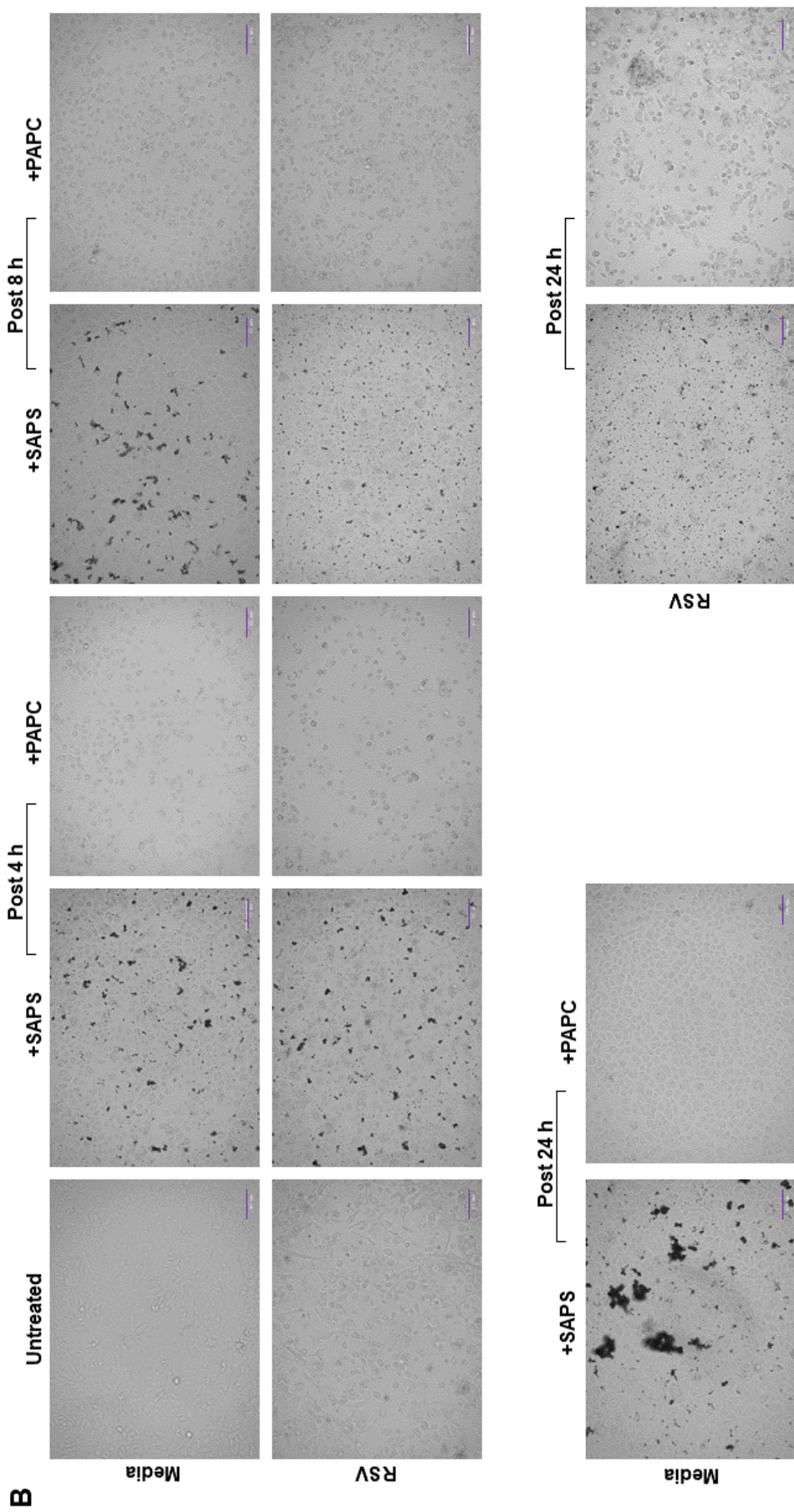


Figure 3.22 100 µg/ml SAPS/PAPC treatments causes visible cytotoxic effects on HEBC3-KT monolayers. HEBC3-KT cells were infected with RSV A2 or stimulated with media control for 2 h. After the 2 h incubation, cells were washed to remove any unbound virus. Designated cells were then treated with SAPS/PAPC (100 µg/ml) at 4 or 8 (24 h samples only) or 4, 8 or 24 h (48 h samples only) post RSV infection. After 24 h (A) and 48 h (B), cell monolayers were imaged using BIO-RAD ZOE fluorescent cell imager. Scale bar is 100 µm. Images are from N=1 individual experiment but indicative of samples from N=3.

3.6 Chapter summary

The main aims for this chapter were to explore the effect of SAPS on production of CXCL8 and CCL5 in response to RSV infection utilising a range of AECs. Investigations were primarily conducted in the immortalised BEAS-2B cell line. Studies were then optimised and conducted in the lifespan extended HBEC3-KT cells and, where possible, NHBE cells. Further to this, the efficacy of SAPS as a post-treatment was investigated within HBEC3-KT cells that were incubated with SAPS at a range of times post-infection to determine if/when SAPS would be most efficacious.

Data within this chapter demonstrate that SAPS can significantly reduce the production of CXCL8 and CCL5 (up to and including 48 h after infection) when it is simultaneously co-incubated with airway epithelial cells during RSV infection (**Figures 3.3, 3.7, 3.8, 3.9 and 3.10**). This efficacy was demonstrated in the immortalised BEAS-2B, lifespan extended HBEC3-KT and in NHBE cells with equal effect. In contrast, co-incubation with the comparative liposome PAPC had more modest (and inconsistent) inhibitory effects on CXCL8 and CCL5 production across the different cell types used. The inhibitory effects on cytokine production at the initial doses tested were not due to decreased cell viability and no cytotoxic effects were seen in any of the AECs when co-incubated with either SAPS or PAPC.

The efficacy of SAPS appeared to diminish however when HBEC3-KT cells were treated after RSV infection with significant reductions in CXCL8 (SAPS and PAPC) and CCL5 (SAPS only) levels only at 24 h post infection where the HBEC3-KT cells had been treated with SAPS/PAPC (25 µg/ml) 2 or 4 h post RSV infection (**Figure 3.12 and 3.13**). Attempts to increase the efficacy of SAPS by increasing the number of applications and the overall concentration of SAPS did not improve its activity as a post-treatment but in fact, led to cytotoxic effects within the HBEC3-KT cells (**Figure 3.15 – Figure 3.22**).

Chapter 4: Results – SAPS Modulates the Life Cycle of RSV in Airway Epithelial Cell Cultures

4.1 Hypothesis and Aims

Published data from my research group demonstrated the ability of SAPS to perturb RV-induced inflammatory signalling in both immortalised and primary airway epithelial cells (Stokes et al., 2016). In chapter 3, I presented data that shows SAPS reduces the inflammatory response to RSV, particularly when cells were co-incubated with SAPS during the initial infection stage. In a previous report by Stokes et al. (2016), SAPS treatment had no impact on the productive life cycle of RV whereby the infection of airway epithelial cells and subsequent levels of viral replication were not reduced despite reports suggesting that RV use MM for attachment and productive infection (Dreschers et al., 2007; Grassmé et al., 2005). It was hypothesised that SAPS may have more efficacy against an enveloped virus such as RSV where lipid membrane fusion at MM is required for viral entry (Chang et al., 2012; San-Juan-Vergara et al., 2012). I therefore wanted to explore if SAPS would impact on the life cycle of RSV including the infection of, and subsequent replication within, airway epithelial cells. In addition to this, I wanted to employ high resolution microscopy techniques to try and visualise the interactions of RSV during infection of airway epithelial cells and investigate if SAPS was impacting these interactions.

Another aspect of my project was to explore the impact of viral-bacterial co-infections in airway epithelial cells and determine if SAPS may moderate these interactions. As we hypothesise that SAPS may be able to inhibit RSV infection of airway epithelial cells, I considered that SAPS treatment may also prevent the subsequent bacterial infections that can occur after viral-induced inflammation. As discussed in Section 1.4, bacterial co-infections, particularly with *Streptococcus pneumoniae* (*Spn*) and non-typeable *Haemophilus influenzae* (*NTHi*) are commonly associated with hospitalised individuals with severe RSV disease and may exacerbate airway pathology (Bosch et al., 2013; Brealey et al., 2015; Duttweiler et al., 2004;

Godefroy et al., 2020; Jung et al., 2020; Liu et al., 2021; Wieggers et al., 2019). I therefore sought to determine if SAPS would reduce RSV infection and the associated factors that enable the increased adherence and uptake of bacteria in RSV-infected airway cells.

The aims of this chapter were to;

- Optimise and employ viral plaque assays to determine infectivity of normal human bronchial epithelial cells with RSV in the presence/absence of SAPS.
- Quantify the levels of viral replication using RT-qPCR to determine if SAPS was modifying the subsequent infection and replication of RSV.
- Optimise and employ confocal microscopy to visualise RSV infection of airway epithelial cells in presence/absence of SAPS.
- Investigate how RSV infections may predispose the cells to bacterial co-infection (focussing on adherence and invasion) with *Streptococcus pneumoniae* and if SAPS can moderate this process.

4.2 SAPS significantly reduces RSV infection of NHBE cells

4.2.1 Viral plaque assay optimisation in NHBE cells

It was hypothesised that SAPS may modify the MM that RSV target during infection of airway epithelial cells. To investigate this, NHBE cells were infected with RSV in the presence/absence of SAPS and the number of infected cells quantified 24 h later. Additionally, to determine if the effect of SAPS was concentration dependent, a lower (10 µg/ml) and higher (25 µg/ml) concentration of SAPS/PAPC was used.

To investigate viral infectivity, a variation of the traditional viral plaque assay was utilised that allows for the quantification of infected cells through immunostaining instead of viral lysis. This method was also used to determine the viral titre when propagating RSV (Section 2.2.5.2). This is termed a focus forming assay, where infected NHBE cells are detected using antibodies that specifically target intracellular RSV antigens, which are then subsequently

labelled using an HRP-conjugated antibody and immunostaining (Section 2.2.6.2). Infected cells are termed focus forming units (FFU) and appear a darker brown colour relative to uninfected cells, and can therefore be identified and quantified using an inverted light microscope (Baer and Kehn-Hall, 2014).

This technique had not been established for the NHBE cells and thus required optimisation to first establish a suitable MOI that would result in a quantifiable level of virus that could be counted by eye (up to 100 plaques per well in a 12-well plate), as summarised in Table 4.1. In the wells infected with the higher MOIs (0.2-1), there were too many FFU to accurately quantify the total number of FFU in the whole well. A snapshot of one area of the infected well visualised through the microscope is shown in **Figure 4.1**. By reducing the MOI much further in the following experiment, I was able to quantify viral-infected cells more accurately from each well. As expected, there were no visible FFU in the uninfected NHBE cells however, there were 260 FFU/well quantified from the triplicate wells infected with RSV MOI 0.001 (**Figure 4.2**). From these experiments it was determined that the best MOI to infect the NHBE cells was MOI 0.001 as it gave rise to a level of infected cells that could be accurately quantified by this method.

Experimental Attempt	Range of MOI used	Additional methods altered	Result
1	1.0, 0.8, 0.4		No clear stain
2	0.4 0.3. 0.2	Doubled concentration of DAB stain in one row	1. Level of stained cells too high to count. 2. Double DAB made FFU harder to see.
3	0.1, 0.05, 0.01, 0.001 (Based on more accurate cell count in NHBE)	Doubled RSV ab concentration to (1:50) in additional wells	1. Higher concentration (1:50) RSV ab did not improve darkness of stain. 2. The lowest MOI (0.001) had level of FFU that I could attempt to count.

Table 4.1 Summary of the steps taken to optimise viral plaque assay to quantify RSV-infected cells.

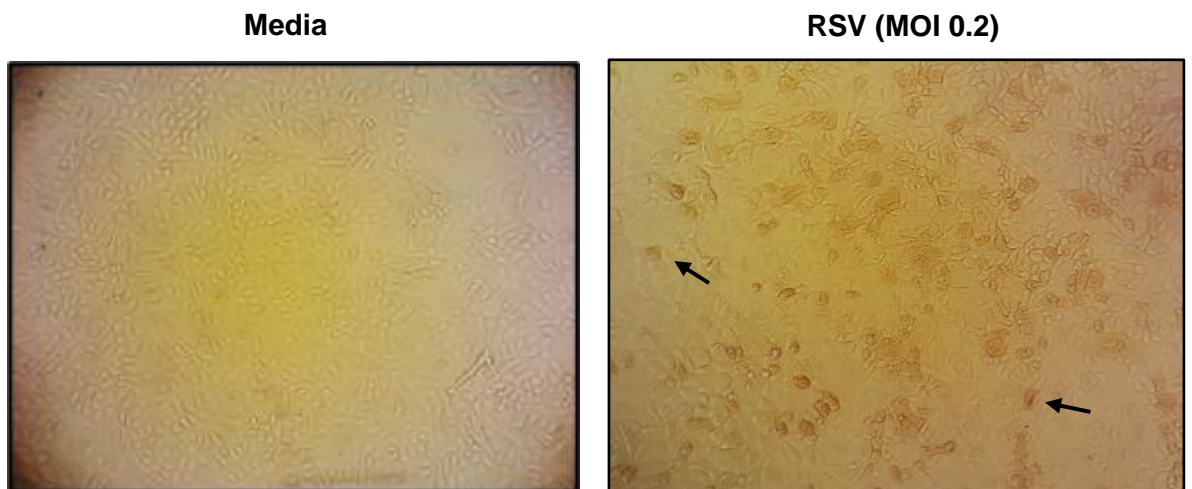


Figure 4.1 Images from viral plaque assay optimisation. Representative images showing uninfected (media) NHBE cells and cells that had been infected with MOI 0.2 and the resultant staining to identify RSV-infected cells or, focus forming units FFU. Images were taken using an inverted light microscope. Magnification is x40. Arrows indicate RSV-infected cells which are darker brown in colour FFU.

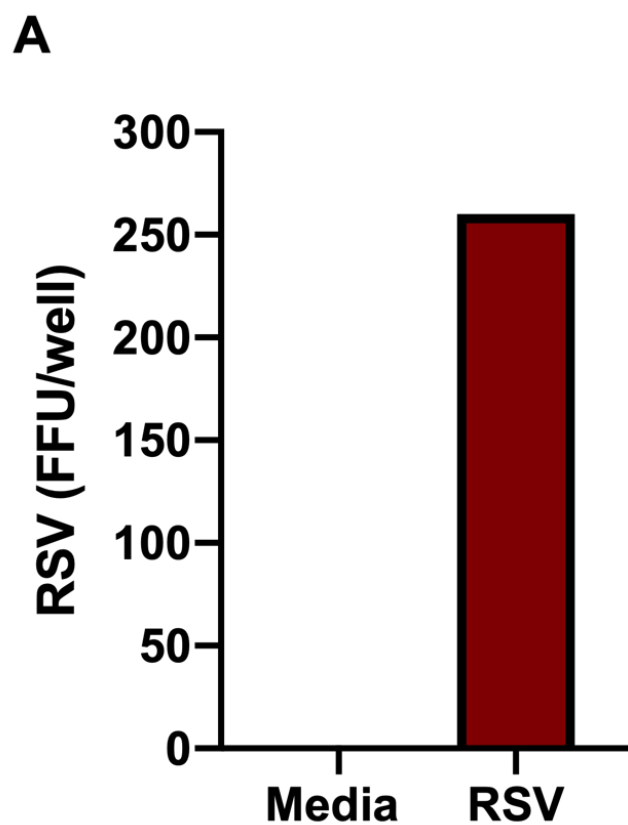


Figure 4.2 Optimising viral plaque assay in NHBE cells. NHBE cells were stimulated with media or infected with RSV A2 (MOI 0.001) for 2 h. Unbound virus was washed off and cells incubated for a further 24 h in fresh basal media. Cells were permeabilised and fixed with 4% PFA. Cells were stained using an RSV-antibody and DAB staining. Viral-infected cells (FFU/well) were counted using an inverted light microscope. Pictures were taken to demonstrate the difference in FFU visible in one focal area under an inverted light microscope.

4.2.2 SAPS significantly reduces the number of NHBE cells infected with RSV

Two different concentrations of SAPS/PAPC (10 and 25 µg/ml) were used to determine the efficacy of either liposome to modulate infectivity of NHBE cells. Based on the observations made in **Section 4.2.1**, RSV MOIs were further reduced to 0.001 and 0.0001 with investigations carried out using a 96-well plate, where the smaller area of each well would allow for easier counting of infected cells. The number of infected cells were quantified (represented as FFU/well) 24 h after RSV infection.

Low numbers of NHBE cells became infected using MOI 0.0001, thus no significant differences were observed between the RSV-infected cells that had received either SAPS or PAPC treatment (**Figure 4.3**). However, NHBE cells infected with MOI 0.001 RSV resulted in 77.67 (\pm 13.42) FFU/well and co-incubation with either concentration of SAPS reduced the number of infected cells by ~95% at 24 h (**Figure 4.3**). Unexpectedly, the highest concentration of PAPC (25 µg/ml), also significantly reduced the number of RSV infected cells by 94% in comparison to NHBE cells infected with virus alone (**Figure 4.3**).

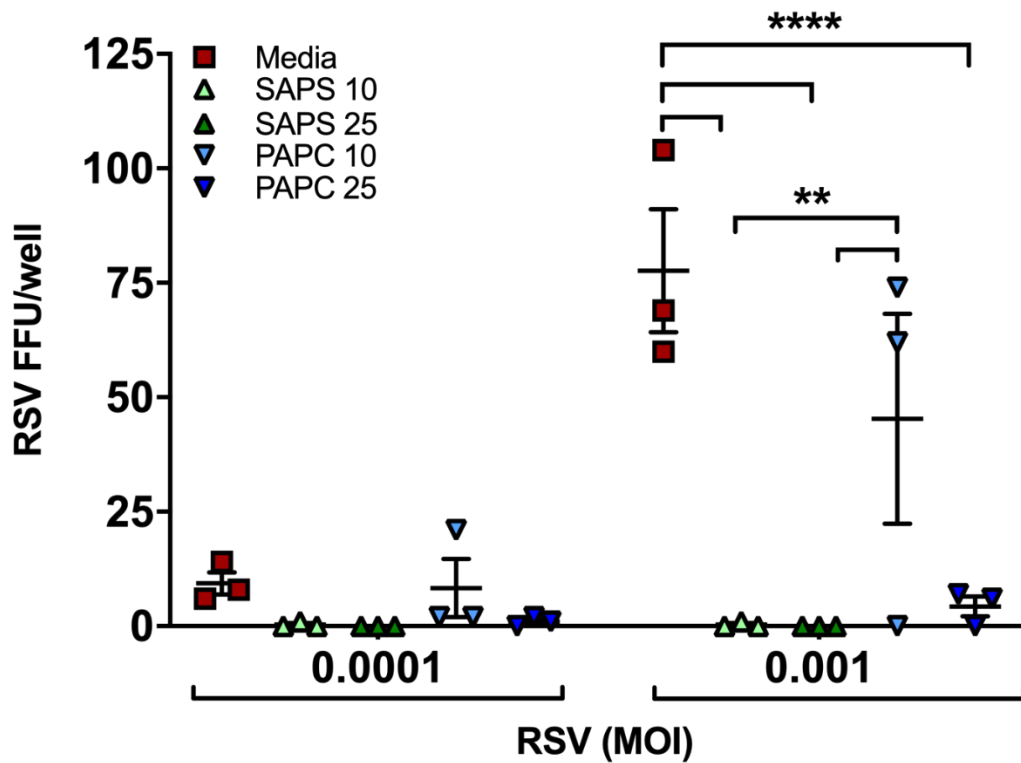


Figure 4.3 Both concentrations of SAPS significantly inhibit viral infection of NHBE cells. NHBE cells were infected with a range of RSV A2 (MOI 0.01, 0.001 and 0.0001) for 2 h. Designated cells were incubated with SAPS or PAPC (10 or 25 $\mu\text{g}/\text{ml}$) which remained on the cells throughout the 2 h incubation. After incubation, cells were washed to remove any unbound virus and designated cells treated once more with SAPS or PAPC (10 or 25 $\mu\text{g}/\text{ml}$). After 24 h, cells were stained and the quantity of viral infected cells counted. MOI 0.01 media control are set at the upper limit of 100 FFU (quantifiable by eye) and therefore not represented in the graph. Data were analysed using a two-way ANOVA and Tukey's multiple comparisons test. Significant differences are indicated by ** $p < 0.01$, and **** $p < 0.0001$. Data are N=3 technical repeats from one independent donor #365.

4.3 SAPS may modulate RSV infection of, and subsequent viral replication within, airway epithelial cells

RSV is thought to preferentially bind to cholesterol-rich MM of the host cell to allow successful attachment, entry, and replication of viral RNA before subsequent release of new virion (Section 1.4). Perturbing MM with SAPS modulates RSV viral entry (as demonstrated in Section 4.2) and it was hypothesised that it was also likely to affect the subsequent viral replication within airway epithelial cells. To validate these findings, viral replication was quantified using RT-qPCR as described in Section 2.5 and using an assay established during my MSc lab project with the advice of Dr Fiona Culley, Imperial College London (Culley et al., 2002).

4.3.1 Viral replication in BEAS-2B cells

The data shown in **Figure 4.4** represents N=1-3 individual experiments in BEAS-2B cells, although some samples failed during the RNA extraction procedure and are therefore omitted from the final RT-qPCR analysis. Due to this, no statistical analysis and conclusive remarks can be made from this data.

The data suggest BEAS-2B cells infected with RSV (MOI 0.4 and 1), that had also been co-incubated with SAPS, had reduced levels of detectable RSV at both 24 and 48 h (**Figure 4.4 A, B**). In contrast, RSV-infected cells that had been treated with PAPC showed little to no reduction in detectable viral copies at 24 h (**Figure 4.4 A**) however, there was a slight reduction of RSV (MOI 0.4) detected at 48 h where PAPC treatment had been used (**Figure 4.4 B**).

As expected, no virus was detected in cells treated with infection media alone, UV-inactivated RSV or filtrate control (**Figure 4.4 A, B**). In addition, no viral RNA was detected at either time point in the uninfected (indicated as MOI 0) media controls (**Figure 4.4 A, B**).

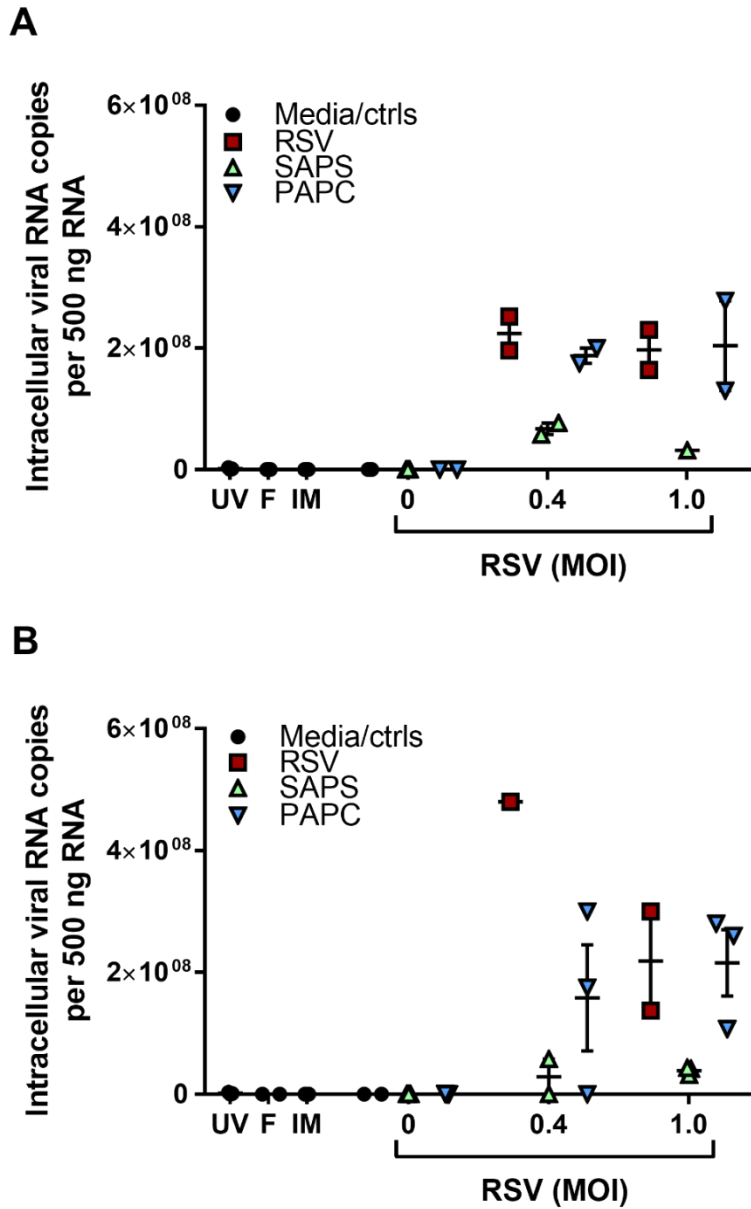


Figure 4.4 SAPS treatment may reduce RSV viral copies at 24 and 48 h. BEAS-2B cells were infected with RSV A2 (MOI 0.4 or 1), UV-inactivated (UV) RSV, filtrate (F) or stimulated with infection (HEp-2) media (IM) or mock infected with normal growth media (MOI 0). Designated cells were incubated with SAPS or PAPC (50 µg/ml) which remained on the cells throughout the 2 h incubation. After incubation, cells were washed to remove any unbound virus and designated cells treated once more with SAPS or PAPC (50 µg/ml). After 24 (A) and 48 h (B), RNA samples were generated, and viral RNA measured by RT-qPCR. Data range between N=1-3 due to sample loss during RNA sample generation. No statistical analysis completed.

4.3.2 SAPS significantly reduces viral RNA from RSV-infected NHBE cells

Due to the limited sample number in the BEAS-2B cell data set (**Section 4.3.1**), it was not clear what effect SAPS or PAPC had on RSV replication. In addition, BEAS-2B cells have limitations in modelling the airway epithelium during viral infection and experiments were therefore conducted in the NHBE cells. NHBE cells were infected with RSV (MOI 0.4) for 2 h in the presence/absence of SAPS/PAPC at a concentration of 10 or 25 µg/ml. Unbound virus was removed and selected wells retreated with SAPS or PAPC, which remained on the cells for the remaining infection period of 24 or 48 h at which point sample RNA was recovered from the cells and RT-qPCR completed. Data were performed on multiple replicates of a single airway cell donor.

These data indicated that at 24 h post RSV infection (**Figure 4.5 A**), NHBE cells contained around 2.3×10^8 ($\pm 4.21 \times 10^7$) copies of the RSV L-gene per 1 µg of RNA. SAPS treatment resulted in a concentration-dependent inhibition of viral replication (**Figure 4.5 A**). A similar trend was also noted at the 48-h time point where significantly less viral RNA was detected from cells co-incubated with increased concentrations of SAPS (**Figure 4.5 B**).

RSV-infected NHBE cells that were co-incubated with PAPC were more varied in their response, which was dependent upon the concentration used (**Figure 4.5 A, B**). Only the highest concentration of PAPC significantly reduced viral RNA whereas the lower concentration had no effect at either time point (**Figure 4.5 A, B**).

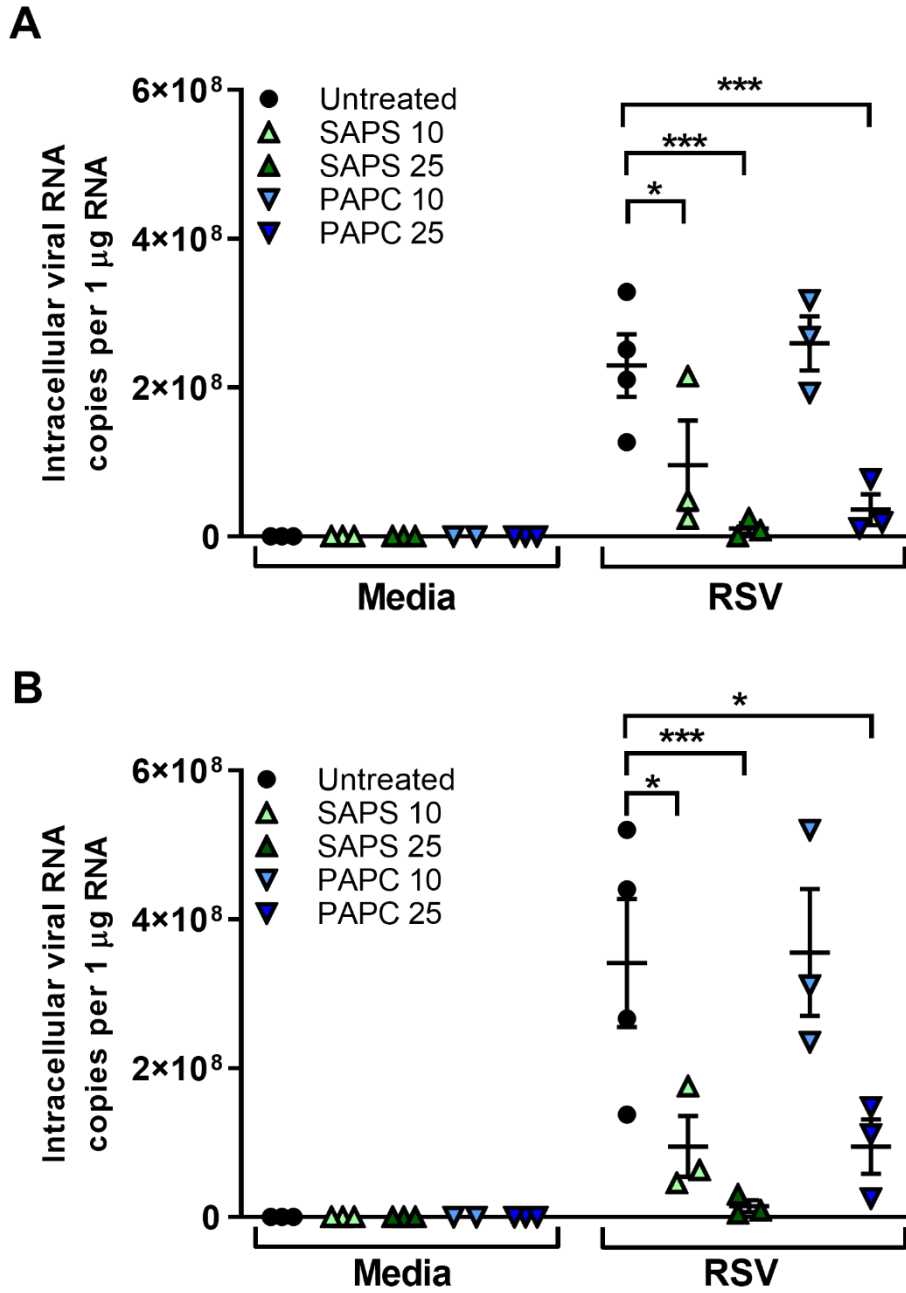


Figure 4.5. NHBE cells treated with SAPS have significantly lower levels of detectable viral RNA at 24 and 48 h. NHBE cells were infected with RSV A2 (MOI 0.4) or stimulated normal growth media. Designated cells were incubated with SAPS or PAPC (10 or 25 $\mu\text{g}/\text{ml}$) which remained on the cells throughout the 2 h incubation. After incubation, cells were washed to remove any unbound virus and designated cells treated once more with SAPS or PAPC (10 or 25 $\mu\text{g}/\text{ml}$). After 24 (**A**) and 48 h (**B**), RNA samples were collected, and levels of viral RNA quantified using RT-qPCR. All data are \pm SEM of $N=3/4$ technical repeats in D365. Data were analysed using a two-way ANOVA and Tukey's multiple comparisons test. Significant differences are indicated by * $p < 0.05$, *** $p < 0.001$.

4.3.3 SAPS significantly reduces viral RNA in RSV-infected HBEC3-KT cells

Following on from the data demonstrated in section 4.3.2, experiments were conducted in HBEC3-KT cells to confirm if SAPS (and PAPC) would have comparable inhibitory effects on viral replication in the HBEC3-KT cells (**Figure 4.5**). Based on the data obtained from the NHBE cells where both liposomes seemed to be most effective at the highest concentration used (25 µg/ml), it was decided that remaining investigations would use this highest concentration only. The experimental plan was carried out in the same way as detailed previously and the corresponding levels of viral RNA quantified at 24 and 48 h post-RSV infection and relative to RSV L-gene copy number/ 1 µg RNA.

Figure 4.6 A illustrates that RSV-infected HBEC3-KT cells co-incubated with SAPS had significantly reduced L-gene copy number at both 24 and 48 h with ~93% less L-gene copies compared to untreated cells infected with RSV. In contrast, RSV-infected HBEC3-KT cells that were co-incubated with PAPC did not have significantly reduced copies of the RSV L-gene at either time point in comparison to untreated, RSV-infected cells (**Figure 4.6 A, B**).

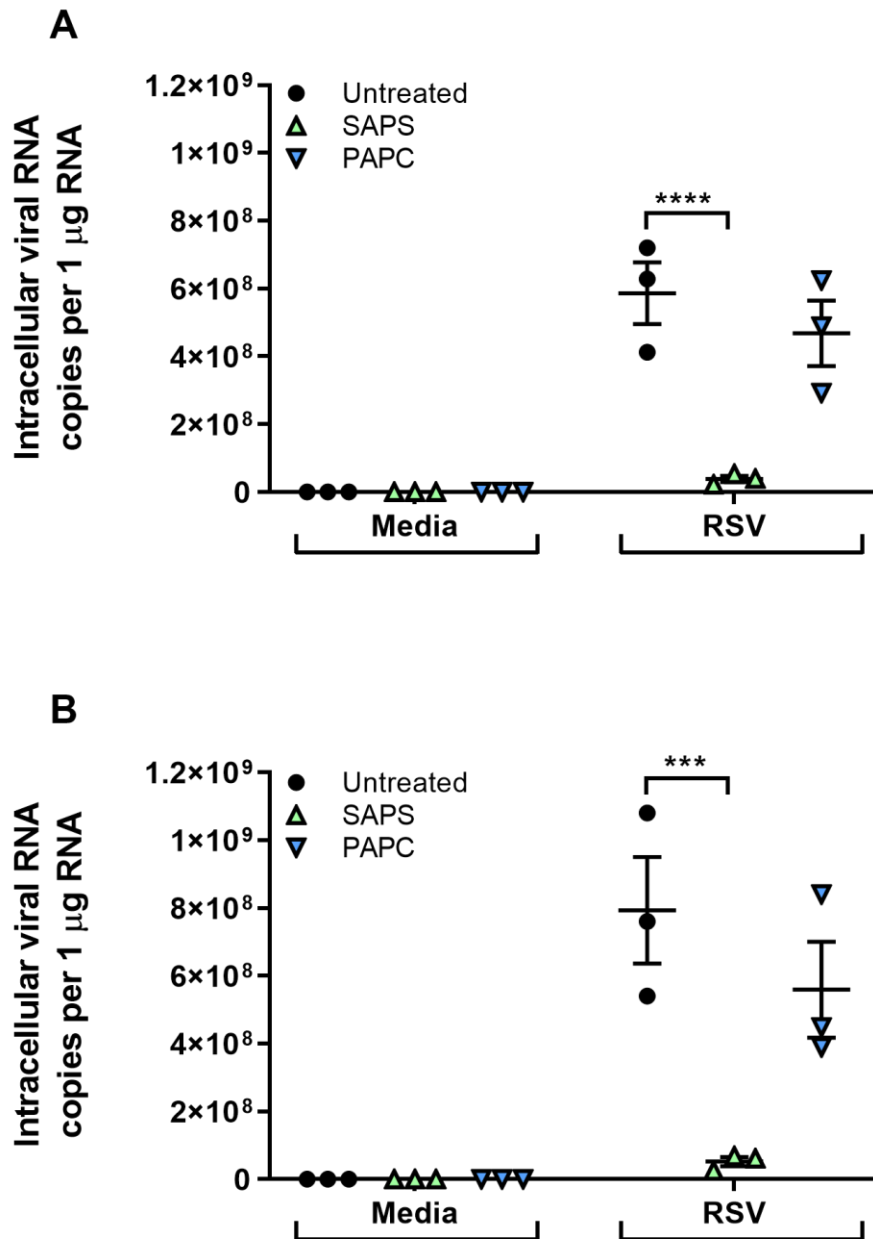


Figure 4.6 HBEC3-KT cells treated with SAPS have significantly lower levels of detectable viral RNA at 24 and 48 h. Cells were infected with RSV A2 (MOI 0.4) or stimulated with normal growth media. Designated cells were incubated with SAPS or PAPC (25 $\mu\text{g}/\text{ml}$) which remained on the cells throughout the 2 h incubation. After incubation, cells were washed to remove any unbound virus and designated cells treated once more with SAPS or PAPC (25 $\mu\text{g}/\text{ml}$). After 24 (**A**) and 48 h (**B**), RNA samples were collected, and levels of viral RNA quantified using RT-qPCR. All data are \pm SEM of N=3 independent experiments. Data were analysed using a two-way ANOVA and Tukey's multiple comparisons test. Significant differences are indicated by ***p < 0.001 **** p < 0.0001.

4.3.4 SAPS does not impact viral replication in HBEC3-KT cells when applied as a post-treatment

The data presented in this chapter thus far demonstrate evidence that SAPS (and to some extent PAPC) may be actively preventing the initial infection and associated subsequent viral replication of RSV within a range of airway epithelial cells. Inhibition of viral replication could result from reduced initial viral entry, and potentially also from direct effects on virus replication and release from infected cells. However, it was not known whether SAPS would be able to inhibit further replication and spread in cells already with an established RSV infection. To explore this further, HBEC3-KT cells were infected with RSV in the absence of SAPS to enable efficient viral uptake. Liposomes were applied at a range of times post-RSV infection including 2, 4 or 8 h post infection (RNA samples collected and analysed at 24 h) or 2, 4, 8 or 24 h post infection (RNA samples collected and analysed at 48 h).

These data collectively demonstrate that SAPS, when applied post-RSV infection, did not reduce copy numbers of the RSV L-gene at 24 or 48 h (**Figure 4.7**). In addition, RSV-infected HBEC3-KT cells that had received PAPC as a post treatment, had elevated levels of L-gene copies relative to HBEC3-KT cells that had not received any liposome treatment (**Figure 4.7 A, B**).

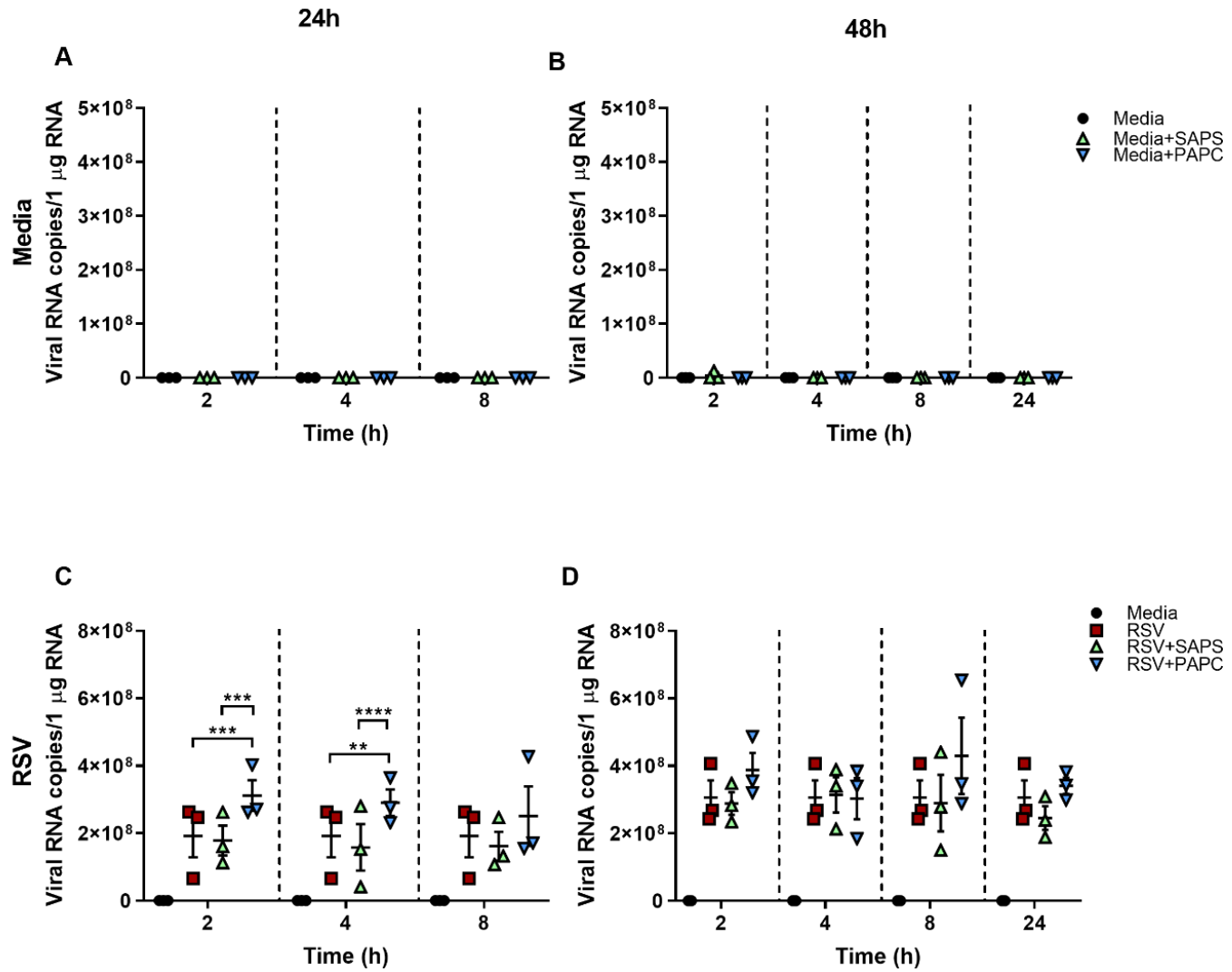


Figure 4.7 SAPS post-treatment does not impact on viral replication in HBEC3-KT. HBEC3-KT cells were infected with RSV A2 (C, D) or treated with media (A, B) for 2 h. After the 2 h incubation, cells were washed to remove unbound virus. The indicated cells were then treated once with SAPS/PAPC (25 µg/ml) at either 2, 4, 8 or 24 h after RSV infection. At 24 (A, C) and 48 h (B, D), RNA samples were collected, and levels of viral RNA quantified using RT-qPCR. All data are \pm SEM of N=3 individual experiments. Data were analysed using a two-way ANOVA and Tukey's multiple comparisons test. Significant differences are indicated by **p < 0.01, ***p < 0.001 and ****p < 0.0001.

4.4 Confocal microscopy for visualising RSV infection

In addition to the quantitative methods so far employed to determine the effect of SAPS and PAPC on viral infection and replication in airway cells, the interactions of RSV with airway epithelial cells were also explored using fluorescence microscopy. It was hoped that these techniques could then be advanced to live microscopy imaging however, due to the disruption of the COVID-19 pandemic, this was ultimately not achieved.

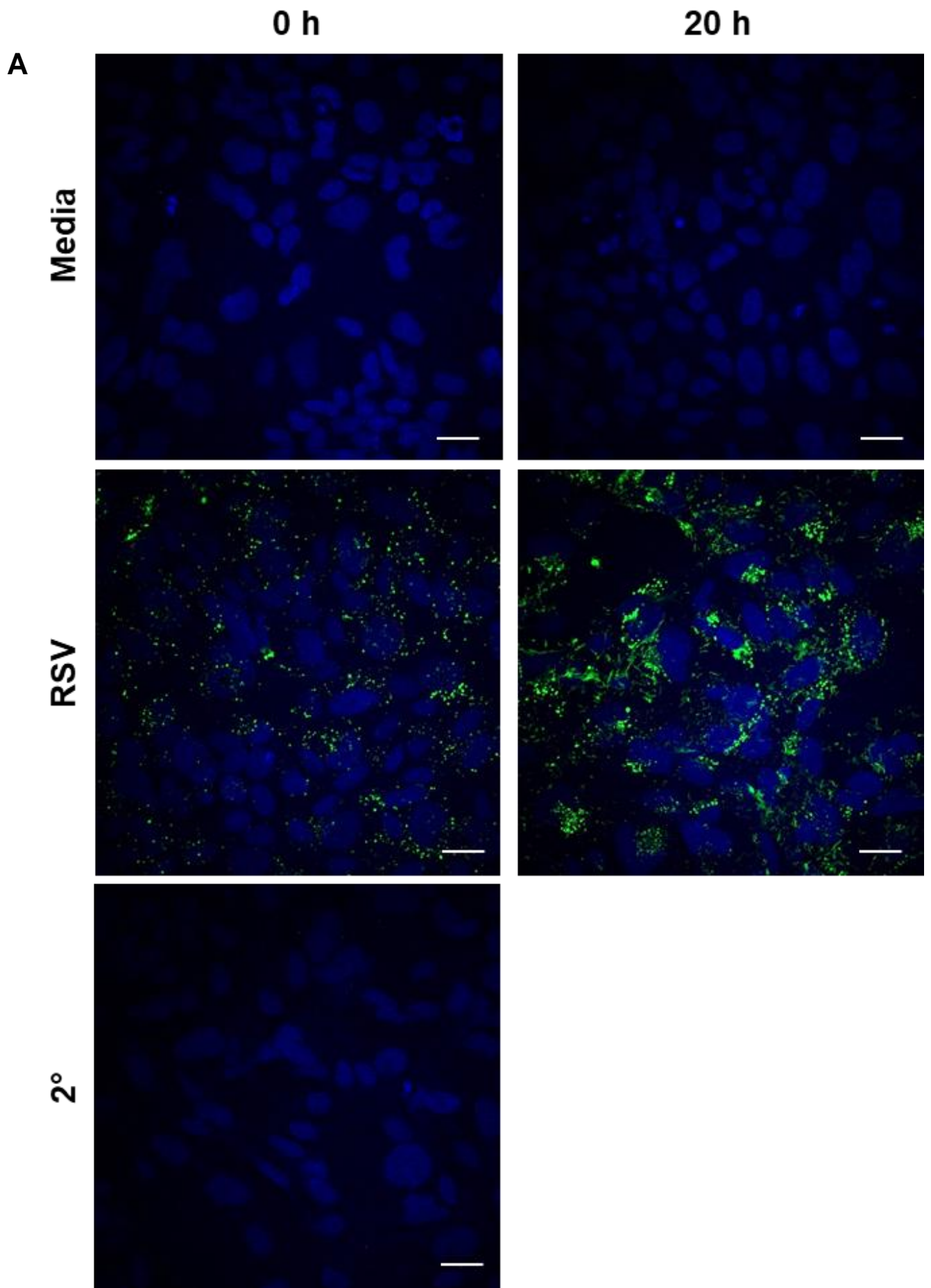
The rapid distribution of SAPS to both the external and inner membrane leaflets throughout BEAS-2B cells has previously been published by my research group where fluorescent SAPS was shown to distribute to membranes of the endosome and Golgi (Stokes et al., 2016) and has also been described in (Leventis and Grinstein, 2010). However, the mechanism of SAPS and PAPC integration into host cell membranes, and how this relates to their ability to modulate cellular responses and the RSV life cycle, remains unknown. Confocal microscopy techniques were therefore employed, first and foremost, to determine if RSV infection could be visualised and quantified within BEAS-2B cells using an anti-RSV fusion (F) antibody (Table 2.4). The results of these experiments would then be applied to future investigations to explore the modulatory effects of SAPS/PAPC on the infection, replication, or egress of RSV within airway epithelial cells, as well as imaging the colocalisation of RSV at MM.

4.4.1 Optimisation of RSV anti-fusion (F) antibody in BEAS-2B

To explore if RSV infection of BEAS-2B cells could be visualised and quantified using fluorescent microscopy, the cells were infected with RSV (MOI 1) for 2 h and then fixed with 4% PFA at either 0 h (immediately after the 2 h incubation with RSV) or at 20 h (when RSV would have had more time to replicate). Cells were stained using an antibody against the fusion (F) glycoprotein of the RSV virion and then stained with a secondary AlexaFluor 488 antibody (shown in green). DAPI staining (blue) was used to stain the cell nuclei of BEAS-2B cells so that cell number could be quantified. A secondary only control was included to ensure

that no non-specific binding was occurring and only RSV was being detected. It was predicted that there would be lower levels of RSV F protein detected at 0 h (and therefore less green fluorescent signal) in comparison to RSV-infected cells left for an additional 20 h with higher levels of F protein (emitting increased green fluorescent signal) indicative of increased RSV replication. Uninfected cells were also included for each time point to act as negative controls to confirm that green fluorescent signal should only be apparent in cells infected with RSV. Images were taken using a Nikon A1 Confocal and three separate fields of view captured for each sample to acquire a representative value for mean fluorescent intensity (MFI). Fields of view were selected using the DAPI only channel to avoid selective bias.

As illustrated in **Figure 4.8 A**, DAPI was used to stain the nuclear material of BEAS-2B cells (blue) which allowed quantification of cell number. As expected, no RSV F protein (green) was detected in the uninfected media control cells at either time point, whilst visible green fluorescence was observed in RSV-infected cells at both 0 and 20 h post infection (**Figure 4.8 A**). The levels of green fluorescence at 20 h appeared to have increased when visually compared to the 0 h time point in RSV-infected cells (**Figure 4.8 A**). This finding was confirmed by quantifying the mean fluorescent intensity (MFI) from the cells, where a 1.4-fold increase of green fluorescence was detected from 0 h to the 20 h time point (**Figure 4.8 B**). These data indicate that green fluorescence was observed within cells that had been infected with RSV but was not detected in uninfected cells and no non-specific binding occurred, as indicated by the secondary only (2°) control (**Figure 4.8 A**). The results therefore support the application of the anti-F antibody and confocal microscopy technique to help visualise and quantify RSV infection within BEAS-2B cells.



B

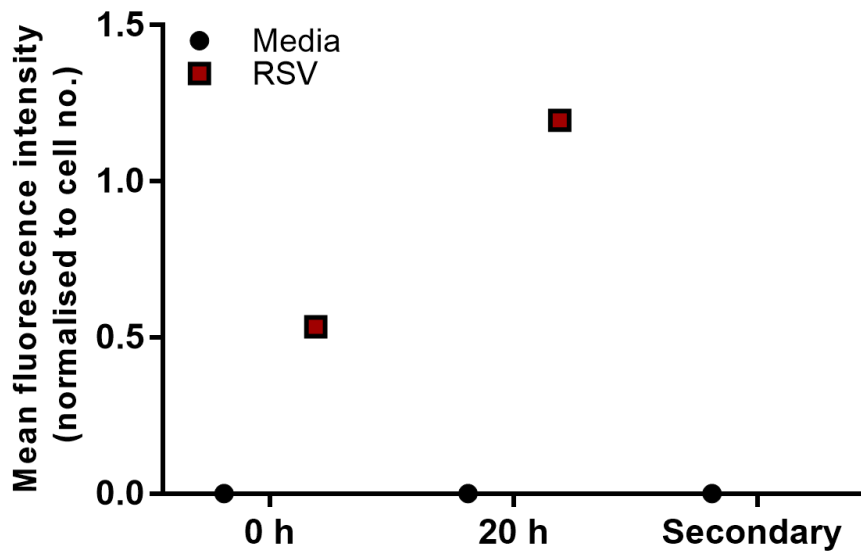


Figure 4.8 Confocal microscopy to visualise and quantify RSV infection. BEAS-2B cells were grown to 80% confluence on coverslips and infected with RSV A2 (MOI 1) for 2 h. Unbound virus were removed and cells either fixed immediately (0 h) or incubated for a further 20 h before fixation with 4% PFA. Cell nuclei were stained using DAPI (blue) and viral infected cells stained using a primary antibody targeting the RSV anti-F (fusion) protein and then secondary staining with AlexaFluor-488 (green). Confocal microscopy was used to visualise levels of RSV infection at 0 h and 20 h. A secondary only control (2^0) was also included to determine if any non-specific binding was occurring (A). Mean fluorescence intensity was calculated relative to cell number (B). Data is N=1. Magnification = x 600. Scale bar is 22 μ m.

4.4.2 Optimisation of RSV F antibody staining in NHBE Cells

It was important to confirm that the fluorescent staining achieved in the BEAS-2B cells would also work effectively in NHBE and HBEC3-KT cells. Two independent NHBE donors were infected with RSV (MOI 0.4) as in Section 4.4.1. In addition to a secondary only (2°) antibody control, an additional well was incubated with an isotype control (Table 2.4), to further determine that non-specific binding had not occurred (**Figure 4.9 A**). Mean fluorescence intensity (MFI) was quantified for each NHBE cell donor at 0 h and 20 h post viral infection.

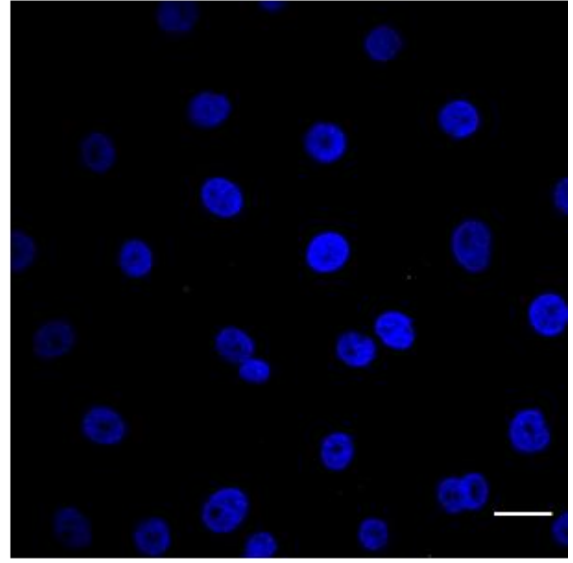
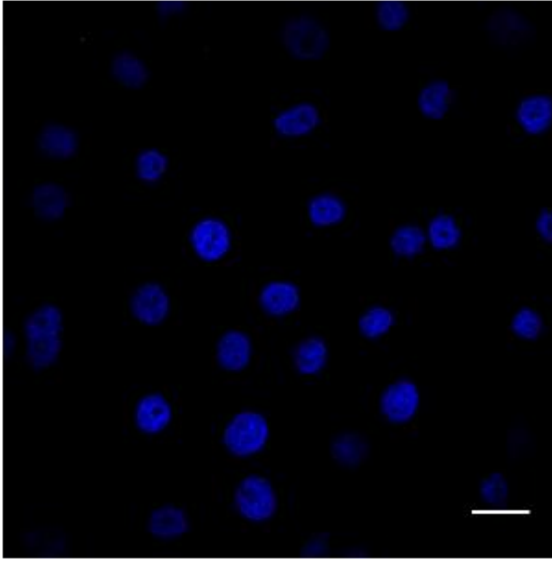
Images were collated using ImageJ software and demonstrate a representative image from three separate fields of view (randomly selected) from each sample (**Figure 4.9 A**). The collated images demonstrate that there was visibly more green fluorescence in the later time point (20 h) in comparison to 0 h in both NHBE cell donors infected with RSV (**Figure 4.9 A**). This was confirmed through quantification of the mean fluorescence intensity (MFI) values for each image, which indicated that green fluorescence (RSV F-protein) was augmented over the 20 h period from 0.14 MFI at 0 h up to 2.52 MFI at 20 h (**Figure 4.9 B**). Uninfected cells that had been stimulated with media, secondary, or the isotype control alone, had no visible green fluorescence and the MFI remained below 0.1 MFI (**Figure 4.9 B**).

A

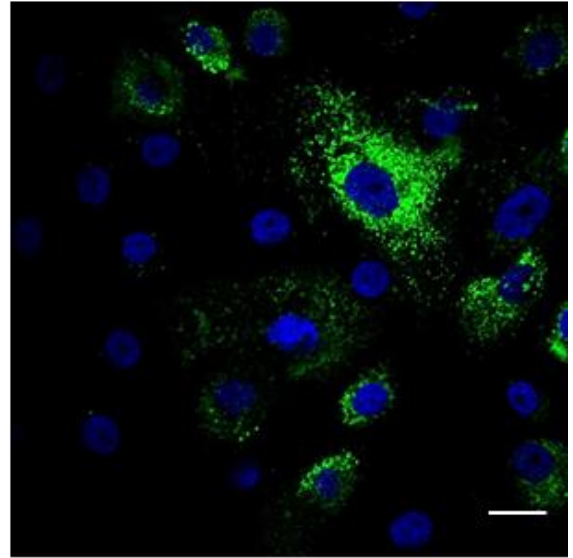
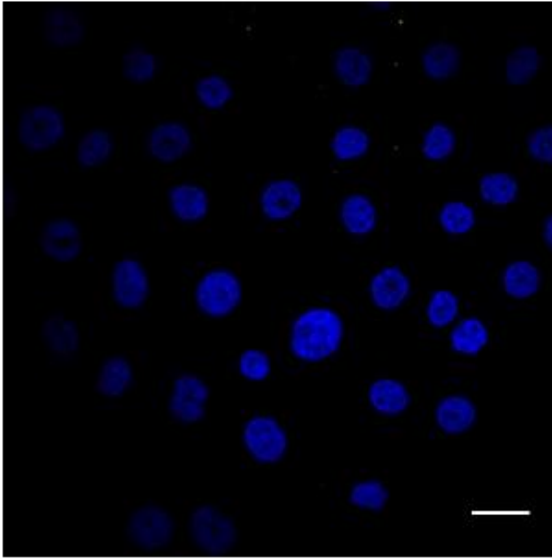
0 h

20 h

Media

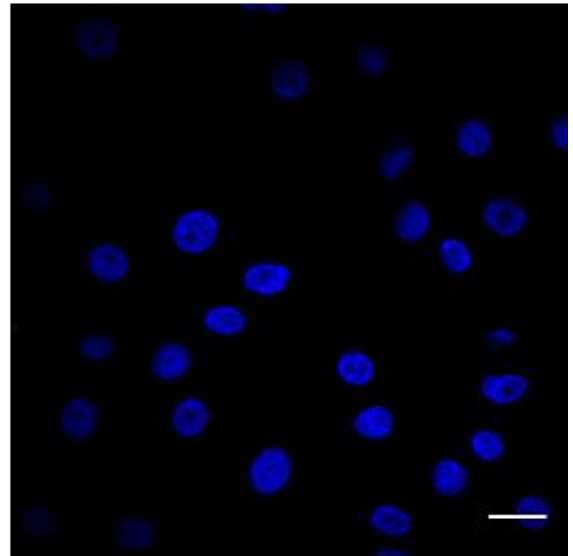
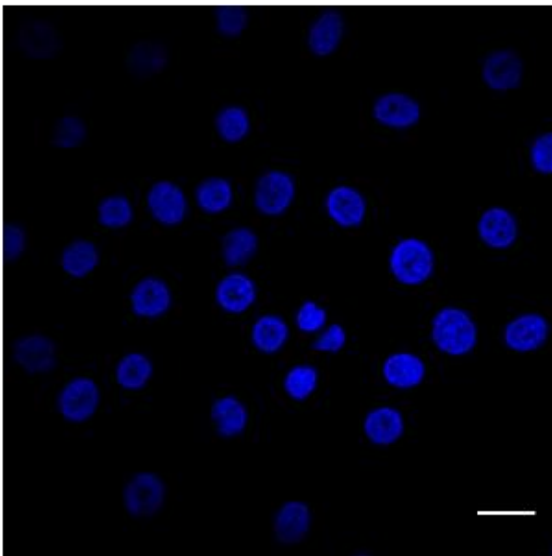


RSV



2° only

Isotype



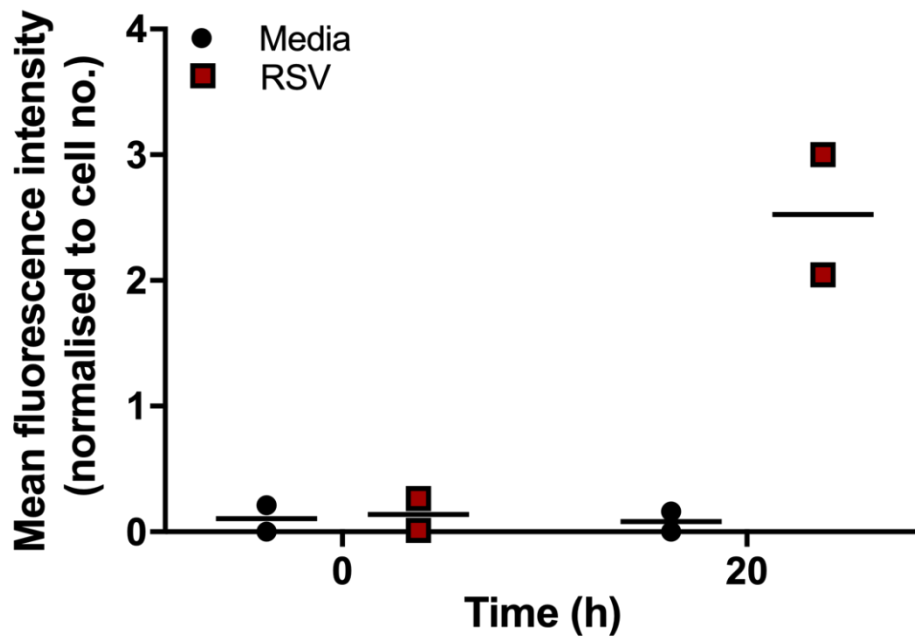
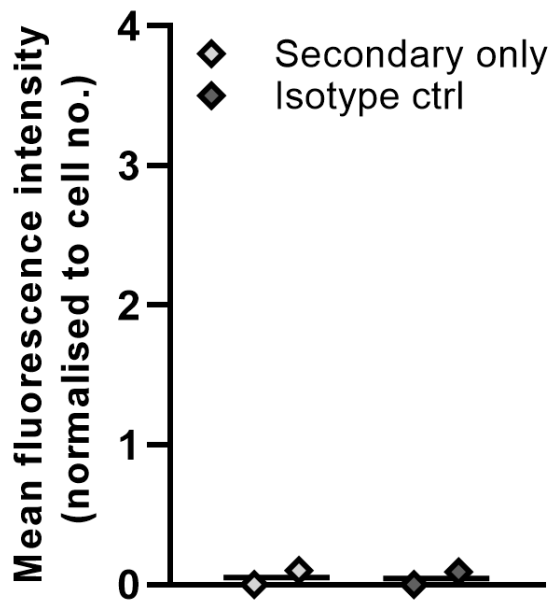
B**C**

Figure 4.9 Confocal microscopy can be used to quantify viral infected cells. NHBE cells were grown to 80% confluence on coverslips and infected with RSV A2 (MOI 0.4) for 2 h. Unbound virus was removed, and cells were either fixed immediately (0 h) or incubated for a further 20 h before fixation with 4% PFA. Cell nuclei were stained using DAPI (blue) and viral infected cells stained using a primary antibody targeting the RSV anti-F (fusion) protein and then secondary staining with AlexaFluor-488 (green). Control cells were incubated with secondary antibody (AlexaFluor 488) or the isotype control only to confirm that no unspecific binding occurred. Confocal microscopy was used to visualise levels of RSV infection at 0 h and 20 h in two independent NHBE donors and representative images are shown (A) Mean fluorescence intensity was calculated relative to cell number (B, C). Data are N=2 from two independent NHBE cell donors. Magnification = x 600. Scale bars are 22 μ m.

4.4.3 Phalloidin staining in HBEC3-KT cells to visualise the interaction of RSV at filament rich microdomains

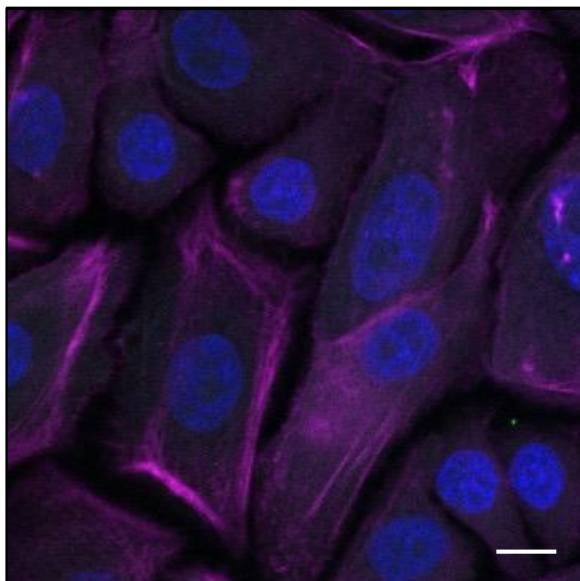
The difficulties associated with imaging MM has often meant that their existence has been extensively critiqued (**Section 1.5.1**). There is published evidence for the role of actin filament rearrangement within host cells to enable the formation of MM (Head et al., 2014; Jumat et al., 2015, 2014), and therefore in the following experiments the staining of actin using a lipophilic probe (phalloidin) was incorporated to identify potential MM regions within the cell. For these studies, a Zeiss Airyscan confocal microscope was used as it offers better opportunities for live-microscopy imaging. The Airyscan enables better visualisation of the field by increasing spatial resolution compared to a standard confocal microscope, but without the increased excitation power of super resolution microscopy which may bleach samples (Korobchevskaya et al., 2017).

Quantification of the mean fluorescent intensity (MFI) for HBEC3-KT cells indicated that there was more background green fluorescence in the uninfected HBEC3-KT cells stimulated with media only, than observed using the Nikon A1 confocal microscope. Therefore, the average background green fluorescence from all four fields of view were quantified and the average value subtracted from the RSV-infected cells to confirm that any green fluorescence was indeed due to the presence of RSV-F protein. As demonstrated in **Figure 4.10 A**, visible green fluorescence was observed in the HBEC3-KT cells infected with RSV at MOIs of 0.2, 0.4 or 0.8, indicative of detectable RSV fusion (F) protein (**Figure 4.10 B**). Of note, and as indicated by the white arrows, there were multiple images where the localisation of green fluorescent protein appeared to be accumulating at areas of the cell membrane that was additionally rich in actin (as demonstrated by the density of purple stain) (**Figure 4.10 A**).

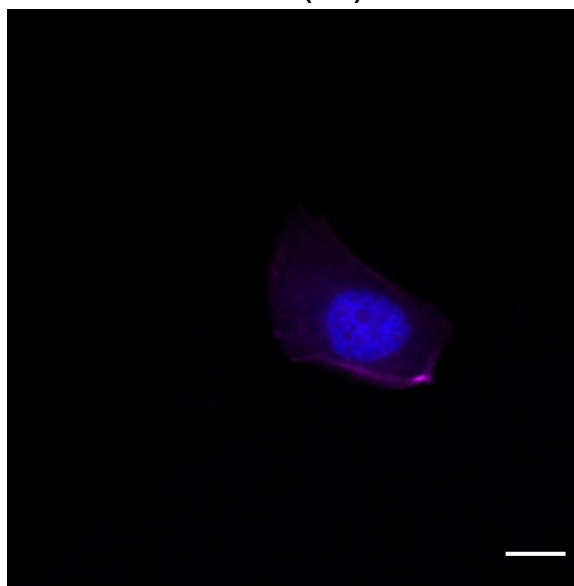
These data indicate that increased green fluorescence was observed with increased RSV MOI. As the collated images demonstrate the interaction of RSV with localised points of the cell membrane, the next step was to determine the impact of SAPS on this interaction.

A

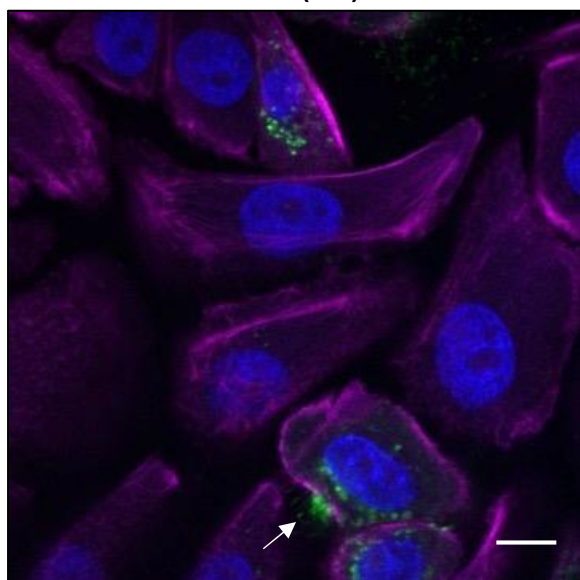
Media



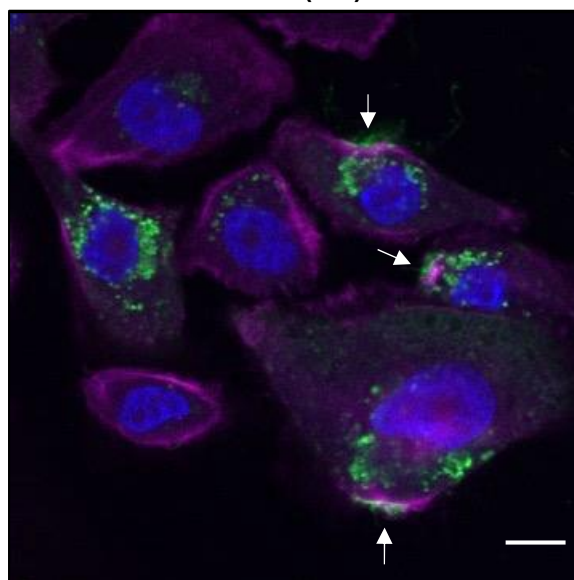
RSV (0.1)



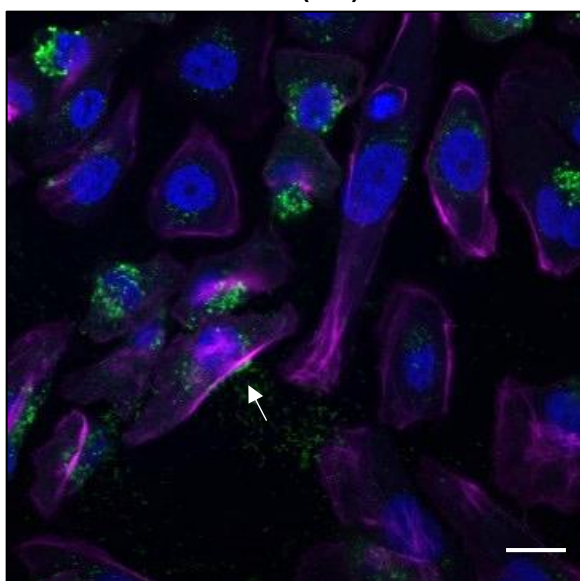
RSV (0.2)



RSV (0.4)



RSV (0.8)



B

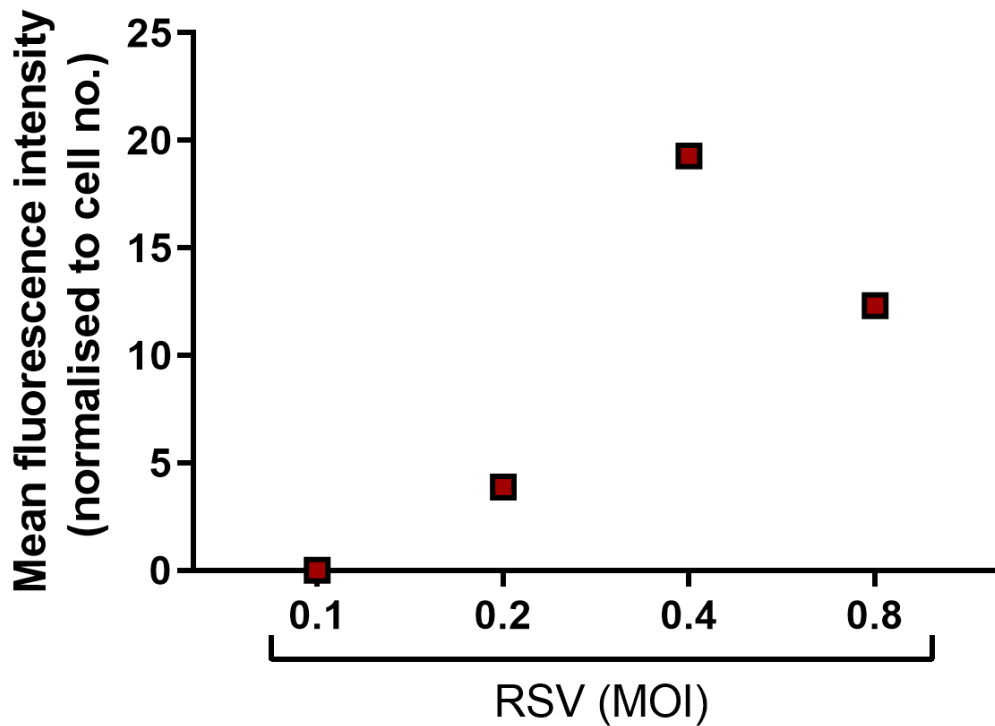


Figure 4.10 Optimisation of phalloidin staining in RSV-infected cells. HBEC3-KT cells were grown to 80% confluence on coverslips and infected with RSV A2 (MOI 0.1, 0.2, 0.4 and 0.8) for 2 h. Unbound virus was removed, and the cells were incubated for 20 h then fixed with 4% PFA. Cell nuclei were stained using DAPI (blue) and viral infected cells were stained using RSV anti-F (fusion) antibody and fluorescent secondary antibody AlexaFluor-488 (green). Actin filaments were stained using Texas Red phalloidin (purple). An Airyscan confocal microscope was used to visualise levels of RSV infection at 20 h. White arrows indicate possible colocalisation of RSV egressing from actin-rich areas of cell membrane (**A**). Mean fluorescence intensity was calculated relative to cell number and background fluorescence of the media control was subtracted from the RSV samples (**B**). Data are from one independent experiment. Images were obtained using the 60X oil lens. Scale bars are 9 μ m.

4.4.4 SAPS visibly reduces levels of viral infection in HBEC3-KT cells

Due to time constraints created by the COVID-19 pandemic, the remaining experiments were streamlined by omitting the use of PAPC with the focus solely on SAPS.

As demonstrated in section 4.4.3, potential RSV colocalisation with actin-rich filaments of the cell membrane was observed, and subsequent experiments explored if SAPS could modify these interactions and reduce the number of virus infected cells.

To explore the mechanism and identify at what point SAPS is affecting RSV binding/fusion to the HBEC3-KT cells, two different incubation temperatures were used to distinguish viral binding and viral fusion events. As demonstrated in (San-Juan-Vergara et al., 2012, 2004), the incubation of RSV with cells at 4 °C allows viral binding but does not allow viral fusion events with the cell membrane, whilst increasing the temperature to 37 °C allows for viral fusion and entry. Thus, the temperature chosen can distinguish what effect SAPS is having on each stage of the viral life cycle and if actin filament rearrangement can be observed during viral entry or release. Viral infection was also compared between HBEC3-KT cells with or without SAPS treatment during the infection stages. As a control, some of the HBEC3-KT cells in each plate were stimulated with media and incubated with SAPS (25 µg/ml) to confirm that SAPS treatment alone would not obscure fluorescent signal.

A summary timeline for this experimental procedure is given below (**Figure 4.11**). To complete these investigations, two duplicate plates of HBEC3-KT cells were exposed to RSV (MOI 0.4) or basal media for 1 h at 4 °C in the presence/absence of SAPS (25 µg/ml). One plate was then washed using ice cold PBS to remove any unbound virus and subsequently fixed with 4% PFA. The second plate was transferred to a humidified incubator for 1 h at 37 °C, 5% CO₂ to allow viral fusion and infection of the HBEC3-KT cells. Cells were washed to remove any unbound virus, required wells treated again with SAPS (25 µg/ml) then the plate put back into the incubator for 20 h. Cells were fixed and stained with DAPI to identify cell nuclei (blue),

RSV fusion (F) protein and secondary antibody staining (green), and actin filaments stained with phalloidin (magenta). Cells were imaged using a Zeiss Airyscan confocal microscope. The mean fluorescence intensity (MFI) was quantified for each sample and is summarised in **Figure 4.12 E**. The media samples for each time point contained a low level of background green fluorescence and this was deducted from all RSV-infected samples and media samples treated with SAPS only to ensure any green fluorescence detected was due to viral infected cells and levels of F-protein rather than background noise (**Figure 4.12 E**). The data and images demonstrate that SAPS treatment alone did not interfere with the green fluorescent signal in either of the channels used and would therefore not obscure the fluorescent MFI values for SAPS-treated cells infected with RSV (**Figure 4.12 A, B**).

HBEC3-KT cells incubated with RSV for 1 h at 4 °C had low baseline MFI values representative of RSV F-protein (**Figure 4.12 E**). Due to low repeats in this sample (N=2 repeats only), no statistical analysis between cells co-incubated with SAPS and those that had not received liposome treatment at this time point. However, there was visibly reduced green fluorescence in HBEC3-KT cells infected with RSV in the presence of SAPS compared to RSV-infected cells that had received no liposome treatment at this early time point (**Figure 4.12 C**).

Green fluorescent staining in the RSV-infected HBEC3-KT cells at 20 h was higher than that in the 0 h samples (**Figure 4.12 C, D**). Of interest, HBEC3-KT cells that had been co-incubated with SAPS during RSV infection demonstrated significantly reduced levels of green fluorescence with a reduction of ~90% MFI (**Figure 4.12 D, E**).

In addition, images from HBEC3-KT cells infected with RSV for 20 h suggested co-localisation at actin-rich membranes where RSV can be seen apparently egressing from the cells (**Figure 4.13 A, B, C**). Interestingly, none of the SAPS-treated cells displayed this morphological event. Furthermore, where virus was identified at the 20 h time point the cells appeared to have different characteristics with the virus appearing perinuclear and the cell membrane appeared

to be ruffling and condensing in size (**Figure 4.14**). This was not apparent in any of the RSV-infected cells that did not receive SAPS treatment. Attempts were made to try and quantify co-localisation of RSV at actin-rich membranes, but these proved challenging and were not completed and thus results are based on visual interpretation only.

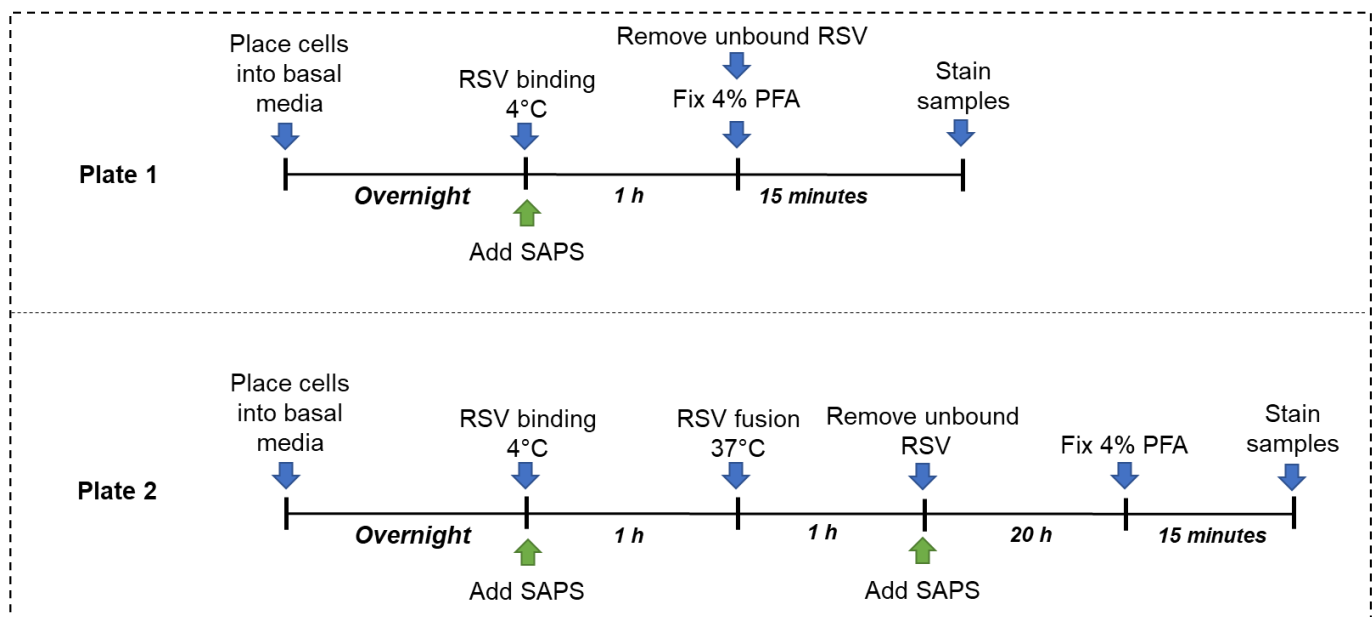


Figure 4.11 Summary timeline indicating the times at which cells are infected with RSV and incubated with SAPS.

HBEC3-KT cells were stimulated with media or infected with RSV A2 (MOI 0.4) for 1 h at 4 °C in the presence/absence of SAPS (25 µg/ml). Plate 1 was then washed using ice cold PBS to remove any unbound virus and subsequently fixed with 4% PFA. Plate 2 was transferred to a humidified incubator for 1 h at 37 °C, 5% CO₂ to allow viral fusion and infection of the HBEC3-KT cells. Cells in plate 2 were washed to remove any unbound virus, required wells treated again with SAPS (25 µg/ml) then put back into the incubator for 20 h before fixing with 4% PFA. After fixation, plates were stained with DAPI to identify cell nuclei (blue), RSV fusion (F) protein and secondary antibody staining (green), and actin filaments stained with phalloidin (magenta). Cells were imaged using a Zeiss Airyscan confocal microscope.

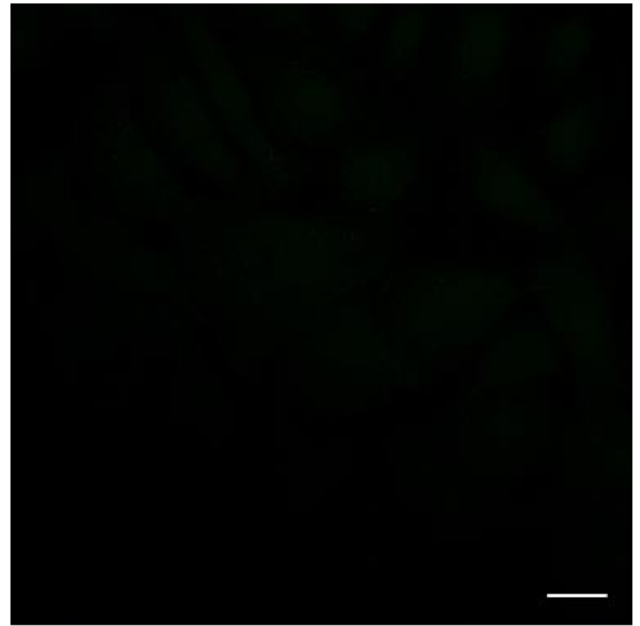
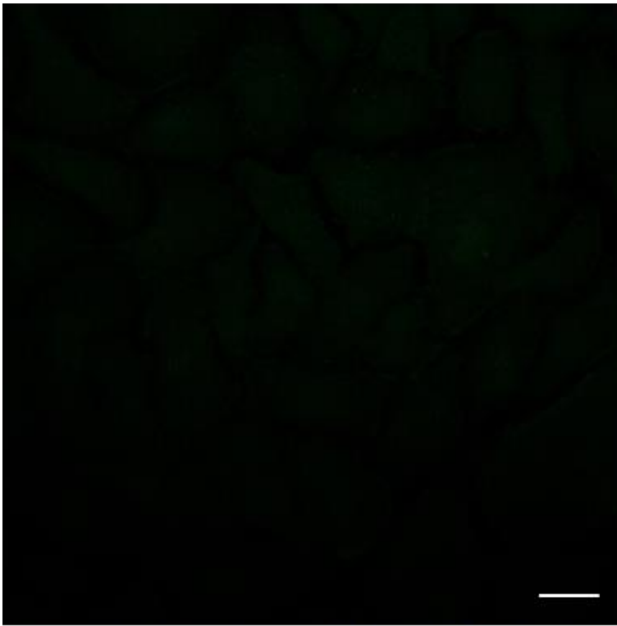
A

1 h at 4 °C

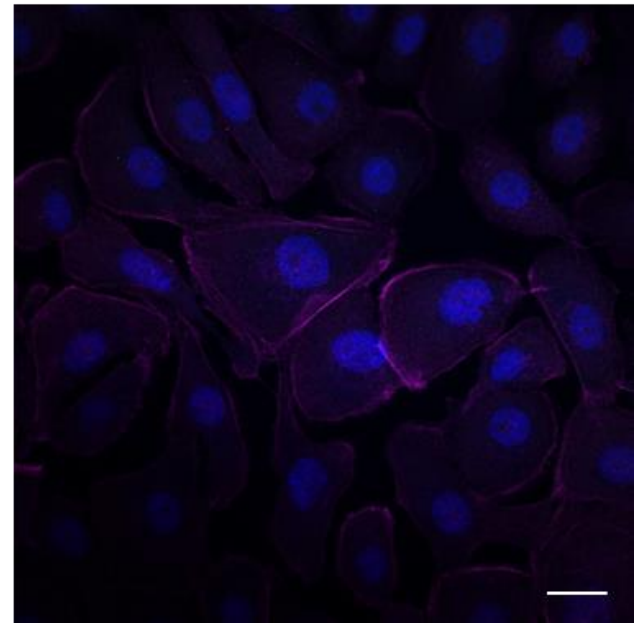
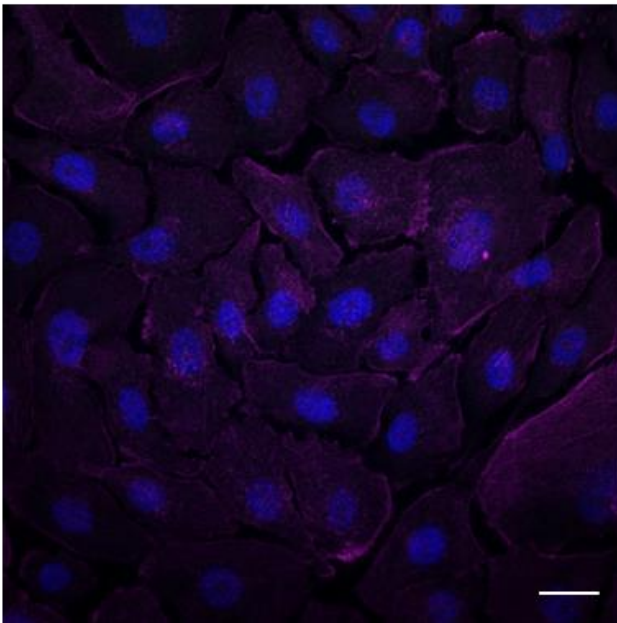
Media

Media+SAPS

RSV F-protein (green)



Merged



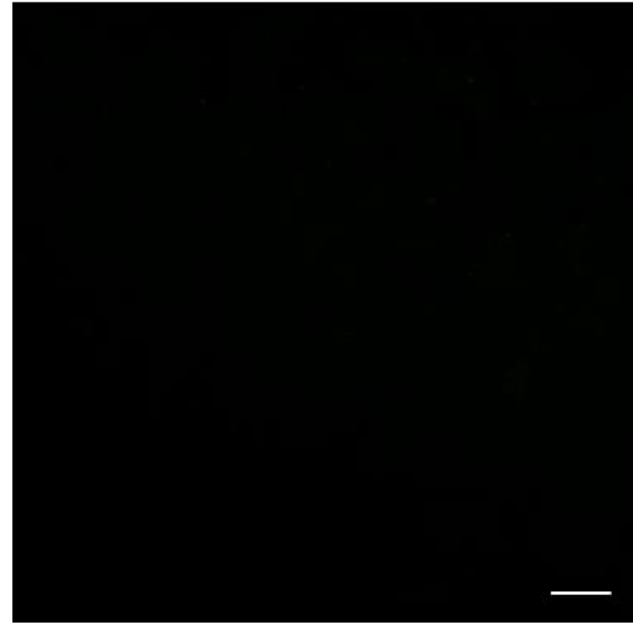
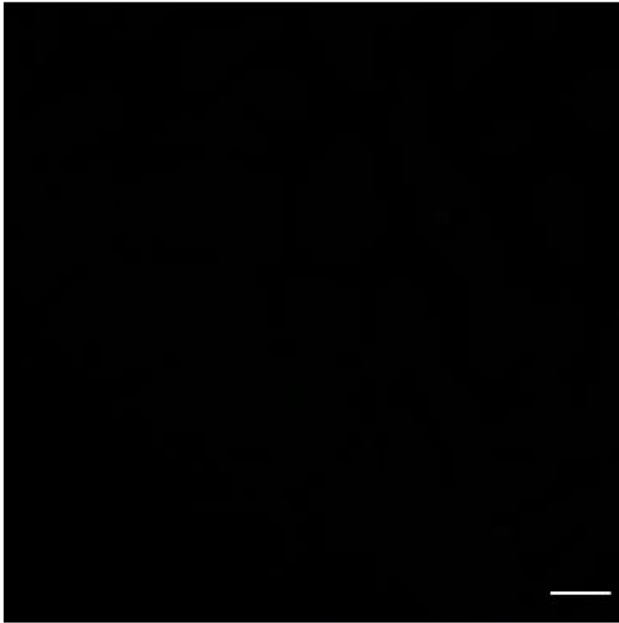
B

20 h at 37 °C

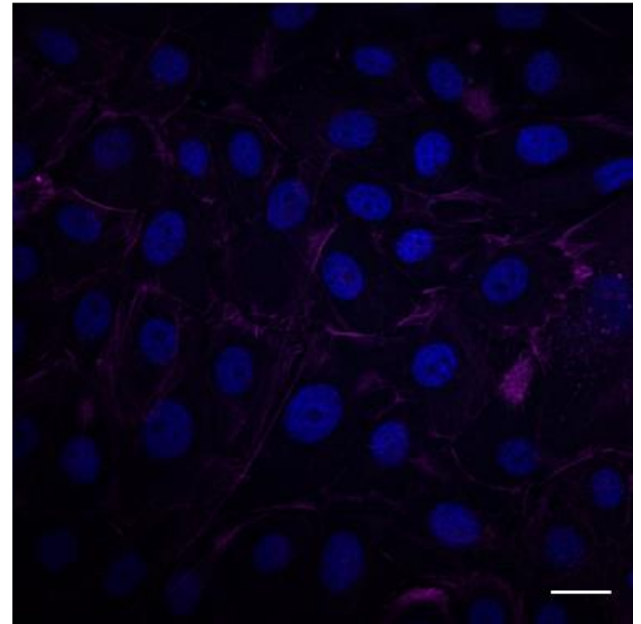
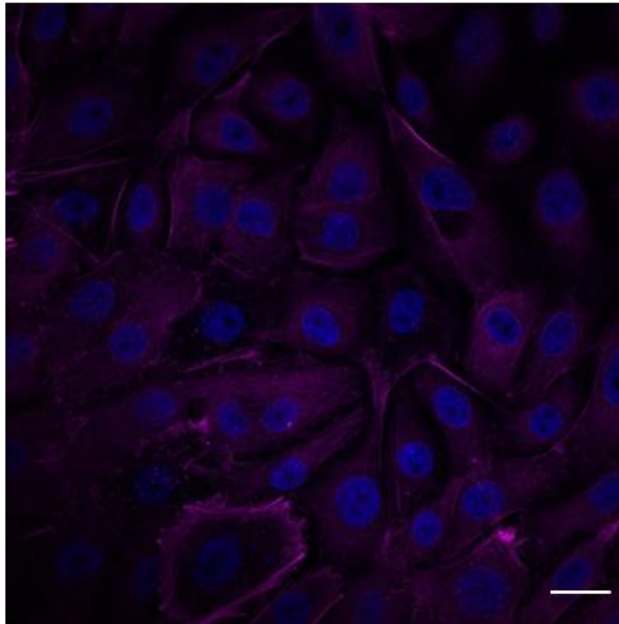
Media

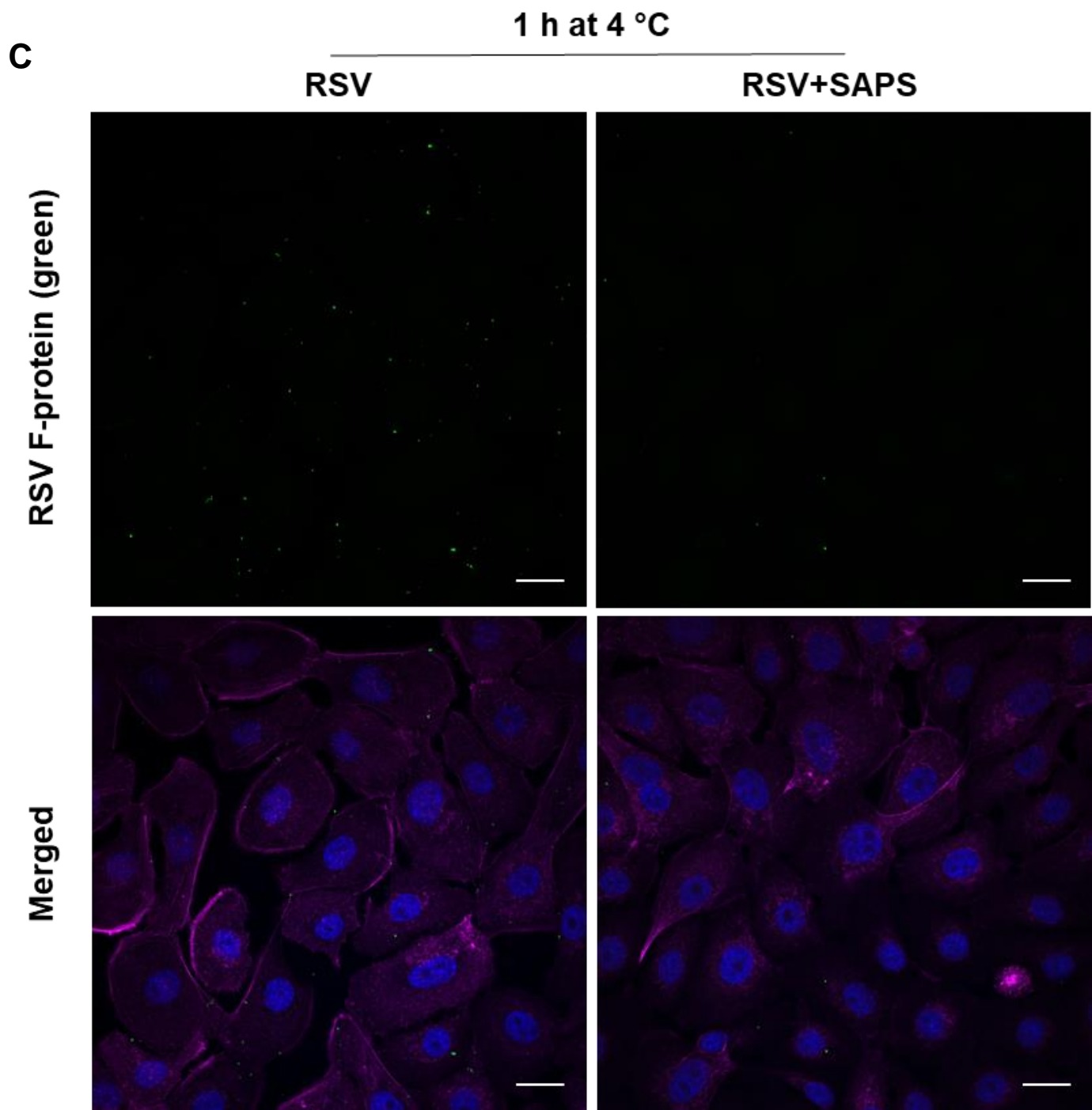
Media+SAPS

RSV F-protein (green)



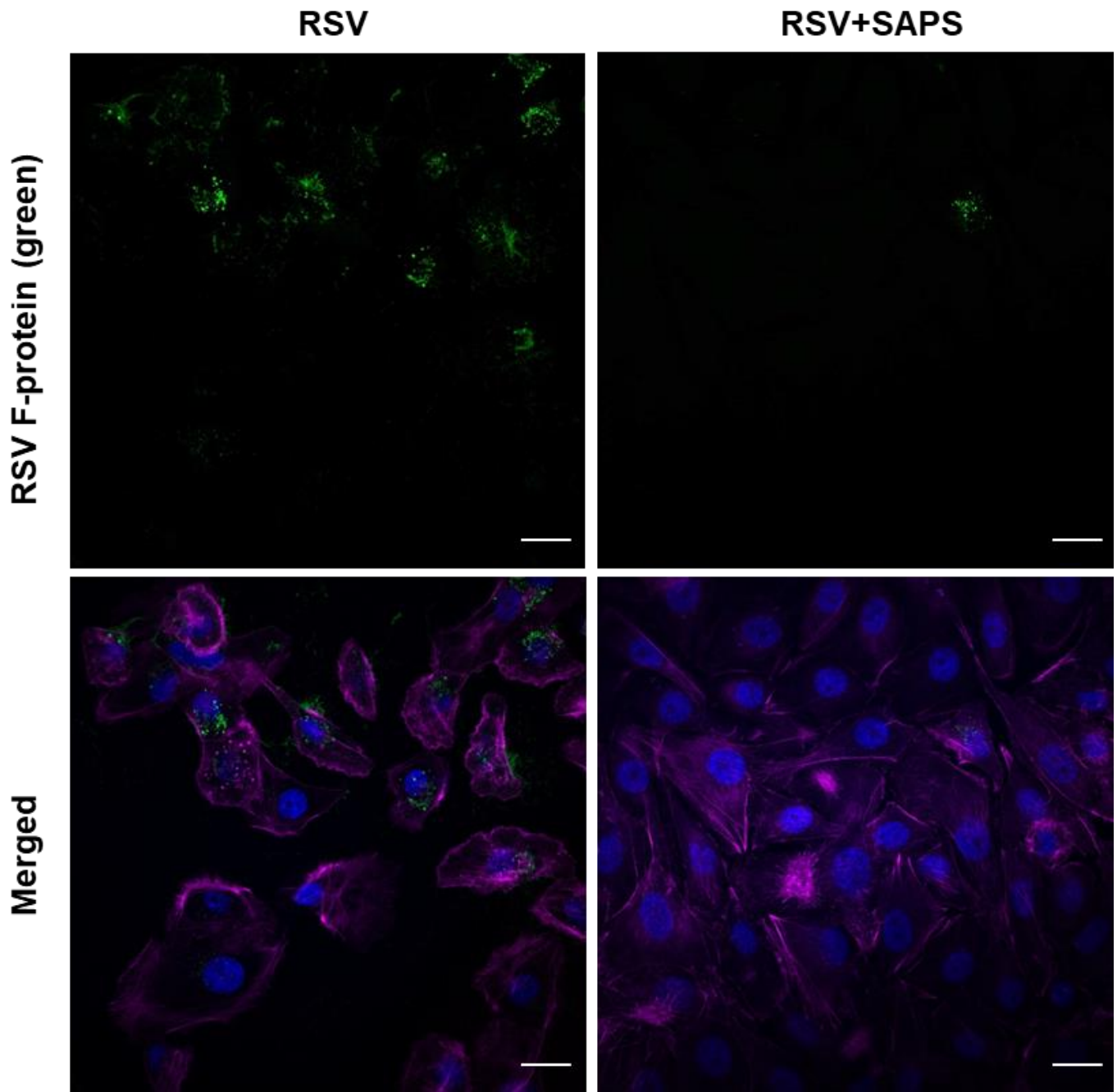
Merged





D

20 h at 37 °C



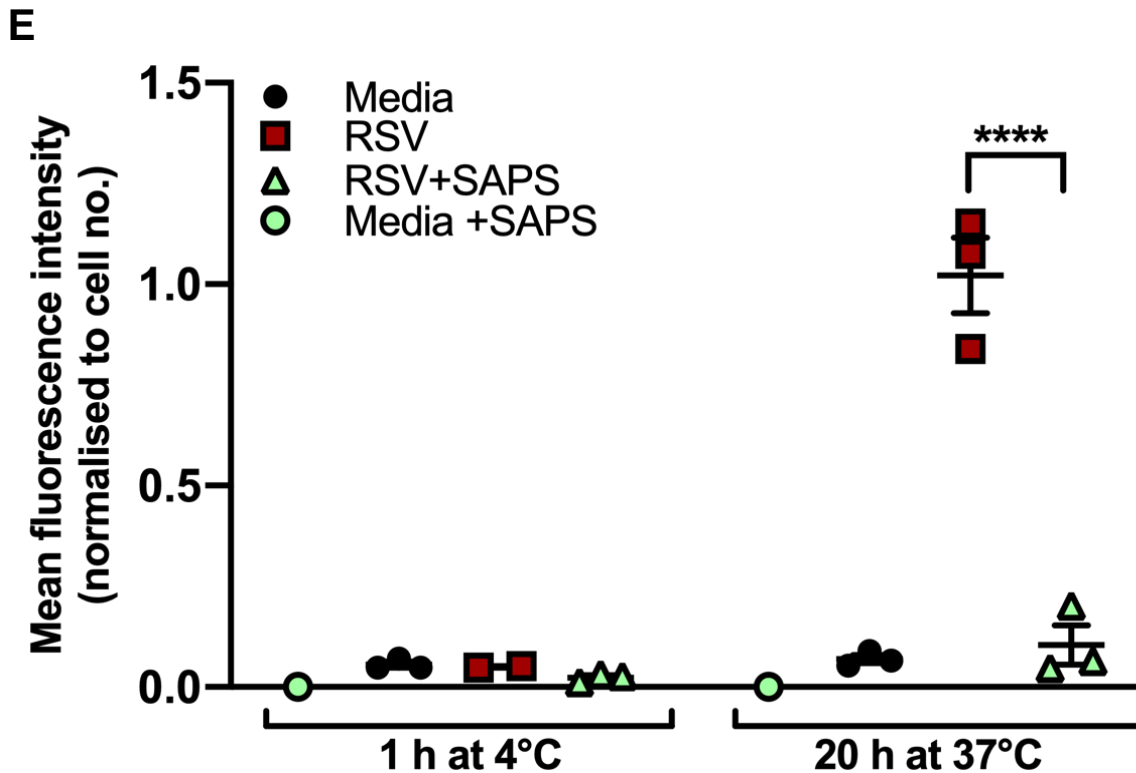


Figure 4.12 Investigating the effect of SAPS on viral infection within HBEC3-KT cells and the role of actin rearrangement. HBEC3-KT cells were grown to 80% confluence on coverslips and stimulated with media or infected with RSV A2 (MOI 0.4) in the presence or absence of SAPS (25 $\mu\text{g}/\text{ml}$). Cells were incubated for 1 h at 4°C to allow for viral binding. Cells were either washed to remove unbound virus and fixed immediately (1 h at 4°C) with 4% PFA or, placed in an incubator for an additional 1 h to allow viral internalisation after which, unbound virus was removed, designated cells retreated with SAPS (25 $\mu\text{g}/\text{ml}$) and the cells incubated for a further 20 h (20 h at 37°C) before cells were washed and fixed with 4% PFA. Cell nuclei were stained using DAPI (blue) and viral infected cells were stained using RSV anti-F (fusion) antibody and fluorescent secondary antibody AlexaFluor-488 (green). Actin filaments were stained using Texas Red phalloidin (purple). An Airyscan confocal microscope was used to visualise cells stimulated with media (**A**, **B**) or infected with RSV (**C**, **D**) (\pm SAPS) after 1 h at 4°C (**A**, **C**) or 20 h at 37°C (**B**, **D**). Mean fluorescence intensity was calculated relative to cell number and background fluorescence of the media control was subtracted from the RSV samples (**E**). Data are from three independent experiments from different population of HBEC3-KT cells. Images were obtained using the 60X oil lens. Scale bars are 22 μm . Significant differences are indicated by ****p < 0.0001

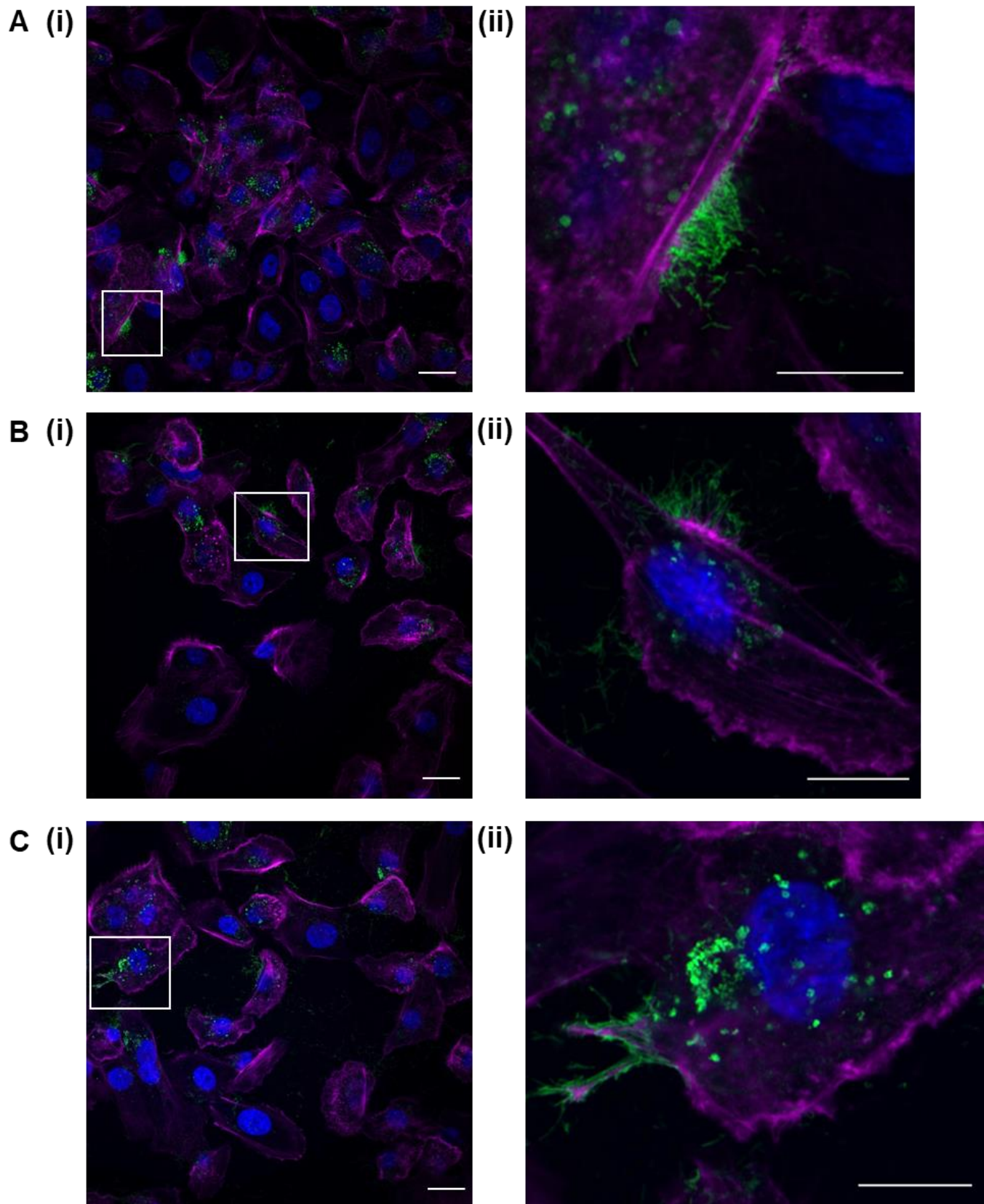


Figure 4.13 Images demonstrating the interactions of RSV at actin-rich membranes of HBEC3-KT cells. HBEC3-KT cells were grown to 80% confluence on coverslips and infected with RSV A2 (MOI 0.4) for 1 h at 4°C to allow for viral binding. Cells were then placed in an incubator at 37°C for an additional 1 h to allow viral internalisation after which, unbound virus was removed, and the cells incubated for a further 20 h (20 h at 37°C). Cells were washed and fixed with 4% PFA. Cell nuclei were stained using DAPI (blue) and viral infected cells were stained using RSV anti-F (fusion) antibody and fluorescent secondary antibody AlexaFluor-488 (green). Actin filaments were stained using Texas Red phalloidin (purple). An Airyscan confocal microscope was used to visualise cells infected with RSV and images were analysed using ImageJ software to obtain images for the selected field of view (i) (22 µm) and relative zoomed in areas (ii) of the image are additionally demonstrated where the scale bar is 10 µm. Images are from three representative independent experiments. Images were obtained using the 60X oil lens.

RSV+SAPS 20 h at 37 °C

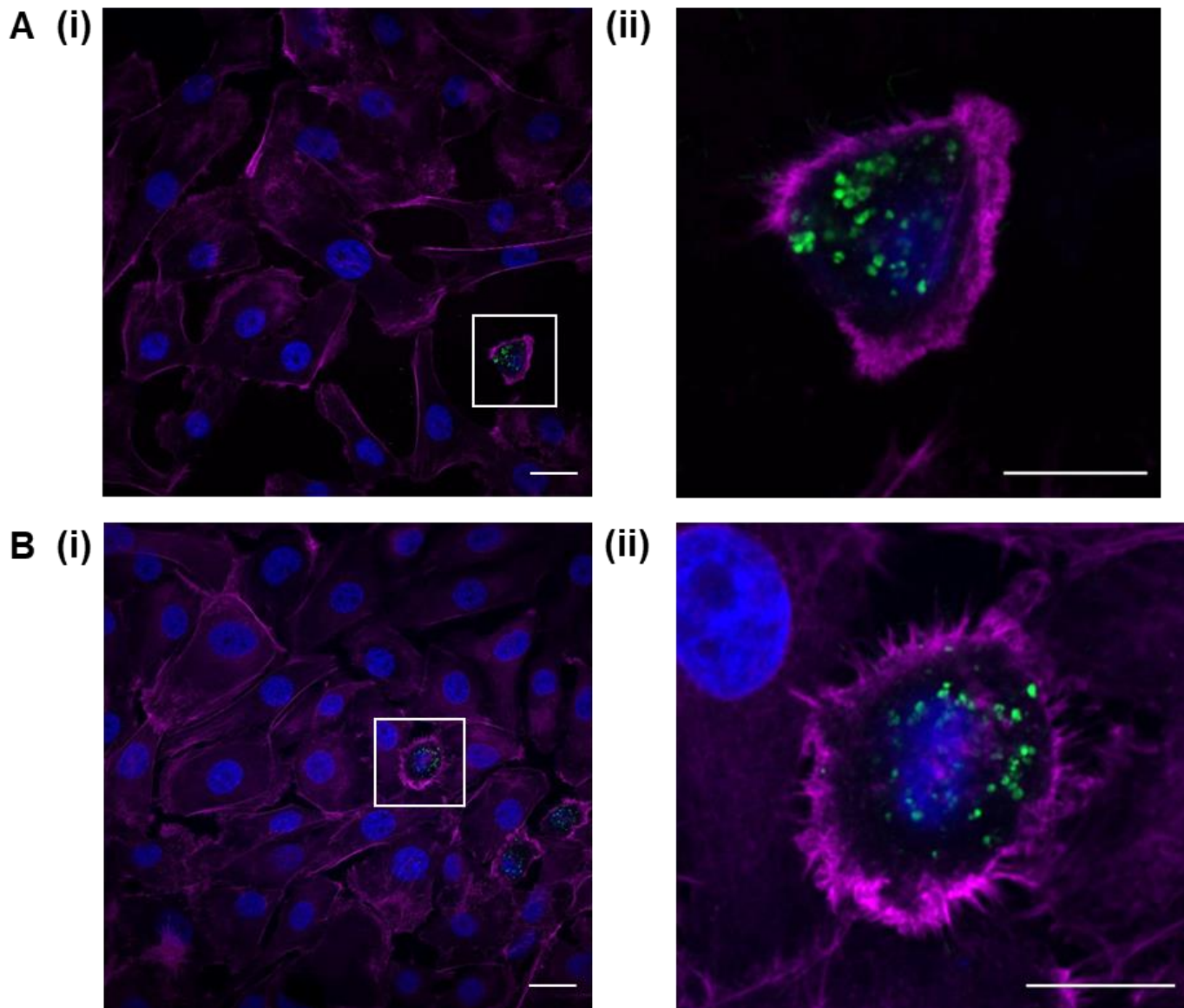


Figure 4.14 Images demonstrating the morphology of HBEC3-KT cells infected with RSV in the presence of SAPS. HBEC3-KT cells were grown to 80% confluence on coverslips and infected with RSV A2 (MOI 0.4) in the presence of SAPS (25 $\mu\text{g}/\text{ml}$) for 1 h at 4°C to allow for viral binding. Cells were then placed in an incubator at 37°C for an additional 1 h to allow viral internalisation after which, unbound virus was removed, and designated cells retreated with SAPS. Cells were incubated for a further 20 h after which, cells were washed and fixed with 4% PFA. Cell nuclei were stained using DAPI (blue) and viral infected cells were stained using RSV anti-F (fusion) antibody and fluorescent secondary antibody AlexaFluor-488 (green). Actin filaments were stained using Texas Red phalloidin (purple). An Airyscan confocal microscope was used to visualise cells infected with RSV and images were analysed using ImageJ software to obtain images for the selected field of view (i) (22 μm) and relative zoomed in areas (ii) of the image are additionally demonstrated where the scale bar is 10 μm . Images are from three representative independent experiments. Images were obtained using the 60X oil lens.

4.5 Section summary

Work within this chapter aimed to explore the effect of SAPS/PAPC treatment on the RSV life cycle events in AECs. Data indicated that co-incubation of NHBE cells with SAPS (and to some extent PAPC) during viral challenge, significantly reduced the number of infected cells after 24 h (**Figure 4.3**). In addition, co-incubation of AECs with SAPS during infection with RSV significantly reduced the level of viral RNA quantified at 24 and 48 h (**Figure 4.5 and Figure 4.6**). In addition, (**Figure 4.10 and 4.13**) demonstrate that RSV may interact with actin-rich areas (indicative of MM formation) of AEC membranes during viral egress. **Figure 4.12 C** also indicates that SAPS may inhibit initial binding events of RSV to AEC.

4.6 Exploring the efficacy of SAPS to perturb bacterial co-infections in RSV-infected cells

As previously discussed, (Section 1.4), viral infections (such as with RSV) can predispose individuals to concurrent or subsequent bacterial co-infections which may potentiate severe disease (Cilla et al., 2008; Honkinen et al., 2012; Thorburn et al., 2006). One of the most common bacterial species isolated from individuals (particularly those that have been hospitalised) with RSV is *Streptococcus pneumoniae* (*Spn*). As summarised in Section 1.4, some of the ways in which RSV infection has been demonstrated to increase the occurrence of bacterial co-infection are through direct destruction of the protective airway epithelium and modulation of immune signalling. Data presented in this thesis demonstrate that co-incubating HBEC3-KT cells with SAPS during infection with RSV protects the cells from viral infection, subsequent viral replication and associated inflammatory responses. In addition, a previous publication by Parker et al. (2008) demonstrated that co-incubation of SAPS with PBMCs diminished IL-1 β (and CXCL8 in unpublished data) production from cells infected with heat killed *Spn*. With these findings in mind, it was hypothesised that SAPS may modulate the ability of *Spn* to co-infect airway epithelial cells after exposure to RSV. To better understand the role RSV may play in predisposing individuals to subsequent bacterial infections, experiments were conducted whereby HBEC3-KT cells were infected with RSV in the presence/absence of SAPS before subsequent infection with *Spn* 24 h later.

4.6.1 HBEC3-KT infections with *Streptococcus pneumoniae*

Over 100 different serotypes of *Spn* have been identified based on their genetically distinct polysaccharide capsule (Ganaie et al., 2020). The capsule is an important virulence factor for *Spn* protecting it from immune-mediated phagocytosis and aiding its ability to colonise the nasopharynx (Morona et al., 2004). Pneumococcal conjugate vaccines (that target the capsule) have been widely used to control *Spn* infections, however, *Spn* can also exist in an unencapsulated form and cases of unencapsulated serotypes have been on the increase

since the use of pneumococcal conjugate vaccines (Ganaie et al., 2020). Unencapsulated *Spn* serotypes may be able to bind airway epithelial cells more readily than capsulated forms, causing more invasive disease (Adamou et al., 1998; Talbot et al., 1996). In addition, more recent work has demonstrated that *Spn* are able to shed their capsule during infection in the airways to allow for better adherence and invasion of airway epithelial cells using a phase transition from transparent (low capsule expression) to opaque (high expression of capsule) (Hammerschmidt et al., 2005).

Due to the increased ability of unencapsulated *Spn* serotypes to adhere to and invade airway epithelial cells and their current clinical importance, unencapsulated strains of *Spn* were selected for the following investigations. The unencapsulated *Spn* serotype, FP22, is an isogenic unencapsulated derivative of serotype 2 strain D39 (Pearce et al., 2002) originally gifted from Professor Tim Mitchell (University of Birmingham). The D39 strain has been used extensively in research for studying the interactions of *Spn* with airway epithelial cells (Adamou et al., 1998; Hammerschmidt et al., 2005; Küng et al., 2014; Marriott et al., 2012; Talbot et al., 1996). For fluorescent studies, the unencapsulated serotype FT4 (originally provided by Dr Andrew Fenton, University of Sheffield) was used which is engineered to express a protein called mKate tagged to histone-like protein A (hlpA), a DNA binding protein which is encoded in the chromosome of FT4 and results in bright red fluorescence as more protein is transcribed during bacterial growth of stocks (Bonnet et al., 2017; Kjos et al., 2015).

4.6.2 Optimising *Streptococcus pneumoniae* infection of HBEC3-KT cells

To my knowledge, investigations looking at viral-bacterial co-infections of HBEC3-KT cells are limited, and it was therefore important to first establish a suitable co-infection model that would support both RSV and *Spn* infections over a 48 h period. Unencapsulated serotypes of *Spn* induce more CXCL8 production from airway epithelial cells in comparison to capsulated strains through exposure of the *Spn* cell wall during infection and exposure of the pneumolysin toxin to TLR2 and TLR4 (Baumgartner et al., 2016; Küng et al., 2014, 2014; Marriott et al., 2012).

It was therefore important to determine which MOI of *Spn* would induce a quantifiable CXCL8 response from the HBEC3-KT cells. It was also important to observe how exposure to *Spn* would affect HBEC3-KT cell viability.

HBEC3-KT cells were infected with a range of bacterial MOI (0.5, 1, 1.5, 5 and 10) and cell viability or CXCL8 release quantified 24 h later by CellTiter-Glo® and ELISA respectively. Infections were carried out as described (Section 2.11.1).

As demonstrated in **Figure 4.15 A**, increasing the bacterial MOI resulted in decreased HBEC3-KT cell viability at 24 h post infection in comparison to uninfected cells. Cell viability was significantly decreased where MOI 5 and MOI 10 were used (**Figure 4.15 A**). Cells stimulated with the PBS control did not result in a marked decrease in cell viability, apart from one outlier where the viability dropped to around 60%. As expected, the staurosporine treated cells (positive control for cell death) demonstrated a significant decrease in cell viability at 24 h in comparison to unstimulated media control cells (**Figure 4.15 A**).

As shown in **Figure 4.15 B**, CXCL8 production at 24 h from HBEC3-KT cells increased with increasing MOI of *Spn*. In comparison to uninfected HBEC3-KT cells (media control), cells infected with MOI 1, 5 and 10 *Spn* resulted in a significant increase of CXCL8 production. HBEC3-KT cells stimulated with media or that were mock infected (PBS control) did not incur increased CXCL8 production (**Figure 4.15 B**).

Based on these data, an MOI of 1 was selected for future studies exploring *Spn* infection in RSV-infected HBEC3-KT cells, as *Spn* alone at this MOI 1 did not induce significant cell death but still induced the release of CXCL8, this lower MOI of *Spn* may also be tolerable in RSV-infected cells.

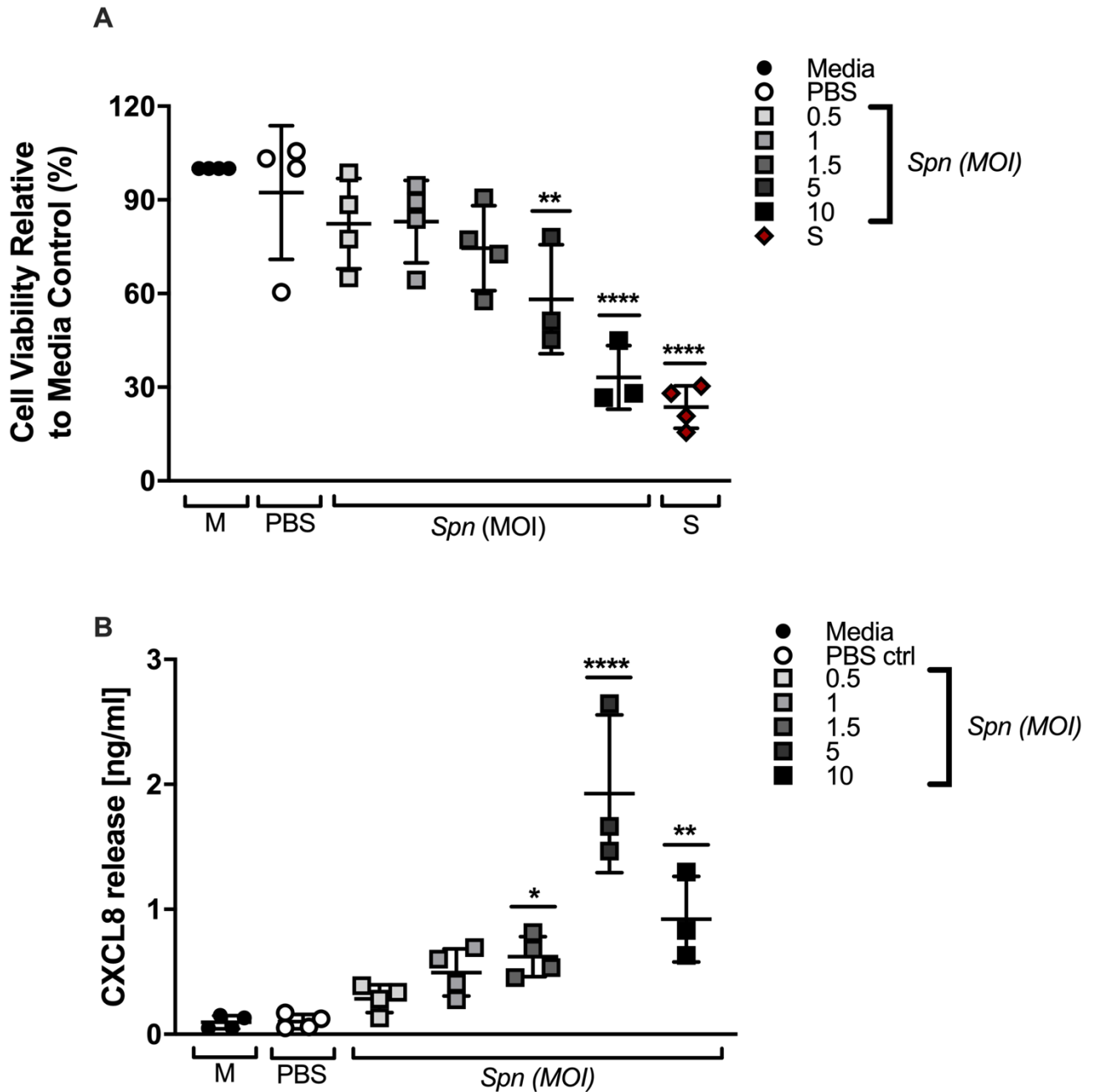


Figure 4.15 Optimisation of *Streptococcus pneumoniae* infection conditions. HBEC3-KT cells were infected with a range of *Spn* MOI (0.5 – 10) for 1 h. Cells were subsequently treated with antibiotics (100 µg/ml Gentamicin/100 µg/ml Streptomycin and 100 U penicillin) for 1 h to prevent overgrowth of bacteria overnight. Cells were washed and fresh basal media added before the plates were incubated overnight. Staurosporine (S) was added as a positive control for cell death. At 24 h a CellTiter-glo® assay was used to determine cell viability (A). Cell-free supernatants were generated and the levels of CXCL8 quantified via ELISA (B). Data are ± SEM of N=3/4 technical repeats. Data were analysed using a one-way ANOVA with Dunnett's post-test relative to the media control. Raw values were used for the analysis of cell viability. The displayed data represents cell viability relative to the media control which has been normalised to 100%. Significant differences are indicated by *p < 0.05, **p < 0.01 and ****p < 0.0001.

4.6.3 SAPS significantly reduces the number of viable *Spn* after 1 h incubation

To investigate if SAPS would have any direct effects on *Spn* viability, bacteria ($\sim 2.31 \times 10^5$ CFU/ well) were incubated in a 12-well tissue culture plate (with no cells) for 1 h in the presence or absence of SAPS (25 $\mu\text{g/ml}$) (Section 2.11.1). Supernatants were collected and serially diluted onto blood agar. **Figure 4.16** demonstrates the quantity of viable bacteria (CFU/ well) after 24 h incubation.

Spn untreated with SAPS grew over the one-hour period, increasing from 2.31×10^5 CFU to 1.92×10^6 ($\pm 2.22 \times 10^4$) CFU/well. However, there was significantly lower levels of growth from *Spn* that had been co-incubated with SAPS for the 1 h incubation period indicating that SAPS may have some bactericidal/bacteriostatic properties (**Figure 4.16**).

The effect of SAPS on bacterial adhesion was next investigated in the presence of HBEC3-KT cells.

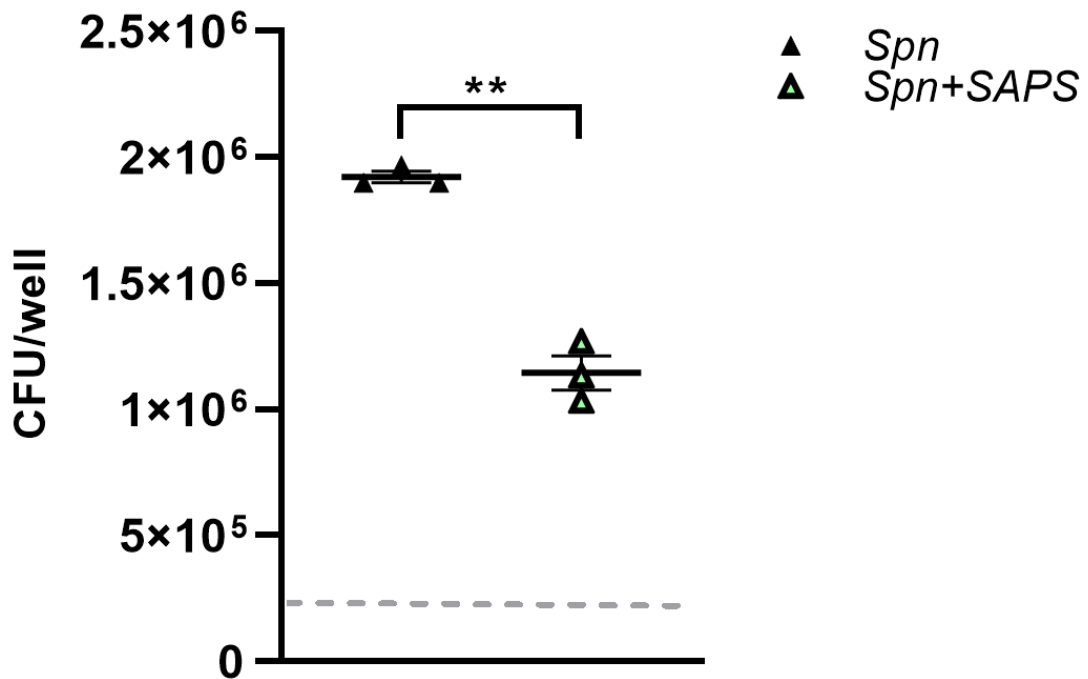


Figure 4.16 Investigating the direct impact of SAPS (25 µg/ml) on *Streptococcus pneumoniae* (*Spn*) growth. One frozen aliquot of *Spn* (FP22) was prepared in basal medium (2.31×10^5 CFU/200 µl) and added to a 24-well plate (200 µl/well) in the presence or absence of SAPS (25 µg/ml). The plate was then incubated for 1 h. The bacterial suspension was collected and gently washed over the well 10x to aid the removal of any bacteria bound to the plastic. Samples of the bacterial suspension from each well were removed and serial dilutions completed. Samples were plated on blood agar and incubated for 24 h where upon Miles Misra calculations were completed. The grey dashed line indicates the approximate number of bacteria (CFU) added to each well at the start of the incubation period calculated as (2.31×10^5 CFU/ml). Data are \pm SEM of N=3 technical replicates from one vial of frozen bacterial stock. Data were analysed using a paired t-test where significant differences are indicated by **p <0.01.

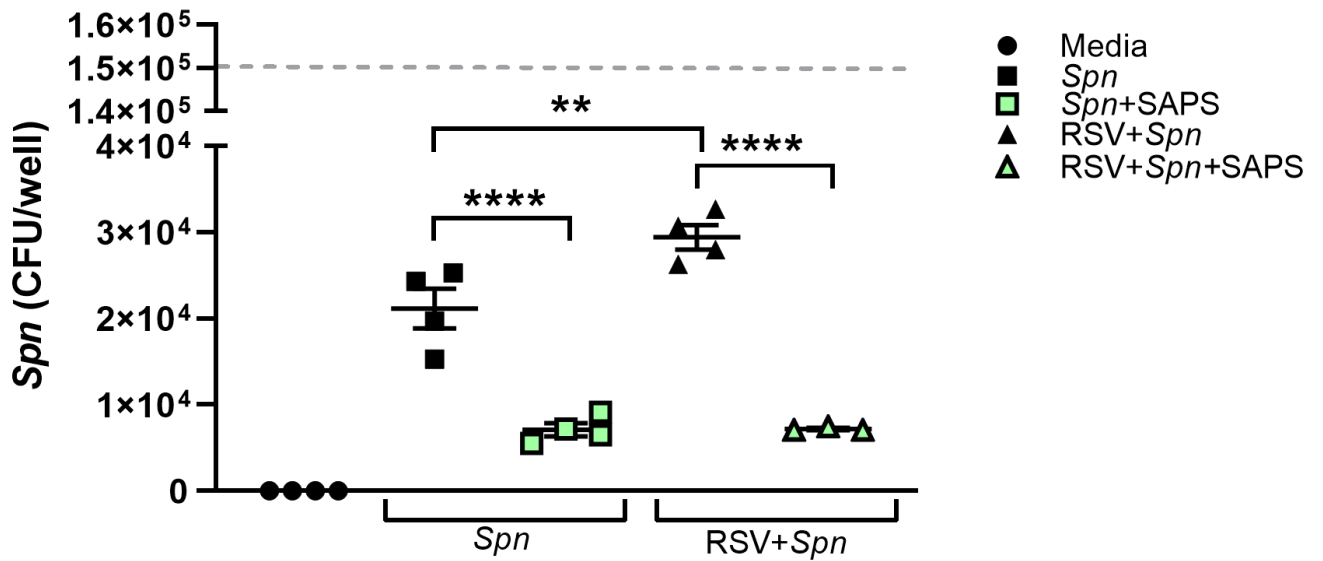
4.6.4 Adherence of *Streptococcus pneumoniae* is upregulated in RSV-infected HBEC3-KT cells but significantly inhibited with SAPS

Published research shows that preceding viral infections (including RSV) can enable increased bacterial adherence of *Spn* to a range of airway epithelial cells (Agarwal et al., 2013; Avadhanula et al., 2006; Hament et al., 2005, 2004; Novick et al., 2017; Park et al., 2021).

A timeline for these investigations is summarised below demonstrating that cells were infected with RSV or stimulated with media for 2 h in the presence/absence of SAPS (25 µg/ml). Cells were incubated for 24 h before subsequent infection with *Spn* (MOI 1) or stimulated with media for 1 h. Cells were detached, and the number of colonies quantified (**Figure 4.17 B**).

As demonstrated (**Figure 4.17 A**), around 14% of *Spn* that were initially added at the start of infection (indicated by the grey dashed line) were able to adhere to the HBEC3-KT cells in the absence of RSV. However, the levels of bacterial adherence were significantly increased in HBEC3-KT cells that had been infected with RSV prior to bacterial infection (**Figure 4.17 A**). Of interest, HBEC3-KT cells that had been incubated with SAPS 24 h prior to bacterial infection resulted in significantly reduced bacterial adherence in both the RSV-infected cells and cells that had not been infected with virus (**Figure 4.17 A**).

A



B

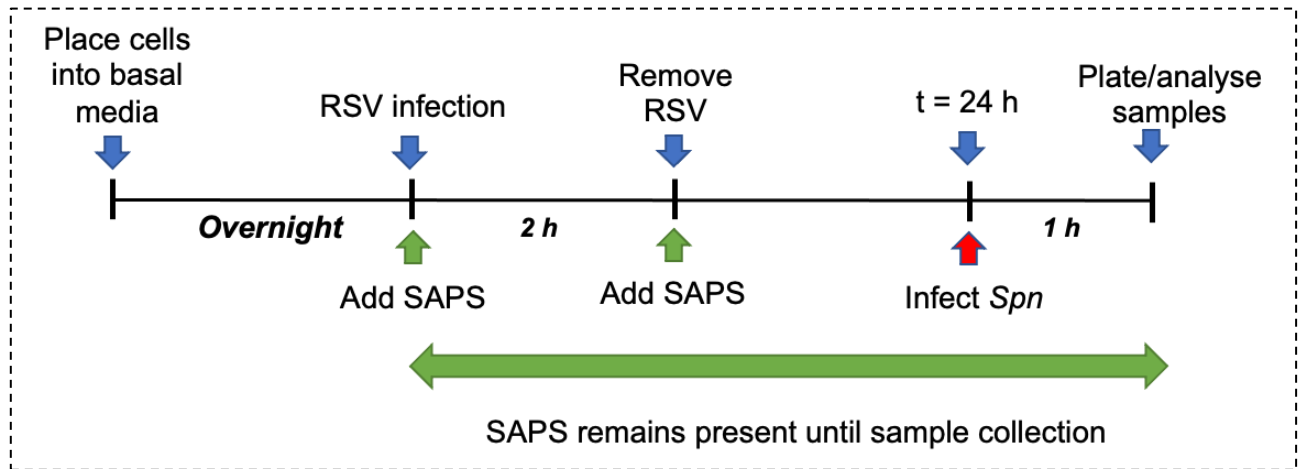


Figure 4.17 The adherence of *Streptococcus pneumoniae* is upregulated in RSV-infected cells but significantly inhibited with the addition of SAPS. A summary timeline demonstrating the experimental process is shown below (B). HBEC3-KT cells were grown to confluence in 24-well plates and placed into basal medium when 80%. On day 1, cells were infected with RSV A2 MOI 0.4 for 2 h ± SAPS (25 µg/ml). Unbound virus was removed and fresh media replaced on the cells ± SAPS (25 µg/ml). After 24 h incubation, cells were then infected with *Spn* MOI 1, for 1 h. Cells were then washed to remove unbound bacteria and cells detached. Serial dilutions of each sample were plated and Miles Misra counts conducted 24 h afterwards. Total CFU/well counts of each well are shown where the average number of bacteria initially added to well is indicated by the grey dashed line = 1.5×10^5 CFU/well (A). All data are ± SEM of N=3/4 from independent experiments completed on different populations of HBEC3-KT cells. Data were analysed using mixed effects analysis and Tukey's multiple comparisons test. Significant differences are indicated by **p < 0.01 and **** p < 0.0001.

4.6.5 Exploring if RSV infection predisposes to increased rates of bacterial invasion with *Streptococcus pneumoniae* in HBEC3-KT cells

In section 4.6.4, it was demonstrated that there was increased bacterial adherence to HBEC3-KT cells that had been infected with RSV 24 h before subsequent infection with *Spn*. Of interest, bacterial adhesion was reduced where HBEC3-KT cells had been co-incubated with SAPS in both RSV-infected cells and cells that had not been infected with virus. As previously discussed, RSV infections can enable bacteria such as *Spn* to progress into the lower airways, preferentially adhering to infected cells and invading the cells which can lead to bacteraemia (Morona et al., 2004). The following experiments were therefore completed to help determine what effect RSV would have on the rates of bacterial invasion of *Spn* in HBEC3-KT cells in the presence/absence of SAPS.

A previous study demonstrated the application of the fluorogenic dye (pHrodo) to label *Spn* in order to discriminate between adherent and internalised bacteria using flow cytometry (Fabbrini et al., 2012). The basis is that the relative fluorescent signal of pHrodo labelled bacteria increase as the environmental pH (such as within a lysosome during infection) decreases from neutral to acidic (Jubrail et al., 2016; Lenzo et al., 2016; Meena and Kimmel, 2018). The following experiments were completed to ensure the pHrodo labelling would result in fluorescent signal (visualised via microscopy) and then applied to co-infection studies to try and quantify relative internalised *Spn* via flow cytometry.

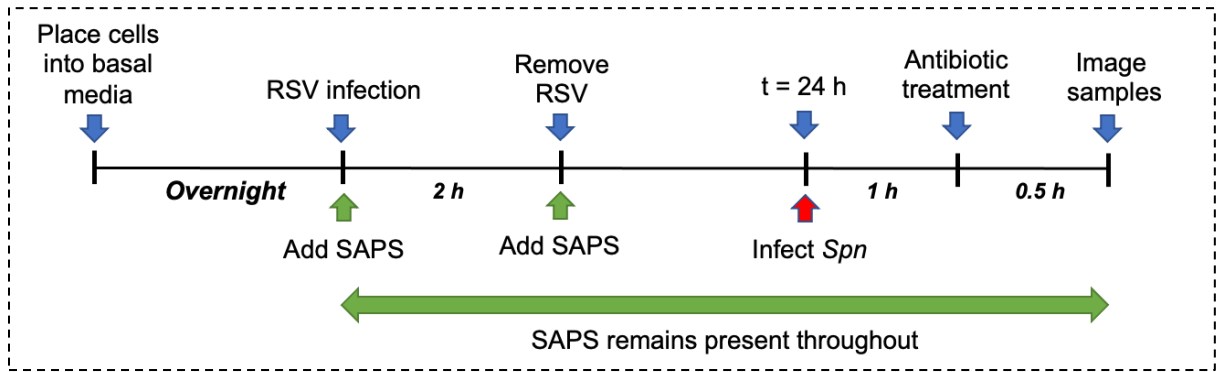
4.6.5.1 Optimisation of techniques to investigate pHrodo-labelled *Spn* invasion in HBEC3-KT cells

A fixed cell control was included to inhibit cell entry during infection with *Spn* and therefore used as a negative control for bacterial invasion. Infections were carried out as described (Section 2.20.2.1) and as summarised in **(Figure 4.18 A)**.

The collated images **(Figure 4.18 B, C)** are representative of N=3 independent populations of HBEC3-KT cells that were simultaneously stimulated/infected. The images indicated that both the uninfected wells stimulated with media only (media ctrl) and those infected with RSV only

(RSV), had no detectable red fluorescence (**Figure 4.18 B, C**). There were limited fluorescent bacteria detected in the 'Fixed ctrl' sample wells which indicate some bacteria may still have adhered to infected fixed cells however, the overall levels of red fluorescence were visibly lower than cells infected with pHrodo-stained *Spn* (**Figure 4.18 B**). Cells that had been treated with SAPS 24 h before infection with *Spn* alone, were observed to have reduced levels of red fluorescence, but this was not quantified (**Figure 4.18 B**). Of note, quantitative analysis of MFI between samples was not attainable due to a technical error in capturing the images, however they do indicate that the pHrodo stained *Spn* was fluorescing and that this fluorescent signal appeared to be restricted to intracellular locations but not on the surface of the HBEC3-KT cells. In addition, to confirm that only intracellular *Spn* was detected, supernatants were collected from each well after antibiotic treatment and plated overnight on blood agar to confirm that no viable extracellular bacteria were present (Section 2.11.4.1). Overall levels of detected fluorescence were low, and further experiments were attempted to increase the working signal for further study.

A

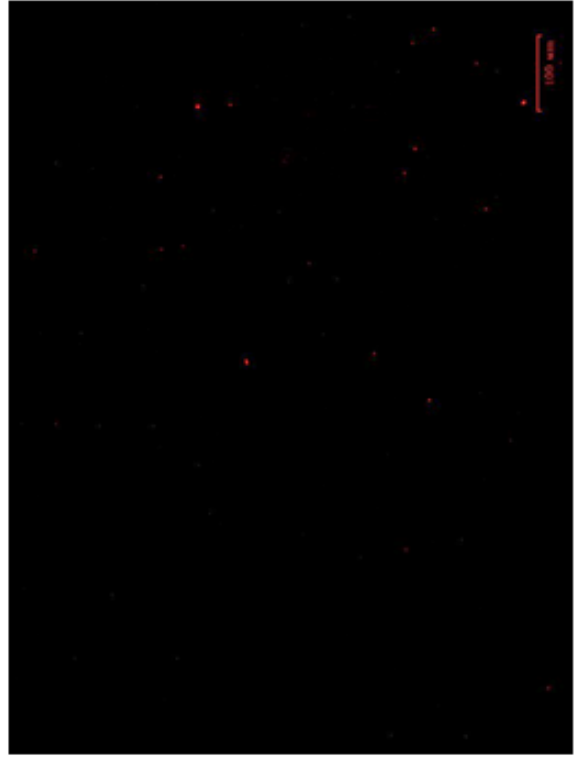


B

Fixed ctrl



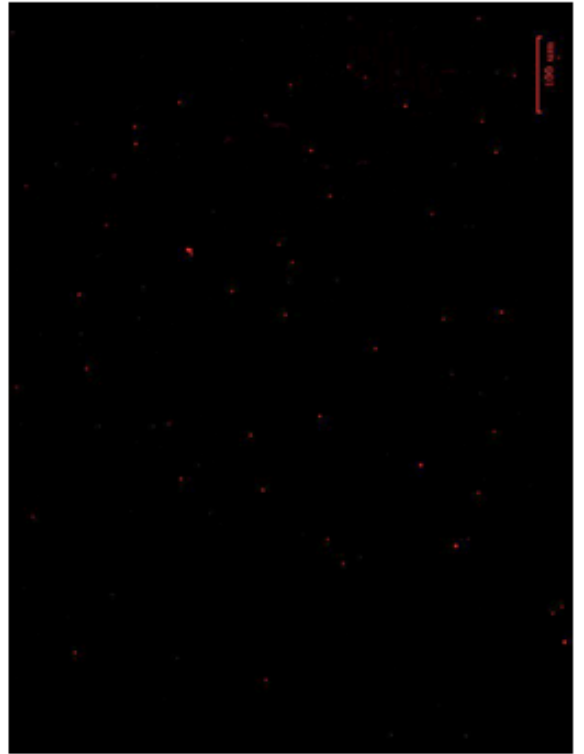
Spn+SAPS



Media ctrl



Spn



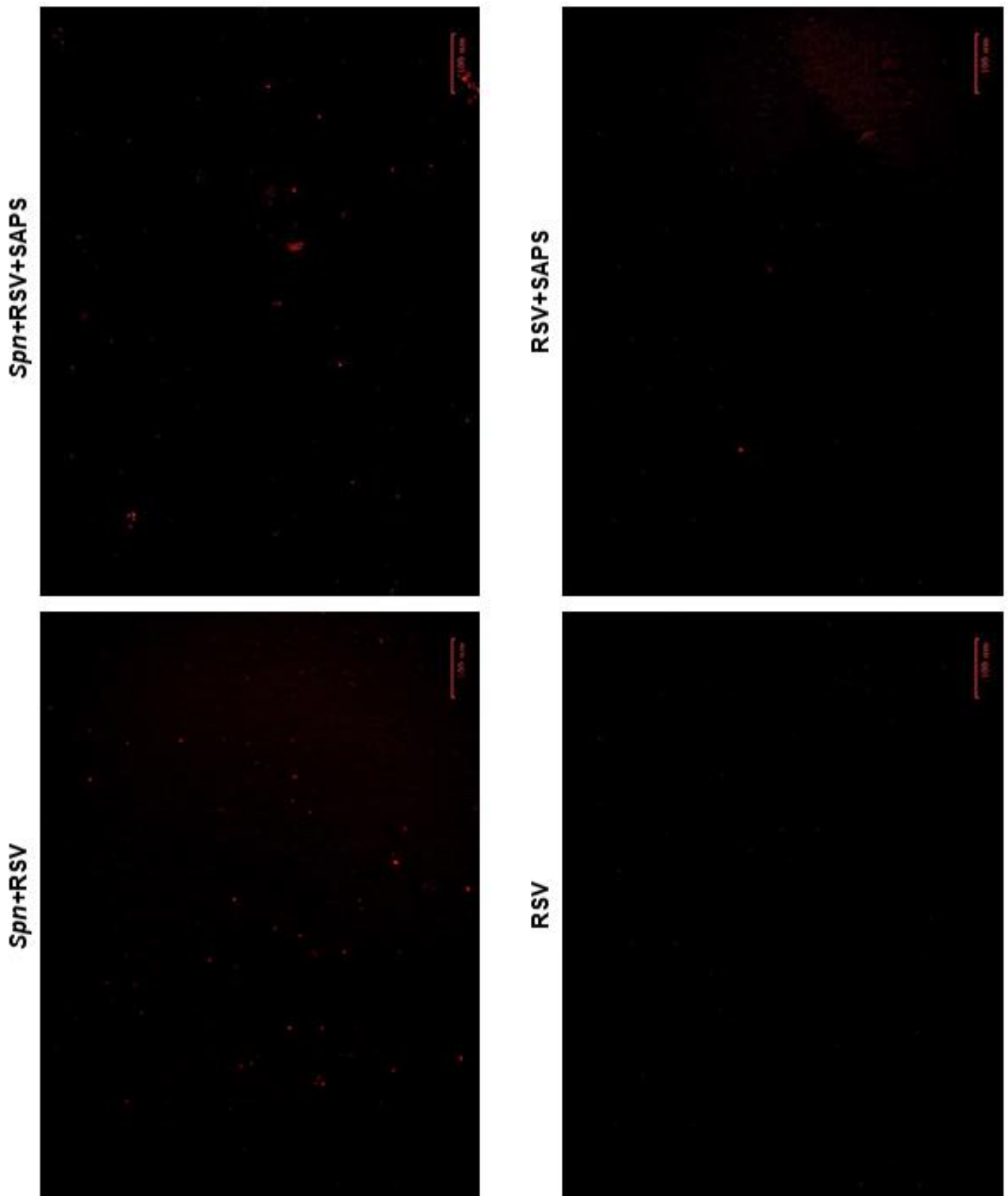
C

Figure 4.18 Investigating the application of pHrodo-stained *Spn* to visualise internalisation in HBEC3-KT cells. A summary timeline demonstrating the experimental process is shown above (A). HBEC3-KT cells were grown until 80% confluent in 24-well plates and then placed into basal medium overnight. On day 1, selected cells were infected with RSV A2 MOI 0.4 for 2 h or stimulated with media \pm SAPS (25 μ g/ml). Unbound virus were removed and fresh media replaced on the cells \pm SAPS (25 μ g/ml). A fixed cell control was included to determine that only intracellular bacteria were present indicative with red fluorescence. 24 h post viral infection, the fixed cell control was fixed with 4% PFA for 15 minutes at room temperature. Selected cells were then infected with pHrodo *Spn* (MOI 1) for 1 h. Cells were subsequently treated with antibiotics (20 μ g/ml Gentamicin/40 μ g/ml Streptomycin and 40 U/ml penicillin) for 30 minutes to selectively kill any extracellular bacteria. Fresh basal medium was then added to each well and cells imaged using a ZOE Fluorescent Cell Imager (BIO-RAD) (B, C). To remove bias, all samples were aligned centrally using the brightfield setting then imaged on the red channel to detect fluorescent *Spn*. Images were taken using the 20X objective lens and the scale bar is 100 μ m. The image contrast of all images was increased by 20% on PowerPoint to allow for better visualisation. These images are representative of N=3 individual experiments.

4.6.5.2 Investigating flow cytometry techniques to quantify *Spn* uptake in HBEC3-KT cells

Given the low levels of pHrodo signal detected using the fluorescent microscope and inability to accurately quantify the mean fluorescent intensity, an alternative technique was explored using flow cytometry to quantify the numbers of intracellular bacteria. HBEC3-KT cells were infected as described (Section 2.11.4.1).

As demonstrated (**Figure 4.19 i**), a broad gate was applied to include the projected forward scatter (FSC) and side scatter (SSC) properties of the HBEC3-KT cells as well as any smaller particles that may have included dead cells (containing bacteria) or bacteria alone based on $FSC = < 50 K$. Detection of pHrodo-labelled *Spn* were selected for using the SSC and 575 or 610 nm detection filters however no pHrodo-labelled bacteria were detected in any of the samples (**Figures 4.19 ii, iii**).

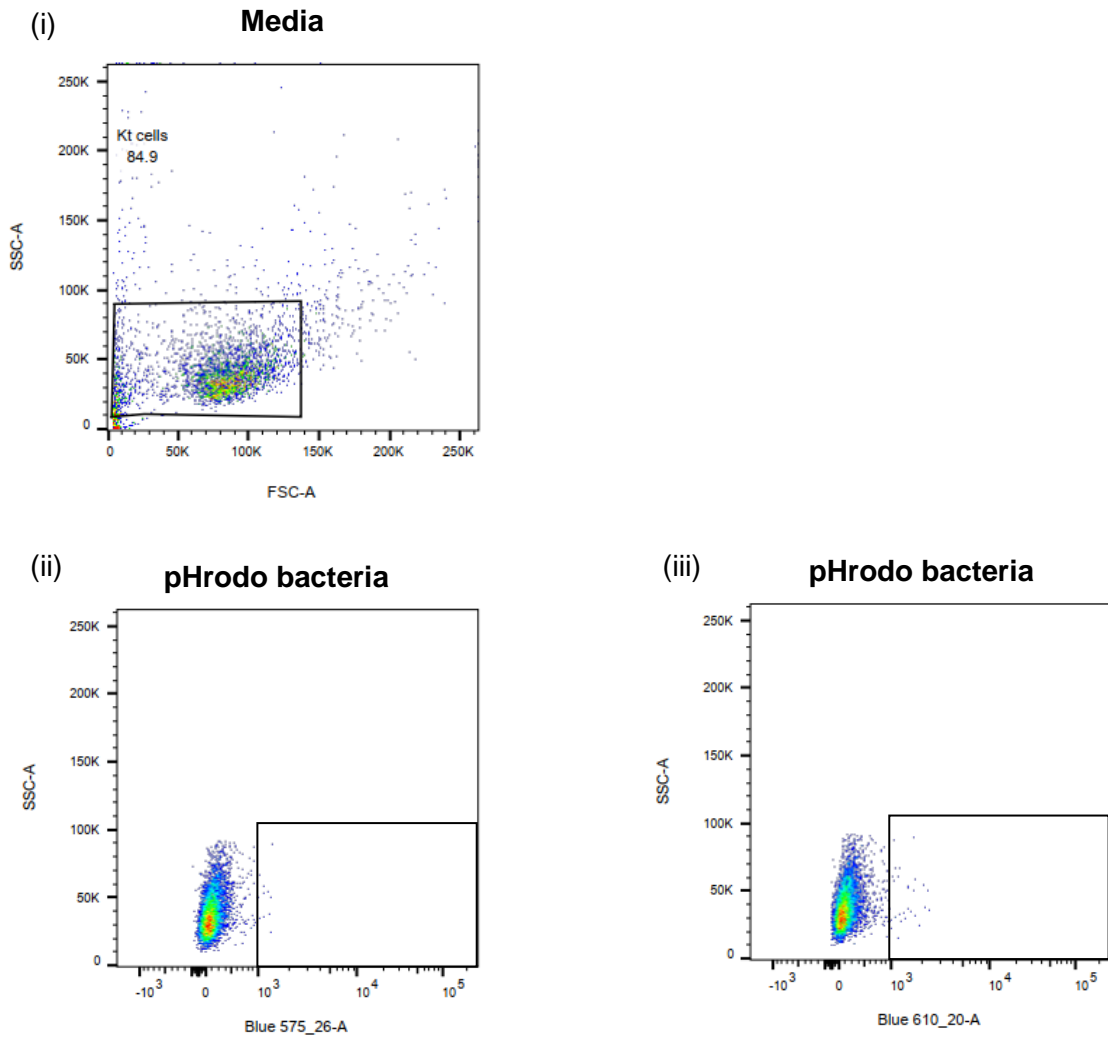


Figure 4.19 Investigating the application of flow cytometry to quantify intracellular *Spn* within HBEC3-KT cells. HBEC3-KT cells were grown to 80% confluence in a 12-well tissue culture plate. Selected cells were stimulated with media or infected with RSV A2 (MOI 0.4) for 2 h \pm SAPS (25 μ g/ml). Unbound virus was removed, cells placed into fresh basal medium \pm SAPS (25 μ g/ml) and incubated for a further 24 h. Selected cells were then infected with pHrodo-stained *Spn* or unstained *Spn* (both MOI 1) for 1 h. Cells were washed to remove adherent bacteria and the cells treated with antibiotics (20 μ g/ml gentamicin/ 40 μ g/ml streptomycin and 40 U/ml penicillin) for 30 minutes to remove any remaining adherent bacteria. Cells were detached with trypsin/EDTA and then fixed with 4% PFA. Samples were analysed using a 4 laser 13 colour LSRII™ (BD Biosciences) and BD FACSDiva software. Cell population was gated to include dead cells and possible fluorescent bacteria (i). Two different detectors were used to try and detect the fluorescent bacteria; 575 nm (ii) and 610 nm (iii).

4.6.5.3 Increased incubation periods of *Spn* on HBEC3-KT cells does not increase invasion

Signals obtained from pHrodo-labelled bacteria remained modest. *Spn* were therefore incubated on the HBEC3-KT cells for longer periods to determine if this would increase the observed signal as a marker of bacterial invasion. The incubation time of *Spn* was increased from 1 h to 2, 3 and 4 h before fixing and processing as previously described (Section 2.11.4.1). Cells were gated as previously described but did not include dead cells/debris to determine that any signal was from pHrodo-labelled *Spn* within viable HBEC3-KT cells. However, no pHrodo positive cells were detected from any of the samples (data not shown).

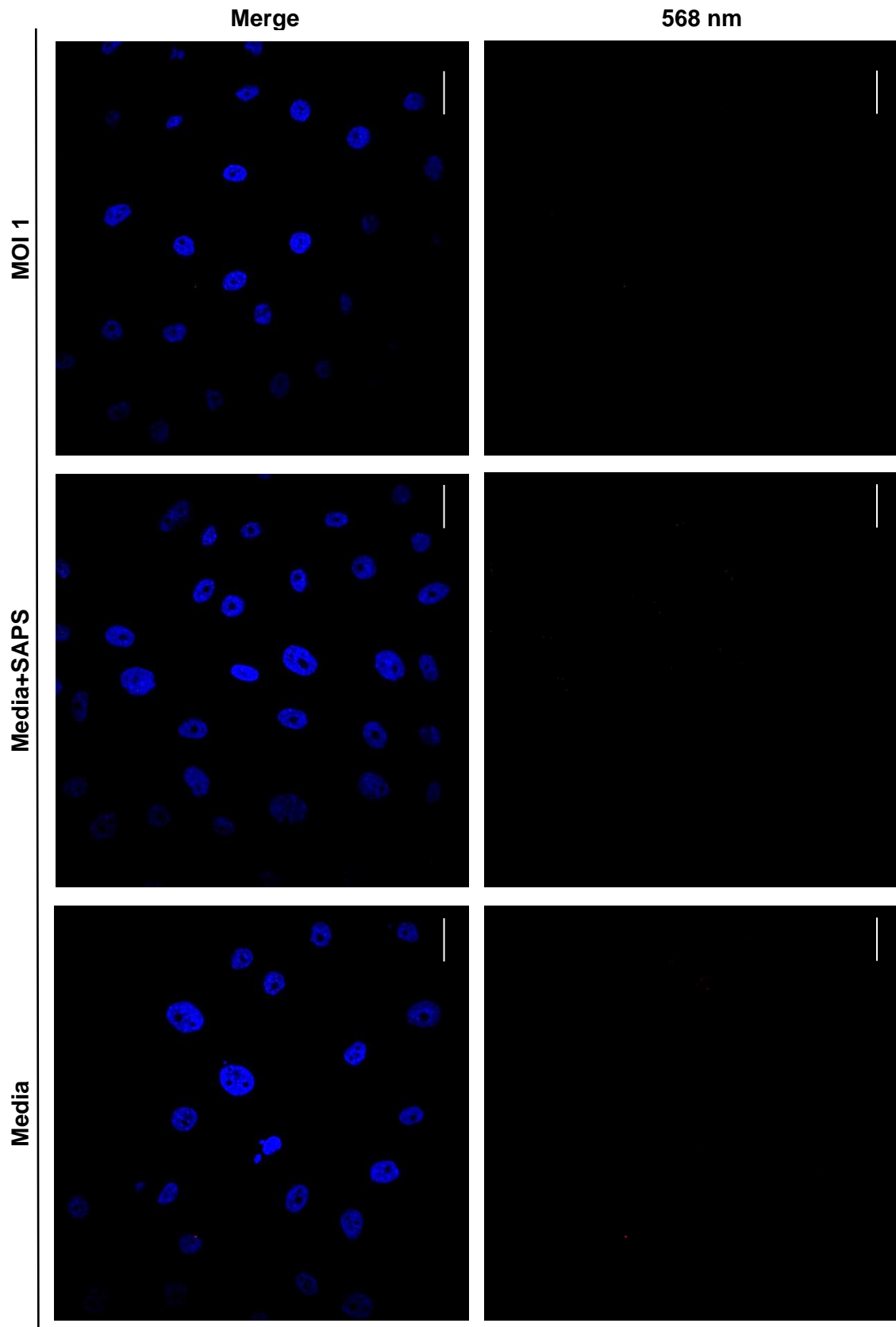
4.6.5.4 Investigating the occurrence of bacterial invasion in RSV-infected HBEC3-KT cells using confocal microscopy

An alternative approach was tested by infecting HBEC3-KT cells with red fluorescent *Spn* (FT4) and using confocal microscopy to analyse bacterial invasion. HBEC3-KT cells were infected with higher quantities of *Spn* (MOI 1, 10, 20 and 30) as described (Section 2.11.4.2) to determine the best MOI to use before conducting experiments in RSV-infected cells.

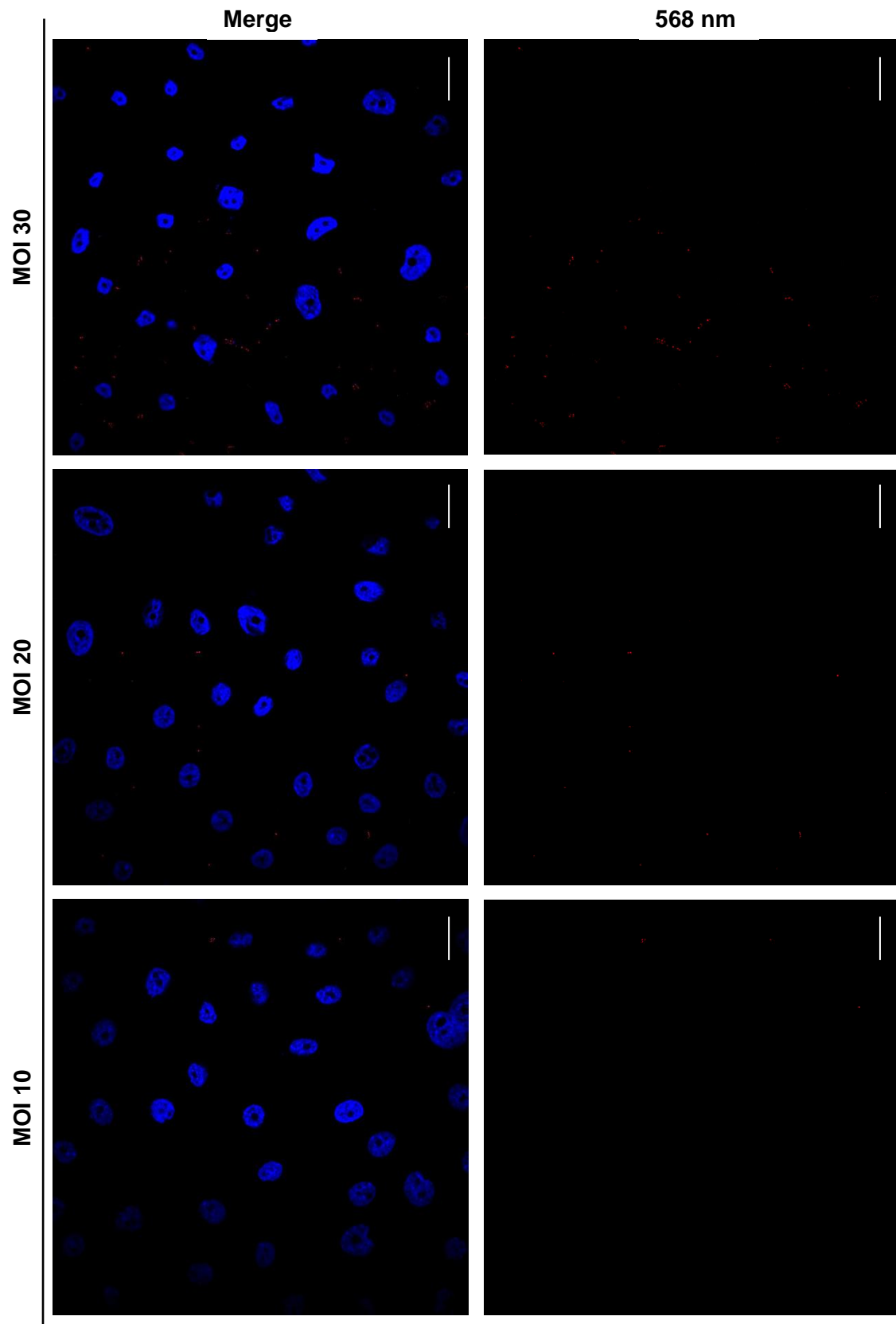
As demonstrated, there was no red fluorescence in HBEC3-KT cells treated with SAPS alone or infected with the lowest MOI of *Spn* (MOI 1) (**Figure 4.20 A**). There was increased red fluorescence observed as the MOI increased from 10 to 30 (**Figure 4.20**) where the MFI quantified also increased (**Figure 4.20 B, C**).

Based on these observations, it was decided that using an MOI of 20 would allow more bacterial invasion without incurring the levels of cell death observed with MOI 30. This MOI was applied in the following co-infection studies.

A



B



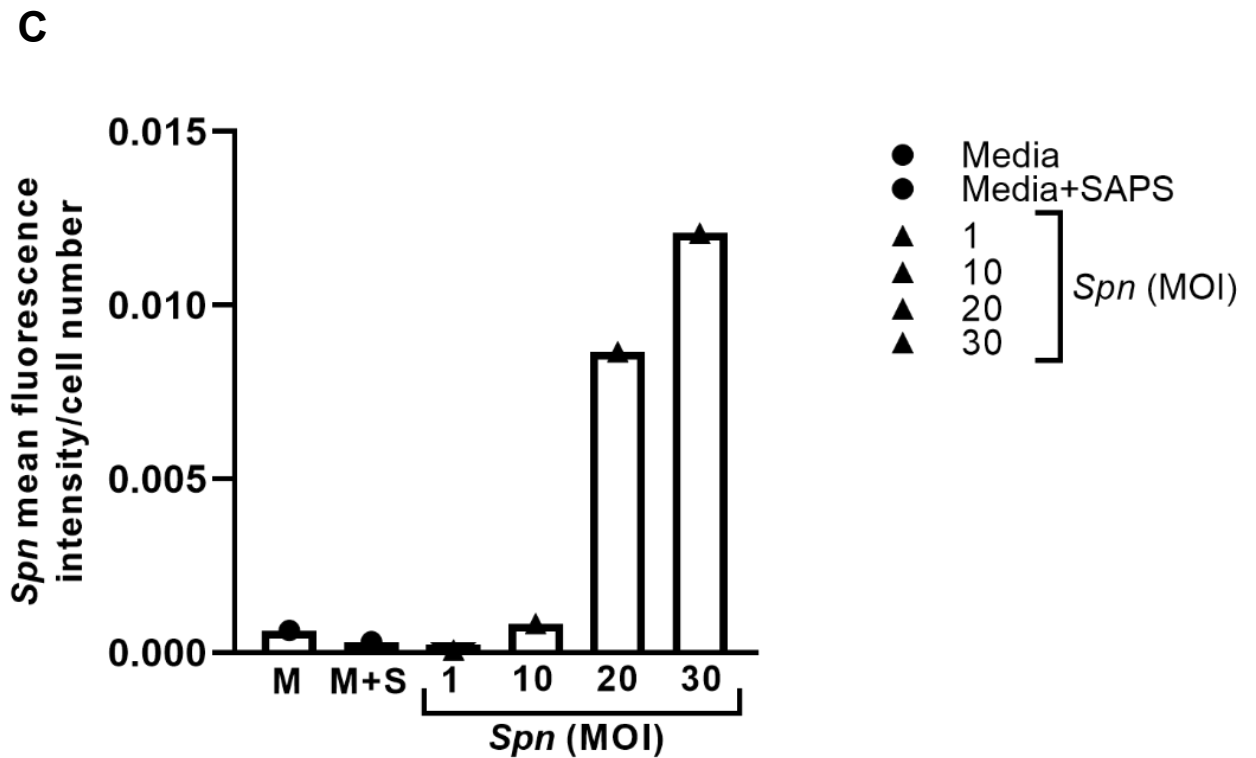


Figure 4.20 Optimisation of fluorescent *Streptococcus pneumoniae* (*Spn*) to visualise and quantify bacterial invasion in HBEC3-KT cells. HBEC3-KT cells were grown to 90% confluence on coverslips and infected with *Spn* (FT4) at a range of MOIs including 1, 10, 20 and 30 or cells were stimulated with media for 1 h. To confirm that SAPS would not auto fluoresce, an additional control was included where cells were stimulated with media and SAPS (25 µg/ml) for 1 h. Cells were then washed with PBS and treated with antibiotics (20 µg/ml Gentamicin/40 µg/ml Streptomycin and 40 U/ml penicillin) for 30 minutes to selectively kill any remaining extracellular bacteria. Cells were again washed with PBS then fixed with 4% PFA for 15 minutes at room temperature. Cell nuclei were stained using DAPI (blue). Confocal microscopy was used to visualise intracellular *Spn* (568 nm). To increase visualisation of the red fluorescence, all the images were modified on PowerPoint to increase the brightness by +40% (A, B). Mean fluorescence intensity of *Spn* was calculated relative to cell number (C). Data are N=1. Magnification = x 600. Scale bar is 22 µm.

4.6.5.5 Investigating the effect of SAPS treatment on bacterial invasion in HBEC3-KT cells using confocal microscopy

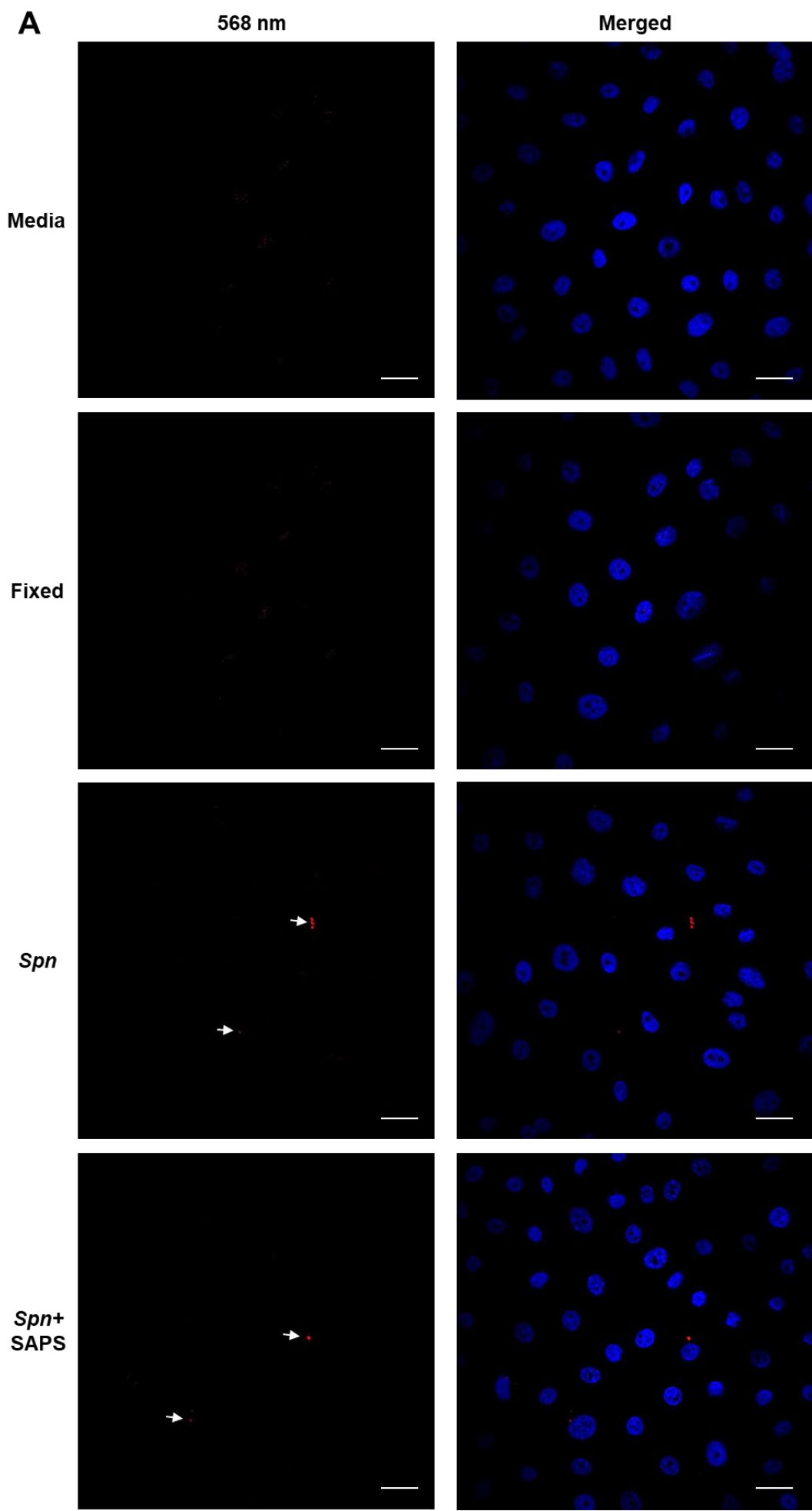
Confocal microscopy techniques were applied to investigate whether bacterial invasion of *Spn* within HBEC3-KT cells would be increased in RSV-infected HBEC3-KT cells, and whether infection could be modified by SAPS.

Cells were infected as previously described (Section 4.6.4.2) except that after the antibiotic treatment and washes, cells were immediately fixed with 4% PFA. Cells were subsequently stained for the anti-fusion (F) protein of RSV (indicative of viral infection) and DAPI stained for identification of cell nuclei. Cells were imaged using a confocal microscope and are summarised in (**Figure 4.21 A, B**). Mean fluorescence intensity (MFI) of *Spn* (568 nm) (**Figure 4.21 C**) and the RSV-F protein (**Figure 4.21 D**) were quantified.

As illustrated, the levels of intracellular *Spn* were relatively low across all the experimental samples whether infected with RSV or not. However, the images indicate that red fluorescence was only detected in samples infected with fluorescent *Spn* (**Figure 4.21 A, B**). There were no notable differences in bacterial fluorescence in HBEC3-KT cells that were infected with RSV before challenge with *Spn* in the presence or absence of SAPS (**Figure 4.21 B, C**).

As expected, there was visible green fluorescence in RSV-infected HBEC3-KT cells but no significant differences in green fluorescence were observed between these cells and those co-infected with *Spn* (**Figure 4.21 D**). Of note, and in line with data presented in section 4.4.4, HBEC3-KT cells that had been infected with RSV in the presence of SAPS had significantly lower levels of RSV F protein compared to cells infected with RSV only, and co-infected cells that had not received SAPS treatment (**Figure 4.21 D**).

These data thus far demonstrate that there was limited bacterial invasion in HBEC3-KT cells regardless of RSV infection and SAPS treatment.

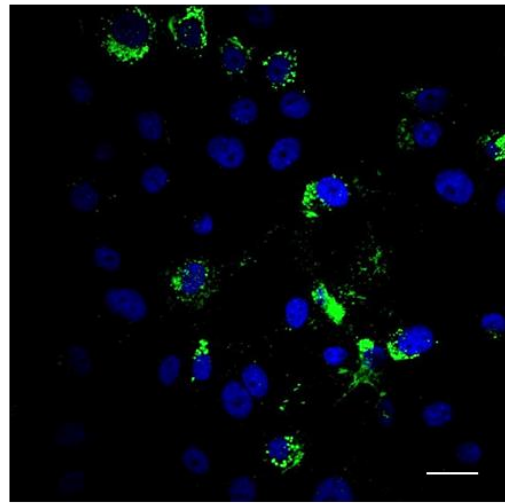
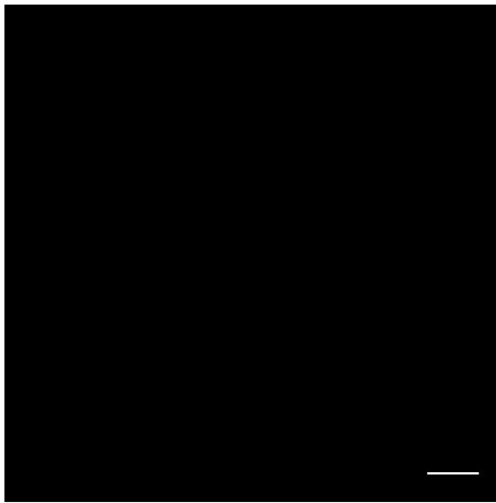


B

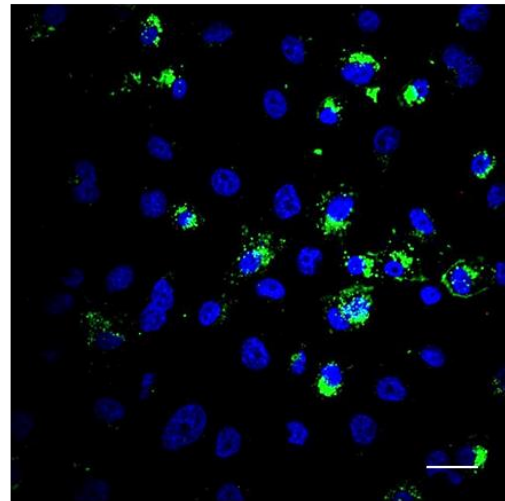
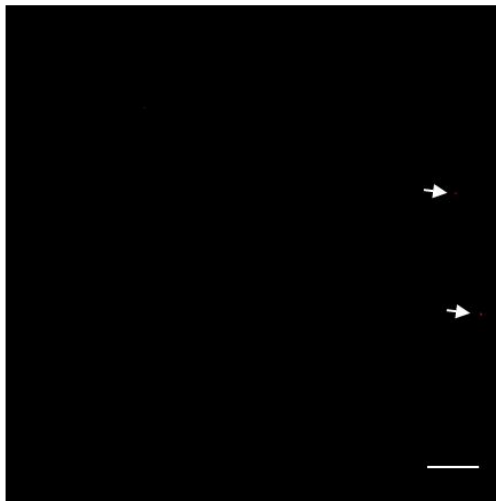
568 nm

Merged

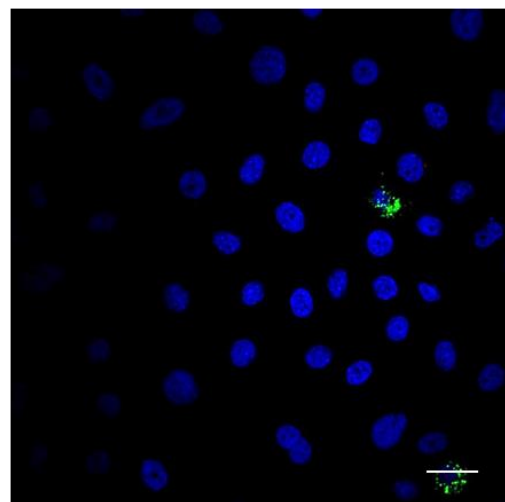
RSV



RSV+
Spn



RSV+
Spn+
SAPS



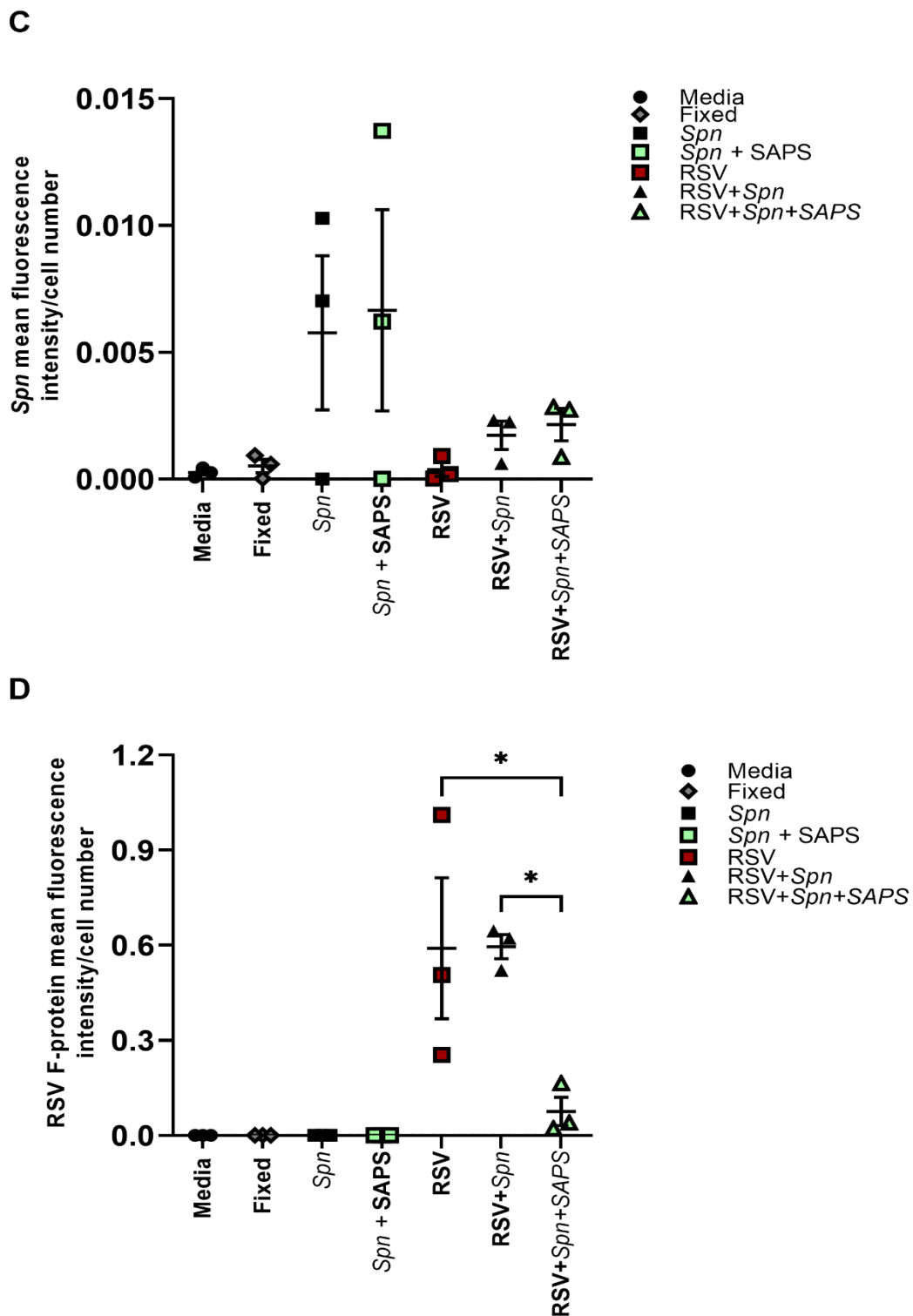


Figure 4.21 Investigating the effect of SAPS on RSV infection and subsequent *Streptococcus pneumoniae* (*Spn*) invasion in HBEC3-KT cells. HBEC3-KT cells were grown to 80% confluence on coverslips and infected with RSV A2 for 2 h or, stimulated with media in the presence or absence of SAPS (25 μ g/ml). Cells were washed to remove unbound virus and designated cells were then treated once more with SAPS (25 μ g/ml). After 24 h, the fixed cell control was fixed for 15 minutes in 4% PFA then washed with PBS. Selected cells were then infected with fluorescent *Spn* (MOI 20) for 1 h. Cells were then washed with PBS and treated with antibiotics (20 μ g/ml gentamicin/40 μ g/ml streptomycin and 40 U/ml penicillin) for 30 minutes to selectively kill any remaining extracellular bacteria. Cells were again washed with PBS then fixed with 4% PFA for 15 minutes at room temperature. Cell nuclei were stained using DAPI (blue) and viral infected cells stained using RSV anti-F (fusion) antibody (green). Confocal microscopy was used to visualise intracellular *Spn* (red) and any viral infected cells stained using RSV anti-F (fusion) antibody (green). To increase visualisation of the red fluorescence, all the images were modified on PowerPoint to increase the brightness by +40% (A, B). Magnification = x 600. Scale bar is 22 μ m. To quantify viral infection and intracellular bacteria, the mean fluorescence intensity (MFI) of *Spn* (C) and RSV anti-F (D) were calculated relative to cell number. Data are \pm SEM of N=3 from individual experiments. Data were analysed using a one-way ANOVA with Tukey's multiple comparisons post-test. Significant differences are indicated by * p < 0.05.

4.7 Chapter summary

The major aims for this chapter were to explore the impact of SAPS on RSV infection and replication in airway epithelial cells. Confocal microscopy techniques were also applied to visualise interactions of RSV at cell membranes to elucidate the possible mechanism of SAPS.

Data presented in this chapter showed that co-incubation of NHBE and HBEC3-KT cells with SAPS significantly reduced RSV infection (**Figure 4.3, Figure 4.12 E**). Moreover, SAPS significantly reduced viral replication in NHBE and HBEC3-KT cells when administered during infection (**Figure 4.5, Figure 4.6**). However, when SAPS was applied to HBEC3-KT cells post infection, no significant differences in RSV replication were seen (**Figure 4.7**). Interrogation of the RSV life cycle was investigated using confocal microscopy techniques. These illustrated co-localisation of RSV with actin rich areas of the HBEC3-KT cell membrane, indicative of possible interactions with MM (**Figure 4.10, Figure 4.13**). Furthermore, co-incubation of HBEC3-KT cells with SAPS during RSV infection appeared to reduce initial viral binding to the HBEC3-KT cells highlighting a possible mechanism of SAPS (**Figures 4.12 C**).

This chapter also aimed to assess whether RSV infection predisposed airway epithelial cells to subsequent bacterial co-infection with *Spn* and, whether SAPS-treatment during RSV infection would inhibit these secondary bacterial infections.

The data within this chapter demonstrated that RSV infection significantly increased *Spn* adhesion to the HBEC3-KT cells (**Figure 4.17**). Of note, these data also indicated that the presence of SAPS during RSV infection significantly reduced subsequent bacterial adhesion with *Spn* (**Figure 4.17**). Surprisingly, treatment of HBEC3-KT cells with SAPS also reduced *Spn* adhesion in the absence of RSV infection (**Figure 4.17**). To conclude the work of this thesis, it was examined whether RSV predisposed airway epithelial cells to *Spn* invasion of cells, but intracellular infection proved challenging to detect.

Chapter 5: Discussion

RSV is a highly ubiquitous virus for which there is currently no licensed vaccine, nor established licensed therapies to control its respiratory disease, which is particularly problematic in infants and the elderly. There remains an urgent need for effective and accessible therapeutics, particularly those which may help to alleviate hyperinflammation associated with severe RSV disease which contributes to pathology. Naturally occurring phospholipids present in pulmonary surfactant have been linked to modulation of the immune response to both bacterial and viral infections (Ji et al., 2021; Kandasamy et al., 2016; Kuronuma et al., 2009; Milad and Morissette, 2021; Numata et al., 2020, 2010). In addition, work within my group has demonstrated that SAPS, a liposome containing the anionic phospholipid phosphatidylserine, may have immunomodulatory mechanisms against rhinovirus (RV) infection, and a range of TLR agonists in airway epithelial cells (AEC)s via modulation of membrane microdomain (MM)-dependent activities (Parker et al., 2008; Stokes et al., 2016). Additional research has identified numerous roles that MM may play in productive infection of RSV in airway cells (Brown et al., 2004; Chang et al., 2012; San-Juan-Vergara et al., 2012; Yeo et al., 2009). The role of MM during viral infection is a growing area of research, however, studying these highly dynamic interactions can be challenging and many questions regarding MM and their potential roles as therapeutic targets remain ambiguous. This project aimed to investigate whether SAPS could inhibit RSV infection of AECs, viral-induced inflammation, and subsequent bacterial co-infection. In addition, this work aimed to decipher the interactions of RSV with MM during infection and evaluate the mechanistic actions of SAPS on these events.

5.1 Airway epithelial cell models

The airway epithelium is both the target of, and an early defence against, respiratory viruses such as RSV. Innate functions of the airway epithelium thus play a crucial role in disease outcome; therefore, exploring these pathways may identify therapeutic targets to either inhibit

viral infection or reduce the associated inflammatory response. For *in vitro* studies, selection of a representative AEC model is therefore crucial.

A range of epithelial cell models have been used to investigate host-pathogen interactions in the context of RSV infection such as immortalised cell lines; HEP-2 (human epithelial type 2), A549 (type II alveolar epithelial carcinoma cell line), and BEAS-2B and 16HBE14o (both simian virus 40 transformed bronchial epithelial cell lines) (Hillyer et al., 2018; Linfield et al., 2021). Other studies have used primary AECs isolated from human volunteers, for example obtained from nasal brushings or via bronchoscopies. Primary AECs can be differentiated into pseudostratified mucociliary epithelium when grown at air liquid interface (ALI), which generates a more accurate airway model for investigating respiratory infections. However, there are several factors that limit the routine use of primary AECs for experimental investigations. A major barrier is that directly obtaining cells involves a specialised clinical team with associated ethical approval in place, and extensive infrastructure support for cell culture. Although commercially available primary cells offer an alternative option, these also have their limitations. Whilst attempts can be made to match donors (for factors such as age, sex and health status), this is dependent on the availability of cells, and clinical data to help interpret donor response patterns is usually very limited. Commercial companies also often limit information on the exact airway source and preparation of cells. Furthermore, not all donors are viable in culture, with individual donors exhibiting genetic or phenotypic differences that can confound data. Primary AECs also require costly reagents for their maintenance and have a reduced and definitive lifespan, limiting availability for continued and comparative work (Reeves et al., 2018). Due to this, immortalised cell lines have proven a popular choice for RSV studies, particularly in the early stages of research.

The initial work presented in this thesis exploring the impact of SAPS on RSV infection was conducted in the immortalised BEAS-2B cell line. This cell type was selected due to the relative ease of maintenance, reproducibility, and their previous applications for viral infection studies within our group (Mills et al., 2019; Parker et al., 2008; Stokes et al., 2016, 2011) and

its wide use elsewhere. BEAS-2B cells are frequently used within pulmonary research due to their durability, longevity, and characteristics that resemble human airways, such as tight junctions and immune signalling pathways (Edwards et al., 2016; Hillyer et al., 2018; Satkunanathan et al., 2014; Stokes et al., 2011; Touzelet et al., 2020; Yoon et al., 2007). However, a recent study has presented evidence that BEAS-2B cells are more representative of mesenchymal stem cell than an epithelial cell type (Han et al., 2020). In addition, previous work has also highlighted the differential effects of using foetal bovine serum in cell culture which may reduce E-cadherin protein expression and induction of squamous differentiation of cells (Lechner et al., 1984; Stewart et al., 2012; Zhao and Klimecki, 2015). Together, these characteristics of BEAS-2B cells may limit their application as a model for respiratory viral infection.

The aim of this project was to replicate studies in primary normal human bronchial epithelial (NHBE) cells with key experiments recapitulated at ALI as a further, more relevant model of the airway epithelium. However, a major setback for this project was unexpected problems establishing NHBE cells for experimental work. Our group had previously obtained NHBE cells from Promocell, where their growth and maintenance had been established (Manley et al., 2019; Stokes et al., 2016). However, the research group planned to study viral responses in cells from people with asthma, which were not at the time available in sufficient numbers from Promocell, so, Lonza was selected as a commercial provider. Unfortunately, despite extensive optimisation, and continued communication with Lonza, only two donors were successfully propagated and utilised to generate the data in this thesis. It was eventually discovered, through personal communication with Dr Michael Edwards (Imperial College London), that the recommended seeding densities in the Lonza protocols were too low and that this contributed to the rapid senescence of cells. The lengthy optimisation (and ongoing cost) rendered the NHBE cells unsuitable for their continued use, especially in the light of major delays in experimentation caused by the impact of the COVID-19 pandemic, and thus alternative cell models had to be considered.

After careful consideration, the HBEC3-KT cells were selected as an alternative model to the NHBE cells. A major deciding factor was that, unlike the BEAS-2B cells, the HBEC3-KT cells were not immortalised using virus but transfected using cyclin dependent kinase 4 (CDK4) and telomerase reverse transcriptase (hTERT), where CDK4 can sequester and inhibit p16, forcing the constitutive expression of telomerase thus preventing the senescent properties demonstrated in NHBE cells (Ramirez et al., 2004; Vaughan et al., 2006). In addition, unlike BEAS-2B cells, the HBEC3-KT cells retain their capacity to differentiate into basal, mucin-producing, and ciliated cells when grown at ALI suggesting preservation of more primary AEC characteristics (Kaisani et al., 2014; Nakauchi et al., 2019; Ramirez et al., 2004; Vaughan et al., 2006). For example, Kaisani et al. (2014) have demonstrated that in submerged culture, HBEC3-KT cells can express markers from that of both the central (stem cell marker p63 and cytokeratin 7, 14, 17, 19) and distal (surfactant proteins A, C, D and CCSP) lung, supporting the credible role of HBEC3-KT cells as an intermediate model for continued investigations in the project. However, there are limited investigations that have used HBEC3-KT cells for viral infection studies and therefore required optimisation for this project. Of note, Nakauchi et al. (2019) recently demonstrated the use of HBEC3-KT cells as a suitable model for the propagation of RV-C, a subclass of RV that cannot be propagated in standard cell models and requires an ALI model (Nakauchi et al., 2019). HBEC3-KT cells have also been used to investigate the induction of TLRs to protect against influenza infection (Kirkpatrick et al., 2019).

Selecting a relevant *in vitro* cell model was important to evaluate RSV-induced host responses that could be compared to SAPS-treated cells. Differences between and within AEC models in the context of viral infection have been described, with variations in viral tropism (characterised by available host cell receptors that may hinder/promote viral infectivity), viral replication, and differential immune signalling that may modify experimental outcomes such as cytokine production (Ferreira Lopes et al., 2017; Fonseca et al., 2012; Glaser et al., 2019; Rijsbergen et al., 2021).

Data generated during my MSc (not shown) and previous research within our group had determined 0.4 and 1 as suitable multiplicity of infections (MOI)s for RSV infection studies within the BEAS-2B cells based on cell viability and induction of CXCL8. However, work using the NHBE, and HBEC3-KT cells required initial optimisation experiments to confirm a suitable MOI for investigations. Previous work in our lab has indicated that primary cells may be more permissive and more sensitive to viral infections, with potential for greater viral-induced cell death. Therefore, the NHBE and HBEC3-KT cells were challenged with a lower range of RSV (MOI 0.2 – 0.8) than was used in the BEAS-2B cells over the required maximum 48-hour time point. Within these optimisation experiments, the levels of pro-inflammatory chemokines CXCL8 (a principal mediator for neutrophil recruitments) and CCL5 (which recruits lymphocytes, monocytes, and eosinophils) were quantified up to and including 48 hours post RSV infection. Our lab group is particularly interested in these two key chemokines as they are routinely identified in cases of severe RSV disease. In addition, CXCL8 is indicative of NF- κ B and MAPK-dependent signalling whilst CCL5 coordinates both innate and adaptive processes and its production is also dependent upon the IFN-stimulated gene (ISG) pathways (Culley et al., 2006; Fitzgerald et al., 2003; Monick et al., 2001; O'Neill and Bowie, 2007). Due to their roles in disease severity during RSV infection, both CXCL8 and CCL5 were used to assess the impact of SAPS on inflammatory (via NF- κ B signalling) and anti-viral signalling (via IRF signalling) respectively. Therefore, establishing an MOI that induced these signalling pathways without causing major cell death was required.

Data presented in chapter 3 demonstrate that there was some variation in both RSV-induced cell viability and chemokine production between AEC models. In the BEAS-2B cell line, cells infected with RSV had a 22% (MOI 0.4) or 42% (MOI 1) reduction in cell viability at 48 hours post-infection (**Figure 3.4**). In similar experiments conducted in the NHBE (**Figure 3.5 C**) and HBEC3-KT cells (**Figure 3.6 E, F**), infection with the highest MOI of RSV (0.8) had the greatest impact on cell viability 48 hours post infection, reducing viability by more than 10%. The lower MOIs (< 0.8) of RSV did not reduce cell viability by more than 10%. The differences in viability

between AEC types in response to RSV infection were surprising as published data generally demonstrates that BEAS-2B cells are less permissive to viral infection in comparison to NHBE cells as well as other cell lines such as A549 (Fonceca et al., 2012; Hillyer et al., 2018). Fonceca et al. (2012) demonstrated that NHBE cells had ~25% decreased cell viability 24 hours after RSV infection (MOI 0.25) whereas only minor effects were seen in BEAS-2B cells. In addition, Hillyer et al. (2018) demonstrated that BEAS-2B cells were less permissive to RSV infection in culture and demonstrated an anti-viral state. Differences observed between published work and data presented in this thesis may be attributed to the number of cells infected which may vary between cell types, or differences between batches of RSV used in the different cell types. All cell types were screened for mycoplasma (Section 2.2.5) ruling out the possibility of mycoplasma contamination. Ultimately, different cell types will exhibit variable responses to viral infection based on differential gene expression levels (e.g receptor expression), which would be interesting to assess using RNAseq. Therefore, optimisation of the MOI of RSV for each cell type was essential to establish an MOI that stimulated a robust immune response without inducing high levels of cell death.

NHBE (**Figure 3.5 A, B**) and HBEC3-KT cell data (**Figure 3.6 A-D**) indicated that increased RSV MOI correlated with increased production of CXCL8 and CCL5 up to 48 hours post infection with levels peaking at ~12 ng/ml CXCL8 and ~60 ng/ml CCL5 for both cell types. Based on these results, the MOI of 0.4 was selected for future investigations as moderate levels of CXCL8 and CCL5 were induced without overtly reducing cell viability. Of note, there were observable differences between the two independent NHBE donor cells. Unfortunately, donor variation could not be statistically tested or evaluated in detail, due to the use of only two donors. However, it was noted that with increased MOI, the variation in chemokine levels increased between the two donors with donor 1 generally producing higher levels of CCL5 and having less viable cells after RSV infection whereas donor 2 produced greater levels of CXCL8 to donor one and had higher levels of viable cells.

There was also variation in cytokine production between the different cell types in response to RSV (MOI 0.4) at 48 hours post infection. RSV-infected BEAS-2B cells produced moderate levels of CXCL8 (~6 ng/ml) but much greater levels of CCL5 (~80 ng/ml) 48 hours post infection (**Figure 3.3 B, D**). The levels of CXCL8 in NHBE cells was comparable to the BEAS-2B cells (~7 ng/ml) but CCL5 levels were lower (~40 ng/ml) (**Figure 3.5 A, B**). HBEC3-KT cells produced the lowest levels of CXCL8 (~4.5 ng/ml) but produced considerable amounts of CCL5 (~55 ng/ml) (**Figure 3.6 B, D**). In general, the levels of CXCL8 were comparable between cell types with larger variations in CCL5 production, which may be cell specific and suggest different permissiveness and responses to viral infection. Investigations to explore the induction of signalling pathways (such as IRF) in different AECs may help explore if there are any correlations between chemokine production and levels of viral infection however this may not provide huge additional data given a broadly stable pattern between cell types, which is reassuring when studying signalling patterns. Publications generally suggest that BEAS-2B cells produce lower levels of both CXCL8 and CCL5 than NHBE cells and other cell lines (e.g. A459), however, this was not the case in my own work. Hillyer et al. (2018) demonstrated that baseline levels of CXCL8 and CCL5 were similar between the BEAS-2B and A549 cells until 48 hours post RSV infection where A549 cells demonstrated a more pro-inflammatory state, secreting more CXCL8 and CCL5 than BEAS-2B cells. Of interest, the phenotypic characterisation of BEAS-2B cells as being in a more anti-viral state, or more resistant to viral infection, was also mirrored in another study where BEAS-2B cells were less permissive to influenza virus compared with NHBE and A549 cells (Seng et al., 2014).

During optimisation of HBEC3-KT cell cultures, it was noted that the media in the RSV-infected cells had a cloudy appearance that indicated a possible contaminant. After further investigation it was discovered that the original RSV stocks (which had been used to propagate successive viral stocks), were contaminated with bacteria (Section 3.4.1.1). This issue had not been highlighted during initial experiments with NHBE cells, thought to be due to the presence of gentamicin-amphotericin (GA-1000) used in NHBE cell culture that had

effectively inhibited bacterial growth. BEAS-2B and HBEC3-KT cell culture instead included penicillin-streptomycin which was thought to have been ineffective at killing the bacteria present in the virus inoculum. The incorporation of GA-1000 was utilised in HBEC3-KT cell culture and new RSV stocks were propagated in the presence of antibiotics and confirmed to be bacteria free before use. Although there had been no observable indications of bacterial contamination during the BEAS-2B cell work, it is possible that the combination of RSV and bacteria induced this heightened cell death observed in BEAS-2B cells compared with HBEC3-KT and NHBE cells. Moreover, BEAS-2B cells were infected with an earlier passage of RSV containing higher levels of bacterial contamination with later passages of virus stocks exhibiting less contamination due to dilution of the original stocks. The data showing RSV-induced CXCL8 in the BEAS-2B cells may therefore have been impacted by the presence of possible bacterial contaminants such as LPS.

Interestingly, two separate studies have demonstrated evidence that AECs (including BEAS-2B and NHBE cells) treated with heat-inactivated (HI) *NTHi*, secreted increased levels of both IL-6 and CXCL8 after subsequent infection with RSV, compared to *NTHi* infection alone (Bellinghausen et al., 2016; Gulraiz et al., 2015). These data indicate that predisposing bacterial infections may induce increased inflammatory responses, tissue damage and thus permissibility to viral infection. Similarly, Neu and Mainou (2020) highlight the synergistic interactions that viruses and bacteria play in disease susceptibility (Gulraiz et al., 2015; Neu and Mainou, 2020). The possible presence of bacterial products may have confounded data presented in this thesis however, the overall production of CXCL8 (which can be stimulated by LPS) appeared to be in keeping with published data.

Inclusion of antibiotics such as polymyxin B to neutralise possible LPS contaminants remaining in the RSV stocks may have been beneficial here (Domingues et al., 2012). Attempts were made to acquire fresh stocks of RSV from ATCC however there were issues with the product provided and after lengthy discussions with ATCC to replace the virus, they advised that vials of RSV A2 were then out of stock. These issues also occurred just before the national lockdown in response to COVID-19 and thus upon arrival back in the lab, swift

decisions had to be made to progress with the current lab work. A replacement challenge virus would be obtained for any future experimental work to avoid these possible contamination issues. What's more, the application and use of a clinical isolate of RSV for this study would also be considered. Despite the use of commercially available isolates (such as RSV A2 used in this thesis) being widely used in the field, RSV A2 (acquired in 1961) does not circulate within the human population and is therefore not as representative for viral challenge studies investigating RSV-induced immune responses (Van der Gucht et al., 2019). In addition, these commercial isolates have naturally acquired mutations because of continual propagation in cell cultures, obscuring the interactions of RSV with airway epithelial cells during infection *in vivo* (Van der Gucht et al., 2019; Villenave et al., 2011). Thus, the implementation of a more representative airway epithelial cell model infected with a relevant clinical isolate of RSV, would be desirable for the progression of this work.

Data presented in this thesis, and published work referenced above, highlight some of the differences that can occur between different cell types in response to viral challenge. Being aware of these differential responses is important as to ensure the reproducibility of work and to ensure that the cell model is recapitulating events that may occur during "natural" infection as accurately as possible. The data within this thesis illustrate that although there was some variation of CXCL8 and CCL5 production in response to RSV infection, the overall results were comparative, and the effect of SAPS treatment had consistent inhibitory effects on the production of both chemokines despite variable production.

5.2 Mechanism of SAPS when co-incubated during RSV infection

After initial optimisation of RSV infection in AECs, demonstrating a minimal reduction in cell viability with the production of pro-inflammatory chemokines CXCL8 and CCL5, the ability of SAPS to perturb these markers of RSV infection when present during viral challenge was investigated.

Overall, SAPS reduced chemokine production and RSV infection of airway epithelial cells. Each of these pathways and mechanisms will be discussed however it is most likely that the dominant actions of lipid treatments are to inhibit RSV infection, potentially by disruption of membrane microdomains, with a concomitant reduction in the inflammatory response that may also be by reduction in early signalling events from the cell membrane. Interestingly, this appears to be a different mechanism to SAPS inhibition of rhinovirus (RV) infection-induced inflammation, where SAPS inhibits signalling but not infection.

Firstly, the effect of SAPS on AEC viability in the presence or absence of RSV infection was examined. This determined whether SAPS treatment alone reduced AEC viability or any cytoprotective effects in the context of RSV infection were seen. Data presented in chapter 3 demonstrate that SAPS treatment alone had no effect at the tested concentrations on AEC viability up to 48 hours in BEAS-2B cells (**Figure 3.4 C**), and in NHBE cells (**Figure 3.9 C**). These results are in line with published findings from my group where Parker et al. (2008) demonstrated that co-incubation of SAPS (up to 50 µg/ml) with either peripheral blood mononuclear cells (PBMCs) or BEAS-2B cells did not have cytotoxic effects, measured by nutrient uptake and metabolic capabilities (alamarBlue assay), 20 hours after incubation with SAPS. In addition, Stokes et al. (2016) described similar observations in both BEAS-2B and NHBE cells where incubation of cells with either SAPS or PAPC (50 µg/ml) did not induce cytotoxic effects. Furthermore, the presence of SAPS in RSV-infected BEAS-2B (**Figure 3.4 A, B**) and NHBE cells (**Figure 3.9 C**) did not appear to potentiate cell death up to 48 hours post-infection. Overall, these data demonstrate that cells incubated with SAPS during RSV infection had higher levels of cell viability than RSV-infected cells, which may indicate some cytoprotective properties of SAPS against viral infection. In comparison, PAPC appeared to potentiate RSV-induced cell death in BEAS-2B cells at 48 hours post-infection. However, these effects were not recapitulated in two independent NHBE cell donors (**Figure 3.9 C**). Of note, cell viability in BEAS-2B and NHBE cells was evaluated using the MTT or CellTiter-Glo assay. Therefore, the viability of cells in culture was assessed through quantification of

metabolic activity and the production of either NADPH (MTT) or ATP (CellTiter-Glo®). Although these are commercially available and widely used assays to measure cell viability, it is worth highlighting that these are crude measures of cell viability that may not fully capture what is happening in viral infected cells. Viruses require a host cell to replicate their viral genome which requires the transition of the cell metabolic capacity to orientate towards viral progeny production (Connelly et al., 2021; Martín-Vicente et al., 2020; Sumbria et al., 2021). Therefore, viral infection can directly alter metabolic activity within AECs that may result in the increased production of ATP, as was demonstrated in cells infected with dengue virus (Heaton and Randall, 2010). Studies have shown that RSV induces increased glycolysis events and citric acid components during host cell infection which can lead to the production of ATP (Martín-Vicente et al., 2020; Rezinciuc et al., 2020). These studies reveal that viral infection alone has the potential to mediate host cell metabolism and therefore viability assays conducted within these settings must be interpreted with an element of caution. Alveolar lipid metabolism is involved in the continual cycling of lipid generation and degradation within the lung and as such, the addition of exogenous lipids such as SAPS and PAPC into AECs may alter cell metabolism processes (Agudelo et al., 2020). As such, it is important to note that data showing the increased viability of SAPS-treated cells versus RSV-infected cells may not be entirely due to a cytoprotective effect but may also reflect an additional component of the induction of metabolism within the cell in response to excess lipid administration. Due to these limitations of the viability assays, visual analyses of cell cultures during experimental challenge were conducted to note any observable differences between cells that would indicate reduced cell viability or toxicity from either liposome treatment or RSV infection. There was visible cytopathic effect (CPE) in viral-infected BEAS-2B and NHBE cells at 48 hours post infection with cell rounding and visible disruption of the cell monolayer. However, in RSV-infected cells treated with SAPS, the morphology of the cells remained indistinguishable to that of the media control (data not shown), supporting the viability assay data which indicated a cytoprotective effect of SAPS treatment. Of interest, Numata et al. (2010) also described a similar observation where the pulmonary surfactant lipid phosphatidylglycerol (PG) reduced CPE

during RSV infection of both BEAS-2B and NHBE cells, and where PG-treated cells had a similar morphology to that of the uninfected control. In addition, this group confirmed that lipid treatment alone did not alter BEAS-2B cell viability as measured by ³H-leucine incorporation (to measure normal protein synthesis events) over a 48 hour incubation period (Numata et al., 2010).

5.2.1 SAPS possible mechanism on chemokine production

It has been frequently demonstrated that RSV can induce the potent production of CXCL8 and CCL5 from AECs *in vitro* and *in vivo*, e.g. from nasopharyngeal secretions of infants hospitalised with RSV-induced bronchiolitis (Bermejo-Martin et al., 2007; Culley et al., 2006; Hillyer et al., 2018; Russell et al., 2017; Villenave et al., 2012). These soluble mediators are induced via viral-host cell reactions whereby pattern recognition receptors (PRR)s such as surface TLR2 and/or TLR4 and intracellular TLR3 may detect RSV upon infection (Section 1.2.2).

Data shown in chapter 3 demonstrated that co-incubation of AECs with SAPS during viral challenge significantly reduced the production of CXCL8 and CCL5 up to 48 hours post infection (**Figure 3.3, 3.7, 3.8, 3.9 and 3.10**). In BEAS-2B cells, SAPS significantly reduced CXCL8 and CCL5 from cells infected with either MOI (0.4 or 1) with equal effect (**Figure 3.3 A-D**). The inhibitory effects of SAPS were most pronounced against RSV-induced CCL5 production, where the levels of CCL5 were reduced to levels within the vicinity of the matched media control. Numata et al. (2010) also described similar inhibitory effects on cytokine production from BEAS-2B cells infected with RSV in the presence of the surfactant lipid phosphatidylglycerol (PG). PG treatment significantly reduced the production of both IL-6 and CXCL8 at 48 hours post infection. This group also presented comparable findings in NHBE cells with significant reduction of cytokine production in the presence of PG, demonstrating that the effect was maintained across different AECs (Numata et al., 2010). A subsequent study by the same group also noted similar inhibitory effects of another lipid species,

phosphatidylinositol (PI), where co-incubation of BEAS-2B cells with increasing concentrations of PI during RSV infection, correlated with significant reduction of CXCL8 production 48 hours later (Numata et al., 2015). Of note, the significant effects of SAPS demonstrated in the BEAS-2B cell work were also demonstrated in NHBE and HBEC3-KT cell experiments at both 24 and 48 hours post infection (**Figure 3.7-3.10**). SAPS had a concentration dependent inhibitory effect on CXCL8 and CCL5 production in NHBE cells. Concentration dependent effects of SAPS were also demonstrated in co-cultures of PBMC and BEAS-2B cells by Parker et al. (2008) where increasing concentrations of SAPS (0 – 50 µg/ml) were used to antagonise cytokine production in response to LPS stimulation.

Although these data support the role of SAPS to inhibit RSV-induced chemokine production, SAPS treatment may induce elevated baseline levels of CXCL8 production in uninfected AECs. These observations have been previously reported from my group where BEAS-2B cells treated with the highest concentration of SAPS (50 µg/ml) and NHBE cells incubated with either 25 or 50 µg/ml SAPS, resulted in elevated CXCL8 production in uninfected cells (Parker et al., 2008; Stokes et al., 2016). Collectively, these results suggest that co-incubation of cells with SAPS may induce slight inflammatory effects, particularly when used at high concentrations. Of interest, a study by Fonceca et al. (2012) noted that the overall baseline levels of CXCL8 in uninfected NHBE cells was higher than BEAS-2B cells. This group postulated that the higher confluency of the NHBE cells, particularly after 48 hours in culture, may result in cell death and subsequent production of CXCL8 (Fonceca et al., 2012). It is therefore also possible that co-incubation of AECs with SAPS may permit increased cell growth and lead to subsequent over confluence and cell death. However, it is notable that the induction of CXCL8 with increased concentrations of lipids, was not demonstrated by Numata et al. (2010), where the addition of PG to uninfected BEAS-2B or NHBE cells did not induce elevated CXCL8 in comparison to untreated cells despite using a relatively high concentration of PG at 200 µg/ml.

The comparative liposome (PAPC) used in these investigations elicited more variable effects on chemokine production from RSV-infected AECs. In BEAS-2B cells, co-incubation of cells with PAPC during RSV infection significantly reduced production of CCL5 at both 24 and 48 hours post infection, though with less potency than SAPS (**Figure 3.3 C, D**). The highest concentration of PAPC (25 µg/ml) had further significant effects on cytokine production from RSV-infected NHBE cells, inhibiting both CXCL8 and CCL5 equally well as SAPS (**Figure 3.7, Figure 3.8**). These effects were surprising as PAPC had not demonstrated any inhibitory effects on cytokine production in previous studies by my group (Stokes et al., 2016). In addition, PAPC has been routinely used as a negative control lipid in previous studies by Numata et al. (2010, 2012, 2020). However, it has been shown that lipids composed of phosphatidylcholine (PC) may have some immunomodulatory effects on NF-κB induced signalling as was reported in intestinal epithelial cells stimulated with LPS (Chen et al., 2018). PAPC has been reported to have anti-inflammatory effects when in an oxidised form (ox-PAPC) (Kawasaki and Ohnishi, 1992; Ke et al., 2017; Lichtenberger et al., 2001; Treede et al., 2007). The inhibitory effects elicited by SAPS were more consistent across all AECs and therefore may suggest that the varied response of PAPC might be due to subtle variations in PAPC preparations and/or its state of oxidation as all the liposomes are prepared in the lab (Section 2.8). Importantly, there are other potential points at which SAPS and PAPC may target RSV infection, and which may explain differences in the ability of these lipids to target RSV replication vs other viruses such as RV. For example, Stokes et al. (2016) have suggested that SAPS may inhibit TLR3-mediated raft signalling in the endosome. It is possible that PAPC may not translocate to the endosome and therefore have limited effects on certain signalling pathways in response to different viral infections compared to SAPS which has been shown to rapidly locate to the endosome. It's possible that for RSV, SAPS inhibition of signalling events is primarily by preventing early infection, and that maybe PAPC may also moderately inhibit RSV infection and thus the downstream signalling cascades, but just not as well as SAPS. Of note, the prepared liposomes have been previously tested for stability up to 4 weeks when stored at 4°C, however these liposomes were routinely used for longer periods

of time during the investigations outlined in this thesis. Therefore, it may be that the characteristics of PAPC have changed over prolonged use. In the future, it may be appropriate to monitor the lipid biochemistry more closely using analytical tools such as lipid mass spectrometry to monitor the changes in both structure and function of SAPS and PAPC over time and within experimental investigations (Karnati et al., 2018; Li et al., 2014). Data obtained from the different PBMC donors within this study demonstrated high donor variation of baseline CXCL8 production, hindering the more accurate assessment of SAPS/PAPC treatment. The methods used for determining the efficacy of newly generated liposomes in the lab may also be improved by implementing the use of a more consistent cell model such as the THP-1 monocytic cell line, as was previously used in Parker et al. (2008) to investigate SAPS efficacy to reduce LPS induced signalling responses.

It is also worth noting the possible differences in lipids used between the data demonstrated in this thesis and comparative published studies. The comparative PC lipid species used in studies by Numata et al. (2010, 2012, 2020) was 1-palmitoyl-2-oleoyl-sn-glycero-3-phosphatidylcholine (16:0-18:1), whereas the PC lipid species used in this thesis was 1-palmitoyl-2-arachidonoyl-sn-glycero-3-phosphatidylcholine (16:0-20:4). The differences between these two lipid species are the arachidonic acid (used in these studies) which is a polyunsaturated acid with 20 carbon chains and 4 cis double bonds. Oleoyl acid in comparison is a monosaturated fatty acid with 18 carbons and one double bond (<https://avantilipids.com/>). As described in Bakht et al. (2007), the structure of certain lipids may alter their function and interactions with host membranes and this may explain the different results obtained in this thesis compared with other published literature, especially in the context of two different viruses where effects may inhibit different sites such as PRRs that respond to specific viral species (Bakht et al., 2007).

Whilst production of CXCL8 and CCL5 to RSV infection differed across AEC types, SAPS maintained its ability to significantly decrease the production of both these chemokines when co-incubated during viral infection. Moreover, a range of alternative lipid species have also

been detailed to inhibit chemokine production in response to RSV and other clinically relevant respiratory viruses, suggesting a role for lipids to modulate immune signalling.

5.2.2 Viral infection and replication

Data presented in this thesis demonstrate that co-incubation of AECs with SAPS during viral challenge exhibited significant inhibitory effects on viral infection of NHBE cells and viral replication within NHBE and HBEC3-KT cells. Both concentrations of SAPS significantly reduced RSV infection of NHBE cells by ~95% regardless of concentration used, as measured by plaque assay (**Figure 4.3**). These results indicate that SAPS may be physically blocking viral infection or that SAPS may be perturbing stages of the viral replication process and thus reducing subsequent viral spread in culture. To this end, viral replication was also quantified at 24 and 48 hours post infection to determine the effect of SAPS on viral load. Data presented in **Figure 4.5** and **Figure 4.6** indicate that SAPS reduced the levels of viral replication in both NHBE and HBEC3-KT cells. There was a dose dependent effect of SAPS within NHBE cells, whereby the highest concentration of SAPS (25 µg/ml) had the greatest effect on viral replication. Of note, the levels of viral replication in the untreated HBEC3-KT cells were almost 2-fold higher than the NHBE cells at both 24 and 48 hours. This may indicate that the HBEC3-KT cells were more permissible to viral infection and/or replication. It would have been interesting to compare the infectivity of the HBEC3-KT cells using the viral plaque assay, however this was not completed due to time restrictions. An interesting observation was that despite overall higher levels of viral replication in the HBEC3-KT cells compared to the NHBE and BEAS-2B cells, SAPS (25 µg/ml) retained significant inhibitory effects up to 48 hours post RSV infection. Collectively, these data indicate that SAPS was able to inhibit not only the initial infection of AECs but also continued to suppress viral replication up to 48 hours post-infection despite variations in viral infectivity and replication between cell types.

These data exploring SAPS effect on the viral life cycle of RSV differ to that which was demonstrated in the study of RV infection, where SAPS treatment had no effect on viral load

of RV within BEAS-2B cells (Stokes et al., 2016). Data have described a role for MMs in RV infection whereby ICAM-1 (a receptor for the majority of RV serotypes) are found to congregate into MMs (Bacsó et al., 2002; Grassmé et al., 2005). However, the interactions and thus reliability of RV on MMs for fusion and entry into AECs may be dissimilar to RSV due to RV virion structure that lacks a lipid envelope.

Numata et al. (2010, 2015) reported similar findings to that demonstrated in this thesis using an alternative lipid species (PG and PI) to antagonise RSV infection of AECs. Data from their earlier study (2010) demonstrated that co-incubation of PG (200 µg/ml) with RSV reduced viral infection of HEp-2 cells by 4 log units. Further to this, Numata et al. (2010) demonstrated that these inhibitory effects could be replicated *in vivo* where BALB/c mice were infected with RSV in the presence or absence of PG (75-150 µg/ml). Treatment significantly reduced the viral burden within the lungs, as quantified by viral plaque assay as well as inflammatory cell mediators (Numata et al., 2010). In a later publication, Numata et al. (2015) replicated these investigations using PI and indicated similar efficacy to that of PG on viral infectivity and immune cell infiltrates *in vivo*. Additional studies by this group investigated whether PG and/or PI would also antagonise infection and subsequent inflammation in response to different strains of Influenza A virus (IAV) including H1N1 pdm09, Philippines 82/H3N2 and H1N1/PR8 (Numata et al., 2020, 2012). Viral infection of Madin-Darby canine kidney (MDCK) and A549 cells was reduced in the presence of either lipid where it was also shown that these lipids could directly bind influenza virions thus blocking their successive binding to cells (Numata et al., 2020, 2012). The exact mechanisms of these observations however remain unclear and there is ambiguity around whether inhibition of influenza binding to the cells is achieved through antagonistic effects of the lipids of the cognate receptor (sialic acids) that influenza requires to bind. The addition of lipids may also be acting directly on the virions alone, or a combination of both these activities may be having this effect. It is therefore difficult to compare SAPS to these effects where the mechanisms remain unclear. An important observation is that both RSV and IAV require receptors that are predominantly found enriched in MMs. Lipids

may therefore be disrupting the binding of the viruses to host cell through the modulation of lipids on MMs (Bukrinsky et al., 2020; Sorice et al., 2021; Verma et al., 2018).

Research from Numata et al. (2015) contradict data presented in this thesis on the role of PS lipids inhibiting RSV infection of AEC. They report that PS (and another anionic lipid species, phosphatidic acid [PA]) did not have any significant inhibitory effects on RSV binding to HEp-2 cells. However, this viral binding assay was their only comparative investigation using PS and was at just one concentration (200 µg/ml). Numata et al. (2015) suggested that PS is not as effective at controlling RSV infections in AECs because it is not naturally found in pulmonary surfactant. However, published work demonstrate that PS is present in surfactant and makes up less than 5% of total surfactant alongside PI and phosphatidylethanolamine (PE), with PG (=7-15%) and PC the major component making up approximately 80% (in disaturated form-DPPC) (Agassandian and Mallampalli, 2013; Ji et al., 2021). It is also worth noting that as previously discussed with PAPC, different forms of PS lipids may have been used in studies by Numata et al. (2015). Although the specifics are not outlined in their paper regarding the structure of PS used, the specific form of PS used in this thesis was the arachidonoyl form of PS which is polyunsaturated and has 4 cis double bonds. This structure results in extensive kinking of the tails and poor 'tight packing' ability within membranes – thus more disruptive to membrane microdomains (Bakht et al., 2007). Collectively, these published findings and my own data suggest that numerous lipids, many of which are found in pulmonary surfactant, may inhibit viral attachment of RSV to a range of AECs *in vitro* and *in vivo* and that the precise structure of lipid classes may hinder or promote this function. Bakht et al. (2007) explain that ordered liquid domains that form MMs rely on tight packing between sphingolipids and sterols and the incorporation of some lipids may disrupt this occurring.

A notable difference between data within this thesis and published work is that PAPC displayed some anti-viral effects in the NHBE cells. In the viral plaque assay, the highest concentration of PAPC (25 µg/ml) exhibited similar inhibitory effects on RSV infection of NHBE cells as the same concentration of SAPS (**Figure 4.3**). Similarly, PAPC demonstrated a

concentration-dependent effect on viral replication within NHBE cells, significantly decreasing viral load at both time points (**Figure 4.5**). Once more, these effects were only demonstrated in the NHBE cells and not in HBEC3-KT cells, where PAPC had no significant inhibitory effects on viral replication (**Figure 4.6**). As previously discussed, there may have been batch variation in suspensions of PAPC where older batches (as were used in the NHBE studies) may have become oxidised and thus had some level of anti-inflammatory properties. However, these data suggest that PAPC may also have antagonistic effects on viral binding of NHBE cells. It may also be that PAPC exhibits differential effects in specific cell types, however, this was not a phenomenon described in previously published work from my group where NHBE cells were incubated with PAPC (Stokes et al., 2016). The work of Stokes et al. (2016) however, was conducted in the context of RV infection and therefore the differences that were seen with PAPC treatments on RSV-infected cells may also indicate that PAPC is virus specific by targeting of RSV and inhibiting viral infection but not having direct effects on viral-induced cell signalling. In addition, studies by Numata et al. (2010) did not demonstrate any inhibitory effects of PC lipids against RSV infection of HEP-2 cells. In viral binding assays, Numata et al. (2015, 2020) also showed data indicating that PC, unlike PG and PI, did not directly bind RSV. Due to potential structural differences that may have affected lipid function, it would have been of benefit to characterise the stability and structural properties of these lipid species over time. Work to do this began before the COVID-19 pandemic arose where additional studies were going to employ a ZetaView® system to compare SAPS and PAPC batches over time. This machine analyses the concentration of liposomes in suspension in addition to determining particle size and electrostatic potential. This may be something that could be employed in future investigations to monitor possible changes in lipids that may affect their characteristics in viral challenge studies.

5.3 Mechanism of SAPS when applied post RSV infection

To explore the impact of SAPS on an established RSV infection, the application of SAPS at a range of post-RSV infection time points was investigated in HBEC3-KT cells. Initial investigations included one treatment of SAPS (25 µg/ml) at 2, 4, 8 or 24 hours post RSV infection. The efficacy of SAPS to significantly reduce chemokine production (**Figure 3.1, Figure 3.13**) diminished the later it was applied. SAPS significantly reduced CXCL8 production at 24 hours relative to the untreated HBEC3-KT cells infected with RSV when applied 2, 4 or 8 hours after viral challenge. Similarly, SAPS had limited effects on CCL5 production with only the 2- or 4-hour post treatment significantly reducing this chemokine. These results differed to earlier data where co-incubation of SAPS during viral challenge had a particularly potent effect against CCL5 induction. The longevity of these inhibitory effects also diminished at 48 hours post infection where the levels of both CXCL8 and CCL5 were not significantly different to that of the untreated RSV-infected cells. In addition, unlike earlier results indicating that co-incubation of SAPS decreased viral load, when given as a post-treatment, SAPS had no significant impact on viral replication at either 24 or 48 hours (**Figure 4.7**). Of interest, post treatments with PAPC resulted in increased copies of the RSV L-gene which was significant at 24 hours where the HBEC3-KT cells had been treated 2 or 4 hours after viral infection. These data indicate that PAPC may enable viral spread or replication of RSV within the cells although there was no plaque assay data to confirm this, and any potential mechanism for this is currently unclear. Whilst SAPS did not appear to be impacting on viral life cycle events as a post-treatment, experiments were conducted to determine if the inhibitory effects of SAPS on inflammatory cytokine production could be improved. The time points 4, 8, and/or 24 hours post infection were selected to determine if recurrent treatment of AECs with SAPS (25 µg/ml) would increase its efficacy (**Figure 3.15**). Parallel experiments using an increased concentration of SAPS (100 µg/ml) were also completed (**Figure 3.19, 3.20**).

Increased concentrations of either liposome, or repeated treatments, did not markedly improve on their ability to inhibit post-infection responses (**Figures 3.16, 3.19, 3.20**). However, repeated treatments did impact on cell viability (**Figures 3.17, 3.21, 3.22**).

These data collectively demonstrated that SAPS had only modest effects as a post-treatment to control RSV-induced chemokine production and that increased concentrations of SAPS induced cytotoxic effects in HBEC3-KT cells. Interestingly, Stokes et al. (2016) showed that SAPS significantly inhibited RV-induced cytokines post-infection indicating a possible viral-dependent effect of SAPS. Stokes et al. (2016) demonstrated that one treatment of SAPS (10/50 µg/ml) was able to significantly reduce the production of CXCL8, CCL5, and CXCL10 from BEAS-2B cells when applied 1, 4, or 8 hours after RV infection. In addition, SAPS inhibitory effects were maintained up to 48 hours post RV infection which was in contrast to the modest short-lived effects observed with RSV (Stokes et al., 2016).

Numata et al. (2013) demonstrated that PG significantly inhibited RSV-induced CXCL8 when applied post-infection. This group showed that increased concentrations of PG (200, 500 and 1000 µg/ml) had a concentration dependent impact on CXCL8 production from HEp-2 cells infected with RSV for 24 hours prior to treatment. Of note, only the higher concentrations (500 and 1000 µg/ml) significantly reduced CXCL8 relative to the RSV-infected HEp-2 cells that had not received treatment. These concentrations of lipid far exceeded the concentrations of SAPS used in this thesis. Furthermore, Numata et al. (2013) did not assess cell viability. Therefore, it is not clear whether PG actively reduced cytokine production or if this was an artefact of lipid-induced cell death. Also of note, previous studies by this group analysed the effect of PG when co-incubated with BEAS-2B and NHBE cells during viral challenge (Numata et al., 2010). However, for their post-treatment investigation, studies were conducted in HEp-2 cells. It would have been of interest to have had post-treatment experiments conducted within the same cell type as a more comparable model.

The use of SAPS as a post treatment in RSV infection also had limited effects on viral replication. However, it was reassuring to note that SAPS did not increase viral replication when applied post RSV infection. This contrasts with PAPC where post-treatments resulted in elevated viral replication at most time points, with this effect significant at 24 hours in HBEC3-

KT cells treated either at 2- or 4-hours post-infection. These results support the possible mechanism of SAPS in reducing the initial attachment of RSV to AECs. In cases where RSV has already infected cells, SAPS does not seem to inhibit subsequent spread or viral replication suggesting direct interactions are needed between SAPS and RSV to reduce infectivity. These published findings, together with the data in this thesis, indicates that SAPS may have both viral-specific and cell specific effects.

Once again, these data suggest that lipids such as SAPS may have broad antiviral actions, but different ways of mediating inhibition of different viruses. For RSV, the predominant actions of SAPS appear to be to inhibit viral infection at the membrane, with possible additional effects on intracellular signalling in response to virus infection. For RV, Stokes et al. (2016) suggested that the main actions of SAPS were to disrupt TLR3 signalling after viral infection. Since TLR3 contributes to RSV-induced inflammatory responses (Rudd et al., 2005), it is to some degree surprising that post-infection treatment with SAPS had little effect on cytokine production (except where cell mortality was increased). It would be interesting in future work to explore in more detail the signalling pathways activated by RSV in the presence and absence of SAPS as a pre- and post-treatment. For example, tracking activation of ISG signalling pathways as described by Stokes et al. (2016) could be undertaken, together with siRNA treatments to target signalling molecules such as TLR3, and determine further which signalling pathways are ameliorated or preserved in SAPS-treated cells that have been infected with RSV.

In contrast to RSV, RV is an unenveloped virus and therefore the reliance on membranes is minor where lipid mixing during infection processes are not required (Grassmé et al., 2005). RSV has also been demonstrated to form syncytia between cells and can therefore spread to adjacent cells through these membrane dependent processes (Jessie and Dobrovolny, 2021). Viral replication data suggests that SAPS was not able to perturb subsequent rounds of infection in the HBEC3-KT cells when applied after an established viral infection. It would have been interesting to investigate how post-treatments also affected infectivity of the cells using a viral plaque assay. This could be used to investigate if PAPC was increasing viral infection,

accounting for the notable increased viral load or, if PAPS modified the viral replication efficiency of RSV when applied 2 or 4 hours after RSV infection. Although my data indicate that SAPS may only have beneficial effects when applied during viral challenge, published data from Numata et al. (2010) demonstrated that PG (200 or 500 µg/ml), could significantly inhibit RSV infection within HEp-2 cells after an established viral infection. However, the application of PG was directly after unbound virus had been removed (designated 0 hour in studies within this thesis) and therefore didn't fully explore the efficacy of PG to inhibit viral spread when given at later time points in a more relevant post-infection model. In addition, most of the work in this particular study explored the effects of PG when co-incubated with BEAS-2B or NHBE cells during viral challenge, but as noted above for this particular experiment, HEp-2 cells were used (Numata et al., 2010). Of interest, in a later publication from the same group, when investigating the effect of PG and PI to alleviate inflammation and viral infection of AECs with RSV, no experiments were conducted to explore the potential application post-RSV infection (Numata et al., 2015). Comments from this study were that both PG and PI were most efficacious when administered during viral challenge of BEAS-2B cells which is in line with the findings in this thesis. Comparative investigations were also completed by this group investigating the efficacy of PG and PI to reduce influenza infection of MDCK and A549 cells (Numata et al., 2020, 2012). These investigations also demonstrated that both PG and PI were most efficacious when administered close to the initial viral challenge time point. Numata et al. (2012) reported that PG (1000 µg/ml) had some inhibitory effects on subsequent viral infection when administered up to 1 hour post influenza infection but was ineffective by 2 hours post-infection. Published data and data presented within this thesis therefore demonstrate that the efficacy of certain lipids to reduce inflammatory responses and viral infection of AECs is highly dependent upon the time of administration in relation to infection. Comparative studies using SAPS against RV infection and RSV infections of AECs also suggests that the efficacy of lipids may be variable against different viral species.

As well as the limitations of SAPS as a post-treatment, this project also revealed some unexpected results whereby increased concentrations of SAPS resulted in markedly high cytotoxic effects within HBEC3-KT cells. Although it had been previously noted that SAPS could moderately increase production of CXCL8 from uninfected AECs, no cytotoxic effects had previously been visualised where SAPS had affected epithelial cell integrity. Therefore, the visible detrimental effect that SAPS had when applied post RSV-infection may indicate that SAPS can exacerbate viral harm if applied to cells already infected with virus.

Lipid homeostasis is a highly regulated process within cells which enables the rapid turnover of different lipid species. The submerged cell culture model used in this thesis and by Stokes et al. (2016) does not fully recapitulate the regulation of lipid metabolism in the lungs. Surfactant lipids such as PS and PC species are catabolically degraded by type II alveolar epithelial cells (which also generate lipids at ER) or alveolar macrophages (Agassandian and Mallampalli, 2013). *In vivo* both toxicity and efficacy may also be affected by accessibility of lipids to the cell surface, and by their metabolism and degradation. Excess PS may be converted, via decarboxylation to other lipid species, including PC and PE, which may also have a role in modulating viral infection and inflammation. Of interest, Numata et al. (2010, 2012, 2015) have demonstrated in multiple *in vivo* studies that the use of exogenous lipids into mouse lungs, were not associated with toxicity.

5.4 SAPS interactions with cell receptors and virus

The data presented in this thesis indicate that SAPS was most efficacious at reducing cytokine production and viral infection of AECs when co-incubated with RSV during viral challenge. Published data from my group showed that SAPS may interact with host cell receptors, impeding inflammatory signalling responses typically driven through PRR interactions (Parker et al., 2008). Many studies have shown that MM are crucial for the induction of transmembrane signalling events in response to a range of pathogens, including RSV (Triantafyllou et al.,

2004b, 2002; Yokoyama et al., 2021). RSV infection initiates the recruitment of TLR2 and/or TLR4 into MM that enables the congregation with their associated co-receptors myeloid differentiation factor 2 (MD-2) and cluster of differentiation 14 (CD14) and subsequent production of proinflammatory cytokines (Broadbent et al., 2018; Haynes et al., 2001; Kurt-Jones et al., 2000). Therefore, disruption of TLR recruitment into MM may be inhibiting RSV-induced inflammation and may be a potential mechanism of SAPS. Previous investigations from my lab group have demonstrated that SAPS reduced the association of PRRs within MM in response to a range of TLR agonists (Parker et al., 2008). FRET technology demonstrated that LPS stimulation of monocytes was disrupted in the presence of SAPS where TLR2/4 were unable to associate with co-receptors MD-2 and CD14. A similar finding was demonstrated by Abate et al. (2010) where inhibition of TLR4 into MM was shown via density gradient ultracentrifugation. In the presence of commercially available surfactant (Survanta®, Curosurf® and dipalmitoylphosphatidylcholine [DPPC]), TLR4 was unable to congregate into MM and thus CXCL8 production from A549 airway epithelial cells was inhibited (Abate et al., 2010). A similar study also showed that TLR2/4 inflammatory signalling in macrophages was disrupted using an alternative anionic phospholipid containing phosphatidylglycerol (PG) which directly bound CD14, antagonizing the binding of LPS and downstream signalling events (Kandasamy et al., 2016). The direct binding of PG to CD14 and MD-2 was also reported by another group, whereby LPS-induced inflammatory signalling in macrophages was directly inhibited using PG, but not PC-containing lipids that were administered in mice (Kuronuma et al., 2009). Parker et al. (2008) also showed that SAPS (50 µg/ml) could inhibit the interactions between LPS and CD14 by directly binding CD14 in both co-cultures (BEAS-2B cells and PBMCs) and independently in THP-1 (macrophage model) cell culture. In a separate study investigating interactions between PS and the brain, it was shown that PS modified ligand receptor binding and associated signalling (Agassandian and Mallampalli, 2013). However, in contrast to published findings by Parker et al. (2008), Kuronuma et al. (2009) demonstrated that PS-containing liposomes (up to 20 µg/ml) had only minor antagonistic effects in comparison to PG and a reduced ability to inhibit nitric oxide and TNF α .

Work from Numata et al. (2013, 2012, 2010) also showed that PG containing liposomes directly modulated the binding of RSV and influenza virus to cells including RSV (HEp-2 cells) and influenza (MDCK cells). These data indicate that specific lipids may have abilities to directly bind signalling receptors, co-receptors, and/or PAMPs to arrest hyperinflammation in the lung and which may be the mechanism by which SAPS inhibited responses to RSV in this study.

In addition to modulation of inflammatory chemokine production, the results presented in this thesis indicate that SAPS treatment reduced RSV infection and replication, suggesting that additional mechanisms (alongside MM modulation) may be involved. The data presented in this thesis show that co-incubation of SAPS as well as reapplication of SAPS immediately after viral infection (0 hours), significantly reduced subsequent viral load of RSV detected up to 48 hours post infection. This may indicate that SAPS is having inhibitory effects on the initial attachment of RSV to AECs.

To determine if SAPS reduced viral binding in the HBEC3-KT cells, fluorescent microscopy was used to visualise the different stages of RSV infection, specifically binding and fusion events. As demonstrated in **Figure 4.12 A-E**, the presence of SAPS during viral challenge significantly reduced the levels of RSV-infected cells 20 hours after viral infection as determined by the presence of F-protein. Furthermore, in **Figure 4.12 C**, cells were incubated at 4°C for 1 hour to allow for the attachment of RSV to HBEC3-KT cells but prevent viral fusion and uptake into the cell. There was reduced expression of F protein (indicative of RSV attachment) on the HBEC3-KT cells that had been incubated with SAPS relative to RSV infection alone. This indicates that SAPS may have directly reduced RSV attachment to the HBEC3-KT cells, with unbound RSV removed in the subsequent cell wash. This raised the possibility that SAPS was either binding HBEC3-KT cell receptors used by RSV, disrupting MMs that were critical for viral attachment and infection, or directly binding RSV virions to disrupt viral-host cell interactions required for successful attachment. Of interest, published work by Numata et al. (2010, 2012, 2013, 2015 and 2020) demonstrated that PG and PI lipids

were able to directly bind to both RSV and influenza virions in a concentration-dependent manner. They also demonstrated that unlike PG or PI, PC lipids had only minor binding capabilities to RSV and influenza and thus only insignificant inhibitory properties. Overall, the findings within this thesis and published data support the potential mechanism of SAPS to directly antagonise RSV binding to airway epithelial cells. However, it would have been of interest to complete additional mechanistic studies to investigate this interaction in more detail. For example, Numata et al. (2010) investigated the binding efficiency of RSV and influenza to solid phase lipids coated on microwell plates. This may have helped determine if SAPS was directly binding to RSV virions and whether this was a temporal effect as well as concentration dependent. As such, this may have enabled determination of whether the minor binding activities of PC lipids demonstrated by Numata et al. (2010, 2012, 2013, 2015 and 2020) may have accounted for the variable data generated with the PC-containing liposome PAPC. The potential binding activities of lipids such as PS demonstrated in the literature and within this thesis have also been observed for other constituents of pulmonary surfactant including surfactant proteins (SP)-A and -D which have been shown to directly bind TLRs of host cells as well as playing crucial roles antagonising responses to fungal, bacterial, and viral pathogens (Numata and Voelker, 2022).

In addition to determining the interactions of SAPS on viral attachment to the HBEC3-KT cells, another important aspect of the fluorescent imaging was to determine if host-viral interactions were occurring at MM, as hypothesised. As discussed, (Section 1.4.1), the presence and activities of MM can be challenging to visualise due to their transient nature. Published data have indicated that the formation of MM is dependent on actin rearrangement to form these platforms during viral infection (Jumat et al., 2015; San-Juan-Vergara et al., 2012; Yeo et al., 2009). It was anticipated that fluorescent microscopy would allow visualisation of actin rearrangement within the cell during various stages of the RSV life cycle, supporting the possible presence of MM during these events. Moreover, the formation of these actin-rich areas within the membrane were disrupted in the presence of SAPS was investigated.

Data presented in **Figure 4.10 A** and **Figure 4.13 A-C**, illustrate that there were defined regions of the membrane that were densely stained purple, indicative of the accumulation of actin filaments. Actin-rich areas of the membrane appeared to colocalise where there was also intense green fluorescence, indicative of the RSV virions. It was difficult to quantify these interactions, and these may have been subject to bias so to reduce this, multiple areas of each sample slide were randomly selected based on DAPI staining alone. The time point of 20 hours post infection suggests that images may capture RSV congregation at the HBEC3-KT cell membrane for budding and egress out of the cell. As such, not all RSV-infected cells demonstrated the accumulation of RSV at actin-filament rich areas of the host cell. This may be due to images capturing cells at different stages of infection. In addition, the nature of confocal microscopy means that these images only capture one focal plane of the cells. This can be overcome by using a Z-stack to visualise the entirety of the infected cells; however, this requires long processing times and can rapidly bleach samples. Similar images were also demonstrated by Jumat et al. (2014) showing human metapneumovirus (HMPV: a virus that is closely related to RSV within the *Pneumoviridae* family) colocalising at actin-rich membranes during viral egress. In addition, the staining of the major surface glycoproteins attachment glycoprotein (G) and fusion (F) protein of HMPV demonstrated that these viral proteins were most abundant at areas of the cell membrane together with areas rich in actin filaments. To better visualise MM, Jumat et al. (2020) stained for the glycolipid, GM-1 which has been shown to be in abundance in MM and therefore used as a marker for identifying MM using Cholera Toxin (CTxB) (Rissanen et al., 2017). By incorporating these different markers, Jumat et al. (2020) illustrated that HMPV appears to interact with MM during viral budding and that HMPV appears to bud in a filamentous morphology. Kinder et al. (2020) also demonstrated similar findings with RSV and HMPV where filamentous projections were seen from infected AECs at ALI although they noted that these filamentous projections were more prominent in HMPV-infected cells (Kinder et al., 2020). Of interest, the images captured within this thesis did not demonstrate characteristics of syncytia (multinucleated cells) formation in

RSV-infected HBEC3-KT cells. Kinder et al. (2020) also reported similar findings where no syncytia were observed at the peak of viral infection (72 hours post-infection). These observations may be due to cell culture methods where virus may be able to bud from apical membranes of the cells easier in submerged culture and not require the fusion and spread to adjacent cells. This may also suggest some limitations to using *in vitro* modelling for observing these processes and how SAPS may be modulating the spread of RSV between cells. An interesting observation, however, was that the RSV-infected HBEC3-KT cells that had been co-incubated with SAPS not only had less infected cells 20 hours after infection but also had distinct morphological features. The RSV-infected cells were condensed in size relative to the surrounding cell monolayer with the membrane of the infected cell appearing ruffled and shrunken (**Figure 4.14**). It is hard to determine from these images whether this may illustrate an apoptotic cell but there did not appear to be characteristic accumulation of RSV at the cell membrane indicating a possible mechanistic modulation. The images also seemed to indicate that although there were some RSV-infected cells, the virus had not been able to egress and spread within culture to adjacent cells. This may indicate that SAPS can impact on viral egress, a feature that would have been interesting to explore using a viral budding assay to characterise the infectivity of RSV in these cases.

5.5 RSV-bacterial co-infections

Studies have shown evidence that peaks in RSV infections (particularly in children) also coincide with peaks in co-infection with *Streptococcus pneumoniae* (*Spn*) (Michelow et al., 2004) and that severe RSV disease is frequently identified as a contributing factor for subsequent bacterial pneumonia (Greenberg et al., 2017; Juvén et al., 2000; Suárez-Arrabal et al., 2015; Thorburn et al., 2006; Vu et al., 2011). A recent report demonstrated that the rates of pneumococcal pneumonia were reduced in Israel during the COVID-19 pandemic and that this may be attributable to the decreased rates of infections with respiratory viruses such as RSV (Danino et al., 2021). In this study, the authors observed that pneumococcal carriage in

children (< 5 years old) was not perturbed but incidence of bacterial pneumonia were reduced suggesting that non-pharmaceutical interventions may have played a minor role in reducing community acquired pneumonia. The rates of carriage were not largely affected and therefore the incidence of illness was more likely associated with reduced frequency of viral infections with influenza, RSV, and human metapneumovirus (Danino et al., 2021). Circulation of RV, adenovirus and parainfluenza virus were not as dramatically affected which may suggest that RSV plays a larger role in predisposing individuals to pneumococcal pneumonia than other common respiratory viruses.

Data presented in this thesis demonstrate that co-incubation of HBEC3-KT cells with SAPS during RSV infection protects the cells from viral infection, subsequent viral replication and associated inflammatory responses. Therefore, it was of interest to determine if these effects would also confer protection against subsequent infection with *Spn*. It was initially planned that these investigations were to be conducted over the last 18 months of my PhD, however due to the COVID-19 pandemic, the funding was delayed by approximately 12 months and the experimental opportunities had also been curtailed due to decreased access to laboratory spaces. Therefore, the experimental design for this part of the project had to be streamlined. In addition, optimisation of the viral-bacterial co-infection model was time consuming and did not allow for extensive interrogation of the role of SAPS in this context.

The pneumolysin toxin of *Spn*, particularly of unencapsulated strains, has been shown to interact with TLR2 and TLR4 on AECs during infection and induce MyD88 and TRIF-dependent signalling pathways leading to the upregulation of CXCL8 (Baumgartner et al., 2016; K ung et al., 2014; Marriott et al., 2012; S anchez-Tarjuelo et al., 2020). A primary objective to optimise the co-infection model was to first assess the effects of *Spn* infection alone in HBEC3-KT cells. HBEC3-KT cells were challenged with increased quantities of *Spn* to assess the interaction with cell receptors and resulting levels of CXCL8 and effect on cell viability (**Figure 4.15 A, B**). These data illustrated that increasing MOIs of *Spn* positively correlated with increased production of CXCL8 and decreased HBEC3-KT cell viability 24

hours after bacterial challenge, except for the highest MOI used (10) which significantly reduced cell viability and subsequently, CXCL8 generation. These data indicate that *Spn* was able to infect the HBEC3-KT cells and trigger CXCL8 production, supporting a possible interaction with TLR2 and/or TLR4.

Bacterial co-infections are particularly common in cases of severe RSV disease where viral-infected cells are susceptible to bacterial colonisation through upregulation of host cell receptors and dysregulated immune responses that occur during viral infection (Section 1.3.4). Data within this thesis demonstrated that SAPS was most efficacious against RSV when incubated with the cells during viral challenge, therefore this was the application time point applied to the subsequent bacterial co-infection experiments. The co-infection experiments conducted within this thesis were designed to model a scenario where RSV would be the predisposing factor for bacterial co-infection, and thus bacterial adhesion and invasion in RSV-infected cells was assessed. In addition, the ability of SAPS to inhibit these predisposing factors was evaluated in HBEC3-KT cells infected with RSV for 24 hours (or stimulated with media). The following day, HBEC3-KT cells were infected with *Spn* (MOI 1), and bacterial adherence quantified. **Figure 4.17** demonstrated that HBEC3-KT cells infected with RSV for 24 hours showed significantly increased adherence of *Spn* to cells. Increased bacterial adherence to RSV-infected cells has also been demonstrated by Hament et al. (2004, 2005) where HEp-2 and A549 cell lines were infected with RSV and subsequently infected with various serotypes of *Spn* associated with invasive pneumococcal disease in children. Hament et al. (2005) observed that *Spn* preferentially accumulated on areas of the monolayer where syncytia were forming with viral-induced CPE also observed. Studies have also shown that *Spn* may directly bind RSV G protein when exposed on viral-infected cells (Elahmer et al., 1996; Hament et al., 2005). In addition, Hament et al. (2005) also demonstrated that *Spn* were able to directly bind RSV virions, a process that was inhibited by the addition of heparin during viral infection which interferes with RSV attachment protein G during viral infection. Further to this, a later study by Smith et al. (2014) demonstrated that attachment protein G of RSV can

directly interact with penicillin binding protein 1a (PBP1a) of *Spn*, which increased bacterial adherence to ciliated AECs and CXCL8 production in comparison to cells not infected with RSV (Smith et al., 2014b). Smith et al. (2014b) also showed that protein interactions between RSV and *Spn* led to the upregulation of *Spn* virulence genes, such as pneumolysin, that further contributed to increased inflammatory signalling processes *in vivo*. These published findings may indicate why increased CPE was observed in the co-infected cells in this thesis, compared to infection with RSV or *Spn* alone (visual observation). Data presented within this thesis also support published findings that viral-infected cells can predispose to bacterial co-infection and that this can be attributed to either viral-induced effects or host cell responses to virus. Of note, the *Spn* used in these investigations was an unencapsulated serotype. Novick et al. (2017) demonstrated that unencapsulated serotypes of *Spn* were shown to adhere and invade A549 cells more easily than capsulated *Spn* serotypes (Novick et al., 2017). The importance of the capsule was also highlighted in a recent review which revealed that the polysaccharide capsule of *Spn* can affect the virulence of that specific serotype and thus its pathogenesis during viral co-infection (Luck et al., 2020).

RSV infection increased bacterial adherence to the HBEC3-KT cells, however, HBEC3-KT cells co-incubated with SAPS during RSV infection had significantly reduced levels of adherent bacteria compared to RSV-infected cells that had not received SAPS treatment. These data reinforce the importance of RSV as a driver of bacterial airway infection and suggest that treatment of RSV infection may reduce risks of subsequent bacterial pneumonia.

Additional experiments were conducted to investigate whether SAPS interacted with *Spn* to evaluate if SAPS had any potential bactericidal effects. Data presented in **Figure 4.16** indicate that although *Spn* had grown in both conditions over the 1-hour incubation period, *Spn* that had been co-incubated with SAPS (25 µg/ml) resulted in significantly less *Spn* colonies the following day. These results were surprising as it was not expected that SAPS would have any direct effects on the viability or growth of *Spn*. It is difficult to confirm whether SAPS was directly bactericidal as there were still increased bacterial numbers comparative to what was

originally added to the plate indicating that within the 1-hour incubation, *Spn* was able to grow and divide but to a lesser degree in the presence of SAPS. More detailed studies of the effects of exogenous phospholipids on bacterial growth and survival are required.

Published literature and preliminary experiments within this thesis demonstrate that RSV-infected AECs showed increased bacterial adherence with *Spn* (Avadhanula et al., 2006; Brealey et al., 2015). Successful adherence and colonisation of *Spn* to cells lining the respiratory tract can promote bacterial invasion and contribute to pneumococcal disease. As with RSV infections, pneumococcal disease is most prolific in very young infants, immunocompromised and elderly individuals (Brealey et al., 2018; Brooks and Mias, 2018). Viral infections of the respiratory tract, including RSV, have been identified as contributing factors for invasive pneumococcal disease. Therefore, this was explored in the HBEC3-KT cells to determine whether RSV infection increased *Spn* bacterial invasion and whether SAPS-treated HBEC3-KT cells would reduce this through modulation of RSV infection. The assays and experiments conducted here did not show significant bacterial invasion of airway epithelial cells. Novick et al. (2017) have demonstrated that different AECs show variable susceptibility to invasive *Spn* which may account for the minimal uptake of *Spn* in the HBEC3-KT cells. This group also highlighted that after bacterial adhesion, *Spn* choline-binding protein A (CbpA) binding to platelet-activating factor receptor (PAF-R) of host cells is required for bacterial uptake into the host cell, a receptor that may be differentially expressed in different cell types (Novick et al., 2017). Moreover, cells infected with *Spn* resulted in bacterial invasion but at much higher MOIs (MOI 80) than were used in this study (MOI 30). Furthermore, the unencapsulated *Spn* serotype invasion rates in primary cells (nasal and oral cells) peaked earlier (at 60 minutes) than A549 and BEAS-2B cell lines which continued to increase up until 90 minutes post-infection. In addition, A549 cells had significantly higher rates of *Spn* invasion than the primary cells (Novick et al., 2017). Whilst the primary site for *Spn* is the nasal epithelium, some studies have indicated that *Spn* can infect bronchial cells (Adamou et al.,

1998; Novick et al., 2017), however, the results demonstrated within this thesis may show that *Spn* invasion of bronchial epithelial cells are less frequent than those of nasal origin.

These data highlight that predisposing RSV infection increased bacterial adhesion in AECs with SAPS not only reducing RSV infection but permissibility to secondary bacterial infection. Interestingly, in cells not infected with RSV, SAPS also reduced bacterial adhesion. Whilst this is promising data, once more, the mechanism of SAPS in this context is unclear and requires further investigation.

5.6 Limitations and future work

As with all studies, there were notable limitations within this project and thus, further work is required regarding the suitability of SAPS as a potential therapeutic for RSV. A major limitation of this work was the airway epithelial cell model used. The work presented in this thesis uses a range of airway epithelial cells grown at submerged culture, however as discussed in **Section 5.1**, normal human bronchial epithelial (NHBE) cells are a more representative model of the human airway than immortalised cells lines and, as such, the use of these cultures throughout this project would have been optimal. However, due to the limited number of cells obtained within our lab, the NHBE cells were used in experiments up to and including passage 7, however the use of NHBE cells past passage 4 is generally not recommended due to their senescent characteristics and this is something that would be rectified in future work to ensure reproducibility among donor cells. In addition, the use of NHBE cells grown at air-liquid interphase (ALI), had been planned for this project however lengthy optimisation of these commercially acquired NHBE cells severely impacted the planned work. Although MMs have been described in ALI culture, the role of MM's during RSV infection of ALI cultures is limited and thus these studies would have established whether SAPS could inhibit infection of ciliated cells, the primary site for RSV infection. Data presented in this thesis have also highlighted that different AEC models have variable responses (such as chemokine production and permissiveness to viral infection) when challenged with the same strain of RSV. Significant

delays to the project due to the optimisation of the NHBE cells and the problems of laboratory access during COVID-19, led to the use of HBEC3-KT cells as an alternative airway epithelial cell model. Despite HBEC3-KT cells being a more suitable model than the BEAS-2B cells, there are limitations as HBEC3-KT cells are still an immortalised cell that may not fully recapitulate the human airway. Therefore, this may therefore hinder the accurate assessment of SAPS effects during RSV infection. It is also worth noting that primary RSV infection predominantly occurs at ciliated nasal epithelium, however all this work was generated using cells from an anatomically lower region of the airways. As such, the inflammatory responses and efficacy of SAPS on viral infection may differ in nasal epithelial cells. This would be good to explore in the future as well as cells obtained from paediatric and elderly people to assess more accurately the responses to RSV which can be different in these age groups.

Another limitation of this work was the partial assessment of innate immune responses to RSV infection and the effect of SAPS on these. Multiple cytokines and chemokines are produced in response to RSV infection such as IFN- α , TNF α , IL-6 and IL-10 (Bohmwald et al., 2019; Habibi et al., 2020; Openshaw et al., 2017; Vázquez et al., 2019). It would have been valuable to use a multiplex array to simultaneously assess the production of different cytokines and chemokines induced by RSV infection. This would have enabled a wider analysis on the effect of SAPS on RSV-induced inflammatory mediators. A combination of cost, sample number and COVID-19 limitations prevented this. In addition, the signalling pathways triggered by RSV would have been beneficial to explore through western blotting to compare the effect of SAPS on signalling within the cell, as discussed above.

Previous publications from my lab group support the mechanism of SAPS acting on MM however, the data presented in this thesis did not make extensive progress in elucidating the interactions of SAPS specifically on MM. The outlined plans to investigate MMs had involved using live confocal microscopy techniques to fluorescently label GM-1 glycosphingolipids that are abundant in MMs. These have previously been successfully labelled using cholera toxin B-subunit (CTxB) based antibodies that bind GM-1 (Kenworthy et al., 2021). Live confocal

microscopy would also have been a useful tool to visualise the interactions of RSV with MM in the presence/absence of SAPS. This would have been interesting to continue the work to visualise actin filament rearrangement and assess its role in MM formation.

Lipidomic analysis for the study of SARS-CoV-2 have shown evidence that viral infections can modulate lipid membranes of the host cell which may enable efficient viral infection and replication (Ji et al., 2021; Wu et al., 2020). It would be interesting in the future to explore using lipidomics to assess how SAPS treatment affects the lipid composition of cells. Mass spectrometry also has the potential to answer specific questions regarding lipid modification of SAPS-treated AECs or RSV-infected cells. Agudelo et al. (2020) have described that lipid metabolism can vary between different cell types and as such, single cell analysis might also serve as a useful tool to understand the response of different AECs such as alveolar, bronchial, and nasal cells more specifically. However, these studies will have to appreciate that changes in lipid species is a continual process and end point quantification may not represent the dynamic increases and decreases of different lipid species, complicating the analysis of which lipids are exactly responsible for the observed outputs. A recent study has also demonstrated that alterations in lipid metabolism may have longer lasting effects in AECs in response to viral infection with SARS-CoV-2 indicating that this is an area of research that needs more investigation (Ji et al., 2021; Wu et al., 2020).

A further limitation to the project was the COVID-19 pandemic which severely impacted both lab work and delayed funding. The pandemic led to approximately 6 months out of the lab where work could not be completed for the PhD. Within this period, I volunteered with Thushan du Silva as part of the AstraZeneca Oxford vaccine trial. A 3-month extension was granted for my PhD project but did not allow sufficient time to complete all the original planned work. As outlined in the COVID-19 impact form, the pandemic restricted access to the lab to continue experiments, due to social distancing and reduced lab capacities, and the HBEC3-KT cells which had just been optimised for use in the lab had to be destroyed. On return to the lab, equipment broke down after sustained periods of inactivity, such as the incubator which further

affected cell culture which was fundamental to lab work. There were high pressure time frames in place and in the last few months we were forced to shut down our lab once more and relocate to a temporary lab, which was associated with a loss of material due to refrigeration issues, with further delays. The bacterial co-infection work was due to be completed over the second half of my PhD, however, these experiments had to be strictly streamlined. Despite this, data presented within this thesis tentatively show that SAPS may be able to protect AECs from bacterial co-infections, either through inhibition of primary RSV infection, or direct inhibitory effects on bacterial adhesion and colonisation. This is novel data and to my knowledge no data has ever been published assessing the impact of lipids on bacterial infection of AECs and so this may be an exciting area of further research.

5.7 Conclusion

Respiratory syncytial viral infections contribute to increased rates of morbidity and mortality, particularly in the very young and elderly populations. Despite extensive research over the last 50 years, there remains an urgent need for effective therapeutics against RSV that will also ensure equal access to those living in low- or middle-income countries. Data suggests that this may be effective as an early treatment to inhibit RSV infection with SAPS being of a respirable size which would enable its rapid delivery in aerosolised form via nebuliser.

The results of this thesis, and the discussion of other publications in these domains, indicate that the lipids present in airway surfactant may be playing vital antiviral roles. Furthermore, the opportunity to exploit their antiviral properties may provide a range of safe therapies that can be administered alongside other specific antiviral drugs in development to aid control of viral infection and viral inflammation in the lung.

The recent COVID-19 pandemic has brought viruses into the limelight where collaborative research has resulted in rapid progress to understand respiratory viruses. These challenging times have highlighted the need for better therapeutics against respiratory viruses and how

consideration and comparison of different viral species can contribute to our overall knowledge.

References

- Abate, W., Alghaithy, A.A., Parton, J., Jones, K.P., Jackson, S.K., 2010. Surfactant lipids regulate LPS-induced interleukin-8 production in A549 lung epithelial cells by inhibiting translocation of TLR4 into lipid raft domains. *J. Lipid Res.* 51, 334–344. <https://doi.org/10.1194/jlr.M000513>
- Ackerson, B., Tseng, H.F., Sy, L.S., Solano, Z., Slezak, J., Luo, Y., Fischetti, C.A., Shinde, V., 2019. Severe Morbidity and Mortality Associated With Respiratory Syncytial Virus Versus Influenza Infection in Hospitalized Older Adults. *Clin. Infect. Dis. Off. Publ. Infect. Dis. Soc. Am.* 69, 197–203. <https://doi.org/10.1093/cid/ciy991>
- Adamou, J.E., Wizemann, T.M., Barren, P., Langermann, S., 1998. Adherence of *Streptococcus pneumoniae* to Human Bronchial Epithelial Cells (BEAS-2B). *Infect. Immun.* <https://doi.org/10.1128/IAI.66.2.820-822.1998>
- Agarwal, V., Ahl, J., Riesbeck, K., Blom, A.M., 2013. An Alternative Role of C1q in Bacterial Infections: Facilitating *Streptococcus pneumoniae* Adherence and Invasion of Host Cells. *J. Immunol.* 191, 4235–4245. <https://doi.org/10.4049/jimmunol.1300279>
- Agassandian, M., Mallampalli, R.K., 2013. Surfactant phospholipid metabolism. *Biochim. Biophys. Acta* 1831, 612–625. <https://doi.org/10.1016/j.bbalip.2012.09.010>
- Agudelo, C.W., Samaha, G., Garcia-Arcos, I., 2020. Alveolar lipids in pulmonary disease. A review. *Lipids Health Dis.* 19, 122. <https://doi.org/10.1186/s12944-020-01278-8>
- Aizaki, H., Lee, K.-J., Sung, V.M.-H., Ishiko, H., Lai, M.M.C., 2004. Characterization of the hepatitis C virus RNA replication complex associated with lipid rafts. *Virology* 324, 450–461. <https://doi.org/10.1016/j.virol.2004.03.034>
- Anderson, C.S., Chu, C.-Y., Wang, Q., Mereness, J.A., Ren, Y., Donlon, K., Bhattacharya, S., Misra, R.S., Walsh, E.E., Pryhuber, G.S., Mariani, T.J., 2020. CX3CR1 as a respiratory syncytial virus receptor in pediatric human lung. *Pediatr. Res.* 87, 862–867. <https://doi.org/10.1038/s41390-019-0677-0>
- Ascough, S., Paterson, S., Chiu, C., 2018. Induction and Subversion of Human Protective Immunity: Contrasting Influenza and Respiratory Syncytial Virus. *Front. Immunol.* 9.
- Avadhanula, V., Rodriguez, C.A., DeVincenzo, J.P., Wang, Y., Webby, R.J., Ulett, G.C., Adderson, E.E., 2006. Respiratory Viruses Augment the Adhesion of Bacterial Pathogens to Respiratory Epithelium in a Viral Species- and Cell Type-Dependent Manner. *J. Virol.* 80, 1629–1636. <https://doi.org/10.1128/JVI.80.4.1629-1636.2006>
- Bacsó, Z., Bene, L., Damjanovich, L., Damjanovich, S., 2002. INF- γ Rearranges Membrane Topography of MHC-I and ICAM-1 in Colon Carcinoma Cells. *Biochem. Biophys. Res. Commun.* 290, 635–640. <https://doi.org/10.1006/bbrc.2001.6246>
- Baer, A., Kehn-Hall, K., 2014. Viral Concentration Determination Through Plaque Assays: Using Traditional and Novel Overlay Systems. *J. Vis. Exp. JoVE* 52065. <https://doi.org/10.3791/52065>
- Bajimaya, S., Frankl, T., Hayashi, T., Takimoto, T., 2017. Cholesterol is required for stability and infectivity of influenza A and respiratory syncytial viruses. *Virology* 510, 234–241. <https://doi.org/10.1016/j.virol.2017.07.024>
- Bakaletz, L.O., 2017. Viral-bacterial co-infections in the respiratory tract. *Curr. Opin. Microbiol.* 35, 30–35. <https://doi.org/10.1016/j.mib.2016.11.003>
- Bakht, O., Pathak, P., London, E., 2007. Effect of the Structure of Lipids Favoring Disordered Domain Formation on the Stability of Cholesterol-Containing Ordered Domains (Lipid Rafts): Identification of Multiple Raft-Stabilization Mechanisms. *Biophys. J.* 93, 4307–4318. <https://doi.org/10.1529/biophysj.107.114967>
- Barthelemy, A., Ivanov, S., Fontaine, J., Soulard, D., Bouabe, H., Paget, C., Faveeuw, C., Trottein, F., 2017. Influenza A virus-induced release of interleukin-10 inhibits the antimicrobial activities of invariant natural killer T cells during invasive pneumococcal superinfection. *Mucosal Immunol.* 10, 460–469. <https://doi.org/10.1038/mi.2016.49>
- Battles, M.B., Langedijk, J.P., Furmanova-Hollenstein, P., Chaiwatpongsakorn, S., Costello, H.M., Kwanten, L., Vranckx, L., Vink, P., Jaensch, S., Jonckers, T.H.M., Koul, A.,

- Arnoult, E., Peeples, M.E., Roymans, D., McLellan, J.S., 2016. Molecular mechanism of respiratory syncytial virus fusion inhibitors. *Nat. Chem. Biol.* 12, 87–93. <https://doi.org/10.1038/nchembio.1982>
- Baumgart, T., Hammond, A.T., Sengupta, P., Hess, S.T., Holowka, D.A., Baird, B.A., Webb, W.W., 2007. Large-scale fluid/fluid phase separation of proteins and lipids in giant plasma membrane vesicles. *Proc. Natl. Acad. Sci. U. S. A.* 104, 3165–3170. <https://doi.org/10.1073/pnas.0611357104>
- Baumgartner, D., Aebi, S., Grandgirard, D., Leib, S.L., Draeger, A., Babiychuk, E., Hathaway, L.J., 2016. Clinical *Streptococcus pneumoniae* isolates induce differing CXCL8 responses from human nasopharyngeal epithelial cells which are reduced by liposomes. *BMC Microbiol.* 16, 154. <https://doi.org/10.1186/s12866-016-0777-5>
- Beadling, C., Slifka, M.K., 2004. How do viral infections predispose patients to bacterial infections? *Curr. Opin. Infect. Dis.* 17, 185–191. <https://doi.org/10.1097/00001432-200406000-00003>
- Beck, J.M., Young, V.B., Huffnagle, G.B., %J T.R., 2012. The microbiome of the lung 160, 258–266.
- Bellinghausen, C., Gulraiz, F., Heinzmann, A.C.A., Dentener, M.A., Savelkoul, P.H.M., Wouters, E.F., Rohde, G.G., Stassen, F.R., 2016. Exposure to common respiratory bacteria alters the airway epithelial response to subsequent viral infection. *Respir. Res.* 17, 68. <https://doi.org/10.1186/s12931-016-0382-z>
- Bender, F.C., Whitbeck, J.C., Leon, M.P. de, Lou, H., Eisenberg, R.J., Cohen, G.H., 2003. Specific Association of Glycoprotein B with Lipid Rafts during Herpes Simplex Virus Entry. *J. Virol.*
- Bermejo-Martin, J.F., Garcia-Arevalo, M.C., Lejarazu, R.O.D., Ardura, J., Eiros, J.M., Alonso, A., Matías, V., Pino, M., Bernardo, D., Arranz, E., Blanco-Quiros, A., 2007. Predominance of Th2 cytokines, CXC chemokines and innate immunity mediators at the mucosal level during severe respiratory syncytial virus infection in children. *Eur. Cytokine Netw.* 18, 162–167. <https://doi.org/10.1684/ecn.2007.0096>
- Binns, E., Koenraads, M., Hristeva, L., Flamant, A., Baier-Grabner, S., Loi, M., Lempainen, J., Osterheld, E., Ramly, B., Chakakala-Chaziya, J., Enaganthi, N., Simó Nebot, S., Buonsenso, D., 2022. Influenza and respiratory syncytial virus during the COVID-19 pandemic: Time for a new paradigm? *Pediatr. Pulmonol.* 57, 38–42. <https://doi.org/10.1002/ppul.25719>
- Bohmwald, K., Gálvez, N.M.S., Canedo-Marroquín, G., Pizarro-Ortega, M.S., Andrade-Parra, C., Gómez-Santander, F., Kalergis, A.M., 2019. Contribution of Cytokines to Tissue Damage During Human Respiratory Syncytial Virus Infection. *Front. Immunol.* 10.
- Bolourani, S., Brenner, M., Wang, P., 2021. The interplay of DAMPs, TLR4, and proinflammatory cytokines in pulmonary fibrosis. *J. Mol. Med. Berl. Ger.* 99, 1373–1384. <https://doi.org/10.1007/s00109-021-02113-y>
- Bonnet, J., Durmort, C., Jacq, M., Mortier-Barrière, Campo, N., VanNieuwenhze, M., Brun, Y., Arthaud, C., Gallet, B., Moriscot, C., Morlot, C., Vernet, T., Di Guilmi, A., 2017. Peptidoglycan O-acetylation is functionally related to cell wall biosynthesis and cell division in *Streptococcus pneumoniae*. *Mol. Microbiol.* 106, 832–846. <https://doi.org/10.1111/mmi.13849>
- Bont, L., 2013. Why is RSV different from other viruses? *J. Med. Virol.* 85, 933–934. <https://doi.org/10.1002/jmv.23547>
- Bosch, A.A.T.M., Biesbroek, G., Trzcinski, K., Sanders, E.A.M., Bogaert, D., 2013. Viral and bacterial interactions in the upper respiratory tract. *PLoS Pathog.* 9, e1003057. <https://doi.org/10.1371/journal.ppat.1003057>
- Brealey, J.C., Chappell, K.J., Galbraith, S., Fantino, E., Gaydon, J., Tozer, S., Young, P.R., Holt, P.G., Sly, P.D., 2018. *Streptococcus pneumoniae* colonization of the nasopharynx is associated with increased severity during respiratory syncytial virus infection in young children. *Respirology* 23, 220–227. <https://doi.org/10.1111/resp.13179>

- Brealey, J.C., Sly, P.D., Young, P.R., Chappell, K.J., 2015. Viral bacterial co-infection of the respiratory tract during early childhood. *FEMS Microbiol. Lett.* 362. <https://doi.org/10.1093/femsle/fnv062>
- Broadbent, L., Coey, J.D., Shields, M.D., Power, U.F., 2018. The Role of Toll-like receptor 4 in respiratory syncytial virus replication, interferon lambda 1 induction, and chemokine responses. *bioRxiv* 404384. <https://doi.org/10.1101/404384>
- Broadbent, L., Manzoor, S., Zarccone, M.C., Barabas, J., Shields, M.D., Saglani, S., Lloyd, C.M., Bush, A., Custovic, A., Ghazal, P., Gore, M., Marsland, B., Roberts, G., Schwarze, J., Turner, S., Power, U.F., 2020. Comparative primary paediatric nasal epithelial cell culture differentiation and RSV-induced cytopathogenesis following culture in two commercial media. *PLOS ONE* 15, e0228229. <https://doi.org/10.1371/journal.pone.0228229>
- Brooks, L.R.K., Mias, G.I., 2018. *Streptococcus pneumoniae's* Virulence and Host Immunity: Aging, Diagnostics, and Prevention. *Front. Immunol.* 9, 1366. <https://doi.org/10.3389/fimmu.2018.01366>
- Brown, D.A., London, E., 1998. Structure and Origin of Ordered Lipid Domains in Biological Membranes. *J. Membr. Biol.* 164, 103–114. <https://doi.org/10.1007/s002329900397>
- Brown, D.A., Rose, J.K., 1992. Sorting of GPI-anchored proteins to glycolipid-enriched membrane subdomains during transport to the apical cell surface. *Cell* 68, 533–544. [https://doi.org/10.1016/0092-8674\(92\)90189-J](https://doi.org/10.1016/0092-8674(92)90189-J)
- Brown, G., Jeffree, C.E., McDonald, T., McL. Rixon, H.W., Aitken, J.D., Sugrue, R.J., 2004. Analysis of the interaction between respiratory syncytial virus and lipid-rafts in Hep2 cells during infection. *Virology* 327, 175–185. <https://doi.org/10.1016/j.virol.2004.06.038>
- Brügger, B., Glass, B., Haberkant, P., Leibrecht, I., Wieland, F.T., Kräusslich, H.-G., 2006. The HIV lipidome: A raft with an unusual composition. *Proc. Natl. Acad. Sci.* 103, 2641–2646. <https://doi.org/10.1073/pnas.0511136103>
- Brügger, B., Krautkrämer, E., Tibroni, N., Munte, C.E., Rauch, S., Leibrecht, I., Glass, B., Breuer, S., Geyer, M., Kräusslich, H.-G., Kalbitzer, H.R., Wieland, F.T., Fackler, O.T., 2007. Human Immunodeficiency Virus Type 1 Nef protein modulates the lipid composition of virions and host cell membrane microdomains. *Retrovirology* 4, 70. <https://doi.org/10.1186/1742-4690-4-70>
- Budnitz, D.S., Pollock, D.A., Weidenbach, K.N., Mendelsohn, A.B., Schroeder, T.J., Annett, J.L., 2006. National Surveillance of Emergency Department Visits for Outpatient Adverse Drug Events. *JAMA* 296, 1858–1866. <https://doi.org/10.1001/jama.296.15.1858> %J JAMA
- Bukowy-Bieryłło, Z., 2021. Long-term differentiating primary human airway epithelial cell cultures: how far are we? *Cell Commun. Signal.* 19, 63. <https://doi.org/10.1186/s12964-021-00740-z>
- Bukreyev, A., Yang, L., Collins, P.L., 2012. The Secreted G Protein of Human Respiratory Syncytial Virus Antagonizes Antibody-Mediated Restriction of Replication Involving Macrophages and Complement. *J. Virol.* 86, 10880–10884. <https://doi.org/10.1128/JVI.01162-12>
- Bukreyev, A., Yang, L., Fricke, J., Cheng, L., Ward, J.M., Murphy, B.R., Collins, P.L., 2008. The Secreted Form of Respiratory Syncytial Virus G Glycoprotein Helps the Virus Evade Antibody-Mediated Restriction of Replication by Acting as an Antigen Decoy and through Effects on Fc Receptor-Bearing Leukocytes. *J. Virol.* <https://doi.org/10.1128/JVI.01604-08>
- Bukrinsky, M.I., Mukhamedova, N., Sviridov, D., 2020. Lipid rafts and pathogens: the art of deception and exploitation: Thematic Review Series: Biology of Lipid Rafts. *J. Lipid Res.* 61, 601–610. <https://doi.org/10.1194/jlr.TR119000391>
- Caballero, M.T., Serra, M.E., Acosta, P.L., Marzec, J., Gibbons, L., Salim, M., Rodriguez, A., Reynaldi, A., Garcia, A., Bado, D., Buchholz, U.J., Hijano, D.R., Coviello, S., Newcomb, D., Bellabarba, M., Ferolla, F.M., Libster, R., Berenstein, A., Siniawski, S., Blumetti, V., Echavarría, M., Pinto, L., Lawrence, A., Ossorio, M.F., Grosman, A.,

- Mateu, C.G., Bayle, C., Dericco, A., Pellegrini, M., Igarza, I., Repetto, H.A., Grimaldi, L.A., Gudapati, P., Polack, N.R., Althabe, F., Shi, M., Ferrero, F., Bergel, E., Stein, R.T., Peebles, R.S., Boothby, M., Kleeberger, S.R., Polack, F.P., 2015. TLR4 genotype and environmental LPS mediate RSV bronchiolitis through Th2 polarization. *J. Clin. Invest.* 125, 571–582. <https://doi.org/10.1172/JCI75183>
- Carter, G.C., Bernstone, L., Sangani, D., Bee, J.W., Harder, T., James, W., 2009. HIV entry in macrophages is dependent on intact lipid rafts. *Virology* 386, 192–202. <https://doi.org/10.1016/j.virol.2008.12.031>
- Chang, T.H., Segovia, J., Sabbah, A., Mgbemena, V., Bose, S., 2012. Cholesterol-rich lipid rafts are required for release of infectious human respiratory syncytial virus particles. *Virology* 422, 205–13. <https://doi.org/10.1016/j.virol.2011.10.029>
- Charlton, F.W., Hover, S., Fuller, J., Hewson, R., Fontana, J., Barr, J.N., Mankouri, J., 2019. Cellular cholesterol abundance regulates potassium accumulation within endosomes and is an important determinant in bunyavirus entry. *J. Biol. Chem.* 294, 7335–7347. <https://doi.org/10.1074/jbc.RA119.007618>
- Chazal, N., Gerlier, D., 2003. Virus Entry, Assembly, Budding, and Membrane Rafts. *Microbiol. Mol. Biol. Rev.* 67, 226–237. <https://doi.org/10.1128/MMBR.67.2.226-237.2003>
- Chen, M., Pan, H., Dai, Y., Zhang, J., Tong, Y., Huang, Y., Wang, M., Huang, H., 2018. Phosphatidylcholine regulates NF- κ B activation in attenuation of LPS-induced inflammation: evidence from in vitro study. *Anim. Cells Syst.* 22, 7–14. <https://doi.org/10.1080/19768354.2017.1405072>
- Cilla, G., Oñate, E., Perez-Yarza, E.G., Montes, M., Vicente, D., Perez-Trallero, E., 2008. Viruses in community-acquired pneumonia in children aged less than 3 years old: High rate of viral coinfection. *J. Med. Virol.* 80, 1843–1849. <https://doi.org/10.1002/jmv.21271>
- Collins, P.L., Fearn, R., Graham, B.S., 2013. Respiratory Syncytial Virus: Virology, Reverse Genetics, and Pathogenesis of Disease. *Curr. Top. Microbiol. Immunol.* 372, 3–38. https://doi.org/10.1007/978-3-642-38919-1_1
- Connelly, A.R., Jeong, B.M., Coden, M.E., Cao, J.Y., Chirkova, T., Rosas-Salazar, C., Cephus, J.-Y., Anderson, L.J., Newcomb, D.C., Hartert, T.V., Berdnikovs, S., 2021. Metabolic Reprogramming of Nasal Airway Epithelial Cells Following Infant Respiratory Syncytial Virus Infection. *Viruses* 13, 2055. <https://doi.org/10.3390/v13102055>
- Cormier, S.A., Shrestha, B., Saravia, J., Lee, G.I., Shen, L., DeVincenzo, J.P., Kim, Y., You, D., 2014. Limited Type I Interferons and Plasmacytoid Dendritic Cells during Neonatal Respiratory Syncytial Virus Infection Permit Immunopathogenesis upon Reinfection. *J. Virol.* 88, 9350–9360. <https://doi.org/10.1128/JVI.00818-14>
- Coultas, J.A., Smyth, R., Openshaw, P.J., 2019. Respiratory syncytial virus (RSV): a scourge from infancy to old age. *Thorax* 74, 986–993. <https://doi.org/10.1136/thoraxjnl-2018-212212>
- Cromer, D., van Hoek, A.J., Newall, A.T., Pollard, A.J., Jit, M., 2017. Burden of paediatric respiratory syncytial virus disease and potential effect of different immunisation strategies: a modelling and cost-effectiveness analysis for England. *Lancet Public Health* 2, e367–e374. [https://doi.org/10.1016/S2468-2667\(17\)30103-2](https://doi.org/10.1016/S2468-2667(17)30103-2)
- Culley, F.J., Pennycook, A.M.J., Tregoning, J.S., Dodd, J.S., Walzl, G., Wells, T.N., Hussell, T., Openshaw, P.J.M., 2006. Role of CCL5 (RANTES) in viral lung disease. *J. Virol.* 80, 8151–8157. <https://doi.org/10.1128/jvi.00496-06>
- Culley, F.J., Pollott, J., Openshaw, P.J.M., 2002. Age at First Viral Infection Determines the Pattern of T Cell-mediated Disease during Reinfection in Adulthood. *J. Exp. Med.* 196, 1381–1386. <https://doi.org/10.1084/jem.20020943>
- Czerkies, M., Korwek, Z., Prus, W., Kocharczyk, M., Jaruszewicz-Błońska, J., Tudelska, K., Błoński, S., Kimmel, M., Brasier, A.R., Lipniacki, T., 2018. Cell fate in antiviral response arises in the crosstalk of IRF, NF- κ B and JAK/STAT pathways. *Nat. Commun.* 9, 493. <https://doi.org/10.1038/s41467-017-02640-8>

- Danino, D., Ben-Shimol, S., van der Beek, B.A., Givon-Lavi, N., Avni, Y.S., Greenberg, D., Weinberger, D.M., Dagan, R., 2021. Decline in Pneumococcal Disease in Young Children During the Coronavirus Disease 2019 (COVID-19) Pandemic in Israel Associated With Suppression of Seasonal Respiratory Viruses, Despite Persistent Pneumococcal Carriage: A Prospective Cohort Study. *Clin. Infect. Dis.* ciab1014. <https://doi.org/10.1093/cid/ciab1014>
- de Bree, G.J., Heidema, J., van Leeuwen, E.M.M., van Bleek, G.M., Jonkers, R.E., Jansen, H.M., van Lier, R.A.W., Out, T.A., 2005. Respiratory Syncytial Virus—Specific CD8+ Memory T Cell Responses in Elderly Persons. *J. Infect. Dis.* 191, 1710–1718. <https://doi.org/10.1086/429695>
- de Steenhuijsen Pitters, W.A.A., Sanders, E.A.M., Bogaert, D., 2015. The role of the local microbial ecosystem in respiratory health and disease. *Philos. Trans. R. Soc. B Biol. Sci.* 370. <https://doi.org/10.1098/rstb.2014.0294>
- Delgado, M.F., Coviello, S., Monsalvo, A.C., Melendi, G.A., Hernandez, J.Z., Batalle, J.P., Diaz, L., Trento, A., Chang, H.-Y., Mitzner, W., Ravetch, J., Melero, J.A., Irusta, P.M., Polack, F.P., 2009. Lack of antibody affinity maturation due to poor Toll-like receptor stimulation leads to enhanced respiratory syncytial virus disease. *Nat. Med.* 15, 34–41. <https://doi.org/10.1038/nm.1894>
- Deng, J., 2013. Viral–bacterial interactions—therapeutic implications. *Influenza Other Respir. Viruses* 7, 24–35.
- Ding, L., Derdowski, A., Wang, J.-J., Spearman, P., 2003. Independent Segregation of Human Immunodeficiency Virus Type 1 Gag Protein Complexes and Lipid Rafts. *J. Virol.* <https://doi.org/10.1128/JVI.77.3.1916-1926.2003>
- Domingues, M.M., Inácio, R.G., Raimundo, J.M., Martins, M., Castanho, M.A.R.B., Santos, N.C., 2012. Biophysical characterization of polymyxin b interaction with LPS aggregates and membrane model systems. *Pept. Sci.* 98, 338–344. <https://doi.org/10.1002/bip.22095>
- Dreschers, S., Franz, P., Dumitru, C., Wilker, B., Jahnke, K., Gulbins, E., 2007. Infections with Human Rhinovirus Induce the Formation of Distinct Functional Membrane Domains. *Cell. Physiol. Biochem.* 20, 241–254. <https://doi.org/10.1159/000104170>
- Duttweiler, L., Nadal, D., Frey, B., 2004. Pulmonary and systemic bacterial co-infections in severe RSV bronchiolitis. *Arch. Dis. Child.* 89, 1155–1157. <https://doi.org/10.1136/adc.2004.049551>
- Edwards, M.R., Facchinetti, F., Civelli, M., Villetti, G., Johnston, S.L., 2016. Anti-inflammatory effects of the novel inhaled phosphodiesterase type 4 inhibitor CHF6001 on virus-inducible cytokines. *Pharmacol. Res. Perspect.* 4, e00202. <https://doi.org/10.1002/prp2.202>
- Eggeling, C., Ringemann, C., Medda, R., Schwarzmann, G., Sandhoff, K., Polyakova, S., Belov, V.N., Hein, B., von Middendorff, C., Schönle, A., Hell, S.W., 2009. Direct observation of the nanoscale dynamics of membrane lipids in a living cell. *Nature* 457, 1159–1162. <https://doi.org/10.1038/nature07596>
- Eiland, L.S., 2009. Respiratory Syncytial Virus: Diagnosis, Treatment and Prevention. *J. Pediatr. Pharmacol. Ther.* JPPT 14, 75–85. <https://doi.org/10.5863/1551-6776-14.2.75>
- Elahmer, O.R., Raza, M.W., Ogilvie, M.M., Blackwell, C.C., Weir, D.M., Elton, R.A., 1996. The Effect of Respiratory Virus Infection on Expression of Cell Surface Antigens Associated with Binding of Potentially Pathogenic Bacteria, in: Kahane, I., Ofek, I. (Eds.), *Toward Anti-Adhesion Therapy for Microbial Diseases*. Springer US, Boston, MA, pp. 169–177. https://doi.org/10.1007/978-1-4613-0415-9_19
- Empig, C.J., Goldsmith, M.A., 2002. Association of the Caveola Vesicular System with Cellular Entry by Filoviruses. *J. Virol.* <https://doi.org/10.1128/JVI.76.10.5266-5270.2002>
- Fabbrini, M., Sammiceli, C., Margarit, I., Maione, D., Grandi, G., Giuliani, M.M., Mori, E., Nuti, S., 2012. A new flow-cytometry-based opsonophagocytosis assay for the rapid

- measurement of functional antibody levels against Group B Streptococcus. *J. Immunol. Methods* 378, 11–19. <https://doi.org/10.1016/j.jim.2012.01.011>
- Falsey, A.R., Hennessey, P.A., Formica, M.A., Cox, C., Walsh, E.E., 2009. Respiratory Syncytial Virus Infection in Elderly and High-Risk Adults [WWW Document]. <http://dx.doi.org/10.1056/NEJMoa043951>. <https://doi.org/10.1056/NEJMoa043951>
- Falsey, A.R., Walsh, E.E., 2005. Respiratory Syncytial Virus Infection in Elderly Adults. *Drugs Aging* 22, 577–587. <https://doi.org/10.2165/00002512-200522070-00004>
- Feng, Z., Xu, L., Xie, Z., 2022. Receptors for Respiratory Syncytial Virus Infection and Host Factors Regulating the Life Cycle of Respiratory Syncytial Virus. *Front. Cell. Infect. Microbiol.* 12, 858629. <https://doi.org/10.3389/fcimb.2022.858629>
- Ferreira Lopes, S., Vacher, G., Ciarlo, E., Savova-Bianchi, D., Roger, T., Niculita-Hirzel, H., 2017. Primary and Immortalized Human Respiratory Cells Display Different Patterns of Cytotoxicity and Cytokine Release upon Exposure to Deoxynivalenol, Nivalenol and Fusarenon-X. *Toxins* 9, 337. <https://doi.org/10.3390/toxins9110337>
- Fessler, M.B., Parks, J.S., 2011. Intracellular lipid flux and membrane microdomains as organizing principles in inflammatory cell signaling. *J. Immunol. Baltim. Md* 1950 187, 1529–1535. <https://doi.org/10.4049/jimmunol.1100253>
- Fitzgerald, K.A., Rowe, D.C., Barnes, B.J., Caffrey, D.R., Visintin, A., Latz, E., Monks, B., Pitha, P.M., Golenbock, D.T., 2003. LPS-TLR4 Signaling to IRF-3/7 and NF- κ B Involves the Toll Adapters TRAM and TRIF. *J. Exp. Med.* 198, 1043–1055. <https://doi.org/10.1084/jem.20031023>
- Fonceca, A.M., Flanagan, B.F., Trinick, R., Smyth, R.L., McNamara, P.S., 2012. Primary airway epithelial cultures from children are highly permissive to respiratory syncytial virus infection. *Thorax* 67, 42–48. <https://doi.org/10.1136/thoraxjnl-2011-200131>
- Foronjy, R.F., Ochieng, P.O., Salathe, M.A., Dabo, A.J., Eden, E., Baumlin, N., Cummins, N., Barik, S., Campos, M., Thorp, E.B., Geraghty, P., 2016. Protein tyrosine phosphatase 1B negatively regulates S100A9-mediated lung damage during respiratory syncytial virus exacerbations. *Mucosal Immunol.* 9, 1317–1329. <https://doi.org/10.1038/mi.2015.138>
- Fulginiti, V.A., Eller, J.J., Sieber, O.F., Joyner, J.W., Minamitani, M., Meiklejohn, G., 1969. Respiratory virus immunization: A field trial of two inactivated respiratory virus vaccines; an aqueous trivalent parainfluenza virus vaccine and an alum-precipitated respiratory syncytial virus vaccine1. *Am. J. Epidemiol.* 89, 435–448. <https://doi.org/10.1093/oxfordjournals.aje.a120956>
- Gajate, C., Mollinedo, F., 2006. Edelfosine and perifosine induce selective apoptosis in multiple myeloma by recruitment of death receptors and downstream signaling molecules into lipid rafts. *Blood* 109, 711–719. <https://doi.org/10.1182/blood-2006-04-016824>
- Ganaie, F., Saad, J.S., McGee, L., Tonder, A.J. van, Bentley, S.D., Lo, S.W., Gladstone, R.A., Turner, P., Keenan, J.D., Breiman, R.F., Nahm, M.H., 2020. A New Pneumococcal Capsule Type, 10D, is the 100th Serotype and Has a Large cps Fragment from an Oral Streptococcus. *mBio*. <https://doi.org/10.1128/mBio.00937-20>
- Gao, Z., Kang, Y., Yu, J., Ren, L., 2014. Human pharyngeal microbiome may play a protective role in respiratory tract infections. *Genomics Proteomics Bioinformatics* 12, 144–150. <https://doi.org/10.1016/j.gpb.2014.06.001>
- Glaser, L., Coulter, P.J., Shields, M., Touzelet, O., Power, U.F., Broadbent, L., 2019. Airway Epithelial Derived Cytokines and Chemokines and Their Role in the Immune Response to Respiratory Syncytial Virus Infection. *Pathogens* 8, 106. <https://doi.org/10.3390/pathogens8030106>
- GlaxoSmithKline, 2021. A Phase 3, Randomized, Open-label, Multi-country Study to Evaluate the Immunogenicity, Safety, Reactogenicity and Persistence of a Single Dose of the RSVPreF3 OA Investigational Vaccine and Different Revaccination Schedules in Adults Aged 60 Years and Above (Clinical trial registration No. NCT04732871). clinicaltrials.gov.

- Godefroy, R., Giraud-gatineau, A., Jimeno, M.-T., Edouard, S., Meddeb, L., Zandotti, C., Chaudet, H., Colson, P., Raoult, D., Cassir, N., 2020. Respiratory Syncytial Virus Infection: Its Propensity for Bacterial Coinfection and Related Mortality in Elderly Adults. *Open Forum Infect. Dis.* 7. <https://doi.org/10.1093/ofid/ofaa546>
- Gong, T., Liu, L., Jiang, W., Zhou, R., 2020. DAMP-sensing receptors in sterile inflammation and inflammatory diseases. *Nat. Rev. Immunol.* 20, 95–112. <https://doi.org/10.1038/s41577-019-0215-7>
- Goritzka, M., Pereira, C., Makris, S., Durant, L.R., Johansson, C., 2015. T cell responses are elicited against Respiratory Syncytial Virus in the absence of signalling through TLRs, RLRs and IL-1R/IL-18R. *Sci. Rep.* 5, 18533. <https://doi.org/10.1038/srep18533>
- Grassmé, H., Riehle, A., Wilker, B., Gulbins, E., 2005. Rhinoviruses Infect Human Epithelial Cells via Ceramide-enriched Membrane Platforms*. *J. Biol. Chem.* 280, 26256–26262. <https://doi.org/10.1074/jbc.M500835200>
- Greenberg, D., Givon-Lavi, N., Faingelernt, Y., Ben-Shimol, S., Avni, Y.S., Bar-Ziv, J., Dagan, R., 2017. Nasopharyngeal Pneumococcal Carriage During Childhood Community-Acquired Alveolar Pneumonia: Relationship Between Specific Serotypes and Coinfecting Viruses. *J. Infect. Dis.* 215, 1111–1116. <https://doi.org/10.1093/infdis/jiw613>
- Griffin, M.P., Yuan, Y., Takas, T., Domachowske, J.B., Madhi, S.A., Manzoni, P., Simões, E.A.F., Esser, M.T., Khan, A.A., Dubovsky, F., Villafana, T., DeVincenzo, J.P., 2020. Single-Dose Nirsevimab for Prevention of RSV in Preterm Infants. *N. Engl. J. Med.* 383, 415–425. <https://doi.org/10.1056/NEJMoa1913556>
- Griffiths, C., Drews, S.J., Marchant, D.J., 2017. Respiratory Syncytial Virus: Infection, Detection, and New Options for Prevention and Treatment. *Clin. Microbiol. Rev.* 30, 277–319. <https://doi.org/10.1128/CMR.00010-16>
- Gulraiz, F., Rellinghausen, C., Bruggeman, C.A., Stassen, F.R., 2015. Haemophilus influenzae increases the susceptibility and inflammatory response of airway epithelial cells to viral infections. *FASEB J.* 29, 849–858. <https://doi.org/10.1096/fj.14-254359>
- Habibi, M.S., Thwaites, R.S., Chang, M., Jozwik, A., Paras, A., Kirsebom, F., Varese, A., Owen, A., Cuthbertson, L., James, P., Tunstall, T., Nickle, D., Hansel, T.T., Moffatt, M.F., Johansson, C., Chiu, C., Openshaw, P.J.M., 2020. Neutrophilic inflammation in the respiratory mucosa predisposes to RSV infection. *Science*. <https://doi.org/10.1126/science.aba9301>
- Halfhide, C.P., Brearey, S.P., Flanagan, B.F., Hunt, J.A., Howarth, D., Cummerson, J., Edwards, S., Hart, C.A., Smyth, R.L., 2009. Neutrophil TLR4 expression is reduced in the airways of infants with severe bronchiolitis. *Thorax* 64, 798–805. <https://doi.org/10.1136/thx.2008.107821>
- Hament, J.-M., Aerts, P.C., Flier, A., Van Dijk, H., Harmsen, T., Kimpen, J.L., Wolfs, T.F. %J P. research, 2004. Enhanced adherence of Streptococcus pneumoniae to human epithelial cells infected with respiratory syncytial virus 55, 972.
- Hament, J.-M., Aerts, P.C., Flier, A., van Dijk, H., Harmsen, T., Kimpen, J.L.L., Wolfs, T.F.W., 2005. Direct Binding of Respiratory Syncytial Virus to Pneumococci: A Phenomenon That Enhances Both Pneumococcal Adherence to Human Epithelial Cells and Pneumococcal Invasiveness in a Murine Model. *Pediatr. Res.* 58, 1198–1203. <https://doi.org/10.1203/01.pdr.0000188699.55279.1b>
- Hammerschmidt, S., Wolff, S., Hocke, A., Rosseau, S., Müller, E., Rohde, M., 2005. Illustration of Pneumococcal Polysaccharide Capsule during Adherence and Invasion of Epithelial Cells. *Infect. Immun.* <https://doi.org/10.1128/IAI.73.8.4653-4667.2005>
- Han, X., Na, T., Wu, T., Yuan, B.-Z., 2020. Human lung epithelial BEAS-2B cells exhibit characteristics of mesenchymal stem cells. *PLOS ONE* 15, e0227174. <https://doi.org/10.1371/journal.pone.0227174>
- Harcourt, J., Alvarez, R., Jones, L.P., Henderson, C., Anderson, L.J., Tripp, R.A., 2006. Respiratory Syncytial Virus G Protein and G Protein CX3C Motif Adversely Affect CX3CR1+ T Cell Responses. *J. Immunol.* 176, 1600–1608. <https://doi.org/10.4049/jimmunol.176.3.1600>

- Hay, A.D., Tilling, K., 2014. Can 88% of patients with acute lower respiratory infection all be special? *Br. J. Gen. Pract.* <https://doi.org/10.3399/bjgp14X676636>
- Haynes, L.M., Moore, D.D., Kurt-Jones, E.A., Finberg, R.W., Anderson, L.J., Tripp, R.A., 2001. Involvement of toll-like receptor 4 in innate immunity to respiratory syncytial virus. *J. Virol.* 75, 10730–10737.
- Head, B.P., Patel, H.H., Insel, P.A., 2014. Interaction of membrane/lipid rafts with the cytoskeleton: impact on signaling and function. *Biochim. Biophys. Acta* 1838, 10.1016/j.bbamem.2013.07.018. <https://doi.org/10.1016/j.bbamem.2013.07.018>
- Heaton, N.S., Randall, G., 2010. Dengue Virus-Induced Autophagy Regulates Lipid Metabolism. *Cell Host Microbe* 8, 422–432. <https://doi.org/10.1016/j.chom.2010.10.006>
- Hendricks, M.R., Lashua, L.P., Fischer, D.K., Flitter, B.A., Eichinger, K.M., Durbin, J.E., Sarkar, S.N., Coyne, C.B., Empey, K.M., Bomberger, J.M., 2016. Respiratory syncytial virus infection enhances *Pseudomonas aeruginosa* biofilm growth through dysregulation of nutritional immunity. *Proc. Natl. Acad. Sci.* 113, 1642–1647.
- Henson, P.M., Bratton, D.L., 2013. Antiinflammatory effects of apoptotic cells. *J. Clin. Invest.* 123, 2773–2774. <https://doi.org/10.1172/JCI69344>
- Hicks, D., Nalivaeva, N., Turner, A., 2012. Lipid Rafts and Alzheimer's Disease: Protein-Lipid Interactions and Perturbation of Signaling. *Front. Physiol.* 3.
- Hiemstra, P.S., 2001. Epithelial antimicrobial peptides and proteins: their role in host defence and inflammation. *Paediatr. Respir. Rev.* 2, 306–310. <https://doi.org/10.1053/prrv.2001.0165>
- Hillyer, P., Shepard, R., Uehling, M., Krenz, M., Sheikh, F., Thayer, K.R., Huang, L., Yan, L., Panda, D., Luongo, C., Buchholz, U.J., Collins, P.L., Donnelly, R.P., Rabin, R.L., 2018. Differential Responses by Human Respiratory Epithelial Cell Lines to Respiratory Syncytial Virus Reflect Distinct Patterns of Infection Control. *J. Virol.* 92. <https://doi.org/10.1128/JVI.02202-17>
- Homaira, N., Briggs, N., Pardy, C., Hanly, M., Oei, J.-L., Hilder, L., Bajuk, B., Lui, K., Rawlinson, W., Snelling, T., Jaffe, A., 2017. Association between respiratory syncytial viral disease and the subsequent risk of the first episode of severe asthma in different subgroups of high-risk Australian children: a whole-of-population-based cohort study. *BMJ Open* 7. <https://doi.org/10.1136/bmjopen-2017-017936>
- Honkinen, M., Lahti, E., Österback, R., Ruuskanen, O., Waris, M., 2012. Viruses and bacteria in sputum samples of children with community-acquired pneumonia. *Clin. Microbiol. Infect.* 18, 300–307. <https://doi.org/10.1111/j.1469-0691.2011.03603.x>
- Hornef, M.W., Normark, B.H., Vandewalle, A., Normark, S., 2003. Intracellular Recognition of Lipopolysaccharide by Toll-like Receptor 4 in Intestinal Epithelial Cells. *J. Exp. Med.* 198, 1225–1235. <https://doi.org/10.1084/jem.20022194>
- Hosakote, Y.M., Brasier, A.R., Casola, A., Garofalo, R.P., Kurosky, A., 2016. Respiratory Syncytial Virus Infection Triggers Epithelial HMGB1 Release as a Damage-Associated Molecular Pattern Promoting a Monocytic Inflammatory Response. *J. Virol.* 90, 9618–9631. <https://doi.org/10.1128/JVI.01279-16>
- Hueber, A.O., 2003. Role of membrane microdomain rafts in TNFR-mediated signal transduction. *Cell Death Differ.* 10, 7–9. <https://doi.org/10.1038/sj.cdd.4401155>
- Hussain, G., Wang, J., Rasul, A., Anwar, H., Imran, A., Qasim, M., Zafar, S., Kamran, S.K.S., Razzaq, A., Aziz, N., Ahmad, W., Shabbir, A., Iqbal, J., Baig, S.M., Sun, T., 2019. Role of cholesterol and sphingolipids in brain development and neurological diseases. *Lipids Health Dis.* 18, 26. <https://doi.org/10.1186/s12944-019-0965-z>
- Ichinohe, T., Pang, I.K., Kumamoto, Y., Peaper, D.R., Ho, J.H., Murray, T.S., Iwasaki, A., 2011. Microbiota regulates immune defense against respiratory tract influenza A virus infection. *Proc. Natl. Acad. Sci.* 108, 5354–5359. <https://doi.org/10.1073/pnas.1019378108>
- Ioannidis, I., Ye, F., McNally, B., Willette, M., Flaño, E., 2013. Toll-Like Receptor Expression and Induction of Type I and Type III Interferons in Primary Airway Epithelial Cells. *J. Virol.* 87, 3261–3270. <https://doi.org/10.1128/JVI.01956-12>

- Iša, P., Realpe, M., Romero, P., López, S., Arias, C.F., 2004. Rotavirus RRV associates with lipid membrane microdomains during cell entry. *Virology* 322, 370–381. <https://doi.org/10.1016/j.virol.2004.02.018>
- Iverson, A.R., Boyd, K.L., McAuley, J.L., Plano, L.R., Hart, M.E., McCullers, J.A., 2011. Influenza Virus Primes Mice for Pneumonia From *Staphylococcus aureus*. *J. Infect. Dis.* 203, 880–888. <https://doi.org/10.1093/infdis/jiq113>
- Jackson, D.J., Gern, J.E., Lemanske, R.F., 2016. The contributions of allergic sensitization and respiratory pathogens to asthma inception. *J. Allergy Clin. Immunol.* 137, 659–665; quiz 666. <https://doi.org/10.1016/j.jaci.2016.01.002>
- Janssen Vaccines & Prevention B.V., 2022. A Randomized, Double-blind, Placebo-controlled Phase 3 Efficacy Study of an Ad26.RSV.preF-based Vaccine in the Prevention of Lower Respiratory Tract Disease Caused by RSV in Adults Aged 60 Years and Older (Clinical trial registration No. NCT04908683). clinicaltrials.gov.
- Jessie, B., Dobrovolny, H.M., 2021. The role of syncytia during viral infections. *J. Theor. Biol.* 525, 110749. <https://doi.org/10.1016/j.jtbi.2021.110749>
- Ji, J., Sun, L., Luo, Z., Zhang, Y., Xianzheng, W., Liao, Y., Tong, X., Shan, J., 2021. Potential Therapeutic Applications of Pulmonary Surfactant Lipids in the Host Defence Against Respiratory Viral Infections. *Front. Immunol.* 12, 730022. <https://doi.org/10.3389/fimmu.2021.730022>
- Johnston, S.L., Goldblatt, D.L., Evans, S.E., Tuvim, M.J., Dickey, B.F., 2021. Airway Epithelial Innate Immunity. *Front. Physiol.* 12.
- Jozwik, A., Habibi, M.S., Paras, A., Zhu, J., Guvenel, A., Dhariwal, J., Almond, M., Wong, E.H.C., Sykes, A., Maybeno, M., Del Rosario, J., Trujillo-Torralbo, M.-B., Mallia, P., Sidney, J., Peters, B., Kon, O.M., Sette, A., Johnston, S.L., Openshaw, P.J., Chiu, C., 2015. RSV-specific airway resident memory CD8+ T cells and differential disease severity after experimental human infection. *Nat. Commun.* 6, 10224. <https://doi.org/10.1038/ncomms10224>
- Jubrail, J., Morris, P., Bewley, M.A., Stoneham, S., Johnston, S.A., Foster, S.J., Peden, A.A., Read, R.C., Marriott, H.M., Dockrell, D.H., 2016. Inability to sustain intraphagolysosomal killing of *Staphylococcus aureus* predisposes to bacterial persistence in macrophages. *Cell. Microbiol.* 18, 80–96. <https://doi.org/10.1111/cmi.12485>
- Jumat, M.R., Nguyen Huong, T., Wong, P., Loo, L.H., Tan, B.H., Fenwick, F., Toms, G.L., Sugrue, R.J., 2014. Imaging analysis of human metapneumovirus-infected cells provides evidence for the involvement of F-actin and the raft-lipid microdomains in virus morphogenesis. *Virology* 484, 395–411. <https://doi.org/10.1016/j.virol.2015.05.014>
- Jumat, M.R., Yan, Y., Ravi, L.I., Wong, P., Huong, T.N., Li, C., Tan, B.H., Wang, D.Y., Sugrue, R.J., 2015. Morphogenesis of respiratory syncytial virus in human primary nasal ciliated epithelial cells occurs at surface membrane microdomains that are distinct from cilia. *Virology* 484, 395–411. <https://doi.org/10.1016/j.virol.2015.05.014>
- Jung, J., Seo, E., Yoo, R.N., Sung, H., Lee, J., 2020. Clinical significance of viral–bacterial codetection among young children with respiratory tract infections: Findings of RSV, influenza, adenoviral infections. *Medicine (Baltimore)* 99, e18504. <https://doi.org/10.1097/MD.00000000000018504>
- Juvé, T., Mertsola, J., Waris, M., Leinonen, M., Meurman, O., Roivainen, M., Eskola, J., Saikku, P., Ruuskanen, O., 2000. Etiology of community-acquired pneumonia in 254 hospitalized children. *Pediatr. Infect. Dis. J.* 19, 293–298.
- Kaisani, A., Delgado, O., Fasciani, G., Kim, S.B., Wright, W.E., Minna, J.D., Shay, J.W., 2014. Branching Morphogenesis of Immortalized Human Bronchial Epithelial Cells in Three-Dimensional Culture. *Differ. Res. Biol. Divers.* 87, 119–126. <https://doi.org/10.1016/j.diff.2014.02.003>
- Kaiser, H.-J., Lingwood, D., Levental, I., Sampaio, J.L., Kalvodova, L., Rajendran, L., Simons, K., 2009. Order of lipid phases in model and plasma membranes. *Proc. Natl. Acad. Sci.* 106, 16645–16650. <https://doi.org/10.1073/pnas.0908987106>

- Kalinowski, A., Galen, B.T., Ueki, I.F., Sun, Y., Mulenios, A., Osafo-Addo, A., Clark, B., Joerns, J., Liu, W., Nadel, J.A., Dela Cruz, C.S., Koff, J.L., 2018. Respiratory syncytial virus activates epidermal growth factor receptor to suppress interferon regulatory factor 1-dependent interferon-lambda and antiviral defense in airway epithelium. *Mucosal Immunol.* 11, 958–967. <https://doi.org/10.1038/mi.2017.120>
- Kandasamy, P., Numata, M., Berry, K.Z., Fickes, R., Leslie, C.C., Murphy, R.C., Voelker, D.R., 2016. Structural analogs of pulmonary surfactant phosphatidylglycerol inhibit toll-like receptor 2 and 4 signaling. *J. Lipid Res.* 57, 993–1005. <https://doi.org/10.1194/jlr.M065201>
- Karnati, S., Garikapati, V., Liebisch, G., Van Veldhoven, P.P., Spengler, B., Schmitz, G., Baumgart-Vogt, E., 2018. Quantitative lipidomic analysis of mouse lung during postnatal development by electrospray ionization tandem mass spectrometry. *PLoS ONE* 13, e0203464. <https://doi.org/10.1371/journal.pone.0203464>
- Katagiri, Y.U., Kiyokawa, N., Fujimoto, J., 2001. A Role for Lipid Rafts in Immune Cell Signaling. *Microbiol. Immunol.* 45, 1–8. <https://doi.org/10.1111/j.1348-0421.2001.tb01259.x>
- Kawai, T., Akira, S., 2010. The role of pattern-recognition receptors in innate immunity: update on Toll-like receptors. *Nat. Immunol.* 11, 373–384. <https://doi.org/10.1038/ni.1863>
- Kawasaki, K., Ohnishi, S., 1992. Membrane fusion of influenza virus with phosphatidylcholine liposomes containing viral receptors. *Biochem. Biophys. Res. Commun.* 186, 378–384. [https://doi.org/10.1016/S0006-291X\(05\)80818-6](https://doi.org/10.1016/S0006-291X(05)80818-6)
- Ke, Y., Zebda, N., Oskokova, O., Afonyushkin, T., Berdyshev, E., Tian, Y., Meng, F., Sarich, N., Bochkov, V.N., Wang, J.M., Birukova, A.A., Birukov, K.G., 2017. Anti-Inflammatory Effects of OxPAPC Involve Endothelial Cell Mediated Generation of LXA4. *Circ. Res.* 121, 244–257. <https://doi.org/10.1161/CIRCRESAHA.116.310308>
- Ke, Z., Dillard, R.S., Chirkova, T., Leon, F., Stobart, C.C., Hampton, C.M., Strauss, J.D., Rajan, D., Rostad, C.A., Taylor, J.V., Yi, H., Shah, R., Jin, M., Hartert, T.V., Peebles, R.S., Graham, B.S., Moore, M.L., Anderson, L.J., Wright, E.R., 2018. The Morphology and Assembly of Respiratory Syncytial Virus Revealed by Cryo-Electron Tomography. *Viruses* 10, 446. <https://doi.org/10.3390/v10080446>
- Kenworthy, A.K., Schmieder, S.S., Raghunathan, K., Tiwari, A., Wang, T., Kelly, C.V., Lencer, W.I., 2021. Cholera Toxin as a Probe for Membrane Biology. *Toxins* 13, 543. <https://doi.org/10.3390/toxins13080543>
- Kinder, J.T., Moncman, C.L., Barrett, C., Jin, H., Kallewaard, N., Dutch, R.E., 2020. Respiratory Syncytial Virus and Human Metapneumovirus Infections in Three-Dimensional Human Airway Tissues Expose an Interesting Dichotomy in Viral Replication, Spread, and Inhibition by Neutralizing Antibodies. *J. Virol.* 94, e01068-20. <https://doi.org/10.1128/JVI.01068-20>
- King, T., Mejias, A., Ramilo, O., Peebles, M.E., 2021. The larger attachment glycoprotein of respiratory syncytial virus produced in primary human bronchial epithelial cultures reduces infectivity for cell lines. *PLOS Pathog.* 17, e1009469. <https://doi.org/10.1371/journal.ppat.1009469>
- Kirkpatrick, C.T., Wang, Y., Leiva Juarez, M.M., Shivshankar, P., Pantaleón García, J., Plumer, A.K., Kulkarni, V.V., Ware, H.H., Gulraiz, F., Chavez Cavasos, M.A., Martinez Zayas, G., Wali, S., Rice, A.P., Liu, H., Tour, J.M., Sikkema, W.K.A., Cruz Solbes, A.S., Youker, K.A., Tuvim, M.J., Dickey, B.F., Evans, S.E., 2019. Inducible Lung Epithelial Resistance Requires Multisource Reactive Oxygen Species Generation To Protect against Viral Infections. *mBio* 9, e00696-18. <https://doi.org/10.1128/mBio.00696-18>
- Kiss, G., Holl, J.M., Williams, G.M., Alonas, E., Vanover, D., Lifland, A.W., Gudheti, M., Guerrero-Ferreira, R.C., Nair, V., Yi, H., Graham, B.S., Santangelo, P.J., Wright, E.R., 2014. Structural Analysis of Respiratory Syncytial Virus Reveals the Position of M2-1 between the Matrix Protein and the Ribonucleoprotein Complex. *J. Virol.* 88, 7602–7617. <https://doi.org/10.1128/JVI.00256-14>

- Kjos, M., Aprianto, R., Fernandes, V.E., Andrew, P.W., van Strijp, J.A.G., Nijland, R., Veening, J.-W., 2015. Bright Fluorescent *Streptococcus pneumoniae* for Live-Cell Imaging of Host-Pathogen Interactions. *J. Bacteriol.* 197, 807–818. <https://doi.org/10.1128/JB.02221-14>
- Knodler, L.A., Vallance, B.A., Hensel, M., Jäckel, D., Finlay, B.B., Steele-Mortimer, O., 2003. Salmonella type III effectors PipB and PipB2 are targeted to detergent-resistant microdomains on internal host cell membranes. *Mol. Microbiol.* 49, 685–704. <https://doi.org/10.1046/j.1365-2958.2003.03598.x>
- Knudson, C.J., Varga, S.M., 2015. The relationship between respiratory syncytial virus and asthma. *Vet. Pathol.* 52, 97–106. <https://doi.org/10.1177/0300985814520639>
- Kollmann, T.R., Crabtree, J., Rein-Weston, A., Blimkie, D., Thommai, F., Wang, X.Y., Lavoie, P.M., Furlong, J., Fortuno, E.S., Hajjar, A.M., Hawkins, N.R., Self, S.G., Wilson, C.B., 2009. Neonatal Innate TLR-Mediated Responses Are Distinct from Those of Adults. *J. Immunol.* 183, 7150–7160. <https://doi.org/10.4049/jimmunol.0901481>
- Korobchevskaya, K., Lagerholm, B.C., Colin-York, H., Fritzsche, M., 2017. Exploring the Potential of Airyscan Microscopy for Live Cell Imaging. *Photonics* 4, 41. <https://doi.org/10.3390/photonics4030041>
- Kowalski, M.P., Pier, G.B., 2004. Localization of Cystic Fibrosis Transmembrane Conductance Regulator to Lipid Rafts of Epithelial Cells Is Required for *Pseudomonas aeruginosa*-Induced Cellular Activation. *J. Immunol.* 172, 418–425. <https://doi.org/10.4049/jimmunol.172.1.418>
- Kozak, S.L., Heard, J.M., Kabat, D., 2002. Segregation of CD4 and CXCR4 into Distinct Lipid Microdomains in T Lymphocytes Suggests a Mechanism for Membrane Destabilization by Human Immunodeficiency Virus. *J. Virol.* <https://doi.org/10.1128/JVI.76.4.1802-1815.2002>
- Kuek, L.E., Lee, R.J., 2020. First contact: the role of respiratory cilia in host-pathogen interactions in the airways. *Am. J. Physiol.-Lung Cell. Mol. Physiol.* 319, L603–L619. <https://doi.org/10.1152/ajplung.00283.2020>
- Küng, E., Coward, W.R., Neill, D.R., Malak, H.A., Mühlemann, K., Kadioglu, A., Hilty, M., Hathaway, L.J., 2014. The Pneumococcal Polysaccharide Capsule and Pneumolysin Differentially Affect CXCL8 and IL-6 Release from Cells of the Upper and Lower Respiratory Tract. *PLOS ONE* 9, e92355. <https://doi.org/10.1371/journal.pone.0092355>
- Kuronuma, K., Mitsuzawa, H., Takeda, K., Nishitani, C., Chan, E.D., Kuroki, Y., Nakamura, M., Voelker, D.R., 2009. Anionic Pulmonary Surfactant Phospholipids Inhibit Inflammatory Responses from Alveolar Macrophages and U937 Cells by Binding the Lipopolysaccharide-interacting Proteins CD14 and MD-2. *J. Biol. Chem.* 284, 25488–25500. <https://doi.org/10.1074/jbc.M109.040832>
- Kurt-Jones, E.A., Popova, L., Kwinn, L., Haynes, L.M., Jones, L.P., Tripp, R.A., Walsh, E.E., Freeman, M.W., Golenbock, D.T., Anderson, L.J., Finberg, R.W., 2000. Pattern recognition receptors TLR4 and CD14 mediate response to respiratory syncytial virus. *Nat. Immunol.* 1, 398–401. <https://doi.org/10.1038/80833>
- Kwok, Y.H., Hutchinson, M.R., Gentgall, M.G., Rolan, P.E., 2012. Increased Responsiveness of Peripheral Blood Mononuclear Cells to In Vitro TLR 2, 4 and 7 Ligand Stimulation in Chronic Pain Patients. *PLOS ONE* 7, e44232. <https://doi.org/10.1371/journal.pone.0044232>
- Lafont, F., Van Der Goot, F.G., 2005. Bacterial invasion via lipid rafts. *Cell. Microbiol.* 7, 613–620. <https://doi.org/10.1111/j.1462-5822.2005.00515.x>
- Lambert, L., Sagfors, A.M., Openshaw, P.J.M., Culley, F.J., 2014. Immunity to RSV in Early-Life. *Front. Immunol.* 5, 466. <https://doi.org/10.3389/fimmu.2014.00466>
- Laufer, A.S., Metlay, J.P., Gent, J.F., Fennie, K.P., Kong, Y., Pettigrew, M.M., 2011. Microbial Communities of the Upper Respiratory Tract and Otitis Media in Children. *mBio* 2, e00245-10. <https://doi.org/10.1128/mBio.00245-10>

- Lechner, J.F., Haugen, A., McClendon, I.A., Shamsuddin, A.M., 1984. Induction of squamous differentiation of normal human bronchial epithelial cells by small amounts of serum. *Differentiation* 25, 229–237. <https://doi.org/10.1111/j.1432-0436.1984.tb01361.x>
- Lee, A.G., Birdsall, N.J.M., Metcalfe, J.C., Toon, P.A., Warren, G.B., 1974. Clusters in lipid bilayers and the interpretation of thermal effects in biological membranes. *Biochemistry* 13, 3699–3705. <https://doi.org/10.1021/bi00715a013>
- Lee, C.-J., Lin, H.-R., Liao, C.-L., Lin, Y.-L., 2008. Cholesterol Effectively Blocks Entry of Flavivirus. *J. Virol.* <https://doi.org/10.1128/JVI.00117-08>
- Legg, J.P., Hussain, I.R., Warner, J.A., Johnston, S.L., Warner, J.O., 2003. Type 1 and Type 2 Cytokine Imbalance in Acute Respiratory Syncytial Virus Bronchiolitis. *Am. J. Respir. Crit. Care Med.* 168, 633–639. <https://doi.org/10.1164/rccm.200210-1148OC>
- Lenzo, J.C., O'Brien-Simpson, N.M., Cecil, J., Holden, J.A., Reynolds, E.C., 2016. Determination of Active Phagocytosis of Unopsonized *Porphyromonas gingivalis* by Macrophages and Neutrophils Using the pH-Sensitive Fluorescent Dye pHrodo. *Infect. Immun.* 84, 1753–1760. <https://doi.org/10.1128/IAI.01482-15>
- Leventis, P.A., Grinstein, S., 2010. The Distribution and Function of Phosphatidylserine in Cellular Membranes. *Annu. Rev. Biophys.* 39, 407–427. <https://doi.org/10.1146/annurev.biophys.093008.131234>
- Li, D., Wu, M., 2021. Pattern recognition receptors in health and diseases. *Signal Transduct. Target. Ther.* 6, 1–24. <https://doi.org/10.1038/s41392-021-00687-0>
- Li, L., Han, J., Wang, Z., Liu, J., Wei, J., Xiong, S., Zhao, Z., 2014. Mass Spectrometry Methodology in Lipid Analysis. *Int. J. Mol. Sci.* 15, 10492–10507. <https://doi.org/10.3390/ijms150610492>
- Li, X., Zhu, W., Fan, M., Zhang, J., Peng, Y., Huang, F., Wang, N., He, L., Zhang, L., Holmdahl, R., Meng, L., Lu, S., 2021. Dependence of SARS-CoV-2 infection on cholesterol-rich lipid raft and endosomal acidification. *Comput. Struct. Biotechnol. J.* 19, 1933–1943. <https://doi.org/10.1016/j.csbj.2021.04.001>
- Lichtenberg, D., Goñi, F.M., Heerklotz, H., 2005. Detergent-resistant membranes should not be identified with membrane rafts. *Trends Biochem. Sci.* 30, 430–436. <https://doi.org/10.1016/j.tibs.2005.06.004>
- Lichtenberger, L.M., Romero, J.J., Ruijter, W.M.J. de, Behbod, F., Darling, R., Ashraf, A.Q., Sanduja, S.K., 2001. Phosphatidylcholine Association Increases the Anti-Inflammatory and Analgesic Activity of Ibuprofen in Acute and Chronic Rodent Models of Joint Inflammation: Relationship to Alterations in Bioavailability and Cyclooxygenase-Inhibitory Potency. *J. Pharmacol. Exp. Ther.* 298, 279–287.
- Linfield, D.T., Gao, N., Raduka, A., Harford, T.J., Piedimonte, G., Rezaee, F., 2021. RSV attenuates epithelial cell restitution by inhibiting actin cytoskeleton-dependent cell migration. *Am. J. Physiol.-Lung Cell. Mol. Physiol.* 321, L189–L203. <https://doi.org/10.1152/ajplung.00118.2021>
- Liu, Y., Ling, L., Wong, S.H., Wang, M.H., Fitzgerald, J.R., Zou, X., Fang, S., Liu, X., Wang, X., Hu, W., Chan, H., Wang, Y., Huang, D., Li, Q., Wong, W.T., Choi, G., Zou, H., Hui, D.S., Yu, J., Tse, G., Gin, T., Wu, W.K., Chan, M.T., Zhang, L., 2021. Outcomes of respiratory viral-bacterial co-infection in adult hospitalized patients. *EClinicalMedicine* 37. <https://doi.org/10.1016/j.eclinm.2021.100955>
- Llor, C., Bjerrum, L., 2014. Antimicrobial resistance: risk associated with antibiotic overuse and initiatives to reduce the problem. *Ther. Adv. Drug Saf.* 5, 229–241. <https://doi.org/10.1177/2042098614554919>
- Lloyd, C.M., Saglani, S., 2017. Development of allergic immunity in early life. *Immunol. Rev.* 278, 101–115. <https://doi.org/10.1111/imr.12562>
- Lloyd, C.M., Snelgrove, R.J., 2018. Type 2 immunity: Expanding our view. *Sci. Immunol.* 3, eaat1604. <https://doi.org/10.1126/sciimmunol.aat1604>
- London, E., Brown, D.A., 2000. Insolubility of lipids in Triton X-100: physical origin and relationship to sphingolipid/cholesterol membrane domains (rafts). *Biochim. Biophys.*

- Acta BBA - Biomembr., Detergents in Biomembrane Studies 1508, 182–195.
[https://doi.org/10.1016/S0304-4157\(00\)00007-1](https://doi.org/10.1016/S0304-4157(00)00007-1)
- Luck, J.N., Tettelin, H., Orihuela, C.J., 2020. Sugar-Coated Killer: Serotype 3 Pneumococcal Disease. *Front. Cell. Infect. Microbiol.* 10, 817.
<https://doi.org/10.3389/fcimb.2020.613287>
- Ludwig, A., Nguyen, T.H., Leong, D., Ravi, L.I., Tan, B.H., Sandin, S., Sugrue, R.J., 2017. Caveolae provide a specialized membrane environment for respiratory syncytial virus assembly. *J. Cell Sci.* 130, 1037–1050. <https://doi.org/10.1242/jcs.198853>
- Lüfgren, J., Rämelt, M., Renko, M., Marttila, R., Hallman, M., 2002. Association between Surfactant Protein A Gene Locus and Severe Respiratory Syncytial Virus Infection in Infants. *J. Infect. Dis.* 185, 283–289. <https://doi.org/10.1086/338473>
- Lukens, M.V., van de Pol, A.C., Coenjaerts, F.E.J., Jansen, N.J.G., Kamp, V.M., Kimpen, J.L.L., Rossen, J.W.A., Ulfman, L.H., Tacke, C.E.A., Viveen, M.C., Koenderman, L., Wolfs, T.F.W., van Bleek, G.M., 2010. A Systemic Neutrophil Response Precedes Robust CD8+ T-Cell Activation during Natural Respiratory Syncytial Virus Infection in Infants. *J. Virol.* 84, 2374–2383. <https://doi.org/10.1128/JVI.01807-09>
- Ma, H.M., Wu, Z., Nakanishi, H., 2011. Phosphatidylserine-containing liposomes suppress inflammatory bone loss by ameliorating the cytokine imbalance provoked by infiltrated macrophages. *Lab. Investig. J. Tech. Methods Pathol.* 91, 921–931.
<https://doi.org/10.1038/labinvest.2011.54>
- Maguy, A., Hebert, T.E., Nattel, S., 2006. Involvement of lipid rafts and caveolae in cardiac ion channel function. *Cardiovasc. Res.* 69, 798–807.
<https://doi.org/10.1016/j.cardiores.2005.11.013>
- Makris, S., Bajorek, M., Culley, F.J., Goritzka, M., Johansson, C., 2016. Alveolar Macrophages Can Control Respiratory Syncytial Virus Infection in the Absence of Type I Interferons. *J. Innate Immun.* 8, 452–463. <https://doi.org/10.1159/000446824>
- Mangoldt, T.C., Van Herck, M.A., Nullens, S., Ramet, J., De Dooy, J.J., Jorens, P.G., De Winter, B.Y., 2015. The role of Th17 and Treg responses in the pathogenesis of RSV infection. *Pediatr. Res.* 78, 483–491. <https://doi.org/10.1038/pr.2015.143>
- Manié, S.N., Debreyne, S., Vincent, S., Gerlier, D., 2000. Measles Virus Structural Components Are Enriched into Lipid Raft Microdomains: a Potential Cellular Location for Virus Assembly. *J. Virol.* <https://doi.org/10.1128/JVI.74.1.305-311.2000>
- Manley, G.C.A., Stokes, C.A., Marsh, E.K., Sabroe, I., Parker, L.C., 2019. DUSP10 Negatively Regulates the Inflammatory Response to Rhinovirus through Interleukin-1 β Signaling. *J. Virol.* 93, e01659-18. <https://doi.org/10.1128/JVI.01659-18>
- Marks, L.R., Davidson, B.A., Knight, P.R., Hakansson, A.P., 2013. Interkingdom Signaling Induces *Streptococcus pneumoniae* Biofilm Dispersion and Transition from Asymptomatic Colonization to Disease. *mBio.* <https://doi.org/10.1128/mBio.00438-13>
- Marom, T., Nokso-Koivisto, J., Chonmaitree, T., 2012. Viral–Bacterial Interactions in Acute Otitis Media. *Curr. Allergy Asthma Rep.* 12, 551–558. <https://doi.org/10.1007/s11882-012-0303-2>
- Marr, N., Turvey, S.E., 2012. Role of human TLR4 in respiratory syncytial virus-induced NF- κ B activation, viral entry and replication. *Innate Immun.* 18, 856–865.
<https://doi.org/10.1177/1753425912444479>
- Marriott, H.M., Gascoyne, K.A., Gowda, R., Geary, I., Nicklin, M.J.H., Iannelli, F., Pozzi, G., Mitchell, T.J., Whyte, M.K.B., Sabroe, I., Dockrell, D.H., 2012. Interleukin-1 β Regulates CXCL8 Release and Influences Disease Outcome in Response to *Streptococcus pneumoniae*, Defining Intercellular Cooperation between Pulmonary Epithelial Cells and Macrophages. *Infect. Immun.* <https://doi.org/10.1128/IAI.05697-11>
- Martín-Vicente, M., González-Riaño, C., Barbas, C., Jiménez-Sousa, M.Á., Brochado-Kith, O., Resino, S., Martínez, I., 2020. Metabolic changes during respiratory syncytial virus infection of epithelial cells. *PLoS ONE* 15, e0230844.
<https://doi.org/10.1371/journal.pone.0230844>

- McCurdy, L.H., Graham, B.S., 2003. Role of Plasma Membrane Lipid Microdomains in Respiratory Syncytial Virus Filament Formation. *J. Virol.* 77, 1747–1756. <https://doi.org/10.1128/JVI.77.3.1747-1756.2003>
- McLellan, J.S., Chen, M., Joyce, M.G., Sastry, M., Stewart-Jones, G.B.E., Yang, Y., Zhang, B., Chen, L., Srivatsan, S., Zheng, A., Zhou, T., Graepel, K.W., Kumar, A., Moin, S., Boyington, J.C., Chuang, G.-Y., Soto, C., Baxa, U., Bakker, A.Q., Spits, H., Beaumont, T., Zheng, Z., Xia, N., Ko, S.-Y., Todd, J.-P., Rao, S., Graham, B.S., Kwong, P.D., 2013a. Structure-Based Design of a Fusion Glycoprotein Vaccine for Respiratory Syncytial Virus. *Science* 342, 592–598. <https://doi.org/10.1126/science.1243283>
- McLellan, J.S., Chen, M., Leung, S., Graepel, K.W., Du, X., Yang, Y., Zhou, T., Baxa, U., Yasuda, E., Beaumont, T., Kumar, A., Modjarrad, K., Zheng, Z., Zhao, M., Xia, N., Kwong, P.D., Graham, B.S., 2013b. Structure of RSV Fusion Glycoprotein Trimer Bound to a Prefusion-Specific Neutralizing Antibody. *Science* 340, 1113–1117. <https://doi.org/10.1126/science.1234914>
- McNamara, P.S., Flanagan, B.F., Hart, C.A., Smyth, R.L., 2005. Production of Chemokines in the Lungs of Infants with Severe Respiratory Syncytial Virus Bronchiolitis. *J. Infect. Dis.* 191, 1225–1232. <https://doi.org/10.1086/428855>
- Medigeshi, G.R., Hirsch, A.J., Streblow, D.N., Nikolich-Zugich, J., Nelson, J.A., 2008. West Nile Virus Entry Requires Cholesterol-Rich Membrane Microdomains and Is Independent of $\alpha\beta 3$ Integrin. *J. Virol.* <https://doi.org/10.1128/JVI.00008-08>
- Meena, N.P., Kimmel, A.R., 2018. Quantification of Live Bacterial Sensing for Chemotaxis and Phagocytosis and of Macropinocytosis. *Front. Cell. Infect. Microbiol.* 8, 62. <https://doi.org/10.3389/fcimb.2018.00062>
- Michelow, I.C., Olsen, K., Lozano, J., Rollins, N.K., Duffy, L.B., Ziegler, T., Kauppila, J., Leinonen, M., McCracken, G.H., Jr, 2004. Epidemiology and Clinical Characteristics of Community-Acquired Pneumonia in Hospitalized Children. *Pediatrics* 113, 701–707. <https://doi.org/10.1542/peds.113.4.701>
- Milad, N., Morissette, M.C., 2021. Revisiting the role of pulmonary surfactant in chronic inflammatory lung diseases and environmental exposure. *Eur. Respir. Rev.* 30. <https://doi.org/10.1183/16000617.0077-2021>
- Miles, A.A., Misra, S.S., Irwin, J.O., 1938. The estimation of the bactericidal power of the blood. *J. Hyg. (Lond.)* 38, 732–749.
- Mills, J.T., Schwenger, A., Marsh, E.K., Edwards, M.R., Sabroe, I., Midwood, K.S., Parker, L.C., 2019. Airway Epithelial Cells Generate Pro-inflammatory Tenascin-C and Small Extracellular Vesicles in Response to TLR3 Stimuli and Rhinovirus Infection. *Front. Immunol.* 10, 1987. <https://doi.org/10.3389/fimmu.2019.01987>
- ModernaTX, Inc., 2022. A Phase 1, Randomized, Observer-Blind, Placebo-Controlled, Dose Escalation Study to Evaluate the Safety, Reactogenicity, and Immunogenicity of mRNA-1345, an mRNA Vaccine Targeting Respiratory Syncytial Virus (RSV), in Healthy Younger Adults Aged 18 to 49 Years, Women of Child-Bearing Potential Aged 18 to 40 Years, Healthy Older Adults Aged 65 to 79 Years, Japanese Older Adults Aged ≥ 60 Years, and RSV-Seropositive Children Aged 12 to 59 Months (Clinical trial registration No. NCT04528719). clinicaltrials.gov.
- Monick, M.M., Staber, J.M., Thomas, K.W., Hunninghake, G.W., 2001. Respiratory Syncytial Virus Infection Results in Activation of Multiple Protein Kinase C Isoforms Leading to Activation of Mitogen-Activated Protein Kinase. *J. Immunol.* 166, 2681–2687. <https://doi.org/10.4049/jimmunol.166.4.2681>
- Morens, D.M., Taubenberger, J.K., Fauci, A.S., 2008. Predominant Role of Bacterial Pneumonia as a Cause of Death in Pandemic Influenza: Implications for Pandemic Influenza Preparedness. *J. Infect. Dis.* 198, 962–970. <https://doi.org/10.1086/591708>
- Morona, J.K., Miller, D.C., Morona, R., Paton, J.C., 2004. The Effect That Mutations in the Conserved Capsular Polysaccharide Biosynthesis Genes *cpsA*, *cpsB*, and *cpsD* Have on Virulence of *Streptococcus pneumoniae*. *J. Infect. Dis.* 189, 1905–1913. <https://doi.org/10.1086/383352>

- Morris, G.E., Whyte, M.K.B., Martin, G.F., Jose, P.J., Dower, S.K., Sabroe, I., 2005. Agonists of Toll-like Receptors 2 and 4 Activate Airway Smooth Muscle via Mononuclear Leukocytes. *Am. J. Respir. Crit. Care Med.* 171, 814–822. <https://doi.org/10.1164/rccm.200403-406OC>
- Morris, J.A., Blount, R.E., Savage, R.E., 1956. Recovery of Cytopathogenic Agent from Chimpanzees with Goryza. *Proc. Soc. Exp. Biol. Med.* 92, 544–549. <https://doi.org/10.3181/00379727-92-22538>
- Murawski, M.R., Bowen, G.N., Cerny, A.M., Anderson, L.J., Haynes, L.M., Tripp, R.A., Kurt-Jones, E.A., Finberg, R.W., 2009. Respiratory syncytial virus activates innate immunity through Toll-like receptor 2. *J. Virol.* 83, 1492–1500. <https://doi.org/10.1128/JVI.00671-08>
- Nair, H., Nokes, D.J., Gessner, B.D., Dherani, M., Madhi, S.A., Singleton, R.J., O'Brien, K.L., Roca, A., Wright, P.F., Bruce, N., Chandran, A., Theodoratou, E., Sutanto, A., Sedyaningsih, E.R., Ngama, M., Munywoki, P.K., Kartasasmita, C., Simões, E.A., Rudan, I., Weber, M.W., Campbell, H., 2010. Global burden of acute lower respiratory infections due to respiratory syncytial virus in young children: a systematic review and meta-analysis. *The Lancet* 375, 1545–1555. [https://doi.org/10.1016/S0140-6736\(10\)60206-1](https://doi.org/10.1016/S0140-6736(10)60206-1)
- Nakamura, S., Davis, K.M., Weiser, J.N., 2011. Synergistic stimulation of type I interferons during influenza virus coinfection promotes *Streptococcus pneumoniae* colonization in mice. *J. Clin. Invest.* 121. <https://doi.org/10.1172/JCI57762>
- Nakauchi, M., Nagata, N., Takayama, I., Saito, S., Kubo, H., Kaida, A., Oba, K., Odagiri, T., Kageyama, T., 2019. Propagation of Rhinovirus C in Differentiated Immortalized Human Airway HBEC3-KT Epithelial Cells. *Viruses* 11, 216. <https://doi.org/10.3390/v11030216>
- Neu, U., Mainou, B.A., 2020. Virus interactions with bacteria: Partners in the infectious dance. *PLoS Pathog.* 16, e1008234. <https://doi.org/10.1371/journal.ppat.1008234>
- Nicolas de Lamballerie, C., Pizzorno, A., Dubois, J., Julien, T., Padey, B., Bouveret, M., Traversier, A., Legras-Lachuer, C., Lina, B., Boivin, G., Terrier, O., Rosa-Calatrava, M., 2019. Characterization of cellular transcriptomic signatures induced by different respiratory viruses in human reconstituted airway epithelia. *Sci. Rep.* 9, 11493. <https://doi.org/10.1038/s41598-019-48013-7>
- Novick, S., Shagan, M., Blau, K., Lifshitz, S., Givon-Lavi, N., Grossman, N., Bodner, L., Dagan, R., Nebenzahl, Y.M., 2017. Adhesion and invasion of *Streptococcus pneumoniae* to primary and secondary respiratory epithelial cells. *Mol. Med. Rep.* 15, 65–74. <https://doi.org/10.3892/mmr.2016.5996>
- Nuijten, M.J.C., Wittenberg, W., Lebmeier, M., 2007. Cost Effectiveness of Palivizumab for Respiratory Syncytial Virus Prophylaxis in High-Risk Children. *PharmacoEconomics* 25, 55–71. <https://doi.org/10.2165/00019053-200725010-00006>
- Numata, M., Chu, H.W., Dakhama, A., Voelker, D.R., 2010. Pulmonary surfactant phosphatidylglycerol inhibits respiratory syncytial virus-induced inflammation and infection. *Proc Natl Acad Sci U S A* 107, 320–5. <https://doi.org/10.1073/pnas.0909361107>
- Numata, M., Kandasamy, P., Nagashima, Y., Fickes, R., Murphy, R.C., Voelker, D.R., 2015. Phosphatidylinositol inhibits respiratory syncytial virus infection. *J Lipid Res* 56, 578–87. <https://doi.org/10.1194/jlr.M055723>
- Numata, M., Kandasamy, P., Nagashima, Y., Posey, J., Hartshorn, K., Woodland, D., Voelker, D.R., 2012. Phosphatidylglycerol suppresses influenza A virus infection. *Am J Respir Cell Mol Biol* 46, 479–87. <https://doi.org/10.1165/rcmb.2011-0194OC>
- Numata, M., Mitchell, J.R., Tipper, J.L., Brand, J.D., Trombley, J.E., Nagashima, Y., Kandasamy, P., Chu, H.W., Harrod, K.S., Voelker, D.R., 2020. Pulmonary surfactant lipids inhibit infections with the pandemic H1N1 influenza virus in several animal models. *J. Biol. Chem.* 295, 1704–1715. <https://doi.org/10.1074/jbc.RA119.012053>
- Numata, M., Nagashima, Y., Moore, M.L., Berry, K.Z., Chan, M., Kandasamy, P., Peebles, R.S., Murphy, R.C., Voelker, D.R., 2013. Phosphatidylglycerol provides short-term

- prophylaxis against respiratory syncytial virus infection. *J. Lipid Res.* 54, 2133–2143. <https://doi.org/10.1194/jlr.M037077>
- Numata, M., Voelker, D.R., 2022. Anti-inflammatory and anti-viral actions of anionic pulmonary surfactant phospholipids. *Biochim. Biophys. Acta BBA - Mol. Cell Biol. Lipids* 1867, 159139. <https://doi.org/10.1016/j.bbali.2022.159139>
- Okabayashi, T., Kojima, T., Masaki, T., Yokota, S., Imaizumi, T., Tsutsumi, H., Himi, T., Fujii, N., Sawada, N., 2011. Type-III interferon, not type-I, is the predominant interferon induced by respiratory viruses in nasal epithelial cells. *Virus Res.* 160, 360–366. <https://doi.org/10.1016/j.virusres.2011.07.011>
- O’Neill, L.A.J., Bowie, A.G., 2007. The family of five: TIR-domain-containing adaptors in Toll-like receptor signalling. *Nat. Rev. Immunol.* 7, 353–364. <https://doi.org/10.1038/nri2079>
- Openshaw, P.J.M., Chiu, C., Culley, F.J., Johansson, C., 2017. Protective and Harmful Immunity to RSV Infection. *Annu. Rev. Immunol.* 35, 501–532. <https://doi.org/10.1146/annurev-immunol-051116-052206>
- Oppenheim, J.J., Biragyn, A., Kwak, L.W., Yang, D., 2003. Roles of antimicrobial peptides such as defensins in innate and adaptive immunity. *Ann. Rheum. Dis.* 62 Suppl 2, ii17-21. https://doi.org/10.1136/ard.62.suppl_2.ii17
- Palacios-Rápalo, S.N., De Jesús-González, L.A., Cordero-Rivera, C.D., Farfan-Morales, C.N., Osuna-Ramos, J.F., Martínez-Mier, G., Quistián-Galván, J., Muñoz-Pérez, A., Bernal-Dolores, V., del Ángel, R.M., Reyes-Ruiz, J.M., 2021. Cholesterol-Rich Lipid Rafts as Platforms for SARS-CoV-2 Entry. *Front. Immunol.* 12, 796855. <https://doi.org/10.3389/fimmu.2021.796855>
- Park, S.-S., Gonzalez-Juarbe, N., Riegler, A.N., Im, H., Hale, Y., Platt, M.P., Croney, C., Briles, D.E., Orihuela, C.J., 2021. Streptococcus pneumoniae binds to host GAPDH on dying lung epithelial cells worsening secondary infection following influenza. *Cell Rep.* 35, 109267. <https://doi.org/10.1016/j.celrep.2021.109267>
- Parker, L.C., Prestwich, E.C., Ward, J.R., Smythe, E., Berry, A., Triantafilou, M., Triantafilou, K., Sabroe, I., 2008. A phosphatidylserine species inhibits a range of TLR, but not IL-1 β , induced inflammatory responses by disruption of membrane microdomains. *J. Immunol. Baltim. Md* 1950 181, 5606–5617.
- Pearce, B.J., Iannelli, F., Pozzi, G., 2002. Construction of new unencapsulated (rough) strains of Streptococcus pneumoniae. *Res. Microbiol.* 153, 243–247. [https://doi.org/10.1016/S0923-2508\(02\)01312-8](https://doi.org/10.1016/S0923-2508(02)01312-8)
- Pettigrew, M.M., Marks, L.R., Kong, Y., Gent, J.F., Roche-Hakansson, H., Hakansson, A.P., 2014. Dynamic changes in the Streptococcus pneumoniae transcriptome during transition from biofilm formation to invasive disease upon influenza A virus infection. *Infect. Immun.* 82, 4607–4619.
- Pfizer, 2022. A phase 3, randomized, double-blinded, placebo-controlled trial to evaluate the efficacy and safety of a respiratory syncytial virus (RSV) prefusion F subunit vaccine in infants born to women vaccinated during pregnancy (Clinical trial registration No. NCT04424316). clinicaltrials.gov.
- Popik, W., Alce, T.M., Au, W.-C., 2002. Human Immunodeficiency Virus Type 1 Uses Lipid Raft-Colocalized CD4 and Chemokine Receptors for Productive Entry into CD4+ T Cells. *J. Virol.* <https://doi.org/10.1128/JVI.76.10.4709-4722.2002>
- Quintos-Alagheband, M.L., Noyola, E., Makvana, S., El-Chaar, G., Wang, S., Calixte, R., Krilov, L.R., 2017. Reducing Antibiotic Use in Respiratory Syncytial Virus-A Quality Improvement Approach to Antimicrobial Stewardship. *Pediatr. Qual. Saf.* 2, e046. <https://doi.org/10.1097/pq9.0000000000000046>
- Ramirez, R.D., Sheridan, S., Girard, L., Sato, M., Kim, Y., Pollack, J., Peyton, M., Zou, Y., Kurie, J.M., DiMaio, J.M., Milchgrub, S., Smith, A.L., Souza, R.F., Gilbey, L., Zhang, X., Gandia, K., Vaughan, M.B., Wright, W.E., Gazdar, A.F., Shay, J.W., Minna, J.D., 2004. Immortalization of Human Bronchial Epithelial Cells in the Absence of Viral Oncoproteins. *Cancer Res.* 64, 9027–9034. <https://doi.org/10.1158/0008-5472.CAN-04-3703>

- Ramírez-Pérez, S., Hernández-Palma, L.A., Oregon-Romero, E., Anaya-Macías, B.U., García-Arellano, S., González-Estevez, G., Muñoz-Valle, J.F., 2020. Downregulation of Inflammatory Cytokine Release from IL-1 β and LPS-Stimulated PBMC Orchestrated by ST2825, a MyD88 Dimerisation Inhibitor. *Molecules* 25, 4322. <https://doi.org/10.3390/molecules25184322>
- Reddinger, R.M., Luke-Marshall, N.R., Hakansson, A.P., Campagnari, A.A., 2016. Host Physiologic Changes Induced by Influenza A Virus Lead to Staphylococcus aureus Biofilm Dispersion and Transition from Asymptomatic Colonization to Invasive Disease. *mBio*. <https://doi.org/10.1128/mBio.01235-16>
- Reeves, S.R., Barrow, K.A., White, M.P., Rich, L.M., Naushab, M., Debley, J.S., 2018. Stability of gene expression by primary bronchial epithelial cells over increasing passage number. *BMC Pulm. Med.* 18, 91. <https://doi.org/10.1186/s12890-018-0652-2>
- Rezaee, F., DeSando, S.A., Ivanov, A.I., Chapman, T.J., Knowlden, S.A., Beck, L.A., Georas, S.N., 2013. Sustained Protein Kinase D Activation Mediates Respiratory Syncytial Virus-Induced Airway Barrier Disruption. *J. Virol.* 87, 11088–11095. <https://doi.org/10.1128/JVI.01573-13>
- Rezinciuc, S., Bezavada, L., Bahadoran, A., Ingels, J.F., Kim, Y.-Y., Cormier, S.A., Devincenzo, J.P., Shulkin, B.L., Smallwood, H.S., 2020. Respiratory Syncytial Virus Infections Induce Hypermetabolism in Pediatric Upper Airways. <https://doi.org/10.1101/2020.07.18.200964>
- Rijsbergen, L.C., van Dijk, L.L.A., Engel, M.F.M., de Vries, R.D., de Swart, R.L., 2021. In Vitro Modelling of Respiratory Virus Infections in Human Airway Epithelial Cells – A Systematic Review. *Front. Immunol.* 12.
- Rissanen, S., Grzybek, M., Orłowski, A., Róg, T., Cramariuc, O., Levental, I., Eggeling, C., Sezgin, E., Vattulainen, I., 2017. Phase Partitioning of GM1 and Its Bodipy-Labeled Analog Determine Their Different Binding to Cholera Toxin. *Front. Physiol.* 8.
- Rosenberger, C.M., Brumell, J.H., Finlay, B.B., 2000. Microbial pathogenesis: Lipid rafts as pathogen portals. *Curr. Biol.* 10, R823–R825. [https://doi.org/10.1016/S0960-9822\(00\)00788-0](https://doi.org/10.1016/S0960-9822(00)00788-0)
- Rudd, B.D., Burstein, E., Duckett, C.S., Li, X., Lucaks, N.W., 2005. Differential Role for TLR3 in Respiratory Syncytial Virus-Induced Chemokine Expression. *J. Virol.* 79. <https://doi.org/10.1128/JVI.79.6.3350-3357.2005>
- Russell, C.D., Unger, S.A., Walton, M., Schwarze, J., 2017. The Human Immune Response to Respiratory Syncytial Virus Infection. *Clin. Microbiol. Rev.* 30, 481–502. <https://doi.org/10.1128/CMR.00090-16>
- Ruysschaert, J.-M., Loney, C., 2015. Role of lipid microdomains in TLR-mediated signalling. *Biochim. Biophys. Acta BBA - Biomembr.*, Lipid-protein interactions 1848, 1860–1867. <https://doi.org/10.1016/j.bbamem.2015.03.014>
- Sánchez-Tarjuelo, R., Cortegano, I., Manosalva, J., Rodríguez, M., Ruíz, C., Alía, M., Prado, M.C., Cano, E.M., Ferrándiz, M.J., de la Campa, A.G., Gaspar, M.L., de Andrés, B., 2020. The TLR4-MyD88 Signaling Axis Regulates Lung Monocyte Differentiation Pathways in Response to Streptococcus pneumoniae. *Front. Immunol.* 11.
- San-Juan-Vergara, H., Peeples, M.E., Lockey, R.F., Mohapatra, S.S., 2004. Protein Kinase C- α Activity Is Required for Respiratory Syncytial Virus Fusion to Human Bronchial Epithelial Cells. *J. Virol.* 78, 13717–13726. <https://doi.org/10.1128/JVI.78.24.13717-13726.2004>
- San-Juan-Vergara, H., Sampayo-Escobar, V., Reyes, N., Cha, B., Pacheco-Lugo, L., Wong, T., Peeples, M.E., Collins, P.L., Castaño, M.E., Mohapatra, S.S., 2012. Cholesterol-Rich Microdomains as Docking Platforms for Respiratory Syncytial Virus in Normal Human Bronchial Epithelial Cells. *J. Virol.* 86, 1832–1843. <https://doi.org/10.1128/JVI.06274-11>
- Satkunanathan, S., Kumar, N., Bajorek, M., Purbhoo, M.A., Culley, F.J., 2014. Respiratory syncytial virus infection, TLR3 ligands, and proinflammatory cytokines induce CD161

- ligand LLT1 expression on the respiratory epithelium. *J Virol* 88, 2366–73.
<https://doi.org/10.1128/jvi.02789-13>
- Schmidt, M.E., Knudson, C.J., Hartwig, S.M., Pewe, L.L., Meyerholz, D.K., Langlois, R.A., Harty, J.T., Varga, S.M., 2018. Memory CD8 T cells mediate severe immunopathology following respiratory syncytial virus infection. *PLOS Pathog.* 14, e1006810. <https://doi.org/10.1371/journal.ppat.1006810>
- Schmidt, M.E., Varga, S.M., 2020. Cytokines and CD8 T cell immunity during respiratory syncytial virus infection. *Cytokine* 133, 154481.
<https://doi.org/10.1016/j.cyto.2018.07.012>
- Seng, L.-G., Daly, J., Chang, K.-C., Kuchipudi, S.V., 2014. High Basal Expression of Interferon-Stimulated Genes in Human Bronchial Epithelial (BEAS-2B) Cells Contributes to Influenza A Virus Resistance. *PLOS ONE* 9, e109023.
<https://doi.org/10.1371/journal.pone.0109023>
- Sengupta, P., Holowka, D., Baird, B., 2007. Fluorescence Resonance Energy Transfer between Lipid Probes Detects Nanoscopic Heterogeneity in the Plasma Membrane of Live Cells. *Biophys. J.* 92, 3564–3574.
<https://doi.org/10.1529/biophysj.106.094730>
- Shafren, D.R., 1998. Viral Cell Entry Induced by Cross-Linked Decay-Accelerating Factor. *J. Virol.* 72, 9407–9412.
- Shahriari, S., Gordon, J., Ghildyal, R., 2016. Host cytoskeleton in respiratory syncytial virus assembly and budding. *Virol. J.* 13, 161. <https://doi.org/10.1186/s12985-016-0618-z>
- Shi, T., McAllister, D.A., O'Brien, K.L., Simoes, E.A.F., Madhi, S.A., Gessner, B.D., Polack, F.P., Balsells, E., Acacio, S., Aguayo, C., Alassani, I., Ali, A., Antonio, M., Awasthi, S., Awori, J.O., Azziz-Baumgartner, E., Baggett, H.C., Baillie, V.L., Balmaseda, A., Barahona, A., Basnet, S., Bassat, Q., Basualdo, W., Bigogo, G., Bont, L., Breiman, R.F., Brooks, W.A., Broor, S., Bruce, N., Bruden, D., Buchy, P., Campbell, S., Carosone-Link, P., Chadha, M., Chipeta, J., Chou, M., Clara, W., Cohen, C., Cuellar, E. de, Dang, D.-A., Dash-yandag, B., Deloria-Knoll, M., Dherani, M., Eap, T., Ebruke, B.E., Echavarria, M., Emediato, C.C. de F.L., Fasce, R.A., Feikin, D.R., Feng, L., Gentile, A., Gordon, A., Goswami, D., Goyet, S., Groome, M., Halasa, N., Hirve, S., Homaira, N., Howie, S.R.C., Jara, J., Jroundi, I., Kartasasmita, C.B., Khuri-Bulos, N., Kotloff, K.L., Krishnan, A., Libster, R., Lopez, O., Lucero, M.G., Lucion, F., Lupisan, S.P., Marcone, D.N., McCracken, J.P., Mejia, M., Moisi, J.C., Montgomery, J.M., Moore, D.P., Moraleta, C., Moyes, J., Munywoki, P., Mutyara, K., Nicol, M.P., Nokes, D.J., Nymadawa, P., Oliveira, M.T. da C., Oshitani, H., Pandey, N., Paranhos-Baccalà, G., Phillips, L.N., Picot, V.S., Rahman, M., Rakoto-Andrianarivelo, M., Rasmussen, Z.A., Rath, B.A., Robinson, A., Romero, C., Russomando, G., Salimi, V., Sawatwong, P., Scheltema, N., Schweiger, B., Scott, J.A.G., Seidenberg, P., Shen, K., Singleton, R., Sotomayor, V., Strand, T.A., Sutanto, A., Sylla, M., Tapia, M.D., Thamthitawat, S., Thomas, E.D., Tokarz, R., Turner, C., Venter, M., Waicharoen, S., Wang, J., Watthanaworawit, W., Yoshida, L.-M., Yu, H., Zar, H.J., Campbell, H., Nair, H., 2017. Global, regional, and national disease burden estimates of acute lower respiratory infections due to respiratory syncytial virus in young children in 2015: a systematic review and modelling study. *The Lancet* 390, 946–958.
[https://doi.org/10.1016/S0140-6736\(17\)30938-8](https://doi.org/10.1016/S0140-6736(17)30938-8)
- Shukla, S.D., Budden, K.F., Neal, R., Hansbro, P.M., 2017. Microbiome effects on immunity, health and disease in the lung. *Clin. Transl. Immunol.* 6, e133.
<https://doi.org/10.1038/cti.2017.6>
- Sigurs, N., Bjarnason, R., Sigurbergsson, F., Kjellman, B., 2000. Respiratory Syncytial Virus Bronchiolitis in Infancy Is an Important Risk Factor for Asthma and Allergy at Age 7. *Am. J. Respir. Crit. Care Med.* 161, 1501–1507.
<https://doi.org/10.1164/ajrccm.161.5.9906076>
- Simons, K., Gerl, M.J., 2010. Revitalizing membrane rafts: new tools and insights. *Nat. Rev. Mol. Cell Biol.* 11, 688–699. <https://doi.org/10.1038/nrm2977>

- Simons, K., Ikonen, E., 1997. Functional rafts in cell membranes. *Nature* 387, 569–572. <https://doi.org/10.1038/42408>
- Simons, K., Toomre, D., 2000. Lipid rafts and signal transduction. *Nat. Rev. Mol. Cell Biol.* 1, 31–39. <https://doi.org/10.1038/35036052>
- Sims, A.C., Burkett, S.E., Yount, B., Pickles, R.J., 2008. SARS-CoV replication and pathogenesis in an in vitro model of the human conducting airway epithelium. *Virus Res., SARS-CoV Pathogenesis and Replication* 133, 33–44. <https://doi.org/10.1016/j.virusres.2007.03.013>
- Singer, S.J., Nicolson, G.L., 1972. The Fluid Mosaic Model of the Structure of Cell Membranes. *Science*. <https://doi.org/10.1126/science.175.4023.720>
- Smith, C.M., Kulkarni, H., Radhakrishnan, P., Rutman, A., Bankart, M.J., Williams, G., Hirst, R.A., Easton, A.J., Andrew, P.W., O’Callaghan, C., 2014a. Ciliary dyskinesia is an early feature of respiratory syncytial virus infection. *Eur. Respir. J.* 43, 485–496. <https://doi.org/10.1183/09031936.00205312>
- Smith, C.M., Sandrini, S., Datta, S., Freestone, P., Shafeeq, S., Radhakrishnan, P., Williams, G., Glenn, S.M., Kuipers, O.P., Hirst, R.A., Easton, A.J., Andrew, P.W., O’Callaghan, C., 2014b. Respiratory Syncytial Virus Increases the Virulence of *Streptococcus pneumoniae* by Binding to Penicillin Binding Protein 1a. A New Paradigm in Respiratory Infection. *Am. J. Respir. Crit. Care Med.* 190, 196–207. <https://doi.org/10.1164/rccm.201311-2110OC>
- Sorice, M., Misasi, R., Riitano, G., Manganelli, V., Martellucci, S., Longo, A., Garofalo, T., Mattei, V., 2021. Targeting Lipid Rafts as a Strategy Against Coronavirus. *Front. Cell Dev. Biol.* 8.
- Spann, K.M., Tran, K.C., Collins, P.L., 2005. Effects of Nonstructural Proteins NS1 and NS2 of Human Respiratory Syncytial Virus on Interferon Regulatory Factor 3, NF- κ B, and Proinflammatory Cytokines. *J. Virol.* <https://doi.org/10.1128/JVI.79.9.5353-5362.2005>
- Stark, J.M., Stark, M.A., Colasurdo, G.N., LeVine, A.M., 2006. Decreased bacterial clearance from the lungs of mice following primary respiratory syncytial virus infection. *J. Med. Virol.* 78, 829–838. <https://doi.org/10.1002/jmv.20631>
- Stein, R.T., Sherrill, D., Morgan, W.J., Holberg, C.J., Halonen, M., Taussig, L.M., Wright, A.L., Martinez, F.D., 1999. Respiratory syncytial virus in early life and risk of wheeze and allergy by age 13 years. *Lancet Lond. Engl.* 354, 541–545. [https://doi.org/10.1016/S0140-6736\(98\)10321-5](https://doi.org/10.1016/S0140-6736(98)10321-5)
- Stewart, C.E., Torr, E.E., Mohd Jamili, N.H., Bosquillon, C., Sayers, I., 2012. Evaluation of Differentiated Human Bronchial Epithelial Cell Culture Systems for Asthma Research. *J. Allergy* 2012, e943982. <https://doi.org/10.1155/2012/943982>
- Stokes, C.A., Ismail, S., Dick, E.P., Bennett, J.A., Johnston, S.L., Edwards, M.R., Sabroe, I., Parker, L.C., 2011. Role of Interleukin-1 and MyD88-Dependent Signaling in Rhinovirus Infection. *J. Virol.* 85, 7912–7921. <https://doi.org/10.1128/jvi.02649-10>
- Stokes, C.A., Kaur, R., Edwards, M.R., Mondhe, M., Robinson, D., Prestwich, E.C., Hume, R.D., Marshall, C.A., Perrie, Y., O’Donnell, V.B., Harwood, J.L., Sabroe, I., Parker, L.C., 2016. Human rhinovirus-induced inflammatory responses are inhibited by phosphatidylserine containing liposomes. *Mucosal Immunol.* 9, 1303. <https://doi.org/10.1038/mi.2015.137>
<https://www.nature.com/articles/mi2015137#supplementary-information>
- Suárez-Arrabal, M.C., Mella, C., Lopez, S.M., Brown, N.V., Hall, M.W., Hammond, S., Shiels, W., Groner, J., Marcon, M., Ramilo, O., Mejias, A., 2015. Nasopharyngeal bacterial burden and antibiotics: Influence on inflammatory markers and disease severity in infants with respiratory syncytial virus bronchiolitis. *J. Infect.* 71, 458–469. <https://doi.org/10.1016/j.jinf.2015.06.010>
- Subcommittee on Diagnosis and Management of Bronchiolitis, 2006. Diagnosis and Management of Bronchiolitis. *Pediatrics* 118, 1774–1793. <https://doi.org/10.1542/peds.2006-2223>
- Sumbria, D., Berber, E., Mathayan, M., Rouse, B.T., 2021. Virus Infections and Host Metabolism—Can We Manage the Interactions? *Front. Immunol.* 11.

- Sun, K., Metzger, D.W., 2014. Influenza Infection Suppresses NADPH Oxidase–Dependent Phagocytic Bacterial Clearance and Enhances Susceptibility to Secondary Methicillin-Resistant *Staphylococcus aureus* Infection. *J. Immunol.* 192, 3301–3307. <https://doi.org/10.4049/jimmunol.1303049>
- Sun, X., Whittaker, G.R., 2003. Role for Influenza Virus Envelope Cholesterol in Virus Entry and Infection. *J. Virol.* 77, 12543–12551. <https://doi.org/10.1128/JVI.77.23.12543-12551.2003>
- Sun, Y., López, C.B., 2017. The innate immune response to RSV: Advances in our understanding of critical viral and host factors. *Vaccine* 35, 481–488. <https://doi.org/10.1016/j.vaccine.2016.09.030>
- Tal, G., Mandelberg, A., Dalal, I., Cesar, K., Somekh, E., Tal, A., Oron, A., Itskovich, S., Ballin, A., Houry, S., Beigelman, A., Lider, O., Rechavi, G., Amariglio, N., 2004. Association between Common Toll-Like Receptor 4 Mutations and Severe Respiratory Syncytial Virus Disease. *J. Infect. Dis.* 189, 2057–2063. <https://doi.org/10.1086/420830>
- Talbot, U.M., Paton, A.W., Paton, J.C., 1996. Uptake of *Streptococcus pneumoniae* by respiratory epithelial cells. *Infect. Immun.* <https://doi.org/10.1128/iai.64.9.3772-3777.1996>
- Tang, A., Chen, Z., Cox, K.S., Su, H.-P., Callahan, C., Fridman, A., Zhang, L., Patel, S.B., Cejas, P.J., Swoyer, R., Touch, S., Citron, M.P., Govindarajan, D., Luo, B., Eddins, M., Reid, J.C., Soisson, S.M., Galli, J., Wang, D., Wen, Z., Heidecker, G.J., Casimiro, D.R., DiStefano, D.J., Vora, K.A., 2019. A potent broadly neutralizing human RSV antibody targets conserved site IV of the fusion glycoprotein. *Nat. Commun.* 10, 4153. <https://doi.org/10.1038/s41467-019-12137-1>
- Tecle, T., Tripathi, S., Hartshorn, K.L., 2010. Review: Defensins and cathelicidins in lung immunity. *Innate Immun.* 16, 151–159. <https://doi.org/10.1177/1753425910365734>
- Teng, M.N., Collins, P.L., 2002. The Central Conserved Cystine Noose of the Attachment G Protein of Human Respiratory Syncytial Virus Is Not Required for Efficient Viral Infection In Vitro or In Vivo. *J. Virol.* 76, 6164–6171. <https://doi.org/10.1128/JVI.76.12.6164-6171.2002>
- Teng, M.N., Whitehead, S.S., Collins, P.L., 2001. Contribution of the Respiratory Syncytial Virus G Glycoprotein and Its Secreted and Membrane-Bound Forms to Virus Replication in Vitro and in Vivo. *Virology* 289, 283–296. <https://doi.org/10.1006/viro.2001.1138>
- Theken, K.N., Tang, S.Y., Sengupta, S., FitzGerald, G.A., 2021. The roles of lipids in SARS-CoV-2 viral replication and the host immune response. *J. Lipid Res.* 62, 100129. <https://doi.org/10.1016/j.jlr.2021.100129>
- Thorburn, K., Harigopal, S., Reddy, V., Taylor, N., Saene, H.K.F. van, 2006. High incidence of pulmonary bacterial co-infection in children with severe respiratory syncytial virus (RSV) bronchiolitis. *Thorax* 61, 611–615. <https://doi.org/10.1136/thx.2005.048397>
- Thornhill, E.M., Verhoeven, D., 2020. Respiratory Syncytial Virus’s Non-structural Proteins: Masters of Interference. *Front. Cell. Infect. Microbiol.* 10.
- Tian, J., Huang, K., Krishnan, S., Svabek, C., Rowe, D.C., Brewah, Y., Sanjuan, M., Patera, A.C., Kolbeck, R., Herbst, R., Sims, G.P., 2013. RAGE inhibits human respiratory syncytial virus syncytium formation by interfering with F-protein function. *J. Gen. Virol.* 94, 1691–1700. <https://doi.org/10.1099/vir.0.049254-0>
- Tourdot, S., Mathie, S., Hussell, T., Edwards, L., Wang, H., Openshaw, P.J.M., Schwarze, J., Lloyd, C.M., 2008. Respiratory syncytial virus infection provokes airway remodelling in allergen–exposed mice in absence of prior allergen sensitization. *Clin. Exp. Allergy J. Br. Soc. Allergy Clin. Immunol.* 38, 1016–1024. <https://doi.org/10.1111/j.1365-2222.2008.02974.x>
- Touzelet, O., Broadbent, L., Armstrong, S.D., Aljabr, W., Cloutman-Green, E., Power, U.F., Hiscox, J.A., 2020. The Secretome Profiling of a Pediatric Airway Epithelium Infected with hRSV Identified Aberrant Apical/Basolateral Trafficking and Novel Immune

- Modulating (CXCL6, CXCL16, CSF3) and Antiviral (CEACAM1) Proteins. *Mol. Cell. Proteomics* MCP 19, 793–807. <https://doi.org/10.1074/mcp.RA119.001546>
- Treede, I., Braun, A., Sparla, R., Kühnel, M., Giese, T., Turner, J.R., Anes, E., Kulaksiz, H., Füllekrug, J., Stremmel, W., Griffiths, G., Ehehalt, R., 2007. Anti-inflammatory effects of phosphatidylcholine. *J. Biol. Chem.* 282, 27155–27164. <https://doi.org/10.1074/jbc.M704408200>
- Triantafilou, K., Kar, S., Vakakis, E., Kotecha, S., Triantafilou, M., 2013. Human respiratory syncytial virus viroporin SH: a viral recognition pathway used by the host to signal inflammasome activation. *Thorax* 68, 66–75. <https://doi.org/10.1136/thoraxjnl-2012-202182>
- Triantafilou, K., Triantafilou, M., 2004. Coxsackievirus B4-Induced Cytokine Production in Pancreatic Cells Is Mediated through Toll-Like Receptor 4. *J. Virol.* <https://doi.org/10.1128/JVI.78.20.11313-11320.2004>
- Triantafilou, K., Triantafilou, M., 2003. Lipid raft microdomains: key sites for Coxsackievirus A9 infectious cycle. *Virology* 317, 128–135. <https://doi.org/10.1016/j.virol.2003.08.036>
- Triantafilou, M., Brandenburg, K., Kusumoto, S., Fukase, K., Mackie, A., Seydel, U., Triantafilou, K., 2004a. Combinational clustering of receptors following stimulation by bacterial products determines lipopolysaccharide responses. *Biochem. J.* 381, 527–536. <https://doi.org/10.1042/BJ20040172>
- Triantafilou, M., Miyake, K., Golenbock, D.T., Triantafilou, K., 2002. Mediators of innate immune recognition of bacteria concentrate in lipid rafts and facilitate lipopolysaccharide-induced cell activation. *J. Cell Sci.* 115, 2603–2611. <https://doi.org/10.1242/jcs.115.12.2603>
- Triantafilou, M., Morath, S., Mackie, A., Hartung, T., Triantafilou, K., 2004b. Lateral diffusion of Toll-like receptors reveals that they are transiently confined within lipid rafts on the plasma membrane. *J. Cell Sci.* 117, 4007–4014. <https://doi.org/10.1242/jcs.01270>
- Turris, V. de, Teloni, R., Chiani, P., Bromuro, C., Mariotti, S., Pardini, M., Nisini, R., Torosantucci, A., Gagliardi, M.C., 2015. Candida albicans Targets a Lipid Raft/Dectin-1 Platform to Enter Human Monocytes and Induce Antigen Specific T Cell Responses. *PLOS ONE* 10, e0142531. <https://doi.org/10.1371/journal.pone.0142531>
- Ueta, M., Nochi, T., Jang, M.-H., Park, E.J., Igarashi, O., Hino, A., Kawasaki, S., Shikina, T., Hiroi, T., Kinoshita, S., Kiyono, H., 2004. Intracellularly Expressed TLR2s and TLR4s Contribution to an Immunosilent Environment at the Ocular Mucosal Epithelium. *J. Immunol.* 173, 3337–3347. <https://doi.org/10.4049/jimmunol.173.5.3337>
- Ugonna, K., Douros, K., Bingle, C.D., Everard, M.L. %J P. research, 2016. Cytokine responses in primary and secondary respiratory syncytial virus infections 79, 946.
- Ursell, L.K., Metcalf, J.L., Parfrey, L.W., Knight, R., 2012. Defining the Human Microbiome. *Nutr. Rev.* 70, S38–S44. <https://doi.org/10.1111/j.1753-4887.2012.00493.x>
- Van der Gucht, W., Stobbelaar, K., Govaerts, M., Mangodt, T., Barbezange, C., Leemans, A., De Winter, B., Van Gucht, S., Caljon, G., Maes, L., De Dooy, J., Jorens, P., Smet, A., Cos, P., Verhulst, S., Delputte, P.L., 2019. Isolation and Characterization of Clinical RSV Isolates in Belgium during the Winters of 2016–2018. *Viruses* 11, 1031. <https://doi.org/10.3390/v11111031>
- Vandini, S., Biagi, C., Lanari, M., 2017. Respiratory Syncytial Virus: The Influence of Serotype and Genotype Variability on Clinical Course of Infection. *Int. J. Mol. Sci.* 18. <https://doi.org/10.3390/ijms18081717>
- Vareille, M., Kieninger, E., Edwards, M.R., Regamey, N., 2011. The airway epithelium: soldier in the fight against respiratory viruses. *Clin. Microbiol. Rev.* 24, 210–229. <https://doi.org/10.1128/CMR.00014-10>
- Varese, A., Nakawesi, J., Farias, A., Kirsebom, F.C.M., Paulsen, M., Nuriev, R., Johansson, C., 2022. Type I interferons and MAVS signaling are necessary for tissue resident memory CD8+ T cell responses to RSV infection. *PLOS Pathog.* 18, e1010272. <https://doi.org/10.1371/journal.ppat.1010272>

- Vaughan, M.B., Ramirez, R.D., Wright, W.E., Minna, J.D., Shay, J.W., 2006. A three-dimensional model of differentiation of immortalized human bronchial epithelial cells. *Differentiation* 74, 141–148. <https://doi.org/10.1111/j.1432-0436.2006.00069.x>
- Vázquez, Y., González, L., Noguera, L., González, P.A., Riedel, C.A., Bertrand, P., Bueno, S.M., 2019. Cytokines in the Respiratory Airway as Biomarkers of Severity and Prognosis for Respiratory Syncytial Virus Infection: An Update. *Front. Immunol.* 10.
- Verma, D.K., Gupta, D., Lal, S.K., 2018. Host Lipid Rafts Play a Major Role in Binding and Endocytosis of Influenza A Virus. *Viruses* 10, 650. <https://doi.org/10.3390/v10110650>
- Vieira, F.S., Corrêa, G., Einicker-Lamas, M., Coutinho-Silva, R., 2010. Host-cell lipid rafts: a safe door for micro-organisms? *Biol. Cell* 102, 391–407. <https://doi.org/10.1042/BC20090138>
- Villenave, R., O'Donoghue, D., Thavagnanam, S., Touzelet, O., Skibinski, G., Heaney, L.G., McKaigue, J.P., Coyle, P.V., Shields, M.D., Power, U.F., 2011. Differential cytopathogenesis of respiratory syncytial virus prototypic and clinical isolates in primary pediatric bronchial epithelial cells. *Virol. J.* 8, 43. <https://doi.org/10.1186/1743-422X-8-43>
- Villenave, R., Thavagnanam, S., Sarlang, S., Parker, J., Douglas, I., Skibinski, G., Heaney, L.G., McKaigue, J.P., Coyle, P.V., Shields, M.D., Power, U.F., 2012. In vitro modeling of respiratory syncytial virus infection of pediatric bronchial epithelium, the primary target of infection in vivo. *Proc. Natl. Acad. Sci.* 109, 5040–5045. <https://doi.org/10.1073/pnas.1110203109>
- Vincent, S., Gerlier, D., Manié, S.N., 2000. Measles Virus Assembly within Membrane Rafts. *J. Virol.* <https://doi.org/10.1128/JVI.74.21.9911-9915.2000>
- Voelker, D.R., Numata, M., 2019. Phospholipid regulation of innate immunity and respiratory viral infection. *J. Biol. Chem.* 294, 4282–4289. <https://doi.org/10.1074/jbc.AW118.003229>
- Vona, R., Iessi, E., Matarrese, P., 2021. Role of Cholesterol and Lipid Rafts in Cancer Signaling: A Promising Therapeutic Opportunity? *Front. Cell Dev. Biol.* 9.
- Vu, H.T.T., Yoshida, L.M., Suzuki, M., Nguyen, H.A.T., Nguyen, C.D.L., Nguyen, A.T.T., Oishi, K., Yamamoto, T., Watanabe, K., Vu, T.D., Schmidt, W.-P., Phan, H.T.L., Morimoto, K., Le, T.H., Yanai, H., Kilgore, P.E., Dang, A.D., Ariyoshi, K., 2011. Association Between Nasopharyngeal Load of *Streptococcus pneumoniae*, Viral Coinfection, and Radiologically Confirmed Pneumonia in Vietnamese Children. *Pediatr. Infect. Dis. J.* 30, 11–18. <https://doi.org/10.1097/INF.0b013e3181f111a2>
- Waheed, A.A., Freed, E.O., 2009. Lipids and membrane microdomains in HIV-1 replication. *Virus Res., Virus Research - 25th Anniversary Issue* 143, 162–176. <https://doi.org/10.1016/j.virusres.2009.04.007>
- Walsh, E., Falsey, A.R., 2004. Humoral and Mucosal Immunity in Protection from Natural Respiratory Syncytial Virus Infection in Adults. *J. Infect. Dis.* 190, 373–378. <https://doi.org/10.1086/421524>
- Wang, H., Yang, P., Liu, K., Guo, F., Zhang, Y., Zhang, G., Jiang, C., 2008. SARS coronavirus entry into host cells through a novel clathrin- and caveolae-independent endocytic pathway. *Cell Res.* 18, 290–301. <https://doi.org/10.1038/cr.2008.15>
- Wang, J., Li, F., Sun, R., Gao, X., Wei, H., Li, L.-J., Tian, Z., 2013. Bacterial colonization dampens influenza-mediated acute lung injury via induction of M2 alveolar macrophages. *Nat. Commun.* 4, 2106. <https://doi.org/10.1038/ncomms3106>
- Wardle, D.J., Burgon, J., Sabroe, I., Bingle, C.D., Whyte, M.K.B., Renshaw, S.A., 2011. Effective Caspase Inhibition Blocks Neutrophil Apoptosis and Reveals Mcl-1 as Both a Regulator and a Target of Neutrophil Caspase Activation. *PLoS ONE* 6, e15768. <https://doi.org/10.1371/journal.pone.0015768>
- Wiegers, H.M.G., van Nijen, L., van Woensel, J.B.M., Bem, R.A., de Jong, M.D., Calis, J.C.J., 2019. Bacterial co-infection of the respiratory tract in ventilated children with bronchiolitis; a retrospective cohort study. *BMC Infect. Dis.* 19, 938. <https://doi.org/10.1186/s12879-019-4468-3>

- Wilson, S.S., Wiens, M.E., Smith, J.G., 2013. Antiviral Mechanisms of Human Defensins. *J. Mol. Biol., Antiviral Innate Immunity (Part I)* 425, 4965–4980. <https://doi.org/10.1016/j.jmb.2013.09.038>
- Wright, J.R., 2005. Immunoregulatory functions of surfactant proteins. *Nat. Rev. Immunol.* 5, 58–68. <https://doi.org/10.1038/nri1528>
- Wu, D., Shu, T., Yang, X., Song, J.-X., Zhang, M., Yao, C., Liu, W., Huang, M., Yu, Y., Yang, Q., Zhu, T., Xu, J., Mu, J., Wang, Y., Wang, H., Tang, T., Ren, Y., Wu, Y., Lin, S.-H., Qiu, Y., Zhang, D.-Y., Shang, Y., Zhou, X., 2020. Plasma metabolomic and lipidomic alterations associated with COVID-19. *Natl. Sci. Rev.* 7, 1157–1168. <https://doi.org/10.1093/nsr/nwaa086>
- Wu, P., Hartert, T.V., 2011. Evidence for a causal relationship between respiratory syncytial virus infection and asthma. *Expert Rev. Anti Infect. Ther.* 9, 731–745. <https://doi.org/10.1586/eri.11.92>
- Yagi, K., Huffnagle, G.B., Lukacs, N.W., Asai, N., 2021. The Lung Microbiome during Health and Disease. *Int. J. Mol. Sci.* 22, 10872. <https://doi.org/10.3390/ijms221910872>
- Yeo, D.S.-Y., Chan, R., Brown, G., Ying, L., Sutejo, R., Aitken, J., Tan, B.-H., Wenk, M.R., Sugrue, R.J., 2009. Evidence that selective changes in the lipid composition of raft-membranes occur during respiratory syncytial virus infection. *Virology* 386, 168–182. <https://doi.org/10.1016/j.virol.2008.12.017>
- Yokoyama, N., Hanafusa, K., Hotta, T., Oshima, E., Iwabuchi, K., Nakayama, H., 2021. Multiplicity of Glycosphingolipid-Enriched Microdomain-Driven Immune Signaling. *Int. J. Mol. Sci.* 22, 9565. <https://doi.org/10.3390/ijms22179565>
- Yoon, J.-S., Kim, H.-H., Lee, Y., Lee, J.-S., 2007. Cytokine induction by respiratory syncytial virus and adenovirus in bronchial epithelial cells. *Pediatr. Pulmonol.* 42, 277–282. <https://doi.org/10.1002/ppul.20574>
- Zaas, D.W., Duncan, M., Rae Wright, J., Abraham, S.N., 2005. The role of lipid rafts in the pathogenesis of bacterial infections. *Biochim. Biophys. Acta BBA - Mol. Cell Res., Lipid Rafts: From Model Membranes to Cells* 1746, 305–313. <https://doi.org/10.1016/j.bbamcr.2005.10.003>
- Zhao, F., Klimecki, W.T., 2015. Culture conditions profoundly impact phenotype in BEAS-2B, a human pulmonary epithelial model. *J. Appl. Toxicol. JAT* 35, 945–951. <https://doi.org/10.1002/jat.3094>
- Zhou, Y., Wong, C.-O., Cho, K., Hoeven, D. van der, Liang, H., Thakur, D.P., Luo, J., Babic, M., Zinsmaier, K.E., Zhu, M.X., Hu, H., Venkatachalam, K., Hancock, J.F., 2015. Membrane potential modulates plasma membrane phospholipid dynamics and K-Ras signaling. *Science*. <https://doi.org/10.1126/science.aaa5619>
- Zidovetzki, R., Levitan, I., 2007. Use of cyclodextrins to manipulate plasma membrane cholesterol content: evidence, misconceptions and control strategies. *Biochim. Biophys. Acta* 1768, 1311–1324. <https://doi.org/10.1016/j.bbamem.2007.03.026>

Appendix

Appendix 1: Troubleshooting bacterial contaminated RSV stocks

Photo 1

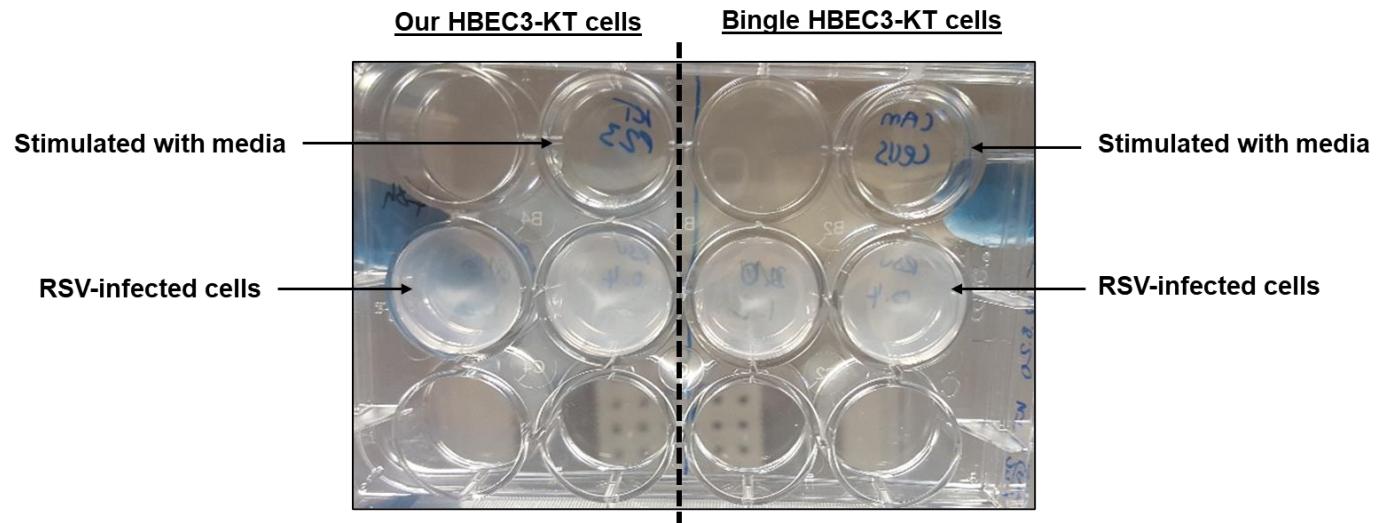


Photo 1: Comparative experiment using HBEC3-KT cells from our lab stocks and HBEC3-KT cells from Professor Colin Bingle's lab group. Cells were either stimulated with our basal media or infected with RSV (0.4 or 1.2) for 2 h. Unbound virus was removed, and fresh basal media added to the cells. The plate was incubated up to 48 h before visualisation and image capture. An opaque effect can be seen in all the HBEC3-KT cells that were infected with RSV.

Photo 2

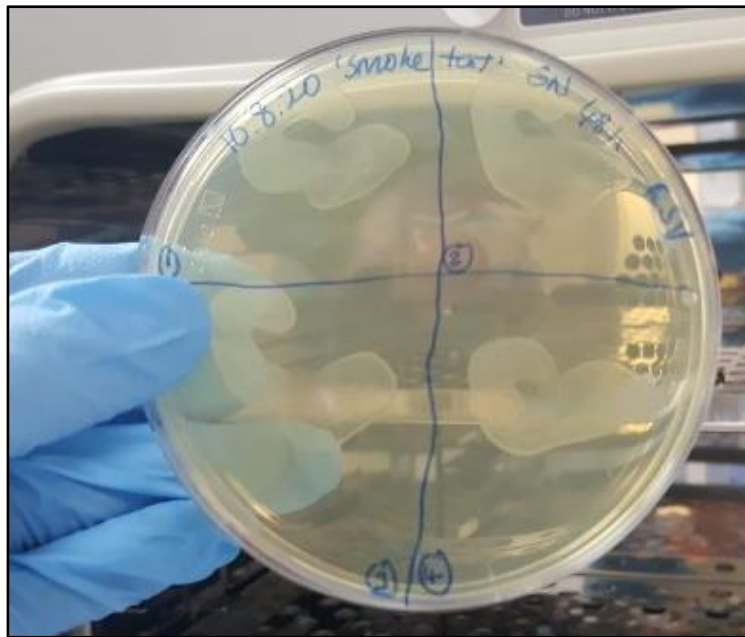


Photo 2: Supernatants were collected from each of the RSV-infected wells from the experiment above. 50 μ l of each supernatant samples were added to an LB agar plate and allowed to air dry. Plates were incubated for 48 h and checked for bacterial growth as indicated by the opaque areas of each sectioned area.

Photo 3



Photo 3: A neat sample (100 μ l) of one frozen RSV stocks (P6) was streaked onto an agar plate and allowed to air dry. The agar plate was incubated for 48 h and checked for bacterial colonies indicated by the white dots.

Photo 4



Photo 4: A neat sample (100 μ l) of older RSV stocks were streaked onto an agar plate and allowed to air dry. Samples included RSV P6 control antigen (CA), RSV P5 and RSV P5 CA. The agar plate was incubated for 48 h and checked for bacterial colonies indicated by opaque area in top right section of plate.

Photo 5

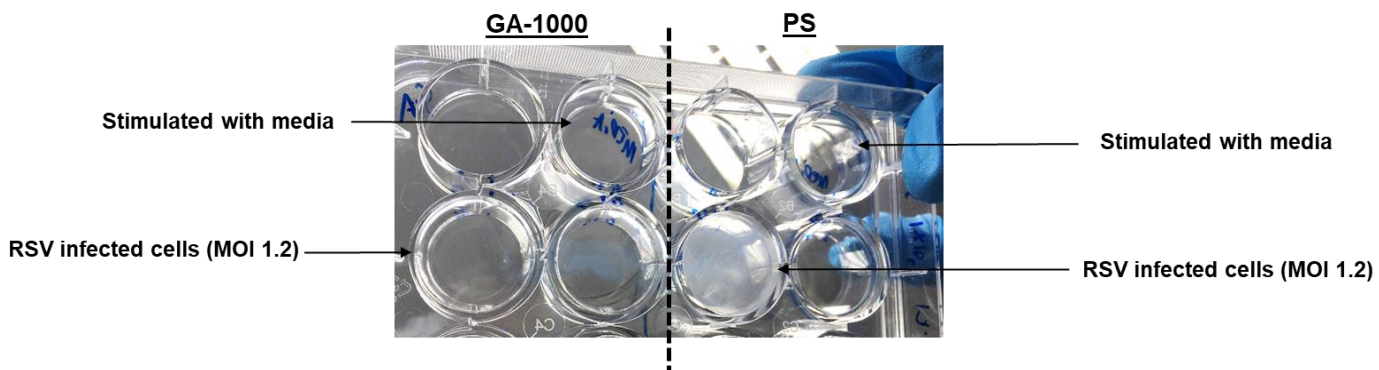


Photo 5: HBEC3-KT cells were either stimulated with media or infected with RSV (MOI 0.4 and 1.2) in media containing either PS or GA-1000. Cells were incubated for 24 h then checked for turbidity in the overlying supernatant. Turbidity was seen in the cells infected with RSV where cells had been incubated in media containing PS but was not seen in GA-1000-containing media. Bacterial contamination was also confirmed on LB agar plates where RSV-infected samples using PS had clear signs of bacterial growth but not GA-1000.